Air induction noise investigation during turbocharger surge events in petrol engines

by

Ajith Venkateswara Pai

A Doctoral thesis

Submitted in partial fulfilment of the requirements for the award of

Doctor of Philosophy

of

Loughborough University

24th March 2015

ABSTRACT

Turbocharging is used as a means to downsize petrol engines, thereby, producing more power for a lower engine size, when compared with a naturally aspirated engine. Due to the presence of a throttle valve in the intake system in petrol engines, flow is restricted at the outlet pipe of the compressor during low load engine operation. For example, during transient tip out – tip in maneuvers. Hence, there is a chance of the turbocharger operating in near surge or surge conditions and, thus, generating surge noise. This Thesis describes an experimental and simulation method to predict and measure the turbocharger surge noise. Initially, experimental transient tip-in and tip-out maneuver was performed on a non turbocharged car with a petrol engine. The measured noise level in the intake manifold, at a low frequency of up to 1200 Hz, was analysed and was shown not to represent surge noise. Next, a one dimensional simulation method was applied to simulate the noise of the engine and this demonstrated an increase in the acoustic pressure level in the intake manifold during the tip – in and tip – out maneuver. However, a surge noise pattern was not observed in the analysis of acoustic pressure signals in the intake system using Short Time Fourier Transform (STFT). The simulation procedure was also used to inform the design of an experimental rig to recreate the surge noise under laboratory conditions. An experimental turbocharger noise rig, designed and built for this purpose, is explained in the Thesis. Important component parts likely to be involved in the surge noise generation such as the intake system, compressor, throttle body, compressor recirculation valve and measurement and control systems were integrated into the test rig. Background noise contributions from the electric motor, AC mains, supercharger pulley, throttle body, inverter fan, throttle body gearing and structural vibration of the supporting structure were identified from the analysed frequency components of the signals from surface microphone measurements taken at the intake system. This helped to clearly identify the surge noise frequency components (3250 Hz) in the STFT analysis. The fundamental mechanism of noise generation was identified using an analysis of the experimental results and a frequency calculation for vortex shedding and the radial acoustic resonances. One of the main conclusions of the Thesis is that the compressor recirculation valve (CRV) open or close position, the CRV delay time and the throttle position are major contributing factors to the cause of the surge noise. Another major conclusion is that the radial acoustic resonance may be a mechanism of surge noise generation. Finally, a passive solution to reduce the surge noise is proposed. A pipe with cross ribs is designed as a passive solution using the radial acoustic resonance calculation and the corresponding nodal patterns. This solution demonstrated a measured intake system noise reduction of up to 10dB under compressor surge conditions.

ACKNOWLEDGEMENTS

TABLE OF CONTENTS

LIST OF FIGURES

LIST OF TABLES

NOMENCLATURE

A	-	Area
A_i	-	Flow area of cell i
A_s	-	Heat transfer surface area
A_{tot}	-	Total flow area of cross section
a_x	-	Acceleration component along the x axis
a_y	-	Acceleration component along the y axis
$C_{f\,\tan}$	-	Tangential velocity component
C_{faxial}	-	Axial velocity component
C_{fi}	-	Gas flow velocity at cell i
$\bar{C}_f$	-	Mean gas velocity at cross section
C_{fo}	-	Velocity through reference bore
C_{fr}	-	Skin friction coefficient
C_p	-	Specific heat capacity at constant pressure
C_{pr}	-	Pressure loss coefficient
C_v	-	Specific heat capacity at constant volume

c	-	Velocity of sound in gas
c_f	-	Fluid velocity
c_{fin}	-	Inlet velocity
c_{gx}	-	Helical wave velocity of propagation
c_x	-	Velocity horizontal
c_z	-	Velocity vertical
D	-	Swirl meter bore reference
d_p	-	Pressure differential across dx
d_x	-	Length of mass element in the flow direction
e	-	Energy (total internal energy per unit mass)
F/A	-	Fuel air ratio
F_r	-	Wall friction per unit volume
F_σ	-	RMS value for frequency range 0-F
$f_{1/2\lambda}$	-	Half wave resonant frequency
g	-	Acceleration due to gravity
h	-	Specific enthalpy
h_{in}	-	Inlet enthalpy

h_{out}	-	Outlet enthalpy
H	-	Total enthalpy
I	-	Shaft moment of inertia
J_{np}	-	Bessel function
k	-	Constant
L	-	Length
$\dot{m}$	-	Mass flow rate
m_{act}	-	Corrected mass flow rate
m_t	-	Time step multiplier
N		Rotational speed of the engine
N_s	-	Strouhal number
N_u	-	Impeller tip speed
n	-	Number of diametral pressure nodes
ni	-	Numbers such as 1,2,3…
p	-	Number of concentric circular pressure nodes
p2	-	Compressor outlet pressure
p_b	-	Power output of the engine

p_m		Brake mean effective pressure
P	-	Pressure
P_2	-	Pressure at compressor outlet
P_{ref}	-	Reference pressure
P_{rms}	-	RMS value of the sound pressure
P_w	-	Power
$\dot{Q}$	-	Heat transfer rate
Q_{HV}	-	Heating value of the fuel
r	-	Radial distance
R	-	Universal gas constant
$r(x)$	-	Radial distance of 1D flow line from the axis of rotation
S_m	-	Swirl meter reading
SM_{const}	-	Swirl meter constant
SM_{corr}	-	Swirl meter correction factor
S_{pp}	-	Power spectral density
T_2	-	Compressor outlet temperature
$T_2^{'}$	-	Temperature after isentropic compression

T_{fluid}	-	Fluid temperature
T_{in}	-	Inlet tempearture
T_{ref}	-	Reference temperature
T_o	-	Torque
$T_{Total,\ in}$	-	Inlet total temperature
T_{wall}	-	Wall temperature
t	-	Time
u	-	Specific internal energy
V	-	Volume
V_s	-	Swept volume of the engine
$\dot{W}$	-	Work transfer rate
Δh_s	-	Isentropic enthalpy change
Δt	-	Time step
Δx	-	Minimum discretized element length
$\Delta \omega$	-	Change in shaft speed
γ	-	Specific heat ratio
η_f	-	Fuel conversion efficiency

μ	-	Dynamic viscosity
ρ	-	Density

Acronyms

bmep	-	Brake mean effective pressure
CFD	-	Computational fluid dynamics
CRV	-	Compressor recirculation valve
dB	-	Decibel
DoE	-	Design of Experiments
FFT	-	Fast Fourier Transform
KE	-	Kinetic energy
MPWR	-	Mean pre whirl ratio
NDSR	-	Non dimensional swirl ratio
NVH	-	Noise, vibration and harshness
PE	-	Potential energy
PID	-	Proportional-integral-derivative

PR   -   Pressure ratio

STFT   -   Short time Fourier Transform

Tfmep   -   Total friction mean effective pressure

CHAPTER 1
INTRODUCTION

1.1 Importance of turbocharger in internal combustion engine downsizing

There is continuous effort in the automotive industry to downsize the engine, i.e. to increase the power to weight ratio of the engine or to increase the power to volume ratio. The major goal of downsizing is carried along with other goals such as higher overall efficiency, low fuel consumption and lower emission of engine. Downsizing is achieved by increasing the power of engine for a given engine weight or by reducing the weight of engine for a given power. The change in weight to power ratio from 1985 for diesel and petrol engines is shown in Fig 1.1.
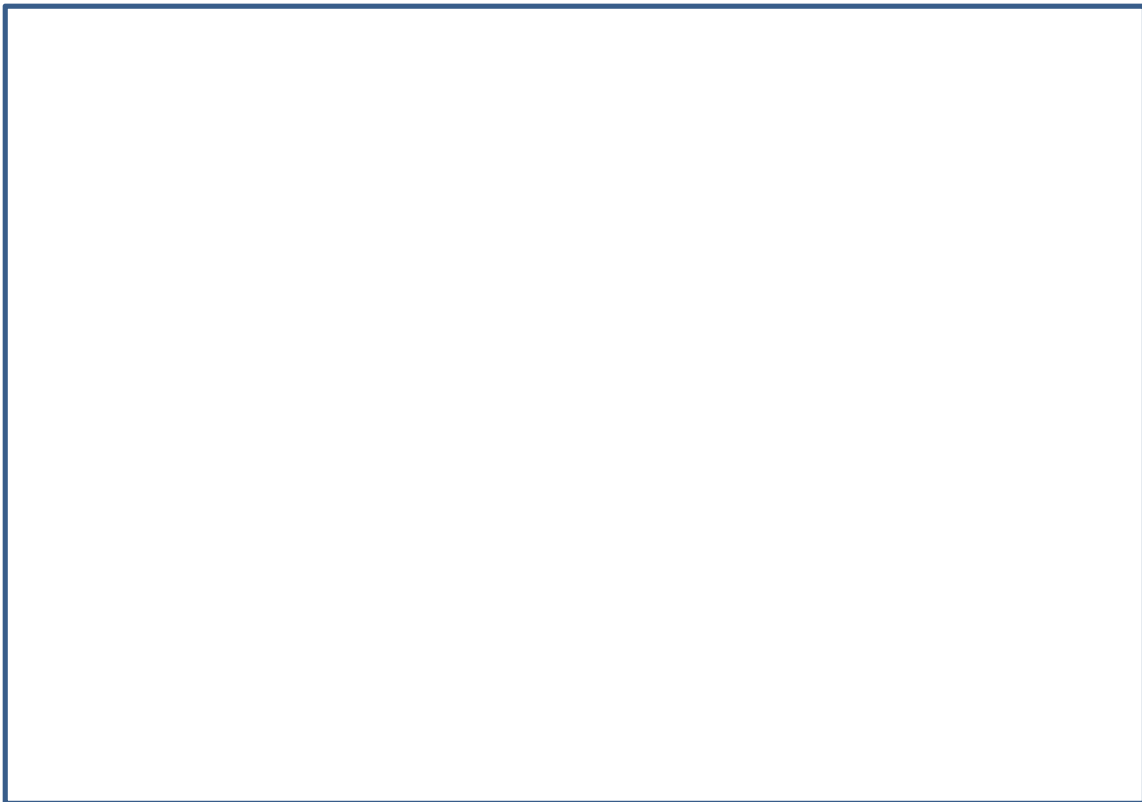
Fig. 1.1 Progress of engine downsizing [1]

The output power of the engine, P_b is defined by the formula

$$p_b = p_{me} \times V_s \times N \qquad \text{-1.1}$$

Hence, power can be increased by increasing brake mean effective pressure (bmep), swept volume, V_s and/or speed of engine in revolutions per minute, N. Increasing the volume will increase the weight of the engine and increasing the rotational speed of engine will increase the frictional losses as defined by the equation :

$$\boxed{} \qquad \text{- 1.2 [2]}$$

The above formula is arrived from several four stroke four cylinder spark ignition engines between 845 to 2000 cc displacements. Hence, increasing mean effective pressure is the method to improve the output power of engine. Brake mean effective pressure is defined by the equation [3] [4]

$$\boxed{} \qquad \text{-1.3}$$

For a given fuel, the heating value and the fuel air ratio is constant. This makes the mean effective pressure proportional to the air density after charging, fuel conversion efficiency and the volumetric efficiency. The density of air in turn, is dependent on charge pressure and inversely dependent on charge air temperature by the formula

$$\rho = \frac{p_2}{R \times T_2} \qquad \text{-1.4}$$

Hence the output of engine of a given volume and speed can be significantly improved by increasing the air charge density by means of a turbocharger. This is illustrated in the following table 1.1 by comparing between a naturally aspirated engine and a turbocharged engine with the same air fuel ratio.
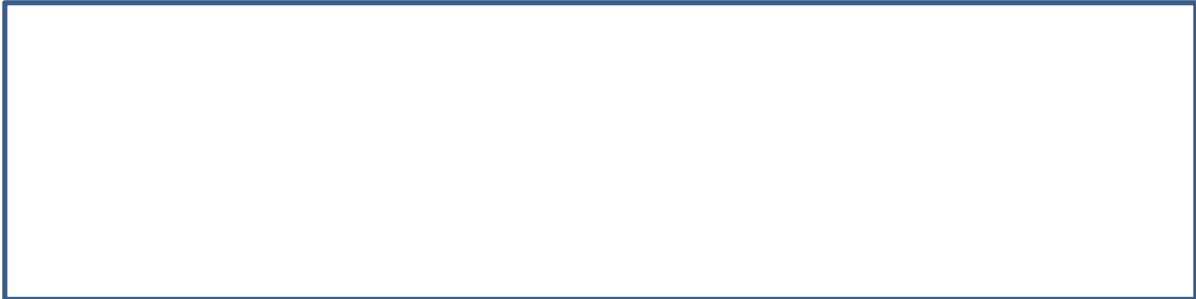
Table 1.1 Effect of charge air density and mean pressure of engines [4]

1.2 Effect of downsizing and introduction of turbocharger on engine noise

One of the important challenges of downsizing the engine is to meet the customer expectations and to achieve the required performance parameters such as driveability and NVH targets. As the engine is downsized, the same or higher power needs to be generated and transmitted using less material. This can increase the NVH of the engine. Also, introduction of turbocharger to a downsized engine can increase the sound pressure level compared to that of an engine of equivalent torque without turbocharger. The increase in noise in the downsized engine during the engine speed range of 1500 to 2800 rpm is attributed to the build-up of boost pressure and hence directly related to the operation of turbocharger. Fig. 1.2 compares radiated noise of a turbocharged and downsized turbocharged engine. The I4 engine as given in the Fig.1.2 is an engine without turbocharger but of much higher displacement than the I3 engine which is turbocharged.

Fig. 1.2 Effect of turbocharger operation on engine noise [5]

Similarly in another study, sound pressure level has been plotted for 9 modern HSDI engines and found that engine noise has increased by 5 dB(A) (Fig. 1.3 and Fig. 1.4) .

Fig. 1.3 Engine noise due to turbocharger operation [6]

Fig. 1.4 Increase in engine overall noise by 5 dBA, contributed by turbocharger whoosh noise [6]

Introduction of turbocharger causes increase in gas flow through the exhaust system and thus causes a high frequency turbulence noise [7]. In the earlier literatures, it is stated that [2] in the intake manifold, the heavy pulsations caused by the operation of intake valves will be suppressed by the introduction of compressor in the system, reducing the low frequency noise. It is also found that the high frequency noise is created due to high rotational speeds of compressor and the blade passing frequency. This is illustrated in Fig. 1.5. The mechanism of silencing is generally attributed to the silencing effect of compressor housing behaving as a small, reactive silencer element. However, there are many types of noise related to turbocharger being listed in various literatures. The main cause of the turbocharger noise is attributed to the higher turbocharger rotor speeds and the air flow interaction with the turbocharger system [8]. Within the turbocharger the audible noise is attributed to the compressor as the turbine is connected to the exhaust system which in turn is having good silencing properties [9].

Fig. 1.5 Effect of turbocharger operation and generation of high frequency noise [2]

Introduction of turbocharger in the spark ignition engine is more difficult than in the compression ignition engine [10]. As the spark ignition engines operate at a wider engine speed range and also include a throttle, the turbocharger compressor need to generate a wider air flow range. This causes difficulty in keeping the operation of compressor away from the surge line and can induce noise under surge conditions. A faster response and also careful control to avoid either pre-ignition or self-ignition is required. This project concentrates on the increase in noise due to introduction of turbocharger in a downsized petrol engine.

1.3 Thesis structure

Internal combustion engine is the major source of noise generated by an automotive vehicle. Downsizing of the internal combustion engine has led to introduction of turbochargers in petrol engines. Normally, the development of engine and vehicle goes through design gates, finally leading to mass production. During the initial development stages, the prototype of engine and vehicle are normally available for testing the noise and other performance. Considerable amount of time is spent to design the engine and manufacture the parts for testing. Hence, it is very important for the NVH engineers to understand the occurrence of surge noise, which is defined as a flow induced phenomena. Also, the noise problem once identified during the development stage of the engine may lead to a costlier solution. The motivation of this thesis is to identify an experimental, simulation method to identify the noise issue in advance, and also to suggest a less costly passive solution.

Review and understanding of the current knowledge available in the field of turbocharger noise is presented in chapter 2 ("Literature Review"). Major classification of turbocharger noise is listed and the causes are explained. This comprises the frequency distribution during each noise occurrence. Further, a detailed explanation on the mechanism of noise generation is listed. The area of interest was covered from system level, i.e. engine interaction to component level, i.e. turbocharger compressor stages. Some of the parameters used for quantification of surge and related noise are explained. Computer based simulation methods used for the prediction of noise occurrence are explained. 3D CFD simulation is removed from the scope of this thesis, as this approach requires extensive geometric data and takes a long time for grid generation and predictions [11]. As this study requires transient operation, over a period of time, with many variables, one-dimensional simulation code along with an experimental rig is used in the current work. The experimental techniques used for the identification of turbocharger noise are explained in detail and the solution methodology adopted is presented.

Experiments on a non turbocharged vehicle was performed and is documented in chapter 2. The aim of the exercise was to identify the noise generated in the intake system of a non turbocharged vehicle and to differentiate that with the turbocharged system. A surface microphone is used to measure the noise inside the intake system of this car. This approach helped to relate the whoosh noise problem to the turbocharged system. The experimental work on this car helped to develop the investigation of the noise problem on an experimental rig in the noise and vibration facility. The characteristic intake system noise in a non-turbocharged vehicle has been documented in this chapter.

After performing experiments and analysis on a vehicle, computer-based one-dimensional simulation has been performed and presented in chapter 3. The theory, discretization and the solution methodology used in the simulation are explained. A simulation model for surface microphone used in the experiment is created and the further processing using Fast Fourier Transform (FFT) is explained. The noise simulated using the simulation model for a non turbocharged engine, is compared with the measured values in experiment. Further, the simulation model is used to perform transient manoeuvres with a combination of parameters to understand the pressure dynamics of the intake system. Even though pressure values gave an indication of increased noise, the characteristic whoosh noise was not observed in the analysed experimental results. Hence, experimental rig and simulation technique was used to conduct further study.

One dimensional simulation technique was selected using the literature review and presented in Chapter 4. GT Power software was used to model the turbocharger and intake system. A surface microphone model was created to perform FFT of the intake pressure signals during the surge operation. Steady state simulation results from a natural aspirated engine model was compared with the experiment explained in chapter 3. Further, transient simulations were performed as a DoE with the parameters of engine speed, throttle profile, compressor recirculation valve (CRV) close or open and the position of the compressor surge line. Finally, the FFT on the simulated data by the surface microphone was conducted to identify any surge noise occurrence.

The concepts developed and the simulation methodology used to arrive at the final design of the experimental rig is given in chapter 5. A modular rig is designed to adapt different intake systems of automotive car. As the surge noise is defined as a compressor based phenomena, a stand-alone supercharger compressor rig is designed. The compressor specification is derived from the one-dimensional simulation results of an automotive engine's model. The selection of the mechanical components of the rig is explained in detail. LabVIEW software along with the data acquisition system is used to control the instruments used. The same facility is used to acquire the noise and other useful data for further analysis.

Background and steady state noise measurement is conducted and documented in chapter 6. The aim is to identify the amplitude and frequency range of the background and steady state operation noise of the compressor rig. Also, operating point on the compressor map is identified during the steady state and transient manoeuvers and the relation with the surge noise identified is explained. Finally, a DoE was conducted to identify the effect of factors such as compressor shaft speed, throttle body position and the compressor recirculation valve position on the surge noise generated.

Development of a passive solution is documented in chapter 7. As a first step, the sound pressure level generated during surge events at different shaft speeds, 'delta T' i.e. the CRV delay is quantified from the measurement and further analysis. Some of the parameters used such as mass flow through from the CRV and the ratio of mass flow through the intake system and through the CRV is obtained using an equivalent one-dimensional simulation model. Further, the mechanism of noise generation is understood from the frequency of sound pressure

level observed during surge noise. This lead to the design of a passive solution. The experiment conducted using passive solution demonstrates a significant reduction in the surge noise.

CHAPTER 2
LITERATURE REVIEW

2.1 Introduction

There are many types of noise related to turbochargers experienced by automotive OEMs during the development phase. The identification of the source of noise is made usually from the frequency, turbocharger speed and engine operating conditions. The mechanisms of the noise generation can be different for different types of noises. More common causes are design related such as imbalance of the shaft, impeller and turbine system, volute construction irregularities and the design of the inlet and outlet passages. In this chapter, more emphasis is given on the flow related noise problems, its mechanism of generation, detection and preventive measures taken. Literature review on other types of noise generation is undertaken to understand the frequency range of interest and also the source of noise. This will then help to identify the noise created during compressor surge in the experimental set up.

2.2 Types of turbocharger noises

Turbocharger noise is broadly classified based on the relation between the frequency of the noise and the turbocharger speed (Fig. 2.1) i.e. a) constant tone noise in which frequency of noise is constant and do not vary with turbocharger speed. b) Unbalancing whistle or pulsation noise. The frequency of noise in this case is proportional to speed of the turbocharger. c) rotating noise in which the frequency is proportional to the product of turbocharger speed and the number of blades of the compressor [12]. d) whoosh noise caused by high engine demand at low engine speeds. Classification is presented in Fig. 2.1
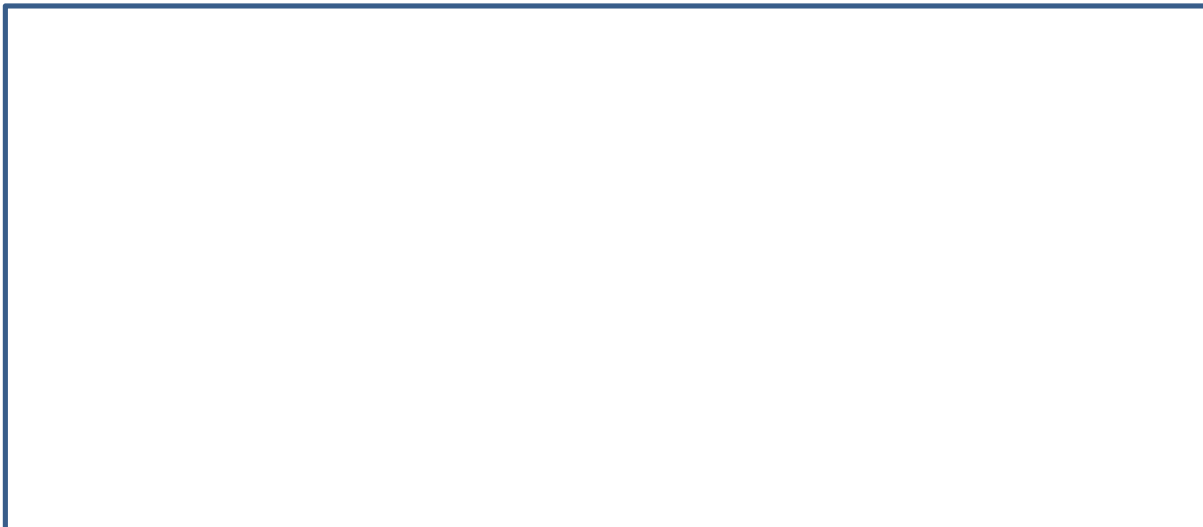
Fig. 2.1 Classification of turbocharger noise based on relation of frequency with turbocharger speed [12]

2.2.1 Constant tone noise

As the name suggests, the frequency of the noise do not change with time. However at lower shaft speeds, the frequency may increase with speed and get stabilised at higher speeds. This kind of noise is mainly due to bending of the rotating shaft in hydrodynamic oil film. The frequency range is 500 – 1000Hz.

2.2.2 Unbalanced whistle and pulsation noise

The frequency range of the noise occurrence is of the order of 1.2 - 4.5 kHz [5]. This type of noise is caused generally by the rotor eccentricities and blade geometry [13] [12] and highly dependent on the rotating speed of turbocharger blades. Generally this type of noise is clearly identifiable against the background noise. In the lab, a test rig is used to detect this noise and also to measure the pulsation rate. Turbocharger manufacturers have extensive experience on methods to keep this type of noise under acceptable level. The usual approach is to get feedback from the vehicle manufacturer regarding acceptable pulsation rates. The vehicle manufacturers are provided with set of identical turbochargers with average to high pulsation rates and requested to give feedback on the interior noise subjective ratings on prototype cars. This method of investigation of correlation between pulsation rate and acceptable interior noise can yield various results. Some cars may produce significant interior noise due to pulsation rate beyond certain limit. But some other cars can cause no objectionable interior noise. Hence this method of determination by means of testing and experimentation can cause rejection of certain

turbochargers with higher pulsation rates and also close quality control. This will add to the cost of turbocharger and subsequently the supplier could suggest certain modification on the intake system to reduce the noise.

2.2.3 Rotating noise

This type of noise is created basically by the pressure difference between the suction and compression side of the blade and also by the blades passing the tongue of housing. The frequency of excitation is determined by the product of turbocharger speed and the number of blades involved. As the passenger car turbocharger shaft can reach rotational speed up to 2,40,000 rpm and that the number of blades are of the order of 5 to 9, the frequency of excitation is likely to be higher than that of audible limit. However, in truck engines, at full load and due to low speed of turbocharger, the frequency can go up to 13 kHz and can be clearly audible to the driver.

2.2.4 Blow noise

This is a broad-band noise (typical range: 1500-3000 Hz, Fig. 2.2) [13] and generally caused during low air flow rate and low turbocharger speed operating conditions. The noise has a similarity to that produced during air leakage.

A similar type of noise is known as whoosh noise [14]and is also of broad band nature. This is typically caused due to high torque demand at lower engine speed which translates to the turbocharger surge operation, i.e. in the event of low air flow across the rotor and high pressure ratio. The phenomenon of surge is explained in the following section. The turbocharger rotor will be in the lower speed range during this event. This condition is generated during the throttle tip in condition, but also found during steady state driving condition, in petrol engines. In diesel engines this is caused by higher loads at low engine speeds. The noise generating steps as shown in Fig. 2.3 explains the engine operating condition of higher engine torque demand or higher load at a lower engine speed. This can also occur during the transient tip-in tip-out manoeuvre of automobiles during which, high pressure is imposed on the compressor outlet followed by lower air flow. This causes the turbocharger to operate at a near surge condition and thereby leading to the generation of whoosh noise.
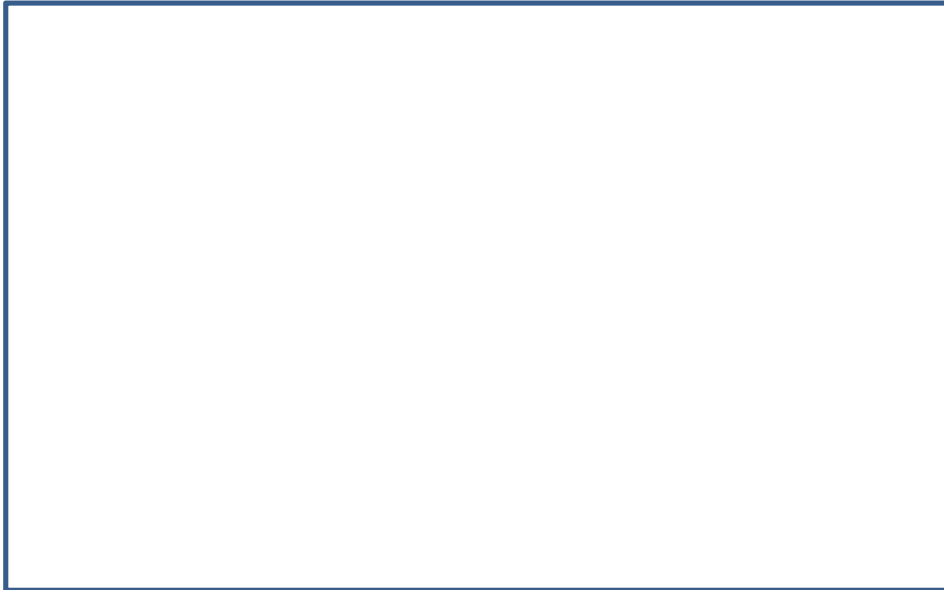
Fig. 2.2 Induct measurement of the airborne noise at compressor exit [13]
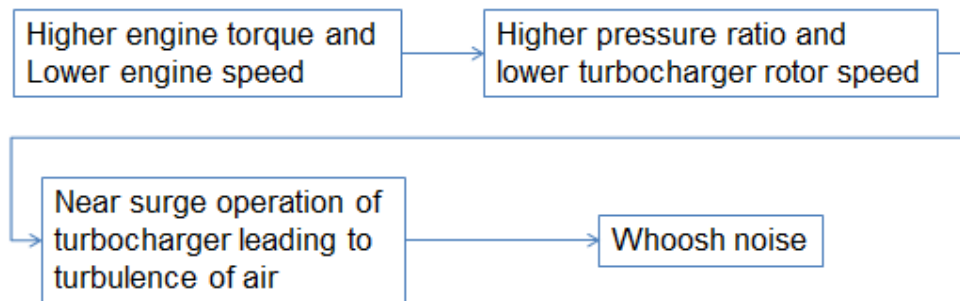
Fig. 2.3 Whoosh noise generation steps

2.3 Mechanisms/causes of turbocharger noise

The mechanisms of turbocharger noise are broadly classified into two 1. inherent causes within the turbocharger system and 2. interaction with the engine and other air intake system components

2.3.1 Inherent causes within the turbocharger system

The major causes are the imbalance of the rotating system, due to improper bearing configuration and position and geometric eccentricities.

Apart from geometric inaccuracies, flow process can cause noise in the turbocharger as suggested by Watson and Janota [2]. The phenomenon is known as component stall and occurs at the flow near the wall, i.e. the boundary layer gets retarded so severely that it can no longer follow the wall surface. The kinetic energy in the boundary layer may not be sufficient to overcome the adverse pressure gradient causing the flow separation near the wall, known as local stall. Referring to the Fig. 2.4, the reduction of mass flow rate at constant speed, causes the axial component (C_x in Fig.2.4) of the absolute velocity of the incident air stream at the leading edge of the inducer to reduce, causing increase in the angle of incidence. When it crosses the critical angle of incidence, the flow can no longer adhere to the suction side of the inducer blade. These conditions can encourage the reversal of flow. During high pressure conditions, the inducer stall can lead to a severe condition known as the surge.

Fig. 2.4 Flow separation in the inducer [2]

The breakdown of flow in one channel (e.g. 'b' in the figure 2.5) of the impeller can cause air to deflect and enter the nearby channel 'a' at an increased angle of incidence [2]. If this angle of incidence is more than the critical angle, channel 'a' can stall causing reduction of incidence angle at channel 'b', thereby restoring the normal flow. This can cause stall to pass from one channel to another and can induce aerodynamically caused vibrations resulting in increased noise level.

Fig. 2.5 Rotating stall [2]

Another interaction which is significant in terms of noise, performance and air flow from the turbo charger compressor is the interaction between the impeller and the diffuser. The impeller is the rotating part of the compressor with blades and diffuser is the adjacent part which converts the kinetic energy of the air into pressure energy. The diffuser can be of vaned or vane less type.

In the case of vaneless diffuser, due to compressibility and viscosity effects in the diffuser region, the streamlines close to the wall have less kinetic energy and follow a path of much reduced spiral angle until the flow is swept back towards the impeller. This is solved by using larger impeller exit flow angle. But the negative effect is that the solution results to low tip width and high associated noise.

In the case of vaned diffuser, stall occurs when the air incidence angle at the diffuser vane inlet reaches a critical value. Disruption of flow due to the effect of non-uniform flow leaving the impeller can also cause rotating stall of the diffuser. If the number of diffuser vanes is less than the impeller blades, the effect of non-uniform flow is reduced.

2.3.2 Noise due to interaction with the engine and other air intake system components

Compressor performance is highly influenced by the interaction with the adjacent component in the engine, i.e. intake pipe and other air inlet system components [15]. The air inlet system layout which provides an optimum turbocharger performance is difficult to package in the automotive engine due to constraints imposed by crash planes, pedestrian protection areas, vehicle styling, power pack components and vehicle chassis components.

Generally the compressor can operate in a satisfactory way, even though some of its components such as the impeller and diffuser are in the stall mode of operation. However, in the case of highly reduced air mass flow rate and at constant speed, critical component or a combination of number of component of the compressor stalls. This introduces a strong reversal of flow. This stage is highly unstable and the phenomenon is described as stage stall [2]. When the disturbance becomes periodic and grows to a large magnitude, the system (comprising the compressor and installation) can become self–exciting. The problem then gets graduated to a system level from the component level.

Generally, turbocharger characteristic map is represented by plotting pressure ratio against mass flow parameter for lines of constant speed parameter. Also contours of constant isentropic efficiency are superimposed [2].
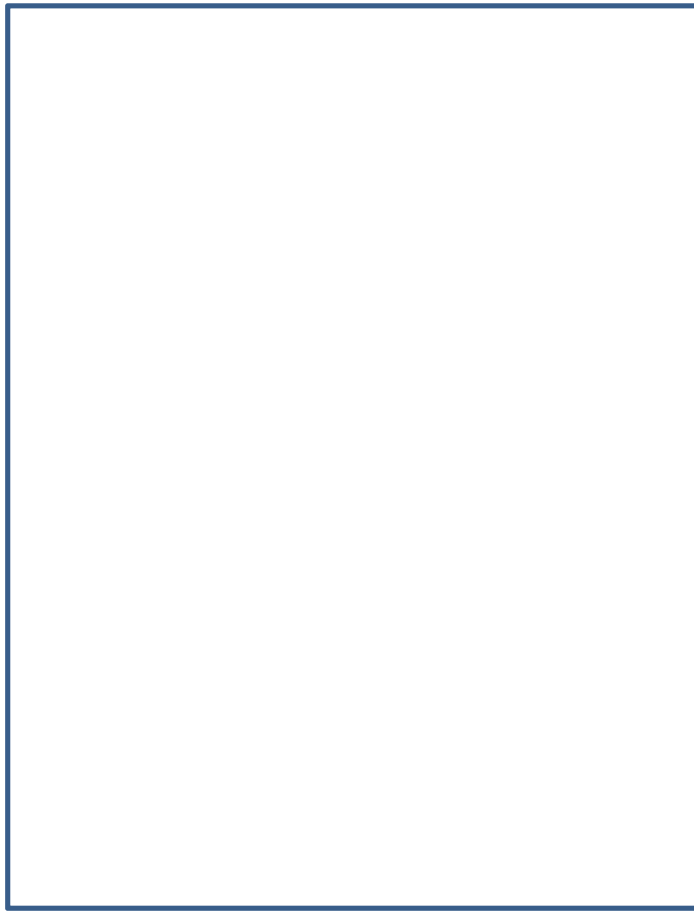
Fig. 2.6 Turbocharger characteristic curve [2]

The entire map is divided into three zones; stable operating zone (centrally placed), surge zone and the choking zone [2], Fig. 2.6. When the mass flow rate through the compressor is reduced at a constant pressure ratio, a point arises when the local flow reversal happens at boundary layers. This will result in low efficiency. If the flow rate is further reduced, complete reversal of flow occurs and will relieve the adverse pressure gradient until a new flow regime and pressure ratio is established. The compressor is then said to be in the surge operation. The area of high gas velocity is known as choking zone. This happens during high speed of the compressor during increased gas velocity, causing diffuser choke. As a result, compressor speed rises substantially with little increase in mass flow rate.

The operating point of the turbocharger on the turbocharger characteristic curve is a good indication of the stable or unstable mode of operation. The operational characteristic of the turbine is highly dependent on the opening and closing of the throttle (Fig. 2.6). In the case of petrol engines, when the throttle (Fig. 2.7) is closed slowly, the delivery pressure of the

compressor increases and the air mass flow rate reduces [2]. This causes increase in the air mass flow rate through the delivery valve and hence reduce the compressor delivery pressure and increase the mass flow rate. This occurs in the stable operating zone as shown in the Fig. 2.8. In the unstable operating zone, when the throttle valve is closed, compressor delivery pressure decreases and hence reduces the flow rate. Eventually mass flow rate will drop to an extent that the pressure downstream the delivery valve will fall below that of the compressor delivery pressure, causing more mass flow from the compressor and the operating point to move towards point 'M' in the Fig. 2.8. The whole cycle repeats and causes surge behaviour.

Fig. 2.7 Schematic of compressor and the throttle [16]

Fig. 2.8 Stable and unstable operating zone [16]

Apart from the position of the operating zone, the positive slope of the flow characteristic curve of the throttled delivery system and that of the constant parameter curve have to be compared for predicting the surge operation. Surge occurs when the positive slope of the speed parameter

curve exceeds that of the delivery system as shown in the Fig. 2.9 [2]. This shows that the surge occurrence is highly interactive with that of the intake system.

Fig. 2.9 Effect of slope of throttle characteristic [2]

Positive pre whirl, i.e. the whirl at an opposite direction to the compressor rotation can lead to high relative velocities at compressor inlet [15]. This along with higher angle of attack can cause turbocharger stall or surge as given in the above passages. To quantify this phenomenon several flow parameters are proposed in literature [15].

    a.   Flow uniformity index (Gamma) index [15]

     -2.1

    Where

C_{fi}- Gas flow velocity at cell i, m/s

$\bar{C}_f$ - Mean gas velocity of cross section, m/s

A_i – Flow area of cell, m^2

A_{tot} – Total flow area of cross section , m^2

b. Mean pre whirl ratio [15]

$$$$ -2.2

Where $C_{f\,tan}$ – Tangential velocity component, m/s

C_{faxial} – Axial velocity component, m/s

Both the above parameters are derived using the CFD analysis of compressor and air inlet system components. Another parameter is explained which is derived from the turbocharger flow test rig.

c. Non dimensional swirl ratio (*NDSR*) [15]

$$$$ -2.3

Where S_m – Swirl meter reading

SM_{const} – Swirl meter constant

SM_{corr} – Swirl meter correction factor

$\dot{m}$ – Mass flow rate

C_{fo} – Velocity through reference bore

D – swirl meter reference bore

Correlation between the *NDSR* and the measured noise level is established in the Fig. 2.10

Fig. 2.10 Measured noise level against measured NDSR [15]

Near surge operation is the major cause of whoosh noise by the turbocharger. When engine is operating in wide open throttle condition and during higher engine speeds, the air flow is more through the turbocharger compressor. As the throttle is moved towards the closed position, the air before the throttle can be of very higher pressure and hence can cause backward flow of air through the compressor to the inlet of the compressor. This will drastically reduce the speed of the compressor and can even cause stall and damage the compressor. Hence a blow off valve is used to vent off the high pressure air between the turbine and the inlet. This will reduce the pressure of the air. However, there could be some time delay for the recirculation valve to open and hence can cause backflow of air through the compressor. This will cause chirpy noise from the turbocharger and is mainly due to the interaction between the air and the compressor. Consideration of proximity of operating line with the marginal surge region can be good indication of surge noise [6]. This tool is valid during steady state operating conditions.

However, the effect of dynamic nature of pressure ratio and the air flow across the compressor is not considered.

The surge line predicted using the gas test stand may not be valid in the engine operating condition. This is because of the interaction of the pulsating flow in the intake due to the piston motion with that of the air flow from the compressor. The volume of the intake system between the compressor and the combustion chamber may not be sufficient to dampen the pulsations caused by the pistons. As the surge line can shift towards the high mass flow rate region, the mean mass flow rate of the compressor must be having sufficient margin with the surge line, due to the interaction. During the surge operation, the interaction with the intake system downstream of the compressor is strongly present.

There could also be considerable difference in pressure and velocity at each inlet channel of the compressor leading to variation in pressure ratio, flow and losses. Further mixing losses occur as the individual flows amalgamate in the vaneless diffuser and volute resulting in reduction in efficiency, mass flow rate and pressure ratio capability.

Another condition is sudden tip in of accelerator and causing high demand of air flow into the engine [8]. This results in the sudden increase of speed of the turbocharger and hence sudden excitation of air causing noise. The flow of excitation from the turbocharger to the passenger compartment is shown in the Fig. 2.10. The flow excitation caused when the turbocharger runs into marginal surge condition splits into structural transfer of vibration to duct and airborne transfer to inlet duct [6]. Structural vibration and the pressure excitation cause radiation of surge noise to the passenger compartment.

Fig. 2.11 Source – transfer path – receiver model for the turbocharger noise [6]

It is generally thought that reversal of flow and hence high turbulence occurs when the operating point is close to the turbocharger surge line. However, the importance of marginal surge is shown in the Fig. 2.11. The full load engine operating line with the speed range causing the turbocharger whoosh noise is presented. At the occurrence of whoosh noise, the operating region of the compressor is away from the surge line. Operating point towards the left of this intersection is the surge region and towards the right of this intersection is the stable region.

Fig 2.12 Whoosh noise detection using the compressor characteristic curve [6]

The above operating points are based on the mean values of air mass flow. However in the real engine, there could be instances of dynamic air mass flow component crossing the surge line to the left, if we examine the cycle to cycle data of the engine. This can cause instantaneous turbulence and hence surge noise [6]. This was predicted using the 1-D thermodynamic simulation software (Ricardo WAVE) as in the Fig. 2.12.

Fig. 2.13 Dynamic air mass flow crossing the surge line [6]

To conclude that increase in pressure pulsation is the root cause of whoosh noise, the temperature at the compressor inlet is measured. It is well known that as the local air temperature at the compressor inlet increases during surge, pressure pulsation also increases as the compressor enters surge operation [14]. To correlate the increase of temperature with that of the whoosh noise, measurement was made using K type thermocouple at the compressor inlet, near the blades by Charlie Teng et al. [14]. The increase in pressure pulsation and the temperature was observed when the compressor is operating near the surge region. The measured temperature increase is shown in the Fig. 2.13. Another experiment conducted by leaking high pressure air through an orifice to increase air flow through the compressor, while maintaining same pressure is conducted by Charlie Teng et al. [14]. It is shown that the leaking air has significantly reduced the compressor whoosh noise and the compressor inlet temperature, as in the Fig. 2.14.

Fig. 2.14 Temperature measured at the compressor inlet vs. whoosh noise [14]

Fig. 2.15 Whoosh noise and temperature baseline vs. with orifice [14]

2.3.3 Vortex shedding and acoustical resonances

Many noise generating mechanisms in the turbocharger surge period is caused by flow [17] [18]. The acoustic resonances were documented at frequencies unrelated to the mechanical frequency by Archibald [19]. Coincidence of vortex shedding with the acoustic resonance results in the amplification of dynamic pressure fluctuations and hence noise problems. Acoustic resonances can be along the length, radial or cross-mode. In the case of acoustic

length resonances, the resonant frequency and the quarter wave resonant frequency is determined by the length and diameter of the air intake system

Half wave resonant frequency is given by:

$$f_{1/2\lambda} = n\frac{c}{2L} \qquad - 2.4$$

n- Number such as 1, 2, 3…
c – velocity of sound in gas
L – Length of the pipe
And the quarter resonant frequency is given by:

$$f_{1/4\lambda} = (2n-1)\frac{c}{2L} \qquad - 2.5$$

Radial acoustic resonance is due to standing pressure waves acting perpendicular to the flow direction and the intake pipe axis and can propagate along the length of the pipe as helical waves.

The resonances involving Bessel function and the velocity of wave propagation is given by the equations [17]

$$f_{np} = J_{np}(c/d) \qquad -2.6$$

J_{np} – Bessel function
c- velocity of sound in gas
d – Basic hydraulic (geometric) diameter of obstruction or constriction (pipe or passage diameter)

$$c_{gx} = \frac{c}{\sqrt{1 - \dfrac{f_{np}}{f}}} \qquad -2.7$$

c_{gx} – Helical wave velocity of propagation
f_{np} – Cross-mode frequency
f – Excitation frequency

A simple model for surge occurrence has been given by Grietzer [20] [21]. Compressor is an energy source and initiates the pressure. The throttle downstream the compressor acts as a damper and the inertia of the fluid between the outlet of the compressor and the throttle acts as a spring mass. The springiness is due to the compressible fluid between the throttle and the compressor outlet. The fluid trapped constitutes the resonant element and the energy from the compressor source is absorbed by the throttle. When the energy delivered by the compressor is

not dissipated through the throttle, any small perturbations could grow into huge disturbance leading to noise.

2.4 Simulation methods used to predict turbocharger noise

Modelling the passive and active properties of sound generation in the turbochargers are described in some literatures [22] [23]. In general, passive properties define the sound propagation through the device while the active properties define the sound generation mechanism in the device. Several methods are used and are described as follows:

2.4.1 Zero Dimensional modelling

This involves modelling techniques using lumped parameter method to detect the surge occurrence developed by Greitzer (1976) for axial compressors and by Yano and Nagata (1971) for centrifugal compressor and stated by Keller et al. [24], [25]. Greitzer model comprises of a set of non-linear equations to estimate the system dynamics in the compression system. A dimensionless number is defined by [21]

$$\boxed{} \quad \text{-2.8}$$

If B<=0.8, No surge and if B>=0.8, surge

N_u – Impeller tip speed,

c - Speed of sound

V_p – volume of the compressed air

A_c-Equivalent compressor cross sectional area

There are simplifying assumptions used in the zero dimensional modelling such as ignoring the wave propagation effects and spatial effects in the compressor system. To overcome the short comings due to these simplifications, one dimensional model are being used [26].

2.4.2 One dimensional modelling

These models are based on non-linear 1 D gas dynamics and basically used to simulate the engine performance. GT Power software is widely used for this purpose. This software uses the pressure waves entering and leaving the compressor and the turbine using the input characteristic map provided. As the characteristic map is measured using a steady state test rig, the pressure waves predicted may not be same as the real pressure wave in the dynamic conditions in the intake system of an engine. The results depend on the accuracy of the characteristic map under dynamic conditions.

One dimensional, non-linear, time dependent equation of conservation of mass, momentum and energy are used for simulation for turbocharger noise by Peat et. Al [27], Fig. 2.16. The time dependent conservation of mass, energy and momentum equations are solved

$$\frac{\partial}{\partial t}\begin{bmatrix}\rho \\ m \\ e\end{bmatrix} + \frac{\partial}{\partial x}\begin{bmatrix}m \\ mV+p \\ hV\end{bmatrix} = \begin{bmatrix}-\dfrac{m}{A}\dfrac{dA}{dx} \\[2mm] -\dfrac{mV}{A}\dfrac{dA}{dx}+\rho(E-F_r) \\[2mm] -\dfrac{hV}{A}\dfrac{dA}{dx}+mE\end{bmatrix} \qquad \text{-2.9 [27]}$$

Where ρ is the density, p is the pressure,

mass, $m = \rho V$

energy, $e = \dfrac{\rho V^2}{2} + \dfrac{p}{\gamma-1}$

wall friction per unit volume, $F_r = \lambda I_p V^3 |8A\|V|$

$E = \Omega^2 r \dfrac{dr}{dx}$

$r(x)$ – radial distance of 1 D flow line from the axis of rotation as in the figure
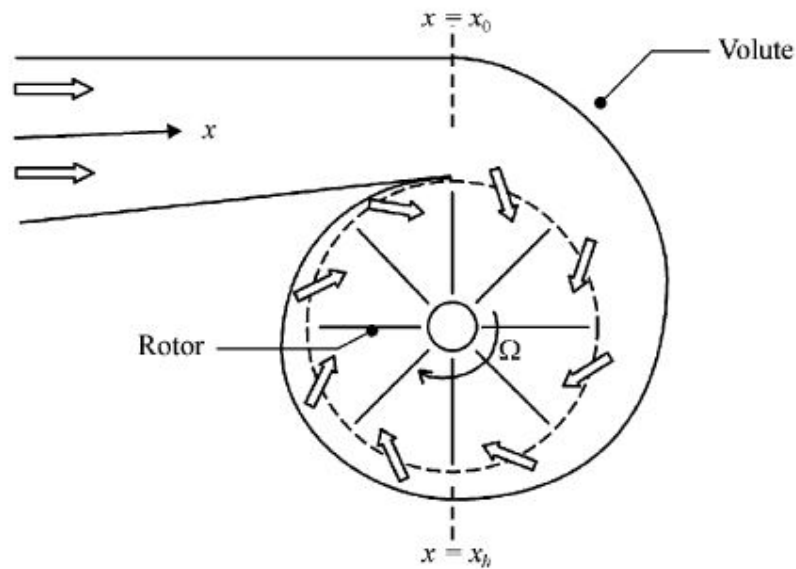
Fig.2.16 Turbine nomenclature [27]

The acoustic parameters are determined using the equation. The acoustic parameters are expressed in the form of transfer function to be further processed into any acoustic property such as transmission loss.

2.5 Testing methods used to measure the turbocharger noise

Two types of testing methods were undertaken generally to measure the turbocharger noise; 1. On a test rig and 2. On an engine

2.5.1 Measurement on a test rig

Test rigs normally consists of a driving mechanism such as compressed air or electrical or hydraulic power. Compressed air is the common means to drive the turbine. The mechanical power to generate compressed air is obtained from diesel or other fuel engines or electrical power. The gas flow is controlled by means of valves and measurement of pressure, temperature, mass flow rate, speed and sound pressure level of the compressor and turbine wheel.

Vibroacoustic measurement of the turbocharger was performed by Aretakis et al. [28] to understand the unsteady flow conditions. The overall schematic of the test rig is shown in

Fig.2.17 In this test rig, compressed air is used to drive the turbine. The intake air to the experimental rig is heated. Throttle valves are provided at the inlet and outlet of the turbine and compressor. The operating points of the turbine and the compressor are set by appropriate adjustment of the throttle valves by regulating the mass flow rate and the pressure across the system. Generally across all the rigs, the operating point is chosen by closing the throttling valve at the compressor outlet and the rotational speed is controlled by adjusting the turbine inlet and outlet valves. The compressor and the turbine mass flow rate are measured with an orifice plate. The total pressure is measured using a total pressure pitot tube and the static pressure is measured using the average pressure of four wall pressure taps. Temperature is estimated using type K thermocouples. The unsteady flow velocities are measured using hot wire anemometers at the compressor inlet. To determine the casing vibrations, two accelerometers are used and also three omnidirectional microphones as in the fig. 2.18

Fig. 2.17 Schematic of the turbocharger test rig [28]

Detection of the surge condition from the non surge condition has been done by Galindo et al. [29] using the frequency domain analysis of the measured variable in an experimental rig.

Fig. 2.18 Positions of accelerometers and the microphones [28]

The measurements were used to diagnose the unstable operating condition of a turbocharger. An acoustic criterion for surge condition detection has been explained. This criterion is given by an equation and is defined as the rms value of acoustic signals filtered in the sub-synchronous part of the spectrum [28].

-2.10
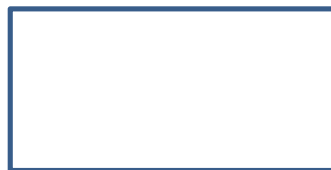
Where F_σ - rms value for frequency range 0-F Hz

f - frequency

S_{pp} - Power spectral density

The limit values of this parameter under different operating condition such as stable, stalled and surged condition has been provided against the rotational speed of the compressor. However there is no concrete indication that these values can be generalised to be applied to other sizes or operational conditions of tubro-compressors.

The input taken from the above experiment setup for this project is the overall experimental setup, the type of measuring equipment used and their location and the analysis performed on the measurements.

2.5.2 Measurement on an engine

Teng et al. [9] have measured the whoosh noise on an engine dynamometer according to SAE standards in a semi anechoic chamber as shown in the fig. 2.19. The measurement taken near the intake orifice i.e. the measurement at the microphone at the left side is studied.

Fig.2.19 Measurement of whoosh noise in an engine test cell [14]

It is noted that the intake orifice at the left side emanates significant whoosh noise at the vehicle interior as shown in the Fig. 2.20. The engine whoosh noise is identified in the engine speed range of 1500 to 3000 rpm and in the frequency range of 1.5-7 kHz.

Fig. 2.20 Radiated noise at the full load run up of engine [14]

2.6 Methods adopted for reducing the turbocharger noise

In this section the various methods adopted for reducing the turbocharger noise after it is detected during testing is listed. The methods are divided based on the region of interest i.e. in the source and transfer path region. The most effective and least expensive will be reduction of noise at source [30]. Reduction in efficiency of noise generation at source will lead to reduction in noise at all observer locations. Whereas, solution at the transfer path region i.e. by providing silencers, barriers are effective only at certain spatial regions. Also adding components such as silencers will lead to increase in cost and weight of the system and also the performance of the engine could be compromised. However many factors need to be considered while choosing the practicality of implementing the solution. The factors could be the freedom of design change which will depend on the development stage of the engine, packaging constraints and performance targets of the engine.

2.6.1 Solution at source

2.6.1.1. Optimising the shaft and bearing configuration

Shaft induced noise are caused mainly due to oil film interaction, high speed of shaft rotation and the bearing configuration. This problem was solved by optimising the bearing configuration of the system.

2.6.1.2. Reduction of imbalance of the shaft, turbine and compressor wheel

This is an important part of reduction of turbocharger noise. This is mostly done at supplier facility and the imbalance is chosen such a way to keep the excitation and noise in an acceptable level.

2.6.1.3. By optimising the engine calibration

Pressure delta, i.e. the difference between the pressures after and before the throttle is an important parameter to determine the position of operating point on the compressor characteristic curve [14]. This value is ensured by the calibration team to have a good turbocharged engine response with respect to vehicle demand and is very important in the case of gasoline engines. By reducing the pressure delta, the compressor can be made to operate in a stable region and thereby whoosh noise can be reduced. The reduction of pressure delta is achieved by reducing the pressure before the throttle plate without adversely affecting the driver demanded performance in tip in manoeuvre as in the Fig. 2.21 and 2.22.

Fig. 2.21 Reduction of pressure delta [14]

Fig. 2.22 Effect of reduction of pressure delta over the radiated sound [14]

2.6.1.4. By modifying the flow at the compressor inlet

Teng et al. [14], Evans et al. [6] and Galindo et al. [31] have documented the influence of quality of air flow at the inlet of compressor on the whoosh noise. Due to packaging constraints many automotive engine are forced to have a 90 degree bend at the inlet to the compressor of

the turbocharger. This bend causes non-uniform entry flow and these instabilities may lead to undesirable instabilities in the operation of the compressor [31]. They have stated that the presence of negative pre whirl is a favourable condition to the reduction of whoosh noise. When the air flow direction is same as that of the direction of rotation of the compressor wheel, it is defined as negative pre whir. The direction of rotation is opposite in the case of positive pre whirl.

But the use of swirl generating devices at the compressor inlet should be done with careful study of the pressure drop it could generate on the system. This pressure drop can move the compressor operating point closer to the surge line and thus cause higher turbulence. Study done by Teng et al. [14] shows that the pre whirl device B has a lower whoosh noise at 2000 to 2500 rpm than another pre whirl device A as shown in the Fig. 2.23. This is because the pre whirl device B moves the operating point away from the surge line as in the Fig 2.24 (shown as circle in the Fig. 2.24). However, the pre whirl device B generates higher turbulence and hence higher whoosh noise at speed of less than 2000 rpm as in Fig. 2.24. This is because pre whirl device B moves the operating line closer to the surge line than the device A (shown as a square).

Fig. 2.23 Effect of pre whirl devices on the noise. [14]

Fig. 2.24 operating point on the compressor characteristic curve [14]

2.6.1.5. By using different sizes of compressor

Different sizes i.e. different trims of the compressor were tried by Teng et al. [9]. Size of the compressor wheel is defined in the form of trim. This is represented as the square of the ratio of the lowest diameter to highest diameter of the wheel as in the Fig. 2.25.

Fig. 2.25 Compressor wheel [32]

- 2.11

By varying the trim, the compressor characteristic curve can be changed. Teng et al. [14] selected two types of trims, i.e. 45 and 55 for the experiment. By selecting the trim size of 55,

they could increase the surge margin only slightly. But by selecting the trim size of 45, the surge margin was increased considerably but the negative impact is that the operating line crossed the choking line. This will limit the compressor performance at high speed operation requirement of the engine as shown in the Fig. 2.26. It is concluded that proper compressor matching is required to each engine based on the operating ranges.

Fig. 2.26 Effect of trim on the characteristic curve of turbocharger [14]

2.6.2 Solution at transfer path

2.6.2.1. By adding a broad band resonator

Broad band resonator consisting of Herschel Quincke tube and two quarter wave resonators were added at the duct between the compressor outlet and the intercooler by Trochon [13]. The arrangement is shown in the Fig. 2.27.

Fig. 2.27 Dimensions of Herschel Quincke tube [13]

The Herschel Quincke tube with one branch twice as long as other is an efficient device which induces transmission loss [13]. If λ is the length of the longest branch, it features 3 resonances at $f_o = c/\lambda$, $f_1 = 2/3 \ c/\lambda$ and $f_2 = 2f_1$, where c is the speed of the sound. The transmission loss of this arrangement was 7.5 dB, with one quarter resonator the transmission loss became 15.5 dB and with the other quarter resonator the transmission loss become 23.5 dB as given in the Fig. 2.28
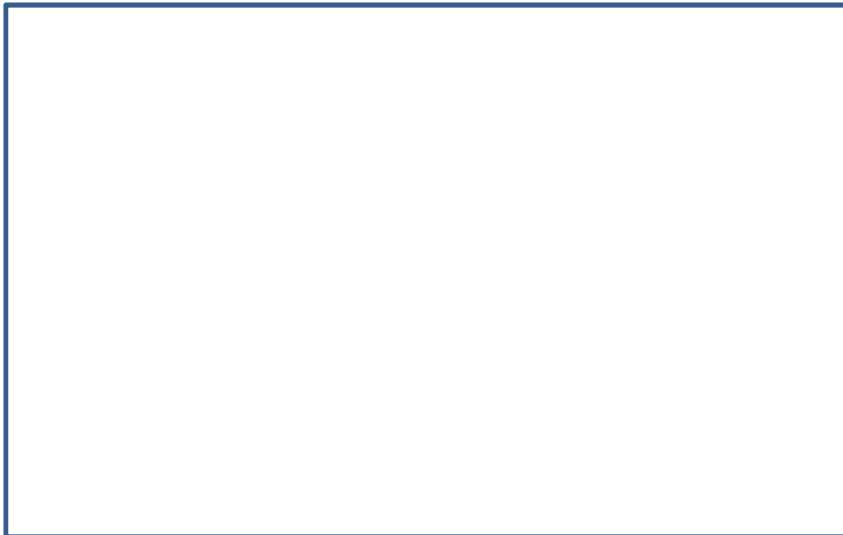
Fig. 2.28 Calculated transmission loss of standard and improved Herschel-Quincke tubes [13]

Resonator very close to the turbocharger compressor outlet has been used by Stoffels et al. [5] to filter out the noise at a certain frequency range. Basically the whining noise due to turbocharger imbalance has been addressed in this case. Measured pressure pulsation given in

Fig. 2.29 shows that whining noise is reduced after the introduction of resonator. The radiated noise is also reduced as in the Fig. 2.30

Fig. 2.29 Introduction of resonator reduces the whining noise [5]

Fig. 2.30 Introduction of resonator reduces the flow noise [5]

2.6.2.2. By changing the intake duct geometry

The strength of contribution of paths in the generation of noise was studied by Evans et al. [6]. It was found that the primary transfer path is the excitation and subsequent radiation of the

intake system ducts. To prove this, intake system was lagged and the sound pressure level reduced to 4.5 dBA.

Another approach followed to reduce the radiated noise was to increase the thickness of the compressor outlet hose. An increase in thickness of the hose wall by 50% gave a noise reduction of 1.5 dBA (Fig. 2.31). Modifying the heat insulator shape and optimising was another approach followed by Usuda et al. [33]. As a result the noise was brought back to same level without a heat insulator.

Fig. 2.31 Effect of heat insulator optimisation [33]

CHAPTER 3
EXPERIMENTS ON A NON TURBOCHARGED VEHICLE

3.1 Aim and objective

Experiments were conducted on Ford Fiesta Car at Loughborough University. The engine of the vehicle is 4 inline, petrol without a turbocharger. The aim of the experiment was to understand the noise and vibration behaviour of the air intake system of the non-turbocharged engine. Another aim was to understand the application of measuring instruments. The experiments performed would be helpful for the measurement and analysis of the parameters in turbocharged engine in the future experiments. Two types of experiments conducted are:

1. To run the engine in idle and measure the noise and vibration of induction system

2. To do tip-in and tip-out manoeuvre and measure the noise and vibration of the induction system

The measurement of sound pressure level inside the air intake system, just before the throttle valve (i.e. after the air filter) and before the air filter is a good indication of the occurrence of abnormal noise during throttle tip in and tip out manoeuvre. During this manoeuvre, it is expected in the turbocharged engines with whoosh noise problems that an abnormal noise is produced which are clearly audible in the passenger compartment. Hence it was decided to place a microphone at the passenger position, i.e. very close to the head rest of the car. Table 3.1 lists the measuring instruments used for the experiments.

Sl No	Instrument	Location	Serial number
1	Free field microphone GRAS 1/2" pre polarized 40 AE and GRAS CCP pre amplifier type 26 CA	At air intake system start	58365 & 57428
2	Free field microphone GRAS 1/2" pre polarized 40 AE and GRAS CCP pre amplifier type 26 CA	After filter element	58364 & 56392
3	Surface microphone B&K 4949	On intake pipe before filter	2574635
4	Surface microphone B&K 4949	On air filter box after filter	2574638
5	Accelerometer PCB 352C44	On air filter box after filter	75449
6	Linear potentiometer, P&G Control	On accelerator pedal	AF145/0150
6	RT Pro Focus software and Focus II real time analyser	-----	

Table No. 3.1 List of instruments used for the experiments.

3.2 Experimental setup

The detailed experimental set up is shown in Fig. 3.1-3.4. Surface microphones are used to measure surface pressure within the intake system. The intake duct is punctured to insert the diaphragm part of the surface microphone into the duct. The flange is used to attach the microphone on the duct wall as shown in the Fig. 3.1. Two free field microphones are used to capture the sound level, one at the intake portion of the air intake system and the other near the surface microphone at the post filter side. An

accelerometer is attached on the post filter side of the air filter box (Fig. 3.4). A linear variable differential transformer (or linear potentiometer) is attached to the movable portion of the accelerator pedal at one end and the stationary portion of the chassis at the other to measure the accelerator pedal travel (Fig.3.3). To confirm the working of accelerator pedal sensor, an electrical output is taken from the throttle body to measure the output voltage and hence to measure the throttle opening (Fig.3.4). RT Pro Focus software along with a Focus II real time analyser is used to capture and analyse the signals.
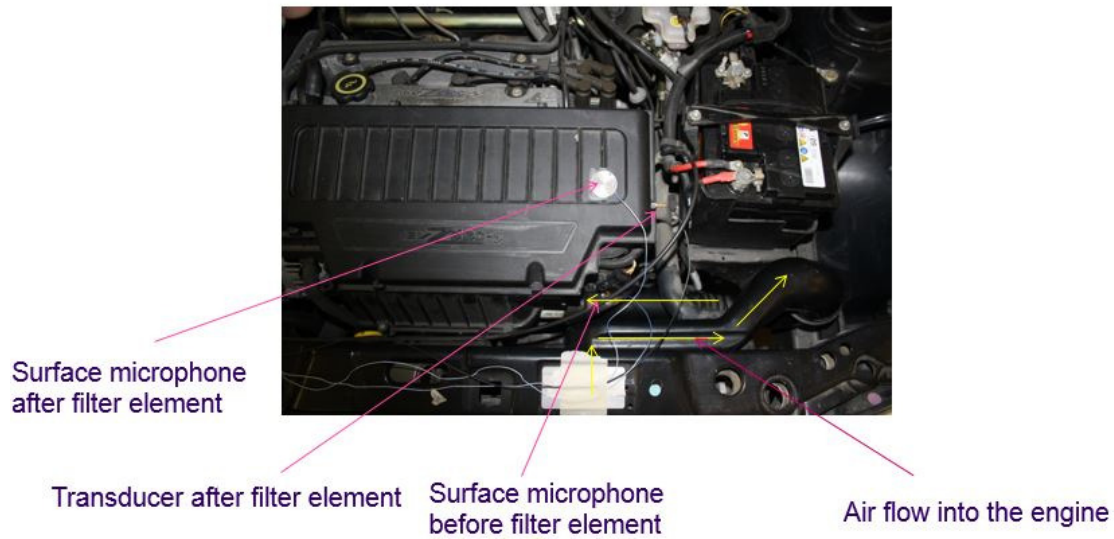
Fig.3.1 Integration of surface microphone on the engine

Free field microphone after filter element   Free field microphone at air intake start

Fig. 3.2 Position of Free field microphones near the vehicle

Linear potentiometer fitted to measure accelerator pedal travel

Fig. 3.3 Arrangement of throttle position sensor on the accelerator pedal

Electrical connection taken from the wire of throttle body to measure throttle angle

Fig. 3.4 Arrangement to measure the throttle angle

3. 3 Procedure

3.3.1 Steady state experiment

Steady state experiments were conducted by operating the engine at an idle speed of 1000 rpm and the measurement was taken.

3.3.2 Transient experiment

The engine is made to run at an idle speed of 1000 rpm and the measurements were recorded. Sudden tip in and tip out of the accelerator pedal of the accelerator pedal was performed.

3.4 Results and conclusion

3.4.1 Steady state experiment - results

Coherence aspect of the test is expressed in the form of Coherence function [34], which is the measure of degree of linear association between two signals i.e. pressure signals at the surface microphone at the pre filter position and that at the post filter position. If the magnitude of the coherence is closer to one it can be inferred that the pressure signal measured at the surface microphone at the pre filter position is linearly associated with the pressure signal measured at the surface microphone at the post filter position. In this case the contribution of noise is very small. But when the coherence is less than

one, two aspects can be analysed. One is the resonance in which the waves cancel each other and gives a low reading of pressure. Another case is the noise contribution into the input signal. This can also cause a low coherence and affects the accuracy of the sound pressure level measured.

Coherence for the engine idle test is provided in the Fig 3.5. This shows that the pressure signals measured by the surface microphone on air intake before and after filter have good coherence until 105 Hz and after this noise dominates in the measurement.
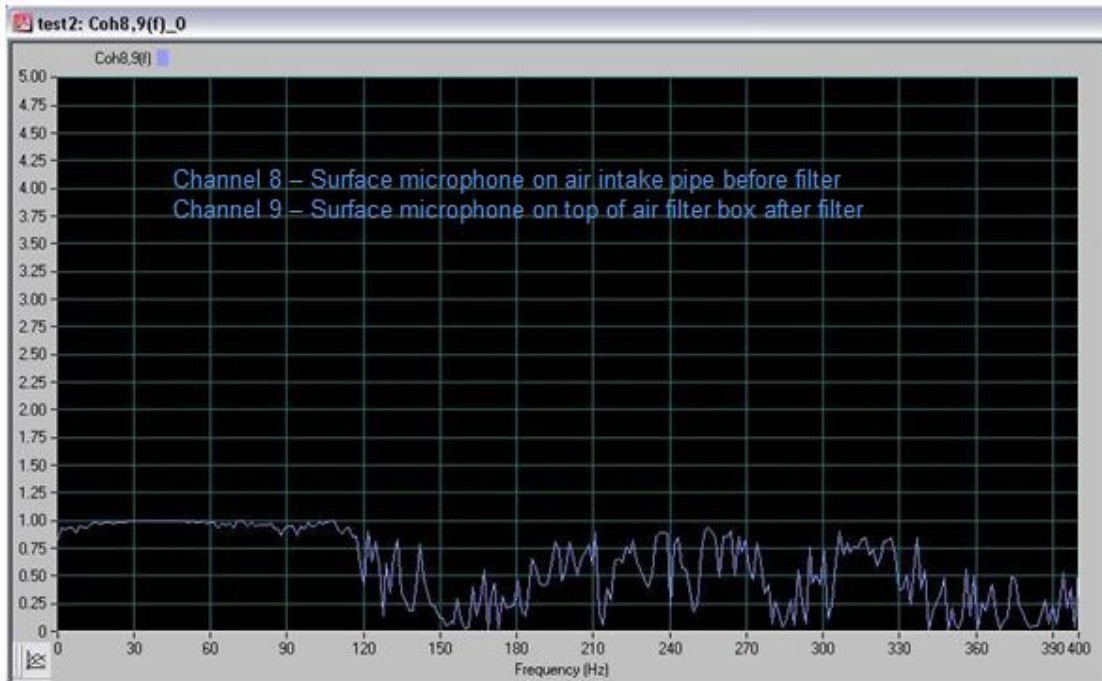
Fig. 3.5 Coherence between the pressure signal measured by surface microphone before and after the filter.

Fast Fourier Transform (FFT) is performed on the measured signals against time to convert that to sound pressure level against frequency using the inbuilt feature of the RT Pro Focus software, as shown in the figure. The FFT is simply a fast way to calculate the discrete Fourier transform (dft), a procedure for calculating discrete frequency components from sampled time data. It is a process by which the time domain sequence is mapped into a continuous function of a frequency variable [35]. Fig. 3.6 shows that the peaks are formed at the multiples of engine idling speed, i.e. 16.5 Hz, 33 Hz, 49.5 Hz and so on.
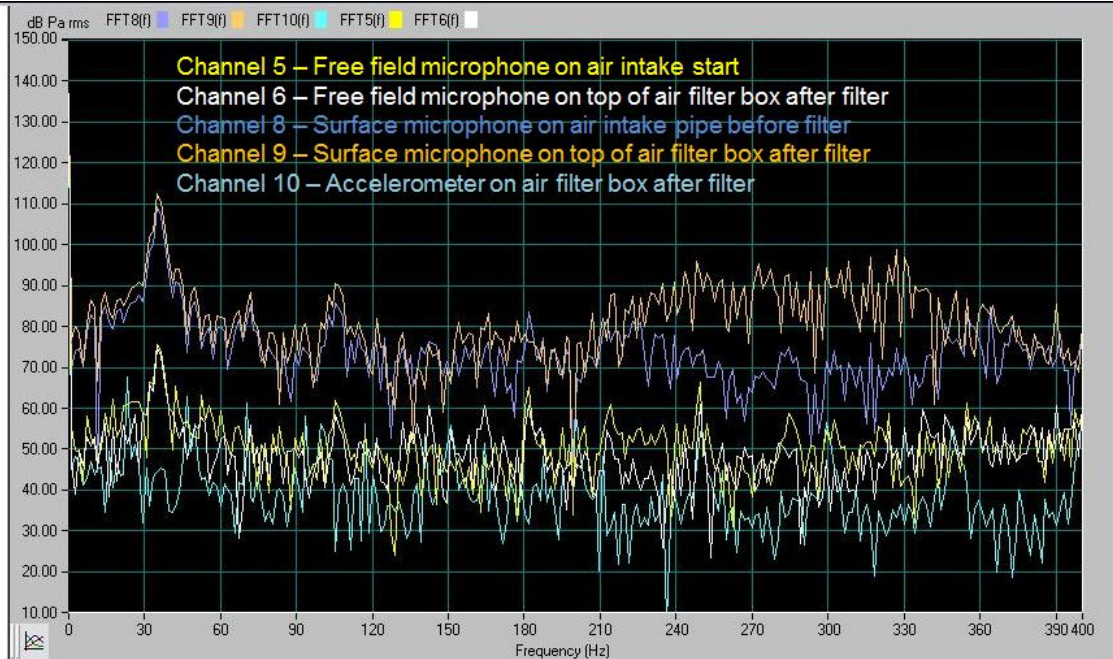
Fig. 3.6 FFT of signals measured

Fig. 3.6 also shows the natural outcome that the readings of the surface microphone which are located inside the intake ducts are higher than that of the microphone located outside the intake system.

3.4.2 Transient experiments -results

The output from the acceleration pedal sensor and the throttle position sensor is shown in Fig. 3.7. The engine is positioned in idle condition for 0 to 13 sec and then accelerator pedal is pressed to until 75%. The throttle position sensor reading shows that the throttle has delayed for a small duration of time due to the lag in the system between the accelerator pedal and the throttle body. The accelerator pedal is released to original position immediately after the tip in.
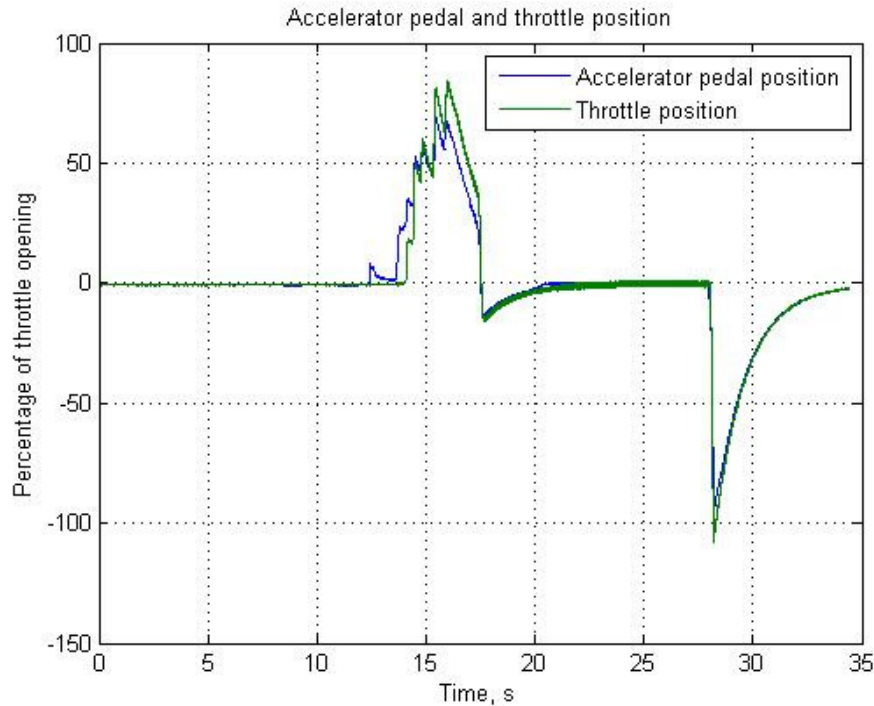
Fig. 3.7 Accelerator pedal position and throttle position.

The reading of the surface microphone in the post filter location is shown in Fig.3.8 The results show that at the post filter surface microphone location, average sound pressure level of 93.9 dB at idle condition is noted. As the accelerator pedal is pressed until 75% at 13th second, the sound pressure level increases to 94.5 to 95 dB. It is noted that increase in sound pressure lags the accelerator pedal travel due to inertia of the engine. Due to same reason, the sound pressure level reduces to original value after a delay.

A short-time Fourier transform (STFT) is performed on the readings of the surface microphone in the post filter location to identify the sound pressure level and the frequency against time. In the case of Fast Fourier Transformation the coefficients are obtained by integrating across time, hence, the information will be lost [36]. In STFT, the FFT is adapted to analyse only a small section of the signal at a time. In other words the signals are windowed at a short duration of time. Hence, STFT is a correct procedure in an experiment having various experimental outputs throughout the time. Also, it would be helpful to correlate the frequency and the sound pressure level against the time as it occurs.
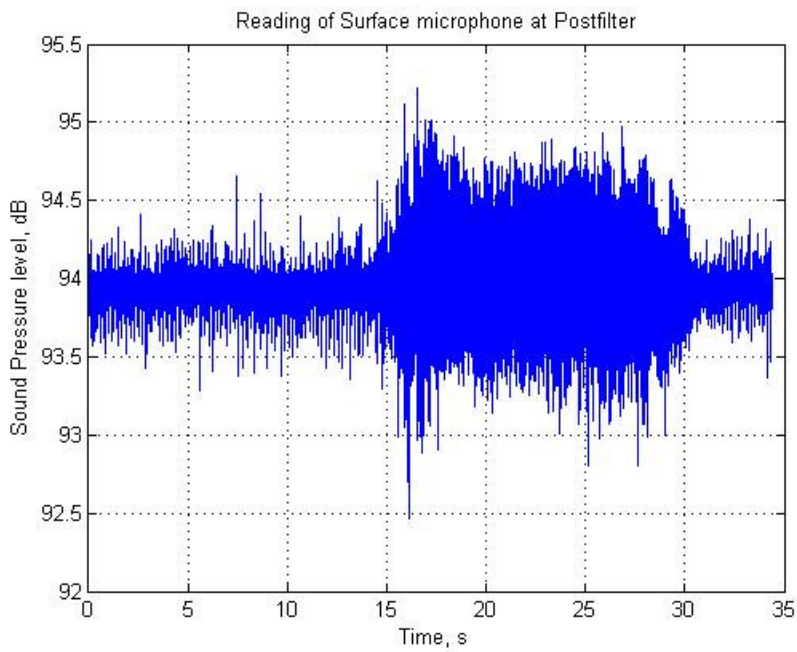
Fig. 3.8 Readings of surface microphone at post filter position.
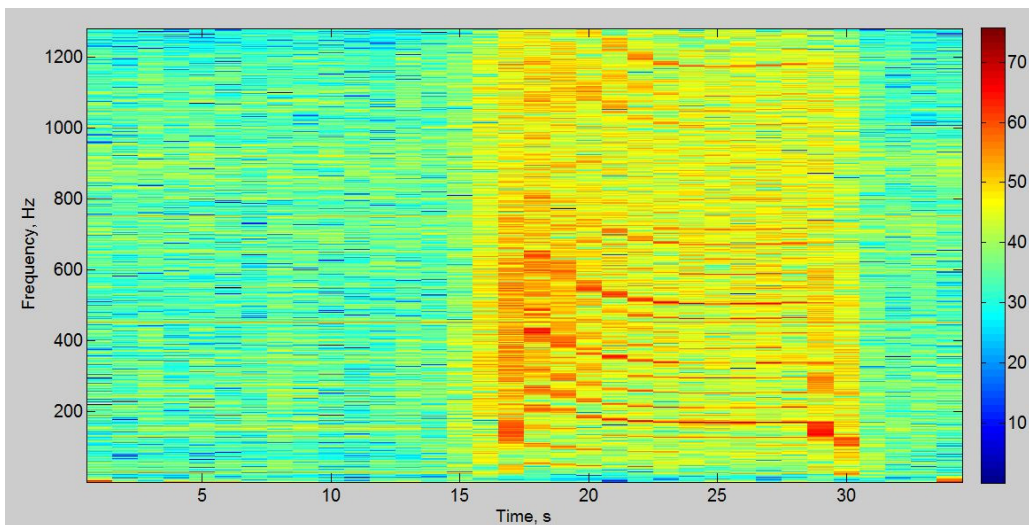
Fig. 3.9 Short time Fourier Transform of surface microphone readings showing sound pressure level in dB.

The above figure shows that there is an increased energy content from 16th second and last just beyond the 30th second. Also the energy content of the sound is more in the frequency range of 150 Hz to 620 Hz.

With the above experiments the sound pressure level of the vehicle is captured for further analysis by correlating with the accelerator pedal position. The engine operating condition is closely associated with that of the sound pressure level output. The above measured readings are useful to compare with that of the turbocharged vehicle and also to arrive at the mechanism of noise generation by correlating with the throttle position, i.e. engine load and speed condition. The above results can also can used to calibrate the 1D thermodynamic model of the engine and hence to simulate the unsteady operating conditions.

The usefulness of surface microphones in the measurement of sound pressure level is understood in the above experiments. From the STFT analysis of the surface microphone readings, (Fig. 3.9), it was observed that much of the energy exists in the lower frequency and doesn't give a characteristic of surge, whoosh or chirpy noise.

CHAPTER 4
SIMULATION TO PREDICT INTAKE SYSTEM NOISE

4.1 Introduction
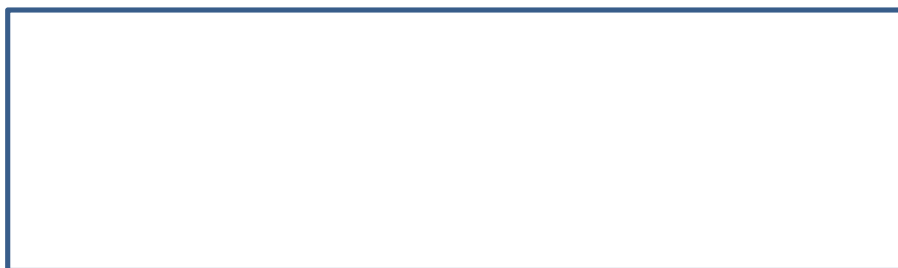
One dimensional engine simulation software known as GT-POWER was used to perform the engine simulation and to predict the intake system noise. Transient analysis such as tip-in and tip-out manoeuvre was performed to simulate the pressure fluctuations in the intake system and the subsequent analysis to compute the sound pressure level. The aim of the chapter is to understand the change in pressure amplitudes in the intake system during tip-in and tip-out manoeuvres and changes in CRV operation, using a turbocharged petrol engine's model.

4.2 Overview of GT Power simulation

GT SUITE is a one-dimensional software used to simulate various aspects of vehicle and engine [37]. One of the solvers in the simulation programme is the solution using one – dimensional fluid dynamics, representing the flow and heat transfer in the piping and other flow components of an engine system.

Flow model:

Navier-Stokes equation is solved in the flow model. It involves the conservation of continuity, momentum and energy equations and applies to laminar and turbulent flow as given by [38]

-4.1

-4.2

Where a_x - acceleration component along the x axis

a_y - acceleration component along the y axis

c_x - velocity, horizontal

c_z - velocity, vertical

 t - time

ρ - density

p - Pressure

g - acceleration due to gravity

These equations are solved in one dimension, which means that the quantities are averaged across the flow direction.

"Staggered grid" type of discretization is used in the GT Power simulation, Fig 4.1. Each pipe in the system is divided into one or two volumes and each flow split is represented as a volume. As a result, the whole system is divided into many volumes. The vector variables such as mass flux, velocity are calculated for each boundary and the scalar variables such as pressure, temperature are assumed to be uniform in each volume.
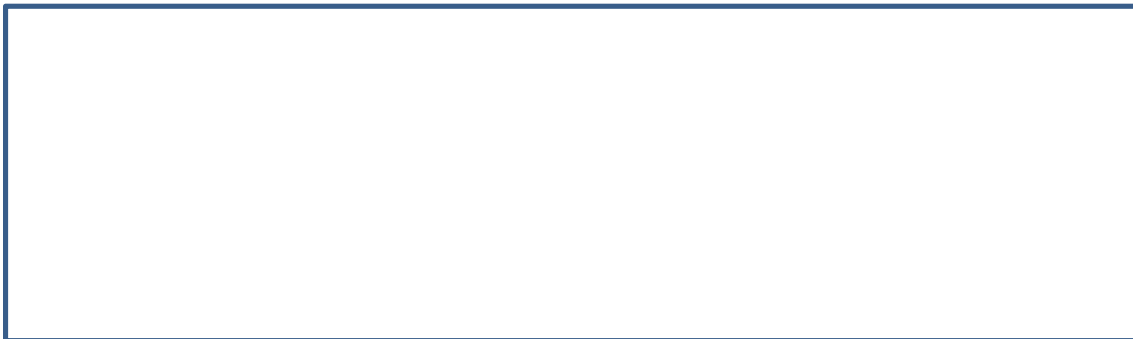
Fig. 4.1 Staggered grid approach used in the one – dimensional simulation [37]

Solution of conservation equation:

-4.3 [37]
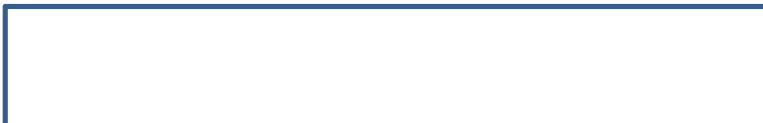
-4.4 [37]

-4.5 [37]

- 4.6 [37]
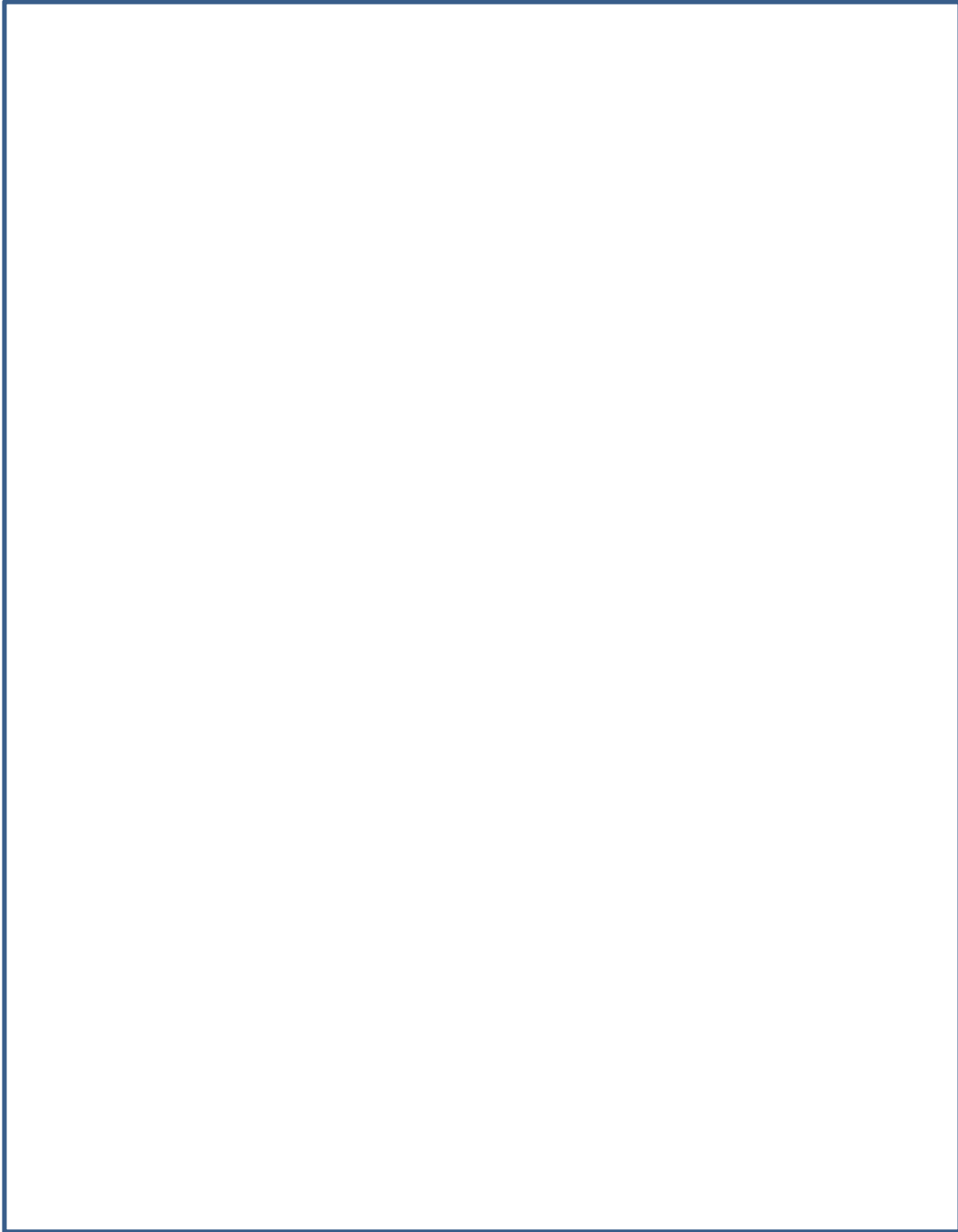
Two types of time integration methods are used in the solver: explicit method having variables mass flow, density and internal energy and implicit method having variables mass flow, pressure and total enthalpy. In the explicit method the values at the right hand side are calculated using the values from the previous time step. This method is highly suitable for the prediction of pressure pulsations in the intake systems and hence appropriate for this project. The disadvantage is that shorter time step required for this process will cause longer simulation time.

At each time step the pressure and temperature are calculated in the following way [37]. Mass and energy is calculated using the continuity and energy equation. Having known the mass and with the given volume, density can be calculated. Equation of state is used to define density and energy of each species as a function of pressure and temperature. Iteration is done on pressure and temperature until they satisfy the density and energy calculated in the time step.

To ensure numerical stability, the time step must be restricted to satisfy the Courant condition. Courant number determines the relation between the time step and the discretization length and the equation defining the condition is given as follows.
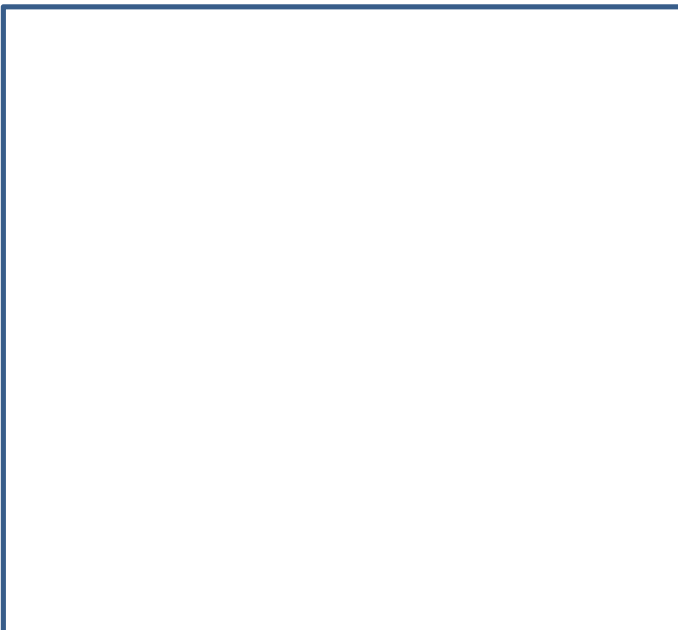
- 4.7 [37]

4.3 Discretization

Discretization is a method to split a complex system or parts into small entities to improve the accuracy of the model. This is achieved by two steps i.e. a) to divide the complex system into several components such as pipes or flow splits and b) to discretize a pipe part into multiple sub volume each undergoing several calculations. A pipe when it is divided into several smaller pipes, i.e. discretized into several smaller components and joined together will provide the same results as that on a single longer pipe. [37]

Careful choice of the discretization length is important for both the accuracy of the results and for the time taken to complete the simulation. Coarse discretization would result in less time to compute, but may sacrifice accuracy. Finer discretization would provide more accuracy; however increase the time to complete the simulation. Ideal solution is to carefully choose the discretisation length to provide best accuracy with good computational time. Generally, a discretization length of approximately 0.4 times the cylinder bore diameter is recommended for the intake system and 0.55 times the bore is recommended for the exhaust system. Different factors are used as the speed of sound varies under different temperatures. For acoustical analysis and hence for this project a discretization length of about half of the value stated above, for general performance analysis is recommended.

4.4 Integration of turbine and compressor model in GT POWER

Turbine and compressor characteristic maps are used as input to the model. The pressure ratio and the speed of the compressor and turbine are predicted by the simulation. The mass flow rate and the efficiency are looked up from the map provided as the input. The turbine and the compressor speed are calculated from the power produced/consumed by the turbine/compressor from the following equations.
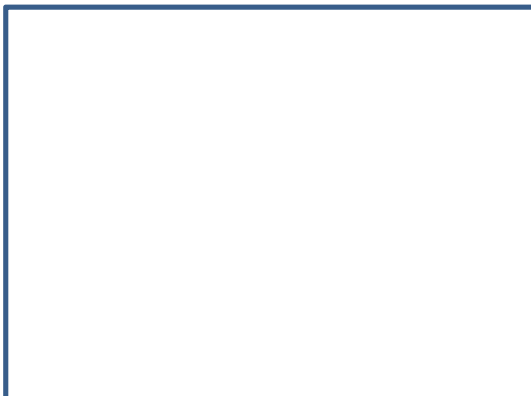
- 4.8 [37]

- 4.9 [37]

- 4.10 [37]

- 4.11 [37]

- 4.12 [37]

- 4.13 [37]

- 4.14 [37]

The turbine and compressor map data set is adjusted against the changes in the temperature and pressure and compositions using a common reference temperature and pressure. The equations used to perform the corrections are given below

-    4.15 [37]

-    4.16 [37]

4.5 Modelling of compressor surge

Map measured under steady condition is used in GT POWER [37] to simulate the turbocharger performance on a time step by time step basis. However, in reality there could be phenomenon as stall or surge which causes the breakdown of flow field. Two methods are used in the GT POWER to simulation the condition under surge: 1. default method and 2. reverse flow method.

1. The default method

    In this method the sudden change in the mass flow rate through the compressor is prevented by adopting two procedures, a. extrapolating the constant speed line beyond the surge line in the compressor map and b. to provide damping to the mass flow rate

    a. Extrapolation of the constant speed line in the compressor map
        This is done by extending the constant speed line beyond the turbocharger surge line by a line with a small negative slop as in the Fig 4.2. If the pressure ratio is below the surge line in one time step and in the next time step it crosses the surge line, the mass flow rate can be suddenly made to zero if the extension of line is not done. This will be a highly unrealistic situation. By adding the extension with a small negative slope this sudden change can be prevented.

    b. By providing damping to the mass flow rate change

In GT POWER the mass flow rate is damped by using the geometry of the system. This will model the inertia within the system and hence cause the change in mass flow rate more gradual and will represent an actual system.

Fig. 4.2. Representation of surge operation [37]

2. Advanced surge model with flow reversal

During the surge conditions, mass flow rate can be negative i.e. the flow can be reversed from the intake system and through the compressor. This phenomenon can be simulated by means of advanced surge model in GT POWER. Extrapolation of the compressor map constant speed lines is used to represent this feature. The extended constant speed lines represent the negative mass flow rates as shown in the Fig. 4.3.

Fig. 4.3 Advanced surge model representing negative mass flow rates [37]

4.6 Simulation of inlet noise using a 4 cylinder Spark Ignition Naturally aspirated Gasoline Direct Injection engine model

Aim: To establish a simulation methodology to predict the pressure pulsations and to derive the sound pressure level in the intake system.

Objective: To simulate the idle operation and intake orifice noise using an acoustic microphone and to interpret the pressure signals measured at the intake pipe near the throttle and to correlate with the experimental results performed on Ford Fiesta. Also to simulate the tip-in and tip-out manoeuvre using one dimensional engine simulation model.

4.6.1. Simulation setup and procedure

The configuration of the engine used for the simulation is shown in table 3. Microphone models and signal processing of the pressure waves in the intake system are done to capture the sound pressure level in the intake system.

Table: 4.1 Configuration of engine

The engine is run at full throttle at different speeds from 1000 RPM to 6000 RPM to capture the brake torque at the crankshaft (Fig. 4.4). This will be useful to compare different engines simulated in future in terms of BMEP, as the engines with higher BMEP output can potentially create higher noise.

Fig. 4.4 Simulated output of torque and BMEP of selected engine

The setup for simulation is shown in the Table 4.2. The engine speed is set as 1000 RPM and the throttle angle is set as 90°, i.e. wide open throttle.

Description	Method used	Remarks
Time control	Cycles	The time control is defined as number of cycles
Solution method for flow	Explicit	Explicit method is used as the wave dynamics are important for this project
Solution method for mechanical motion	Explict - Range Kutta	This method is 5th order accurate and are ideal for non-stiff problems
Simulation duration	40 number of cycles	

Table 4.2 Simulation set up

4.6.2. Microphone component

Exhaust tail pipe and the intake noise are calculated using the microphone component. At the exit of the exhaust system, the calculated pressure is fairly constant because of the continuous outflow. Only disturbance would be the sporadic reversal of flow [39]. The pressure trend at the intake opening cannot be used for the prediction of noise radiation. This is because the calculated pressure exhibits only small departures from the constant atmospheric pressure.

A microphone component is connected to the intake orifice just near to the atmosphere. Microphone component in the GT POWER model predicts the free field sound pressure level from orifice which is connected to the atmosphere more accurately. Hence this component is more suitable to predict the noise for intake orifice and exhaust tail pipe at a distance from the pipe. The pressure at the free-field microphone location is calculated by treating the orifice as a simple pulsating monopole. Landau and Lifshitz [40] states that for small perturbations, in the case of output represented as a monopole source with radiating spherical waves, the pressure field at some distance (several times the diameter of the tube) can be computed from the velocity of the flow. The velocity within the orifice is recorded using a sensor connection and is transformed to pressure at any free field location using the following equation [37] [40].

- 4.16

The above equation is valid for predicting the sound pressure level of components connecting to the atmosphere and hence cannot predict the sound pressure level in the interior engine such as pipes near the turbocharger and throttle. Hence another new method is evolved involving

the Fast Fourier Transform and creating a new model of surface microphone within GT Power console

4.6.2.1. Principle used in the creation of surface microphone module

A variation above and below the atmospheric pressure is known as the sound pressure and is expressed in Pa [30]. A normal ear is most sensitive to frequencies between 3000 and 6000 Hz and a young person can detect pressures as low as about $20\,\mu$ Pa and the normal atmospheric pressure is $101.3\text{x}10^3$ Pa.

The basic step involved is to determine the static pressure within the inlet duct by means of a sensor. The static pressure of a fluid flowing in a duct is that measured at the surface of the wall [2] [28]. The sensor component will output static pressure on the inside surface of the inlet duct in Pa. The dynamic component of the total pressure which is above and below the atmospheric pressure (i.e. $101.3\text{x}10^3$ Pa) is determined thereafter. The next step is to find out the root mean square (rms) value of this dynamic component. The mean value is not a useful measure as the positive part of the signal can get cancelled with that of the negative part. Hence, rms is used which involves squaring the pressure signals at each instant of time and adding and averaging over one or more periods. The rms sound pressure is the square root of this time average, represented by P_{rms}. The sound pressure level, Lp is derived from the reference pressure of $20\,\mu$ Pa (P_{ref}) using the following equation

$$Lp = 20\log_{10}\left(\frac{P_{rms}}{P_{ref}}\right) \qquad\qquad \text{- 4.17}$$

After the determination of rms values, the next step is to convert the time domain signals into frequency domain using the Fast Fourier Transform. This conversion will help to find out the dominant frequencies in the data range. The surface microphone model is summarised as follows (Fig. 4.5).
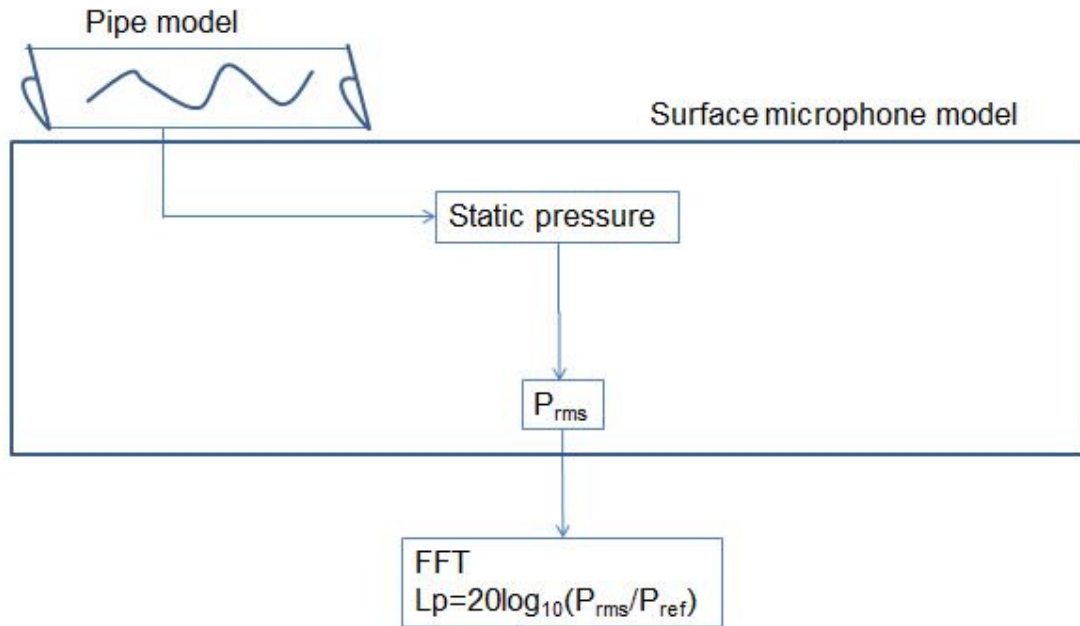
Fig.4.5 Surface microphone model

4.6.3. Simulation of idle operation

The engine is run at a constant speed of 1000 rpm. The surface microphone model used is shown in Fig.4.6. The static pressure, i.e. the pressure at the wall of the pipe just before the throttle is shown in Fig. 4.7, 4.8 and 4.9. The values show a typical intake system pressure of below and above the atmosphere and the maximum fluctuation noted is +0.008 bar above atmospheric pressure and 0.045 bar below the atmospheric pressure. The surface microphone is a flat type of microphone, flush mounted on the wall of the intake system. The diaphragm is placed at the interior of the intake duct. The surface microphone senses the fluctuations of the pressure near the wall of the intake system.

Fig.4.6 Surface microphone model in GT Power
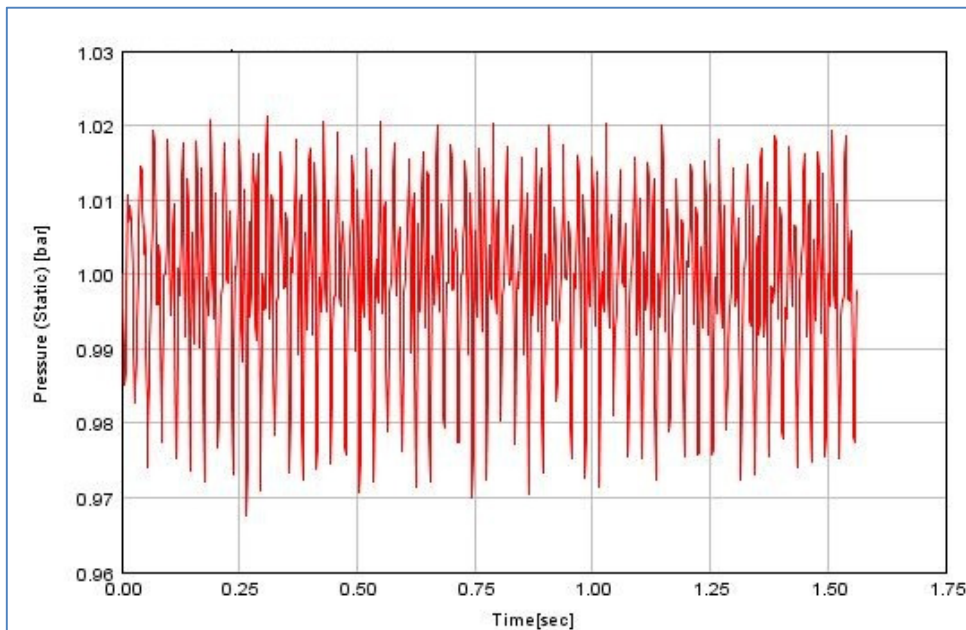
Fig. 4.7 Static pressure simulated at the pipe wall
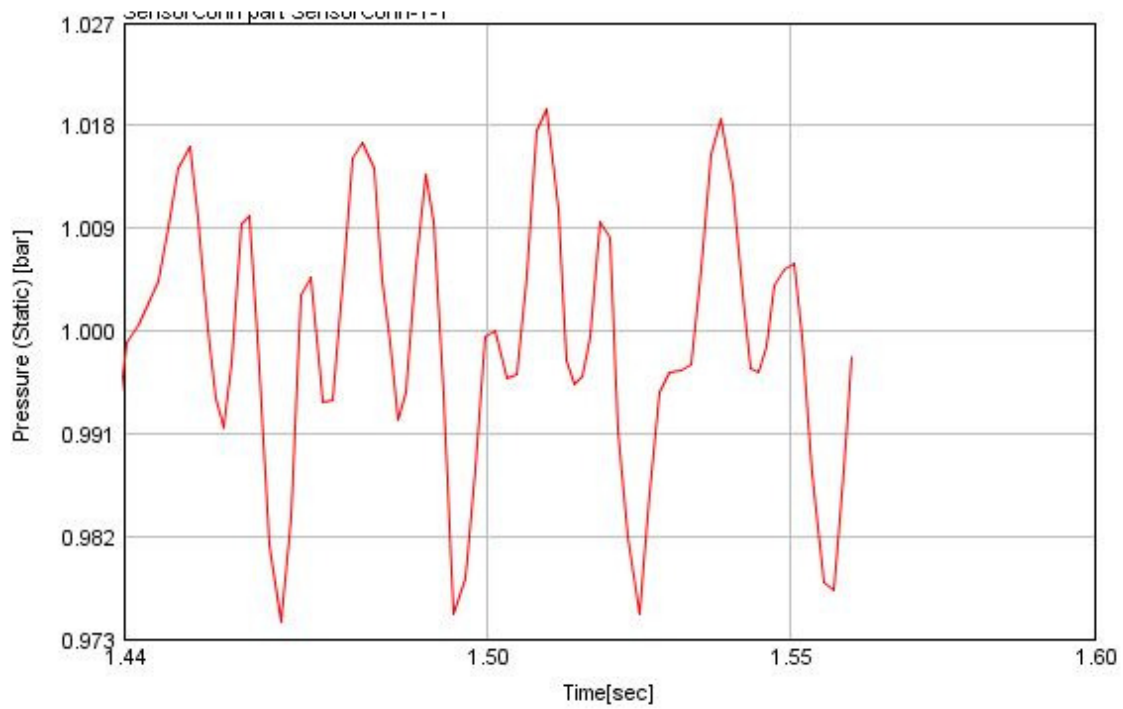
Fig. 4.8 Static pressure during the last cycle
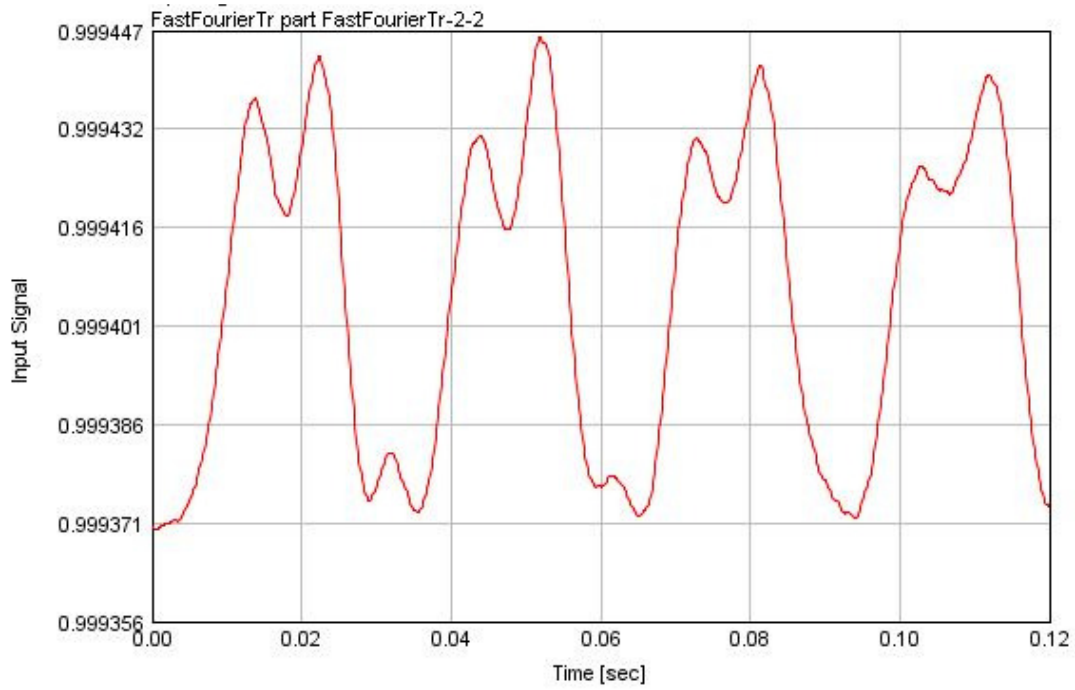
Fig. 4.9 Root mean square of static pressure during the last cycle

Fast Fourier Transform (Fig. 4.10) is performed on the dynamic component of the pressure signal sensed and sound pressure level is obtained using the equation. The reference sound pressure used is 20 μ Pa. The peaks shows clearly the engine orders of the base engine speed (1000 rpm) i.e. 33.33 Hz, 66.67 Hz, 100 Hz and so on. The maximum sound pressure level of 103.75 dB is simulated at the intake pipe wall downstream of the throttle at a corresponding base frequency of 33.33 Hz.
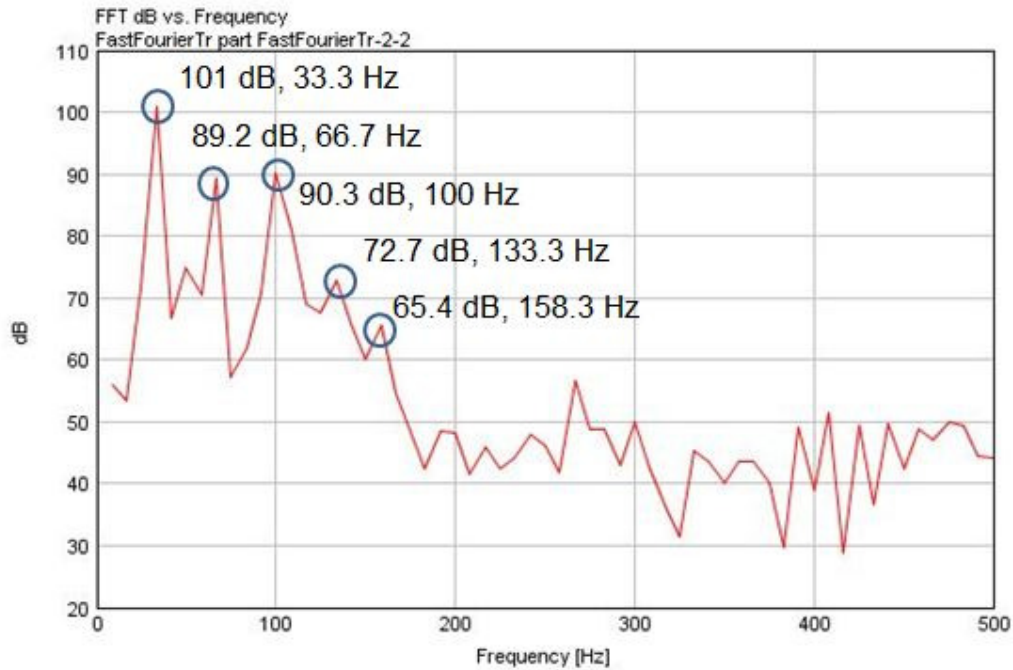
Fig. 4.10 FFT of the sound pressure level

4.6.3.1 Comparison with experimental results

The measured sound pressure level in the Ford Fiesta vehicle at intake duct, post filter position was compared with that of the simulated values. The comparison is shown in the Fig. 4.11 and shows that the simulated frequency peak values are closely matched with the experiment and the sound pressure levels follow the same pattern as that of the experiment. However it is noted that the intake system layout and the engine configuration of the car and the simulated model are different and hence the difference in the values of sound pressure level measured and simulated.
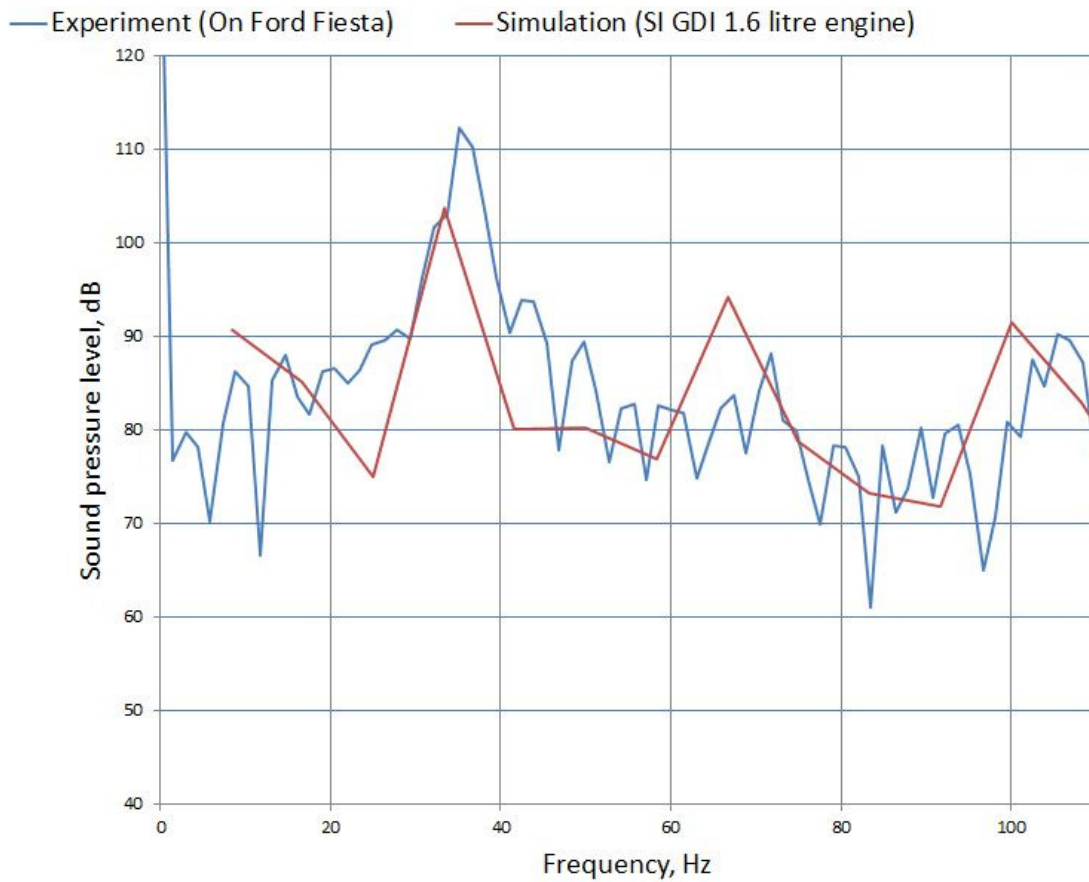
Fig. 4.11 Comparison of experimental and simulated results

4.6.4 Transient simulation

Four sets of simulation were performed

1. Turbocharged engine simulation with constant engine speed, wide open throttle, closed CRV profile and compressor surge line shifted to stable zone
2. Turbocharged engine simulation with experimentally measured engine speed, throttle, CRV profiles and compressor surge line shifted to stable zone
3. Turbocharged engine simulation with experimentally measured engine speed throttle profile, closed CRV profiles and compressor surge line shifted to stable zone
4. Turbocharged engine simulation with experimentally measured engine speed, throttle and CRV closed and with normal compressor surge line

The simulations done are summarised in the following table (Table 4.3).

Simulation No.	Engine speed	Throttle	CRV	Compressor surge line
1	Constant	WOT	closed	Shifted to stable zone
2	Experimental profile	Experimental profile	Experimental profile	Shifted to stable zone
3	Experimental profile	Experimental profile	closed	Shifted to stable zone
4	Experimental profile	Experimental profile	closed	Normal

Table 4.3 Simulation details

4.6.4.1 Simulation 1

Simulation 1 is conducted under steady conditions of throttle valve. This study is performed to form a basis for further simulations under tip-in, tip – out analysis. The pressure signals at 'before air filter' and 'after air filter' shows that the fluctuations are less compared to tip-in tip-out manoeuvres explained in other sections (Fig 4.12).
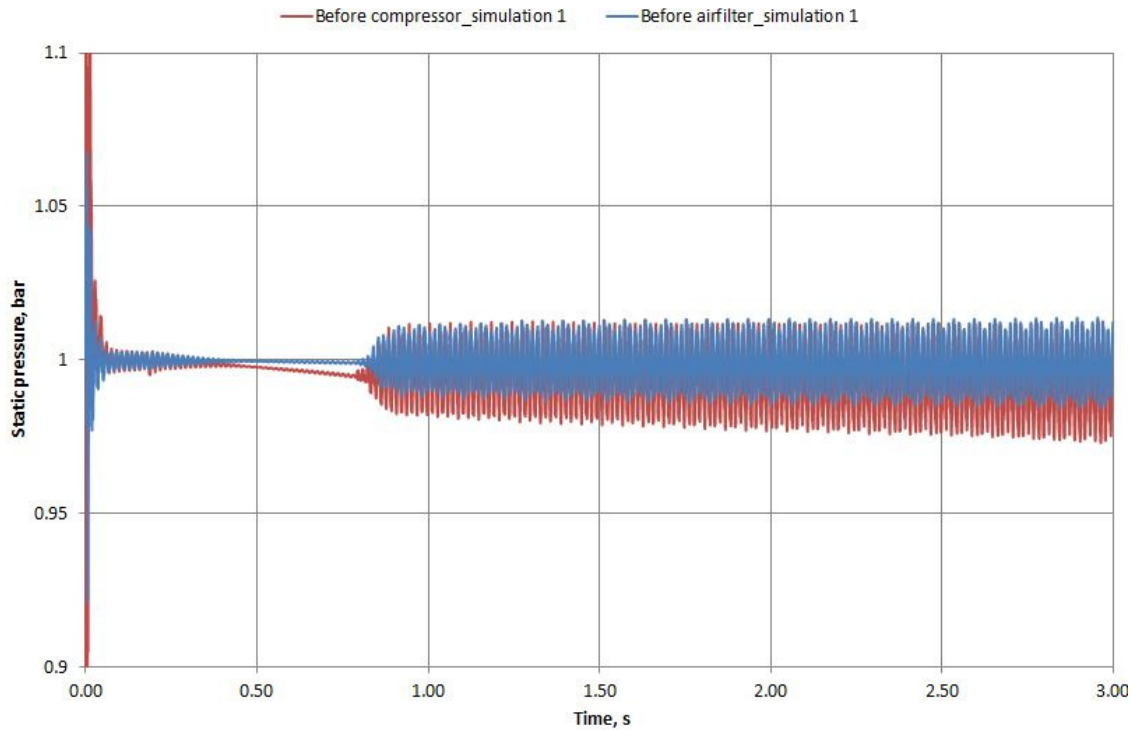
Fig. 4.12 Pressure signals – simulation 1

4.6.4.2 Simulation 2

The objective of this simulation is to theoretically predict the occurrence of noise under surge conditions. The engine speed, throttle opening and CRV opening profile are as per experimental measurements. The compressor surge line is shifted to stable zone to predict extreme operating conditions of the turbocharger. The static pressure during the simulation is presented in Fig. 4.13. Even though the compressor shaft speed curve across time is very smooth and the oscillations of the shaft in the zoomed in region of the curve shows +/-90 rpm, the pressure and the mass flow fluctuations are much higher during the throttle tip – in tip- out manoeuvre. The pressure signal rise is almost parallel to the throttle profile and also engine speed rise. At the initial region of 0 to 1 sec, the entire simulation undergoes a transient phase. After settling down, in the region of 1 to 2 secs, the amplitude of the pressure is almost a constant value. Also the mass flow rate remains as a steady value in this zone. In this area, the flow across the intake system is not disturbed. The throttle valve opening is maintained at a constant value of around 28%. The throttle is tipped in, in the zone of 2 to 4 seconds from the initial value of 28% to around 80%. In this region, the amplitude of pressure and mass flow rate increase. The throttle is kept constant at around 80% region in the 4 to 5.5 seconds. The

pressure continues to rise in this region. The throttle is brought from 80% to 28% in the area 5.5 to 8 sec. The pressure and the mass flow amplitude reduce in this area. However, the values are higher than and hence not equal to that of the 1 to 2 sec region. This is clearly due to high shaft speed and inertia of the turbocharging system.

The simulation results of pressure at different regions shows different trend (Fig 4.14). The air pressure fluctuations before air filter and before compressor locations show a similar trend. However the magnitude of fluctuations is less in the 'before air filter' location than near the compressor. This is because of damping of pressure waves as it progresses through the intake system from the compressor to the air filter. A similar trend is shown in the Fig.4.13. The pattern of pressure fluctuations are similar in the case of 'before throttle' and 'after compressor' locations. The magnitude of pressure fluctuations is similar in the constant engine operating zone, i.e. when the throttle is kept constant (1 to 2 sec). However, the pressure fluctuation magnitude deviates as the throttle is suddenly opened to around 80% and closed suddenly. The pressure fluctuation at the 'after compressor' location shows a lower value than the 'before throttle' location. This is due to restriction of flow created near the throttle as the throttle valve is shut suddenly and the oscillations damp out as it travels to the compressor. In the time zone 5.5 to 6.5 seconds, the pressure fluctuations remain lower due to opening of the CRV. Also mass flow remains lower as the throttle is suddenly closed. The system tries to settle down in the region 5.5 to 6.5 seconds by recirculation of air through the CRV as shown in the fig. 4.15 and 4.16. After this duration, once the system settles down, the pressure, mass flow rate nearly follows the throttle closure profile. Hence, the time zone 5.5 to 6.5 seconds is an interesting and critical time for this study. This region is highly influenced by the opening of the CRV valve. After the time 7.5 seconds, the CRV is suddenly closed. This once again causes a high pressure fluctuation rise. Hence, it is again a region of interest to study the influence of pressure fluctuation and mass flow rate on the noise generated in the system.

The compressor map overlapped with the operating points of mass flow and the pressure ratio is shown in the Fig. 4.18. The map indicates that the compressor works in a region very close to the shifted surge line and also at instances, it has crossed the surge line. The individual time of operating points need to be estimated in the future work.
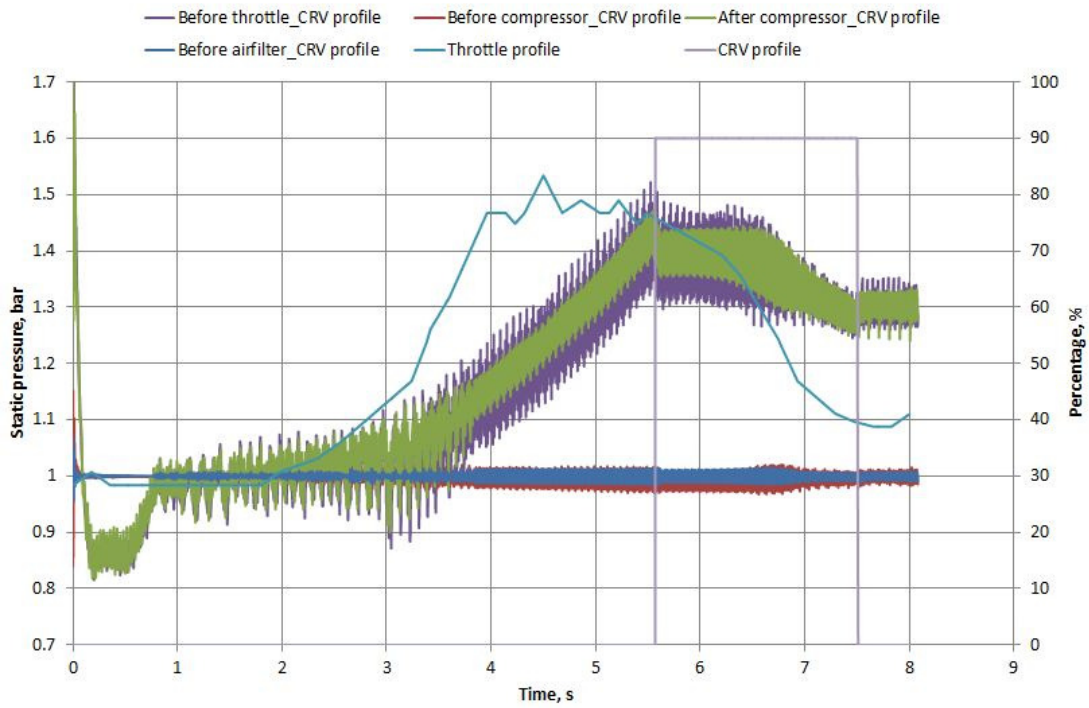
Fig. 4.13 Static pressure, throttle and CRV profiles – simulation 2
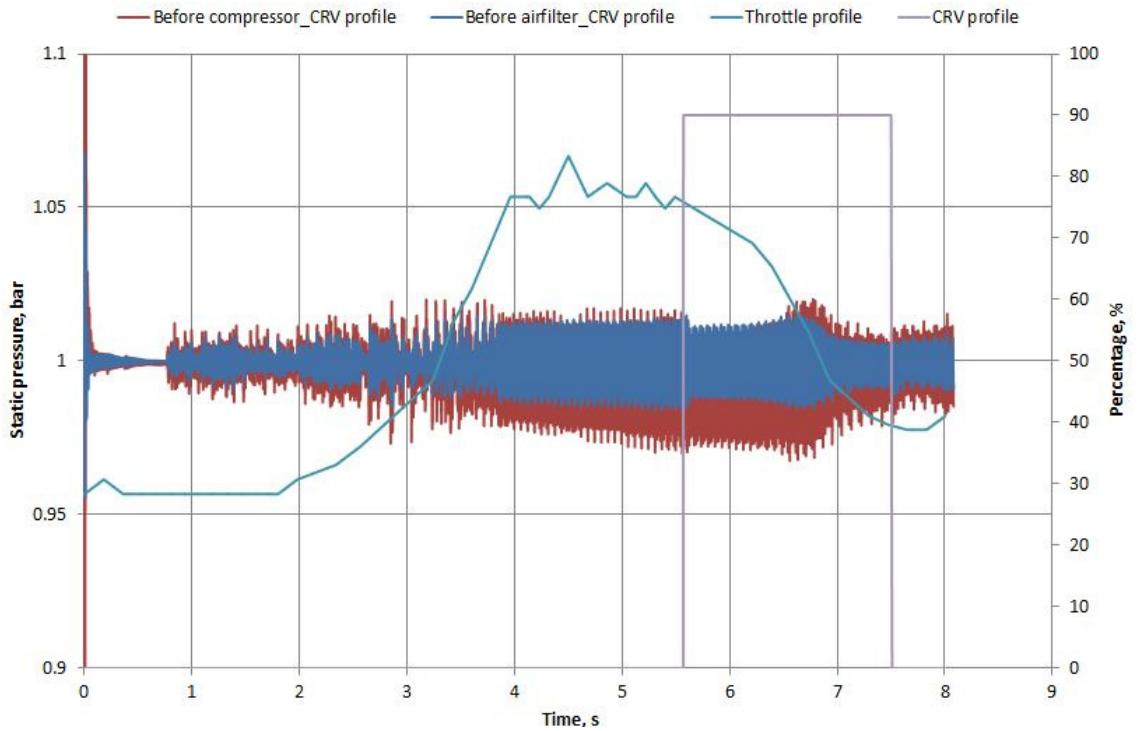
Fig. 4.14 Static pressure, throttle and CRV profiles – simulation 2
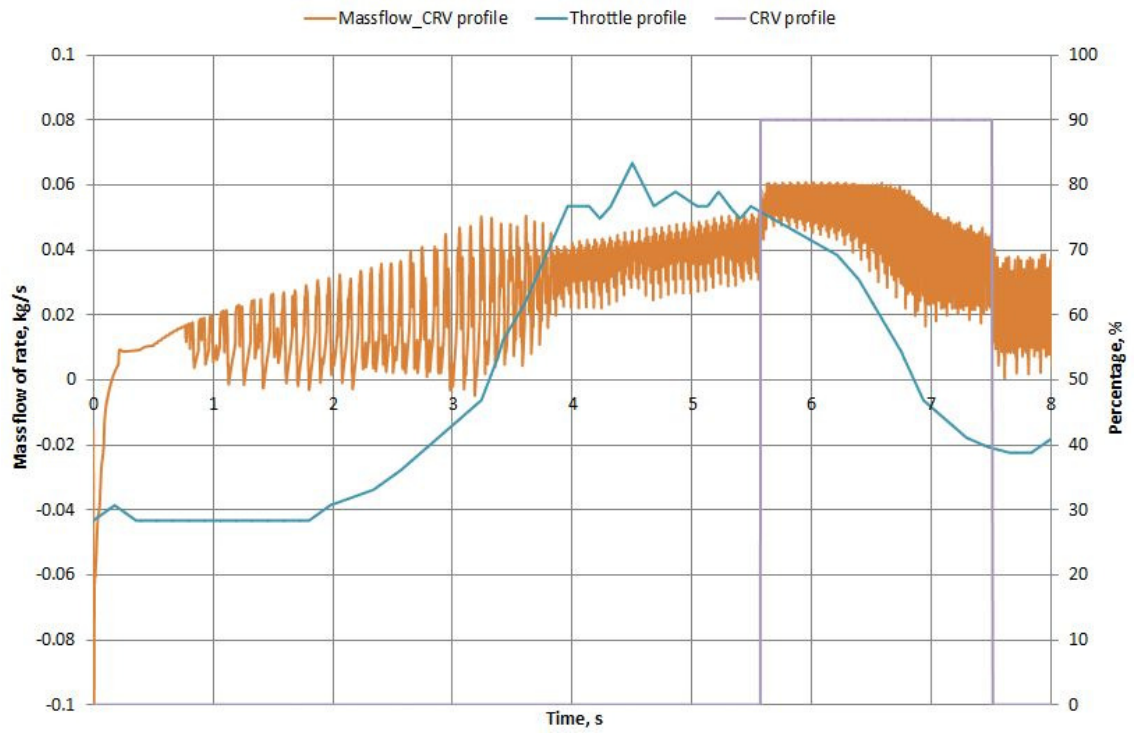
Fig. 4.15 Mass flow rate though intake system – simulation 2
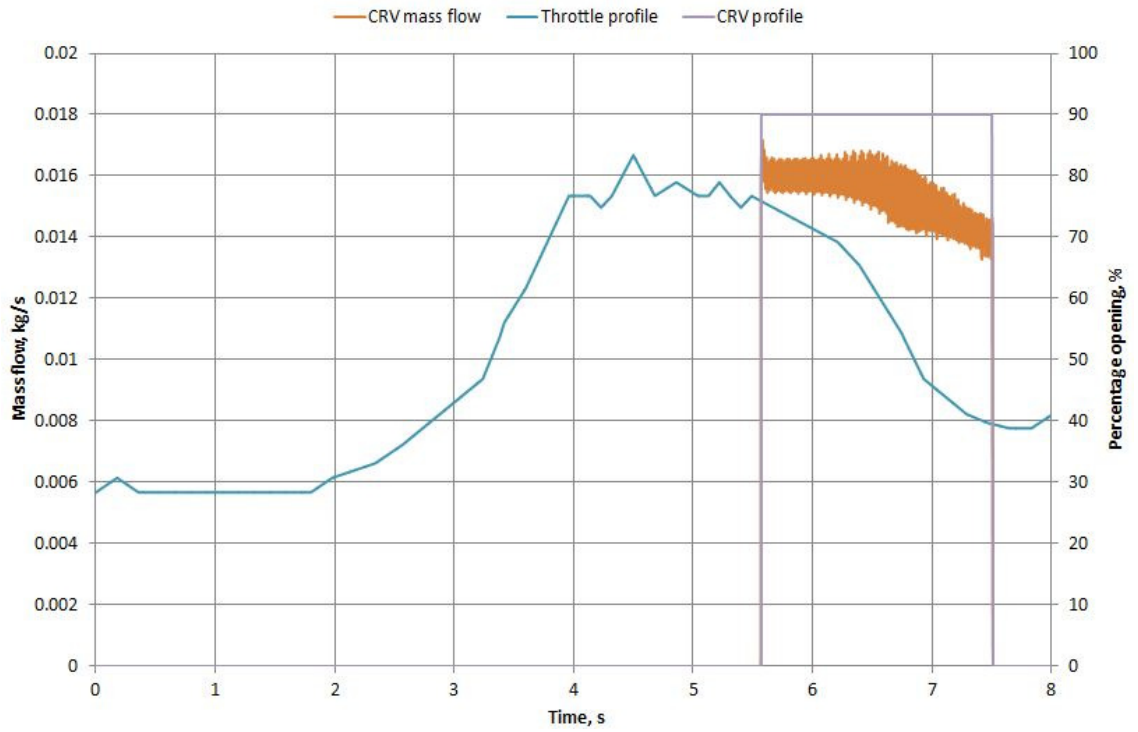
Fig. 4.16 Mass flow through the CRV
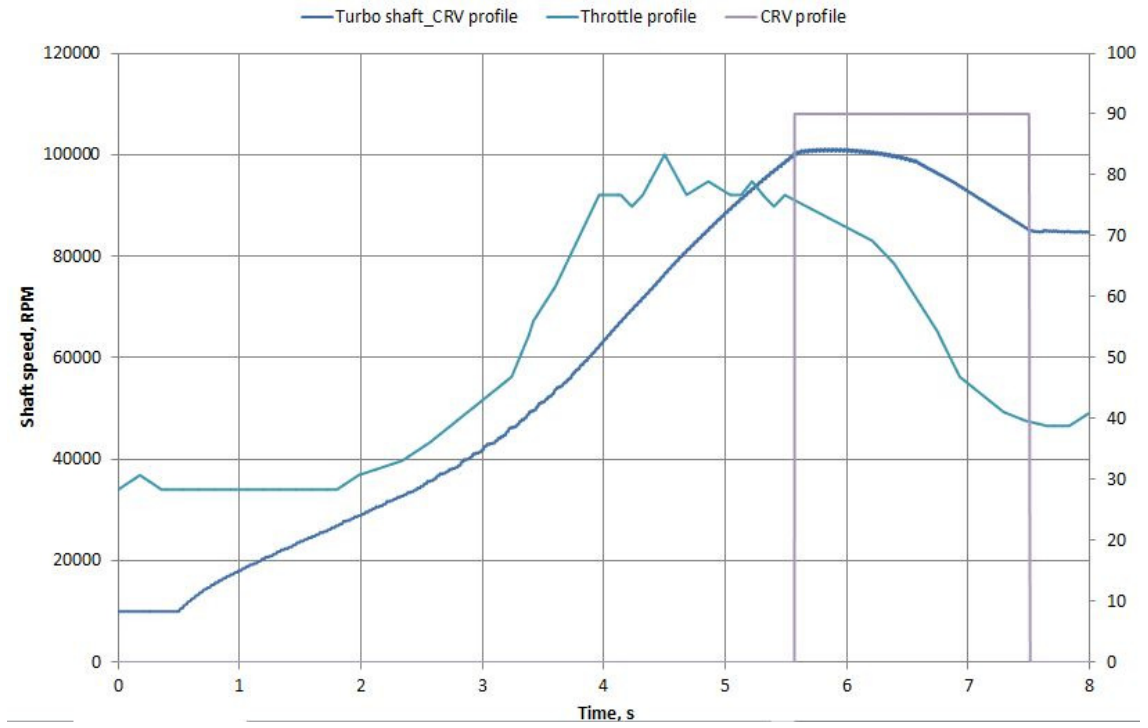
Fig. 4.17 Turbocharger shaft speed

Fig 4.18 Compressor map with operation points

4.6.4.3 Simulation 3

The objective of this simulation run is to understand the influence of CRV on the pressure oscillations and mass flow in the intake system. This simulation is same as that of simulation 2 except that CRV is kept closed. In the case of simulation 2, in the region of 5.5 to 6.5 secs., the magnitude of pressure is lower due to opening of CRV. In the simulation 3, the CRV is closed throughout and hence the pressure magnitudes have increased compared to simulation zone in all the location as shown in Fig. 4.19. This is because of existence of high pressure in the region between the compressor and the throttle. As the CRV is not open, the pressure is not released from the high pressure region between the compressor and the throttle to the low pressure compressor inlet area. In the case of simulation 3, the pressure rises to a high value and then drops as the turbocharger shaft speed drops due to throttle closure.

The mass flow rate simulated at the intake system shows higher oscillations in the values in the case of simulation 3 compared to 2 (Fig. 4.21). The turbocharger shaft speed deviates at 5.5 second in the case of simulation 3 with that of simulation 2. The shaft speed increases in simulation 3 (Fig 4.22). The compressor map shown in the Fig.4.23 indicates much high pressure operation of the system in simulation 3 than in simulation 2. Hence, from the results, it can be concluded that the CRV opening has an important effect on the pressure fluctuation and possibly noise in the system.
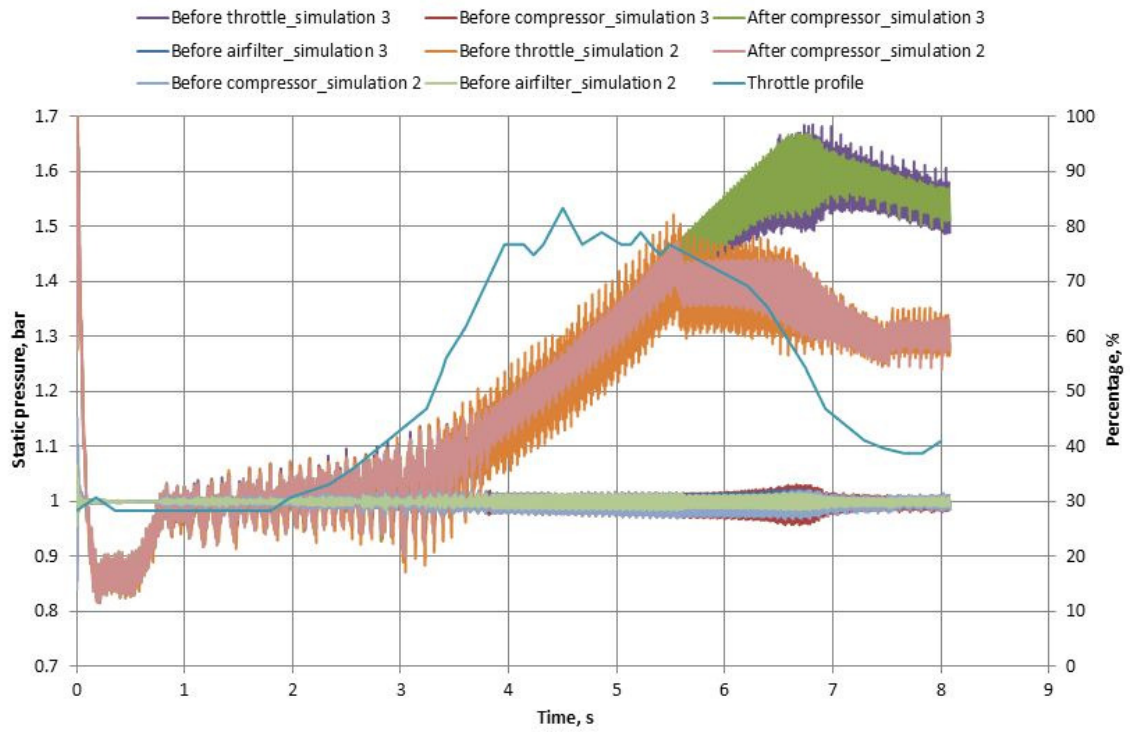
Fig. 4.19 Static pressure, throttle and CRV profiles – simulation 2 and 3 comparison
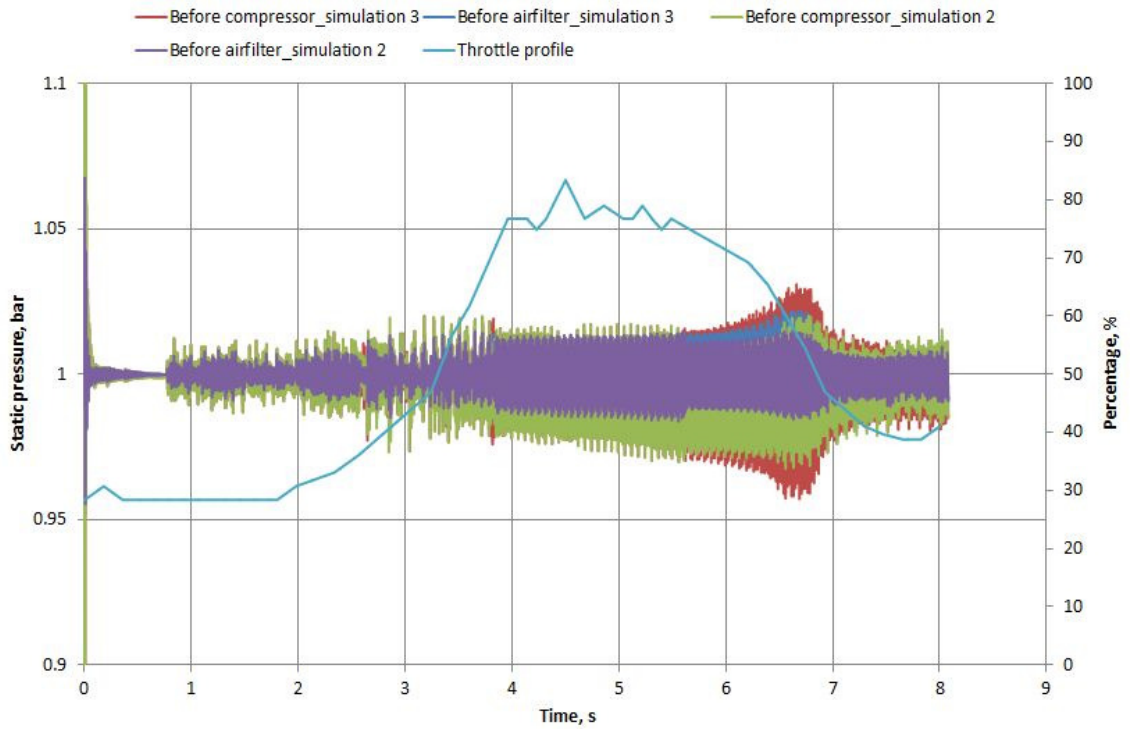
Fig. 4.20 Static pressure, throttle and CRV profiles – simulation 2 and 3 comparison
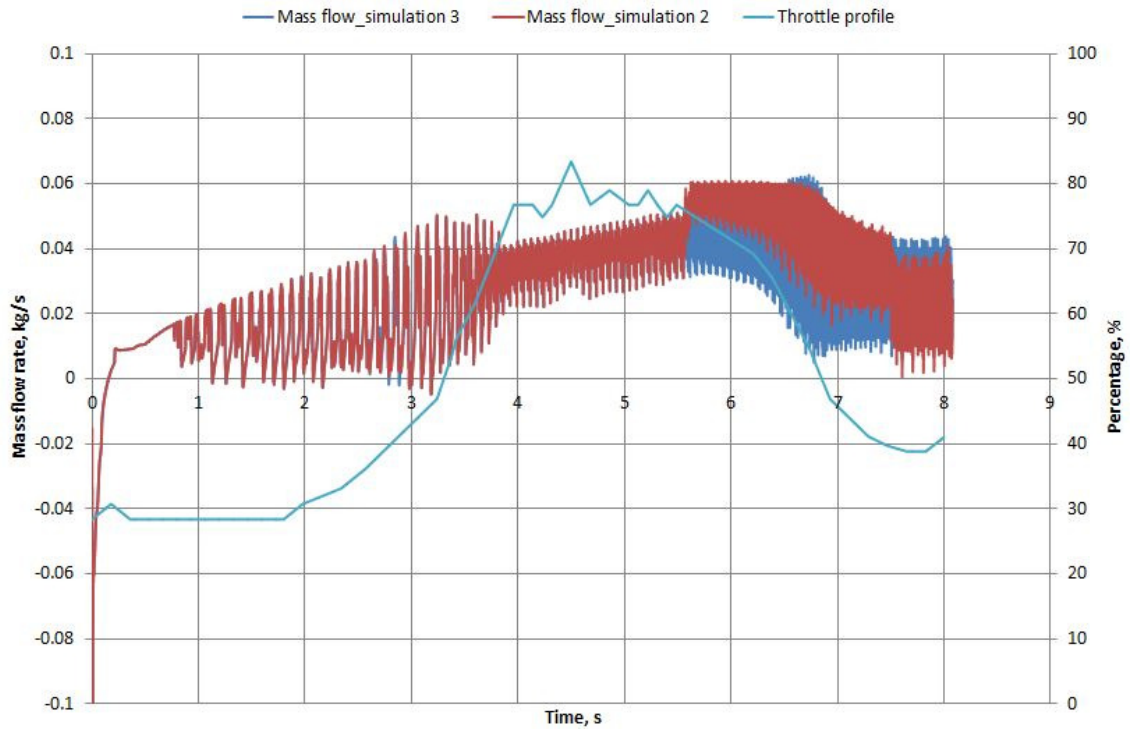
Fig. 4.21 Mass flow rate though intake system – simulation 2 and 3
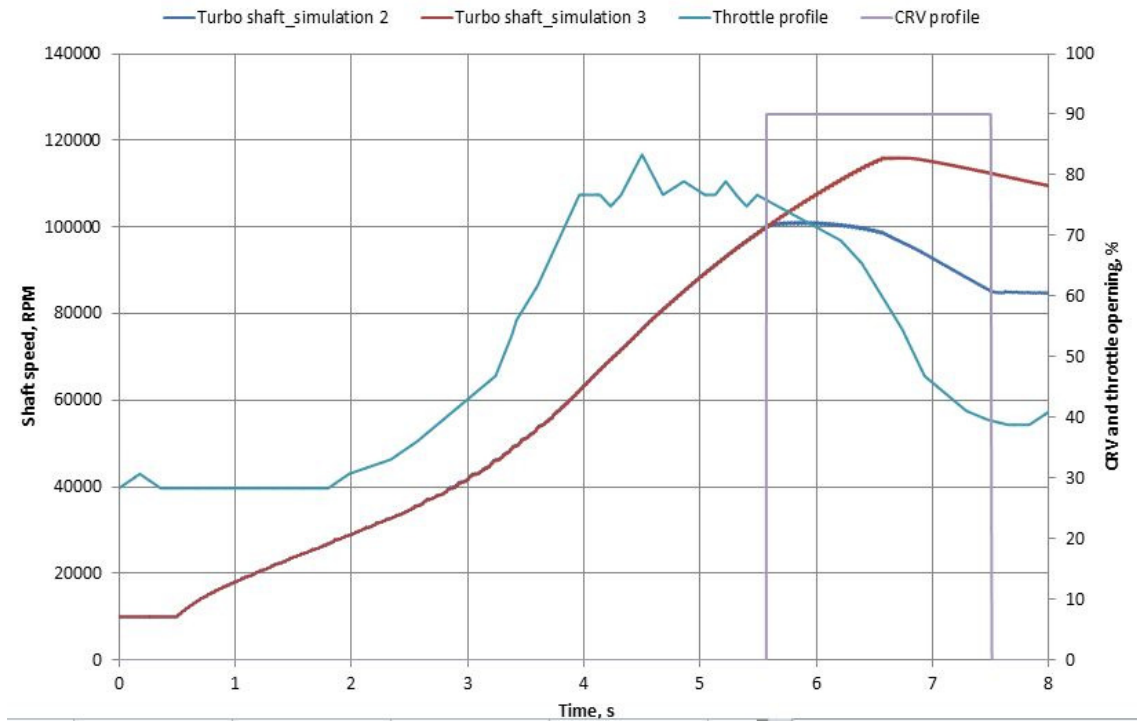
Fig. 4.22 Turbocharger shaft speed – simulation 2 and 3

Fig. 4.23 Compressor with operating points – simulation 3

4.6.4.4 Simulation 4

The objective of this simulation is to compare with simulation 3 by keeping the CRV closed and changing the compressor map to a normal one from that of a shifted one. The pressure signal simulated shows a significant reduction in magnitude in the case of simulation 4 to that of simulation 3. This shows that the shifting of the surge line to the stable zone creates more pressure magnitude and fluctuation in the intake system. This is evident even in the pressure simulated at the downstream of the intake system i.e. at 'before compressor' and 'before air filter' location. The mass flow magnitude remains fairly the same in the magnitude as it is decided by the engine suction.

Fig 4.22 and Fig 4.27 show an interesting result. In Fig.4.22, the compressor speed deviates from the CRV open value at time 5.5 sec, i.e. the time when CRV is open. However in the case of Fig 4.27 the speeds separate even at an earlier stage as the compressor map is different in both the cases and causes different situations with in the compressor.
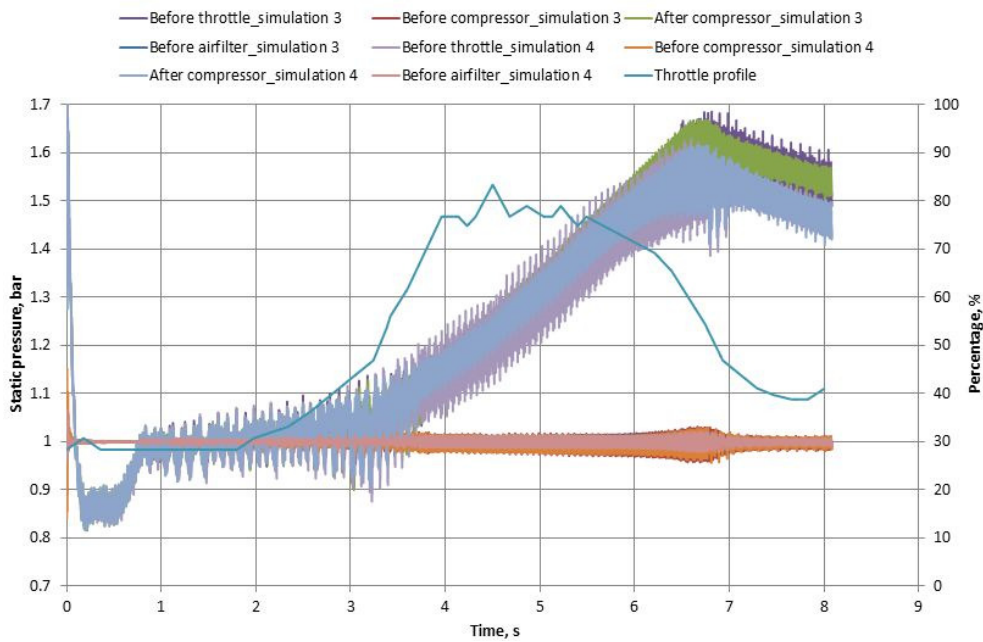
Fig. 4.24 Static pressure, throttle and CRV profiles – simulation 3 and 4 comparison
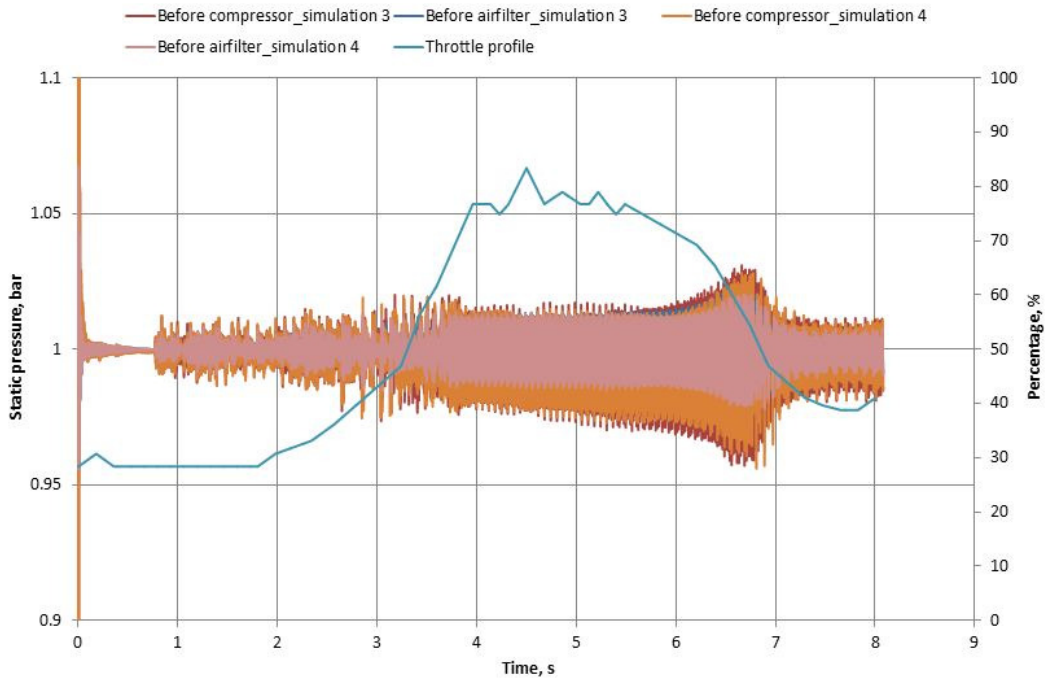
Fig. 4.25 Static pressure, throttle and CRV profiles – simulation 3 and 4 comparison
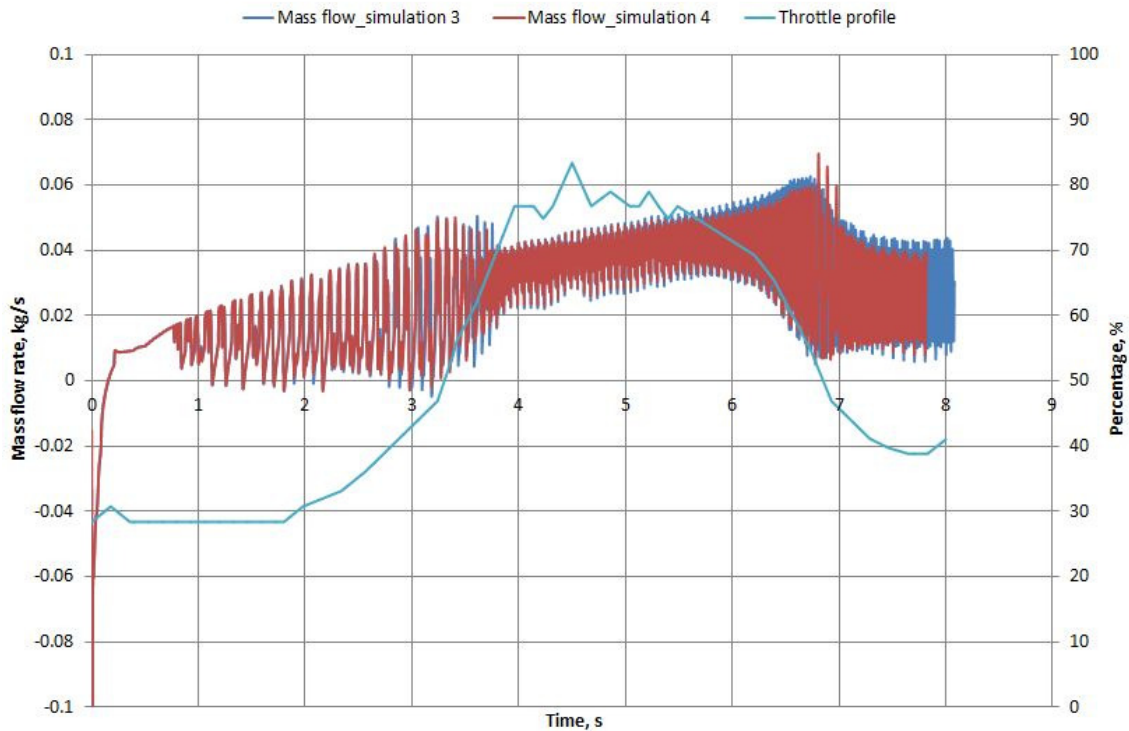
Fig. 4.26 Mass flow rate though intake system – simulation 3 and 4
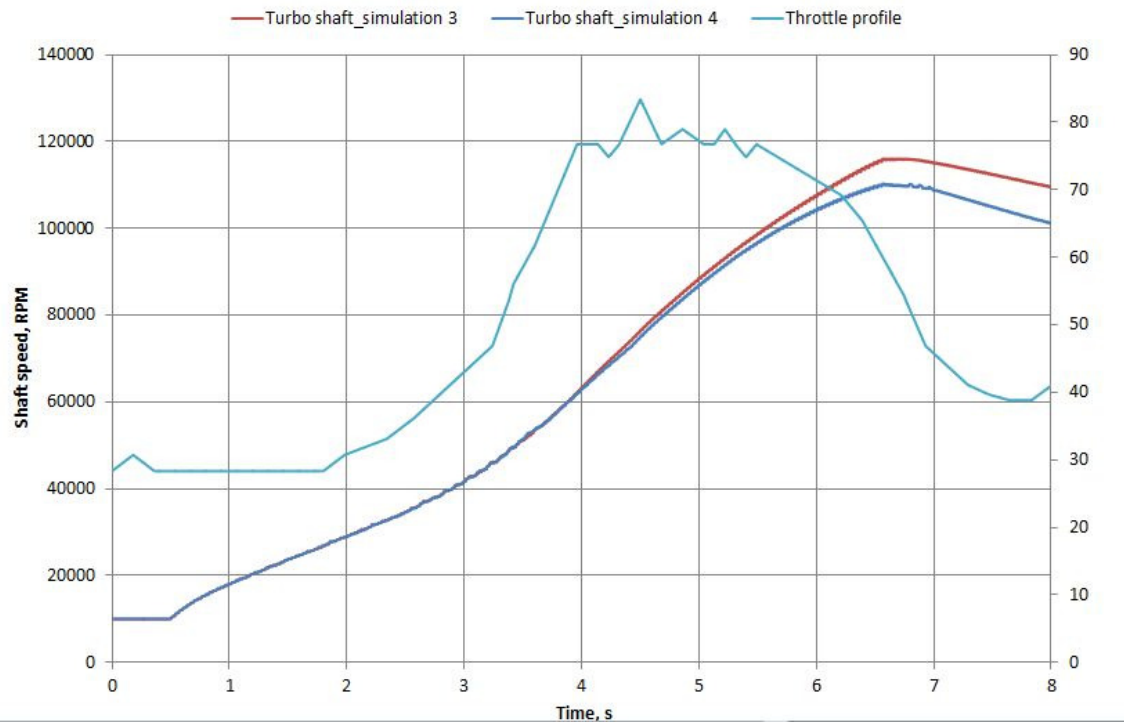
Fig. 4.27 Turbocharger shaft speed – simulation 2 and 3

Fig. 4.28 Compressor with operating points – simulation 4

4.7 Short time Fourier Transform results

Short time Fourier Transform method as described before, was used to analyse the pressure signals at the intake system. The position 'before compressor' was used to study the occurrence of noise during throttle tip-in and tip-out manoeuvre. The results of simulation 2, 3 and 4 are shown in Fig 4.29, 4.30 and 4.31 respectively. The initial transient time signal of the raw pressure data in all the cases is removed from 0 to 1 second to avoid erroneous results. Also, to present a good scaling the energy frequencies below 40 Hz removed in the STFT profile.

Comparing the results of simulation 2 and 3, in the region of 1 to 5.5 seconds (i.e. from the normal throttle opening to start of tip out), it can be seen that the energy levels are almost the same. However, after 5.5 seconds the energy levels in the case of simulation 3 (with CRV closed), are much higher than that of simulation 2. This shows the influence of CRV opening in the intake system noise. The absence of CRV has simulated high intensity sound in the intake system.

Comparing results of simulation 4 with that of 2 and 3, it is noted that the overall energy levels are lower in the case of simulation 4. However, the sound pressure level after 5.5 seconds is still higher as the CRV is closed in this model. This emphasises that the shifting of surge line along with CRV opening are important parameters influencing the sound pressure level of the intake system.

In these results, characteristic chirpy occurrence is not found. Also a short duration high intensity region is not noted in the STFT results. This is possibly due to GT-Power's limitation of predicting frequencies higher than 1500 Hz. Hence the outcome of the chapter is that the surge noise occurs at a higher frequency than 1500 Hz.
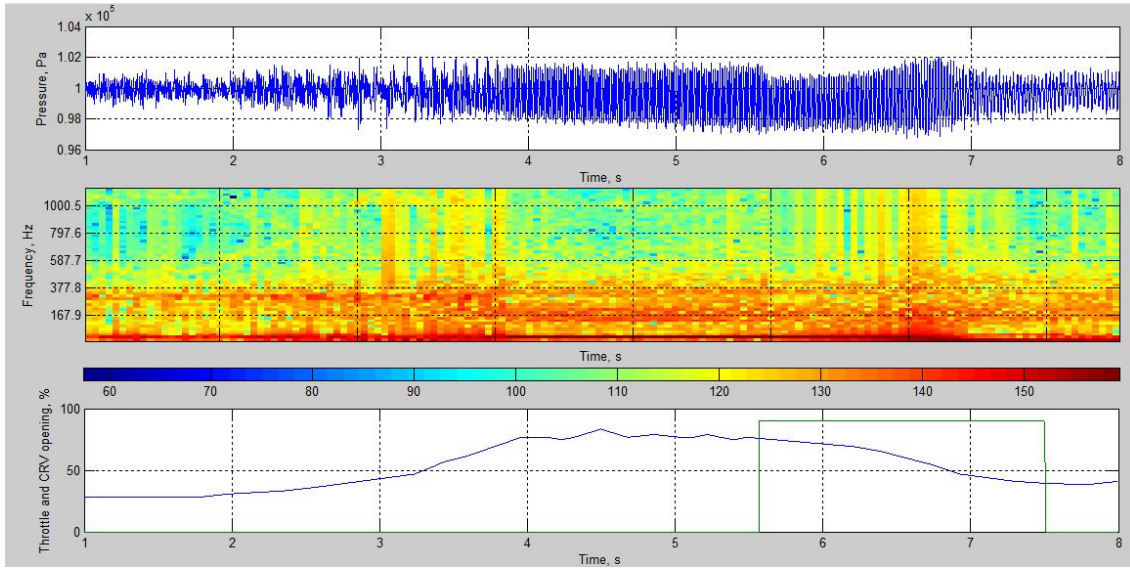
Fig. 4.29 STFT of static pressure at 'before compressor' location (colour coding shows sound pressure level in dBA) – simulation 2
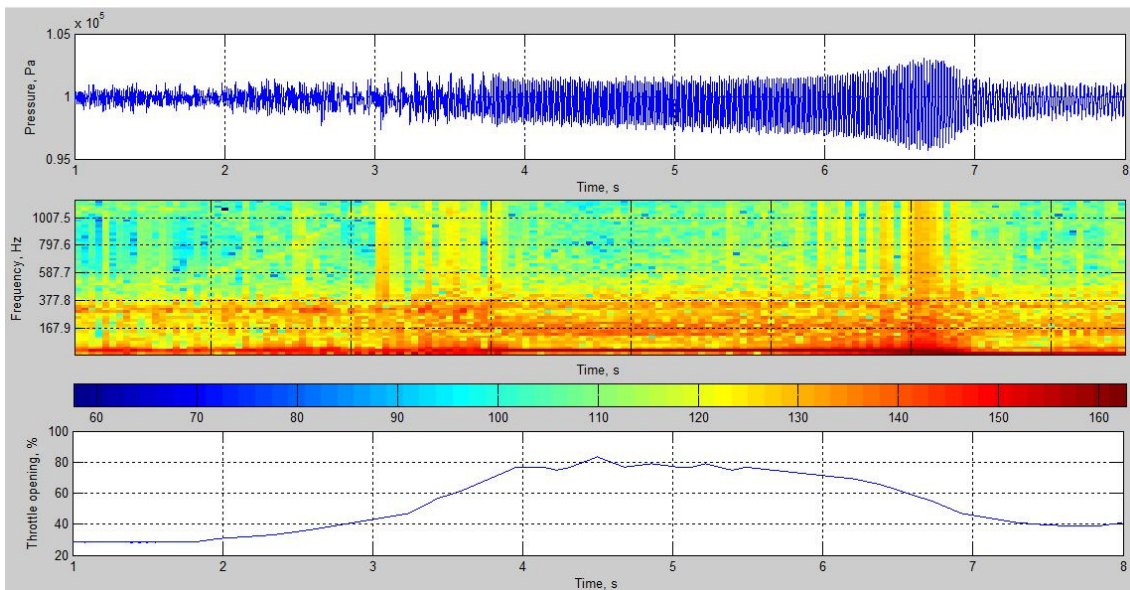
Fig. 4.30 STFT of static pressure at 'before compressor' location (colour coding shows sound pressure level in dBA) – simulation 3
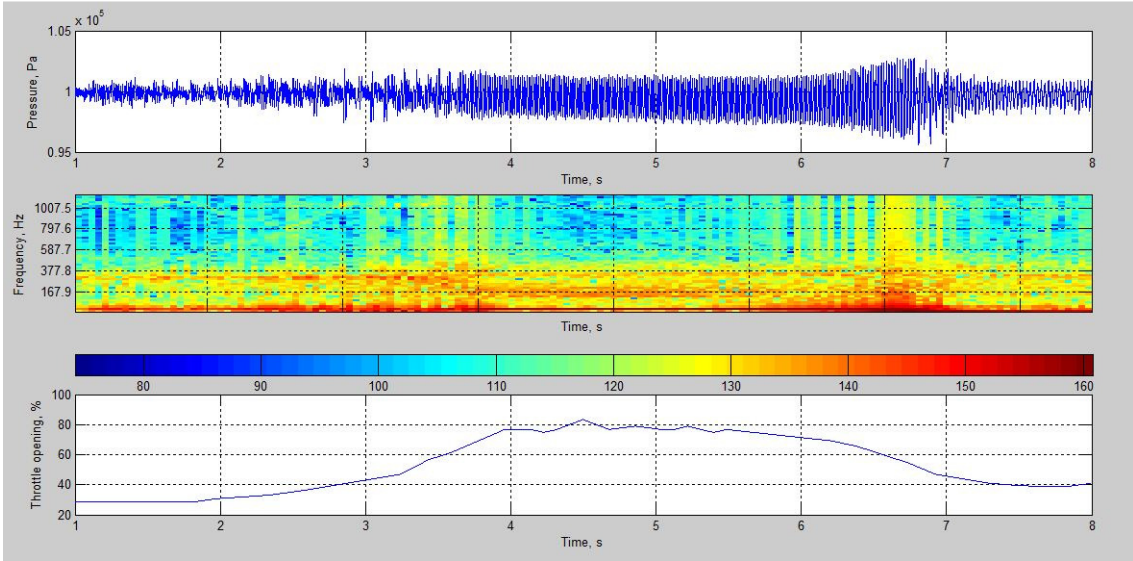
Fig. 4.31 STFT of static pressure at 'before compressor' location (colour coding shows sound pressure level in dBA) – simulation 4

CHAPTER 5
Experimental test rig design and manufacture

5.1 Introduction

In the chapter of literature review, various procedures used to identify the surge noise was discussed. Some of the examples presented mention that the surge noise was measured using experimental rig, engine dynamometer and on a fully functional car. The aim of this chapter is to discuss the methodology used to arrive at concept design of an experimental rig, to discuss the concepts and to explain the design of a selected concept to manufacture and install a functional experimental rig.

The aim of the test rig was to not only replicate the problem in the laboratory condition, but also to identify the mechanism of noise generation. The repeatability of the surge occurance under set condition of the components involved is very important. Hence the component operation was made totally independent from the operation of each other. This means the test rig intended was fully modular and individually controlled using suitable computer programs. The independent operation of the components such as throttle valve, compressor and compressor recirculation valve (CRV) helps to define the operating conditions of each component in the same manner as done on an actual automotive car. Also modularity of the components helps to interchange the components.

In an automotive engine, transient operation of the throttle which triggers the surge noise may occur at a very short interval of time (5 s). The pressure and mass flow rate vary very rapidly during this operation. The factors involved are the speed of the turbocharger, throttle valve angle of operation and the lift and timing of the compressor recirculation valve. The driver operated control which is the accelerator pedal in a car provides input to the throttle system and the variables mentioned are difficult to be controlled manually. Also the throttle valve opening may not operate linearly with the accelerator pedal position. Hence controlling the input boundary conditions is not easy with experiments on a car. The experiment cannot be performed in a controlled way and repeatability of experimental conditions cannot be ensured. The procedure can be time consuming and also subjected to human intervention and error. Also, high operating temperature could cause the usage of transducers such as surface microphone very difficult to adapt in to the air intake systems. Also, the components are difficult to be

modified due to the packaging constraints in a car. Hence the mechanism of noise generation and finding the solution is very difficult.

More controlled operation can be achieved using an engine test rig. In this method of experiment, the throttle opening position and the compressor recirculation valve opening position can be defined using a lift or angle profile against time. However the turbocharger shaft speed cannot be controlled as the operation is defined by the temperature, pressure and the mass flow across the blade of the compressors and the turbine. Hence the operating points on the compressor map cannot be controlled during the experiments. There are several frequencies of noise generated during the operation of the engine and hence the surge noise can be difficult to be identified.

Hence, it was decided to design, manufacture, install and operate an experimental test rig at the noise and vibration lab of Loughborough University. The aim was to design the experimental rig as a modular setup, i.e. to enable the parts to be replaced if required. This helps to adapt intake system of different engine models.

5.2 Experimental rig – design input

The main aim of the test rig is to simulate the pressure and flow dynamics within the intake system of an automotive engine. The operating boundary conditions in the test rig need to be made similar to that of a car during the transient manoeuvre during which the surge noise is generated. Also, the same air intake system parts as that of the car engine need to be used in the rig. The test rig design has to be of modular type. Different type of intake systems must be able to adopt into the test rig. The test rig has the following requirements:-

1. Mass flow and pressure requirements
1.1 The objective is to provide pressurised air as defined by the simulation. These are maximum values and the actual values required need to obtained from an actual or simulated turbocharged engine.
1.2 To be able to control the air flow according to the operating changes in an automotive engine. The operating boundary conditions need to be fed in as an input to the rig.
1.3 To operate the compressor in or near to the surge zone by increasing the pressure ratio across the compressor and reducing the mass flow using a controlled throttle valve at the outlet of the compressor.

1.4 To recirculate air between the compressor and the throttle back in to the compressor inlet. This is to simulate the effect of recirculation valves.

1.5 To change the throttle and compressor recirculation valve position against time according to the vehicle operating conditions.

2. Mechanical requirements

2.1 Shall accommodate the mechanical components such as intake system, sensors and actuators.

2.2 Modular construction : to be flexible to adapt various intake systems of different vehicle models.

The major parts involved in the rig are listed as follows:

Sl No	Description	Function
1	Supercharger	To provide pressurised air to the turbine
2	Motor	To provide mechanical drive to the supercharger and to vary the speed of the supercharger to match with automotive engine
3	Inverter drive	To drive the motor and control the speed
4	Heat exchanger	To maintain temperature of the supercharger oil to an acceptable value of 80 deg C

Table 5.1. Summary of components for test rig

5.3 Concepts

A fully working turbocharger test rig is very complex, time and space consuming and very expensive to build and operate. This is because a typical automotive 1.6 L engine's turbine requires an exhaust pressure at the turbine inlet to a value of around 3 bar and flow rate of 0.3 kg/s. Hence high pressure air is needed to drive the turbine at a high shaft speed of around 75000 rpm. The common methods described in literatures are by using compressed air (Aretakis et al. [28]) and by using exhaust gas from an automotive engine. The use of actual exhaust gases in the turbine avoids the need for pre heating due to its high temperature.

SAE standard (SAEJ1826) provides information on the test setup and test procedure to determine turbocharger and compressor performance characteristics. Hence, this standard can be taken as a design input for generating the concepts.

Fig. 5.1 Schematic diagram of turbocharger test stand (SAEJ1826 [41]) – loop hot gas stand – A-compressor inlet flow straightener, B-compressor stage, C-Compressor discharge flow straightner, D-Compressor flow measuring section, E-compressor throttle valve, F-Turbine throttle valve, G-Turbine flow measuring section, H-Burner, I-Turbine inlet flow straightner, J-Turbine stage, K-Discharge duct, L-Dynamometer, M-Load compressor.

A compressor inlet flow straightener (Fig. 5.1 , A) is recommended to reduce the turbulence of air entering in to the compressor. The temperature of the air in the ducts are suggested to be measured at points 1, 7, 10, 11 and 13. The pressure measurement is suggested at the points 2, 3, 6, 8, 9, 12 and 14 and the flow measurement at the point 4 to measure compressor discharge. Fuel is burnt in burner H to heat the inlet gases to the turbine. The turbocharger was required to be provided with SAE 30 lubricating oil at 350 kPa and 100 deg C. The objective of the test stand is to measure the turbine and the compressor performance characteristics. The resulting

data could be used to match the turbocharger and the engine.Two concepts of turbocharger rig design have been proposed.

5.3.1 Compressor rig which simulates turbocharger flow condition and pressure fluctuations

In this concept, a stand-alone supercharger rig is proposed which comprises of a motor and a selected supercharger. The schematic diagram is shown in the Fig.5.2. The supercharger is selected using the operating point of the engine on the published compressor map. The supercharger is proposed to be driven mechanically by a motor. The objective is to operate the motor and hence the supercharger in a way that the pressure and the flow conditions are similar to that in the automotive intake system. Hence an inverter drive to control the motor using controller and LabVIEW is required. The input to the inverter drive would be then the motor speed. This will in turn make the supercharger to operate in specified operating zones.

Locations for sensors are chosen based on the regions in the intake system where in surge occurrence can be sensed. The main parameters to be measured are the air mass flow through the supercharger, pressure ratio across the supercharger and the compressor shaft speed. This will help to exactly determine the supercharger operating point on the map. The static pressure measured on the intake duct wall and the flow along the duct are helpful to calibrate the simulation model with that of the test rig. The temperature of the air in the intake duct is helpful to do the necessary corrections in the compressor map. The temperature recording can also serve as an indicator of pressure rise. A surface microphone will be mounted on the inlet duct of the compressor to measure the static pressure fluctuation in the form of acoustic signals. Also free field microphones are to be placed in the inlet, outlet and near the supercharger to measure the sound pressure.

The mechanical components comprise of intake duct from a standard automotive engine. The main components are intake duct into the air filter, air filter and duct to the compressor inlet. The outlet duct from the supercharger is to be attached to a throttle valve. The throttle valve is a standard component from an automotive engine and is an electronic type. The throttle valve

is to be opened using an electric signal controlled by USB NI 6341 X series DAQ card. The opening and closing profile against time is variable and is fed into the system. As the throttle is closed rapidly or using a ramp, the pressure build-up between the throttle and the compressor can damage the blades. Hence a recirculation valve is proposed to bypass a portion of air back to the compressor inlet. This will reduce the pressure build-up after the compressor. The recirculation valve operating condition is an important characteristic in the surge dynamics. Hence the lift will be controlled by the NI DAQ card using a predefined profile. The design requirement is to input the coordinated profiles for the supercharger speed, throttle angle and recirculation valve lift profile against time. A cooling system which is integral to the supercharger is to be used. The lubricating oil is proposed to be circulated through a plate type heat exchanger. The objective is to maintain the lubricating oil to a stable operating temperature of 80 deg C.

Advantages: This is a less complex concept with few components involved. Fewer components enable less use of mechanical parts for installation. Also, electrical/electronic installations, control and data acquisitions requirements are lower in this concept. This makes this concept less expensive to manufacture and to operate. The advantage of this concept is that the surge noise occurs at the compressor side. H
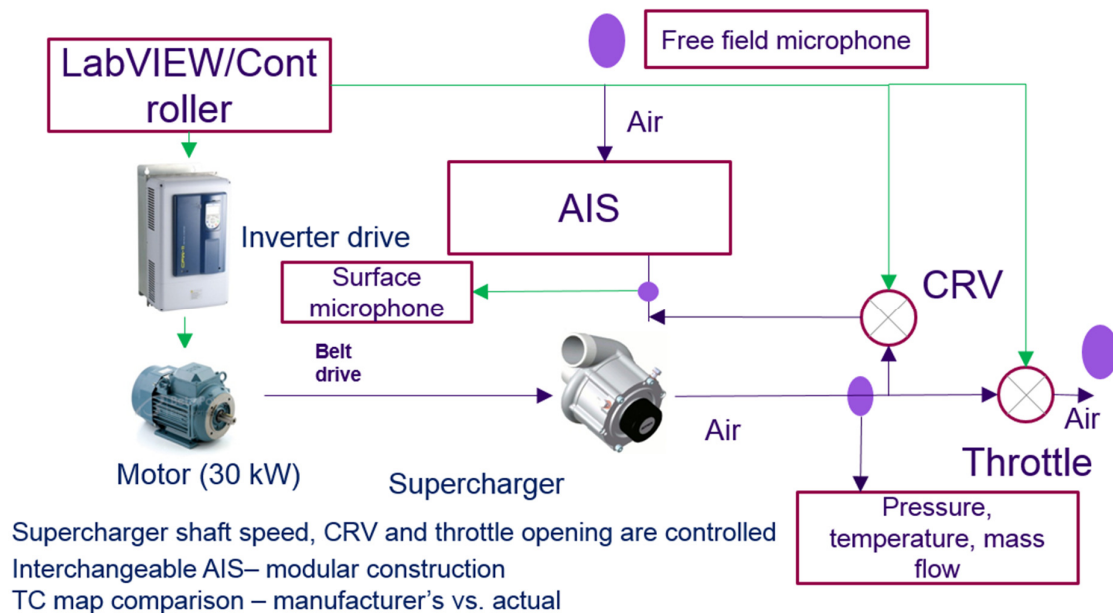
Fig. 5.2 Concept 1 Supercharger rig layout.

5.3.1.1 Feasibility study of concept 1

As the aim of the test rig is to simulate the pressure and flow dynamics under transient throttle conditions, one dimensional simulation of the system was carried out to perform transient simulation.

The supercharger rig concept is modelled in GT Power (Fig.5.3) and the results are compared against standard literature [42]. The aim of this simulation is to analyse if the proposed concept can generate surge conditions given in the literature and the output parameters such as mass flow and pressure are comparable. The supercharger shaft model is driven by a motor model at a constant speed of 40000 rpm. The supercharger shaft is connected to the motor by defining the inertia of the coupling and the shaft. The value of inertia is used to calculate the net torque on the shaft of the compressor. This value along with the moment of inertia of the system can be used to calculate the rotational acceleration. By integrating the rotational acceleration, rotational velocity can be obtained. Further, integration of the rotational velocity can result in rotational position of the shaft. The intake system with the same dimension as in the car is modelled and connected to the inlet side of the compressor. A throttle model is attached to the outlet duct models at the downstream of the compressor. Mass flow, pressure and temperature is measured at the inlet and outlet of the compressor in the simulation model. The throttle is operated from a wide open throttle position to closed throttle position, very rapidly, to cause surge in the compressor system (Fig. 5.4).
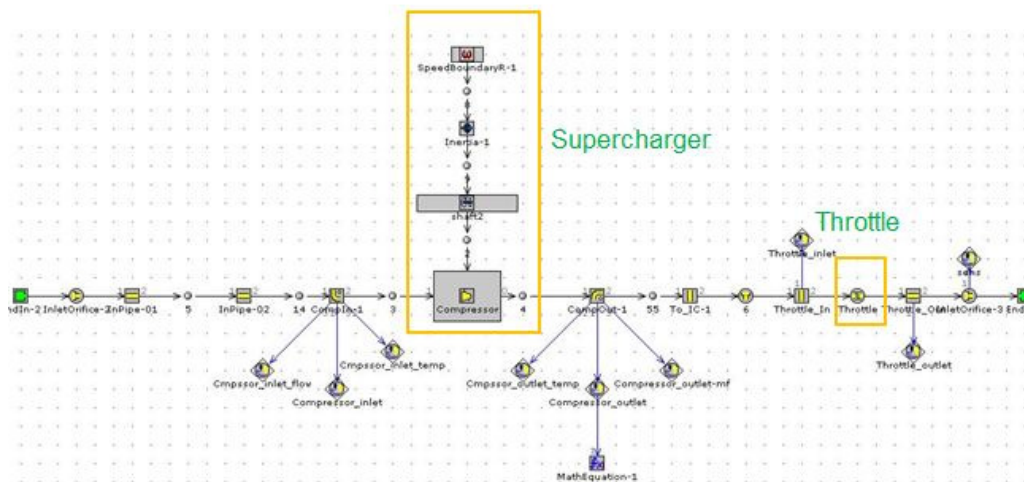
Fig.5.3 Supercharger rig model

The results of the simulation shows that the mass flow rate through the compressor reduces rapidly during sudden closure of throttle and also the pressure after the compressor rises rapidly with more fluctuations and the inlet pressure retains the mean value but the fluctuations have increased. The simulation results are comparable with that of the literature [42]results and are given in Fig 5.5 and 5.6. Hence it is concluded that the supercharger rig (concept 1) is able to simulate deep surge in the intake system.
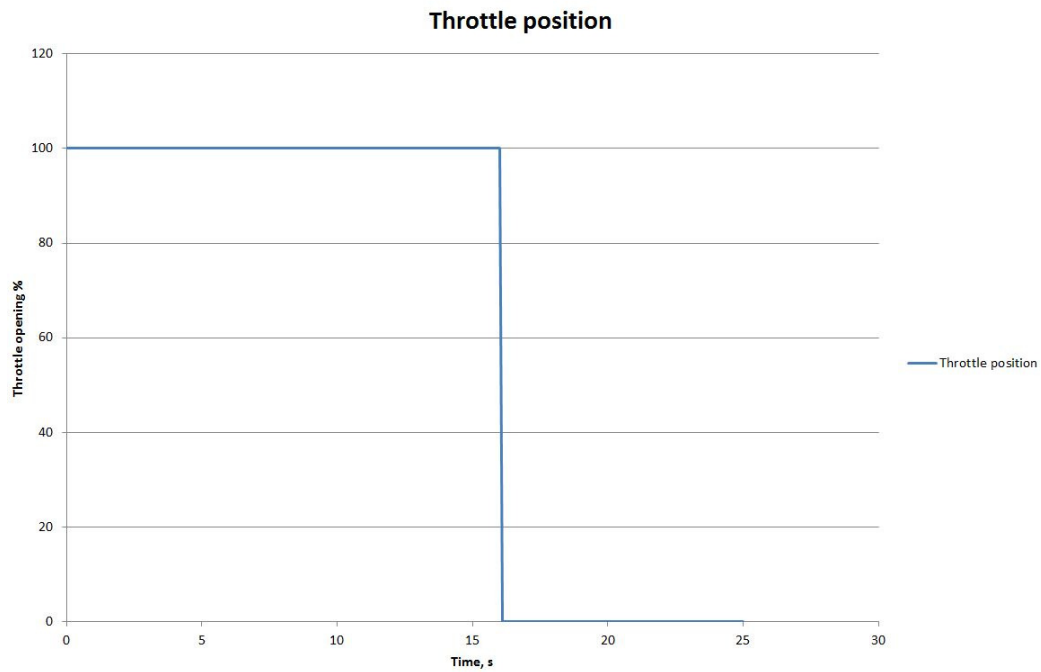
Fig. 5.4 Throttle tip in and tip out to create surge in the supercharger system
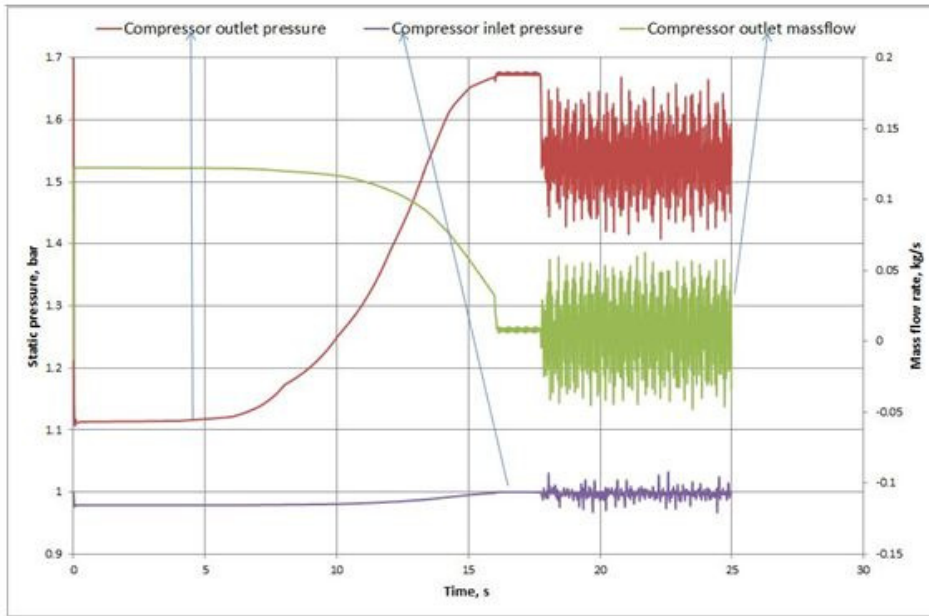
Fig. 5.5 Simulation results of the compressor rig.
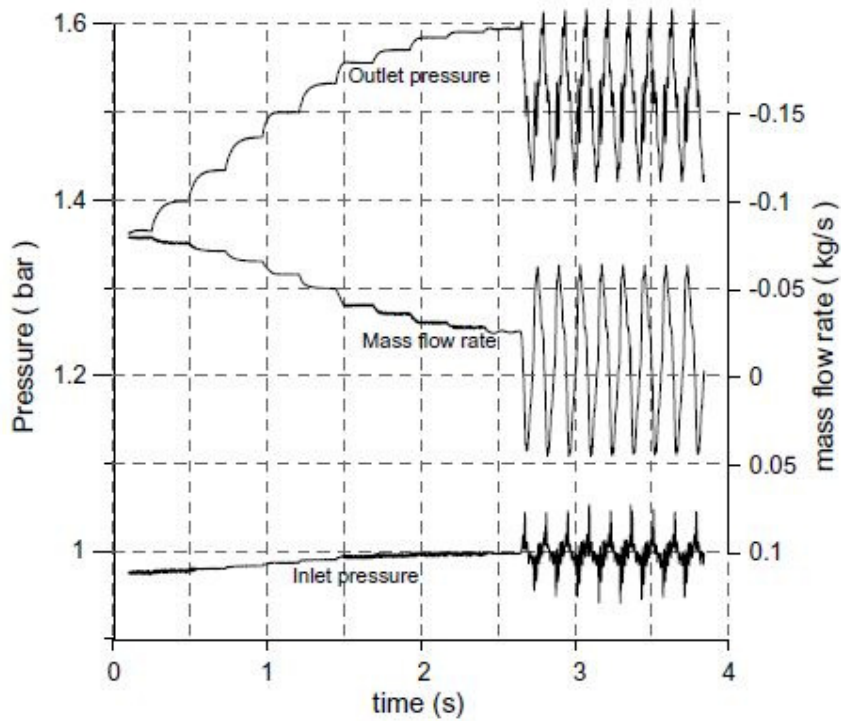
Fig. 5.6 Experimental results on a turbocharger rig [42]

5.3.2 Combined supercharger and turbocharger rig which simulates turbocharger flow condition and pressure fluctuations:

A combined supercharger and turbocharger rig is proposed as a second concept. The air outlet of the supercharger will be used to drive the turbine blades. The air from the supercharger is already compressed and having high temperature. Hence, conventional usage of fuel and a burner to heat the inlet air to the compressor can be avoided. Also, the hot air entering into the turbine cools in the process of expansion and hence can be safely vent to the atmosphere through appropriate exhaust circuits.

The design inputs for the selection of supercharger are the outlet pressure and the mass flow of the air. This must be equivalent to that of a comparable engine's exhaust pressure and mass flow. The function of the turbine in the turbocharger is to convert this pressure and mass flow into mechanical energy to rotate the turbocharger shaft and hence the compressor. The exhaust mass flow and pressure into the turbine inlet is varied as per engine operating conditions and the functioning of waste gate. The similar condition of fluctuation of mass flow of air and the pressure in to the turbine is simulated using the variable speed of supercharger and hence the speed of motor using a profile input.

The pressure, mass flow, temperature sensor and microphone locations are shown in Fig. 5.7. As in the previous concept, LabVIEW can be used to control the motor speed, throttle and CRV opening condition. In this concept, the operating point of the turbocharger is maintained using the control of mass flow, pressure and temperature of air in to the turbine. Another dedicated lubricating system is required to supply oil to the turbocharger bearings as the shaft speed can go up to 125000 rpm. Also, the temperature of the oil need to be maintained to around 80 deg C. This necessitates use of a dedicated cooling system which has an inbuilt temperature control arrangement.
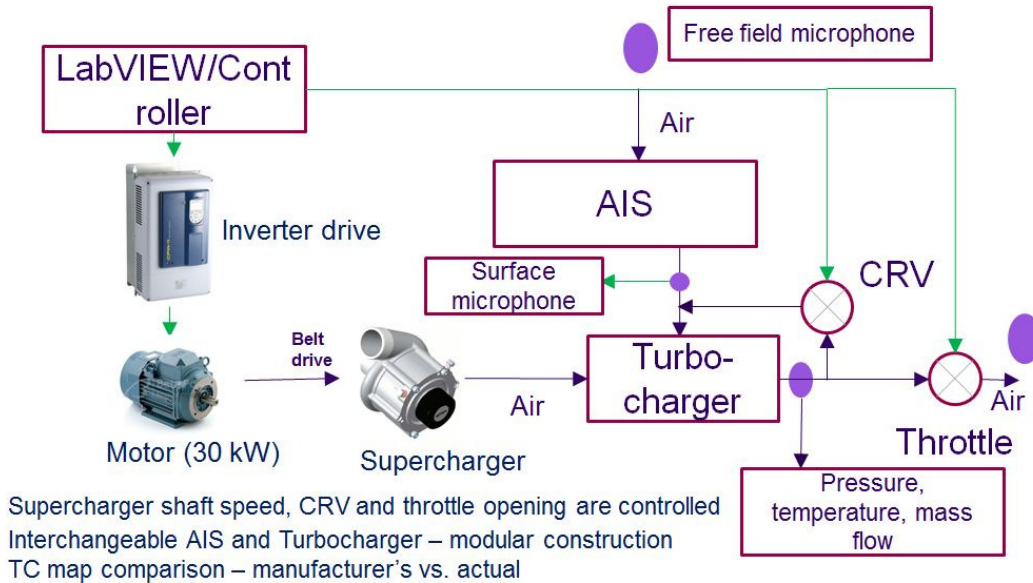
Fig. 5.7 Supercharger rig concept

5.3.2.1 Feasibility study of concept 2.

In the concept 2, the function of the supercharger is to compress ambient air at a very high pressure and provide mass flow and pressure enough to drive the turbine of an automotive turbocharger. In this way, the air outlet from the supercharger would work like the exhaust gases from the automotive engine.

A simulation model using GT Power is created to understand the functioning of rig in the design stage itself. The block diagram of the simulation model is shown in Fig.5.8. A variable speed drive is attached to the supercharger with a pre-defined speed profile. An air inlet duct is given to the supercharger inlet and outlet leads to the turbine model of a turbocharger through outlet duct system. A throttle valve is provided to control the outlet air flow of the supercharger. This is an optional device and the main control of the supercharger pressure and flow is achieved using the speed profile of the motor. The turbine is connected to the compressor using a shaft. A frictional model is provided to the shaft. The shaft drives the compressor and the map is given in Fig.5.9. The outlet of the turbine is lead to atmosphere using an outlet duct. The inlet to the compressor is a standard automotive inlet system through an air filter and inlet ducts. The outlet of the compressor is having an important part, i.e. throttle body which is electronically operated by means of a control system. A compressor recirculation valve model

is built which will open and close at a set profile to avoid pressure rise beyond a safe level in the inlet duct between the compressor and the throttle.
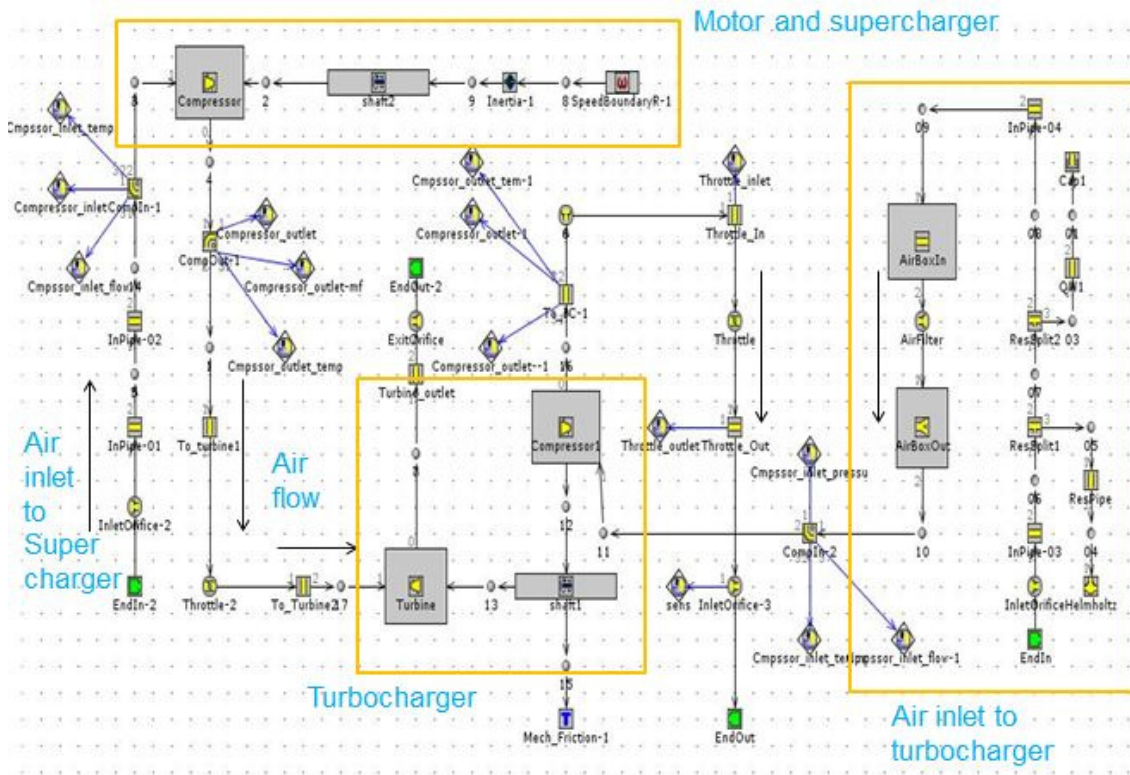
Fig. 5.8 Block diagram of the supercharger rig model

The supercharger selected for the model is of the make Rotrex C38-91 and the compressor map is provided in the Fig.5.9. The maximum mass flow capacity of the supercharger is 0.63 kg/s and the pressure ratio 2.94:1. However these figures are the maximum values and in the dynamic range, i.e. at various speeds of the supercharger and during different load and flow conditions, the pressure ratio and flow can vary. Also the automotive turbocharger has dynamic ranges represented in the maps. Hence a simulation model is required to predict the performance when the dynamic components such as supercharger, turbocharger, throttle valve and the compressor recirculation valve are used as a system. The throttle profile used is given in the Fig. 5.12 and the compressor recirculation valve is given in the Fig. 5.13. The throttle profile is selected based on the tip-in tip-out manoeuvre and the aim is to create surge in the

turbocharger. Also, the throttle valve after the supercharger creates restriction of air flow into the compressor and hence tests the supercharger at variable delivery conditions. The compressor recirculation valve is opened and closed as per standard automotive test data and can be varied against time.

Fig 5.9. compressor map [43]

Fig. 5.10 Supercharger map.
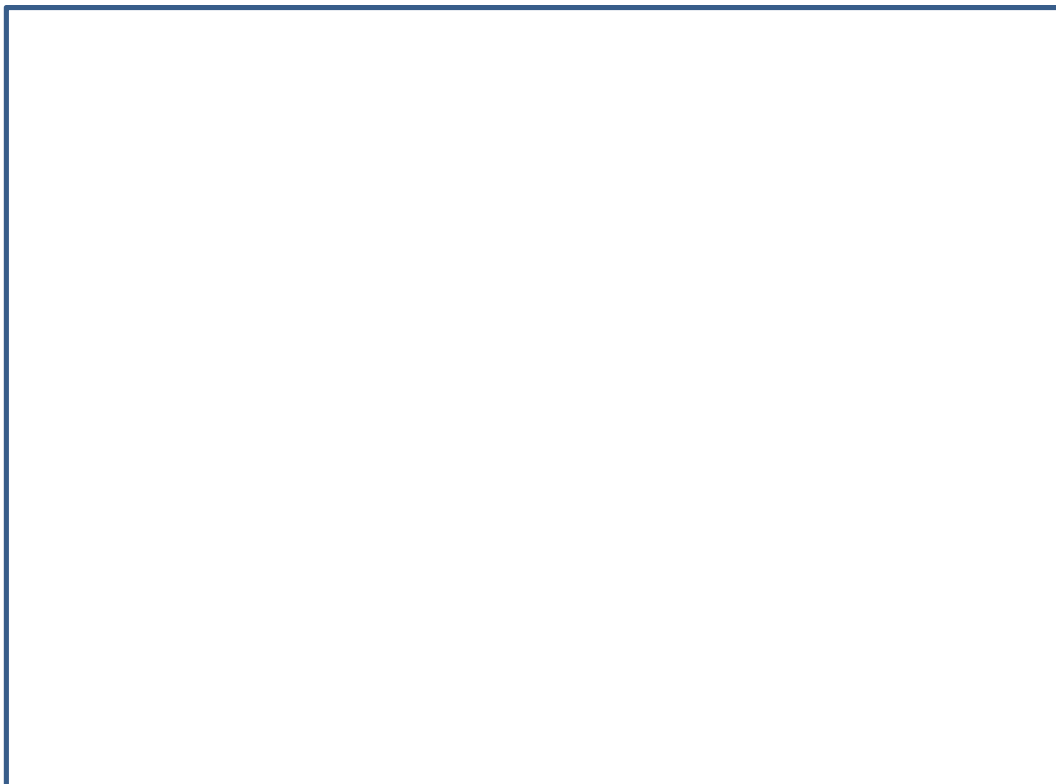
Fig. 5.11 Compressor map.
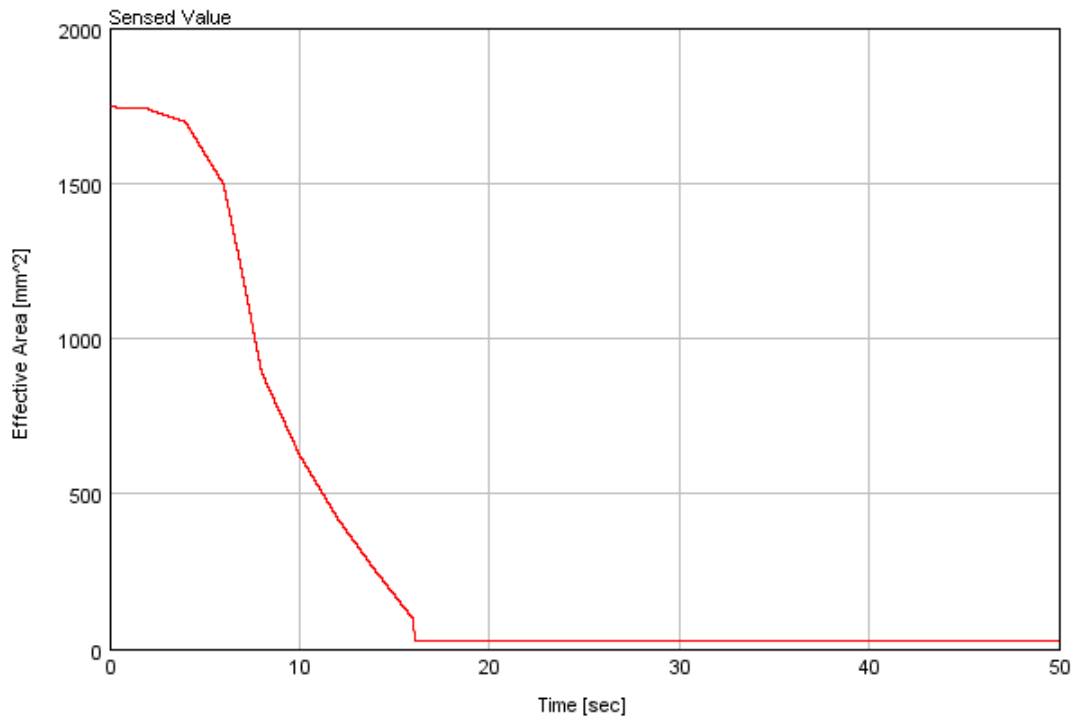
Fig.5.12 Throttle valve profile.
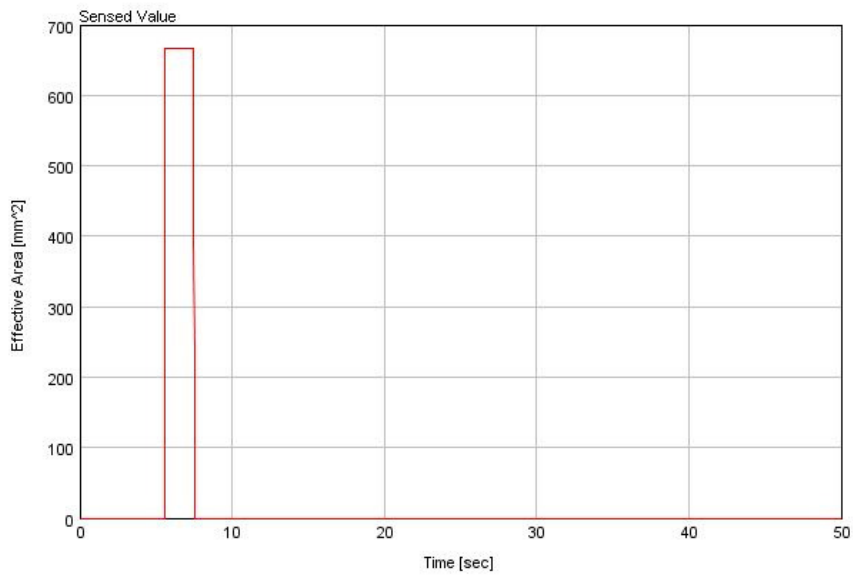
Fig.5.13 Compressor recirculation valve profile.

130

The results are presented on the supercharger and compressor maps in the Fig. 5.10 and Fig. 5.11. The dark lines in the supercharger map and the compressor map show the operating point of the respective components. The supercharger map operating points show that the compressor of the turbocharger operates at a stable operating zone and at a satisfactory speed range.

From the result it is concluded that the supercharger selected is suitable to operate the turbocharger at its operating zone.

5.4 Advantages and disadvantages of concepts

5.4.1 Advantages:

Supercharger rig (concept 1) is a less complex concept with few components involved. Fewer components enable less use of mechanical parts for installation. Also, electrical/electronic installations, control and data acquisitions requirements are lesser in this concept. This makes this concept less expensive to manufacture and operate. As the surge noise occurs at the compressor side of the turbocharger, using a supercharger rig will help to concentrate on the compressor side by eliminating the turbine side. As all the drive mechanisms can be kept closer in a single frame, this concept occupies the least floor area and also facilitates transportation to different facilities.

Combined supercharger and turbocharger rig (concept 2) is having the advantage that operating characteristic of turbocharger can be monitored. However, the control of turbocharger at transient conditions is extremely difficult and requires control of multiple components at the same time in a short span of time. If pulse generating devices are attached on the inlet and exhaust manifold, turbocharger rigs are good to determine the effect of pulses on the turbine and the compressor. However, as this project involves the surge mechanism in a petrol engine which in turn has a throttling device, the pulses due to the valve motion is not a predominant factor in the transient throttle operation.

5.4.2 Disadvantages:

The disadvantage of the concept 1 is that the drive mechanism for the supercharger can be bulkier. The maximum pressure ratio and the flow required at the output to generate the surge mechanism necessitates motor with high capacity. As the motor has to be kept closer to the supercharger due to the drive mechanism requirement, the noise of motor and transmission

system operation can be transmitted to the sensors in the experimental rig. Hence a separate background noise study is required to identify the noise generated sources other than the surge. The concept 2 too include background noise from flow generation mechanism. However, the turbocharger can be placed in a separate chamber with noise insulation and the intake air can be fed through ducts. A disadvantage of this proposal is that the experimental rig can occupy much longer floor area.

5.4.3 Selection of concept

The best design of the experimental rig from concept 1 and concept 2 is selected using the decision matrix approach as given in the table. The criteria for selection are listed at the left side and the concepts are ranked in a scale of 1 to 10. The favourable scores are denoted closer to 10 and less favourable are set closer to 1. The criteria which represents the main aim of the test rig are given in the first 5 rows. However, other important criteria are also included in the decision matrix. The sum of the score denoted in the matrix denotes that concept 1 is a better choice for the rig than concept 2.

Criteria	Concept 1	Concept 2
Surge mechanism prediction capability	10	10
Transient maneuver operation capability	10	8
Ease of analysis for the detection of the problem	9	6
Modularity of the rig to adopt different systems	10	10
Flexibility to do changes to arrive at a solution to the problem	9	9
Ease of instrumentation	9	8
Cost	10	5
Complexity of control systems	8	5
Number of mechanical parts	8	5
Back ground noise	6	9
Total	89	75

Table. 5.2 Ranking of criteria to select the best concept

5.5 Component design/selection of experimental rig

This portion of the chapter concentrates on the individual component design of the experimental rig. Considerable importance has been given to this part to achieve design right at first time. This is to reduce the cost of the rig manufacture and also to reduce time consumed

to build the rig. The major components involved are air intake system, supercharger, motor, drive mechanisms, cooling system, throttle body, compressor recirculation valve (CRV), sensors, data acquisition systems and control systems. The design follows the concept 1 which is described in the previous sections. The aim of the chapter is to arrive at the complete list of components and to arrive at the design specification of the components.

5.5.1 Mechanical components.

5.5.1.1 Supercharger.

This is an important component to be used in the experimental rig. The main function as defined in the previous section is to generate compressed air with pressure and mass flow rate closer to an automotive turbocharger compressor.

a) Engine simulation to obtain supercharger requirements

Concept 1 is evaluated using an one dimensional engine simulation. The objective is to find out of the input air pressure and flow requirement for a turbine of a standard automotive engine. Using an engine model the exhaust pressure and the mass flow on the turbine is determined. The engine model used is shown in Fig 5.14. This pressure is required to transmit the energy to the turbine and hence the compressor. The throttle is set to wide open and hence this simulation results in maximum pressure and mass flow of the exhaust gases on to the turbine. This is due to high mass flow of air into the engine at wide open throttle and thereby causing higher combustion pressures and more mass flow and pressure of the exhaust gases. The pressure in the turbine inlet simulator is provided in the Fig. 5.15.

Fig. 5.14 Engine model in GT Power.
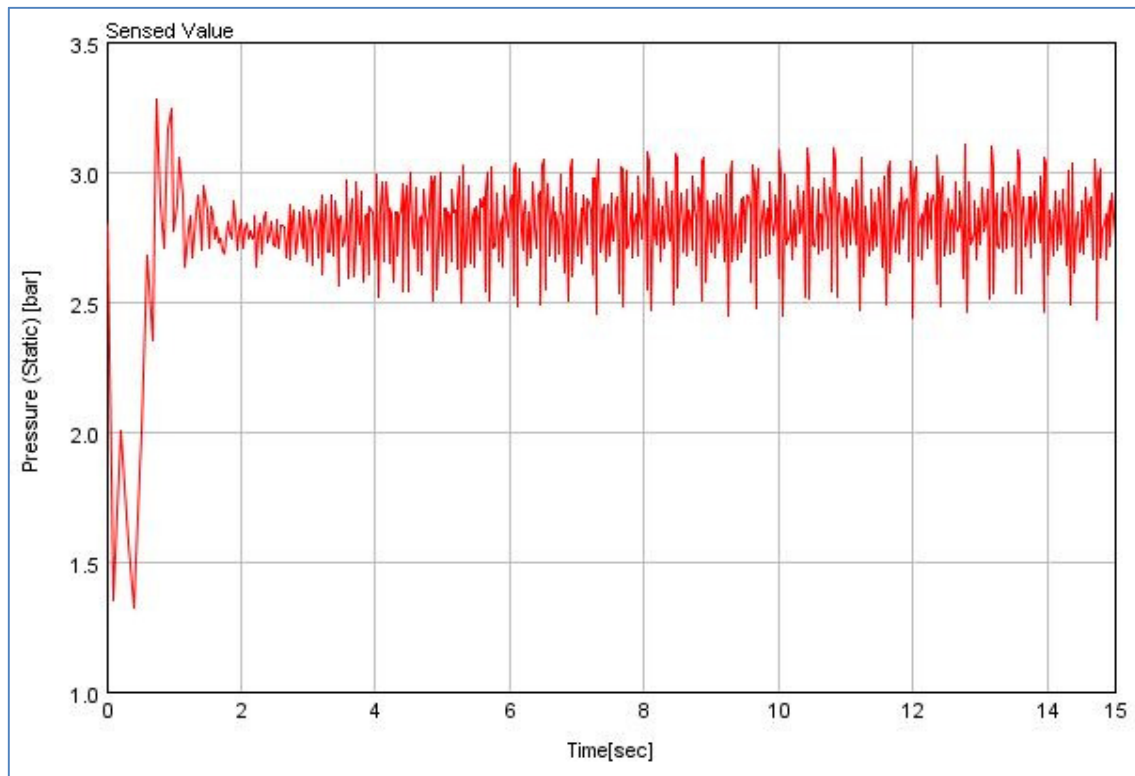
Fig. 5.15 Turbine inlet pressure.
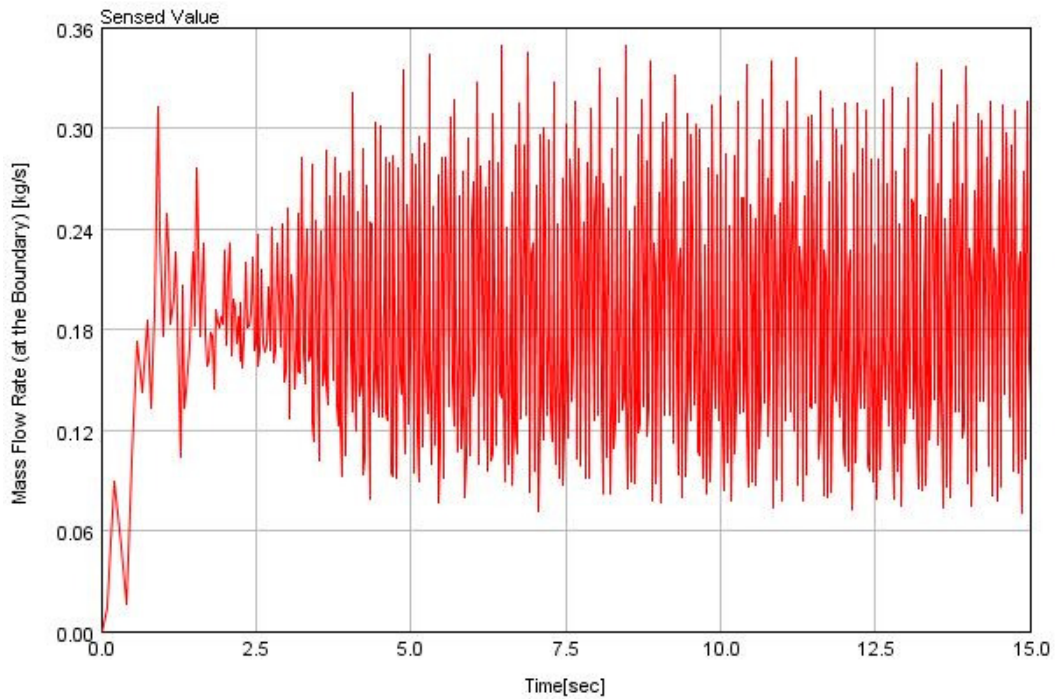
Fig. 5.16 Turbine inlet mass flow.
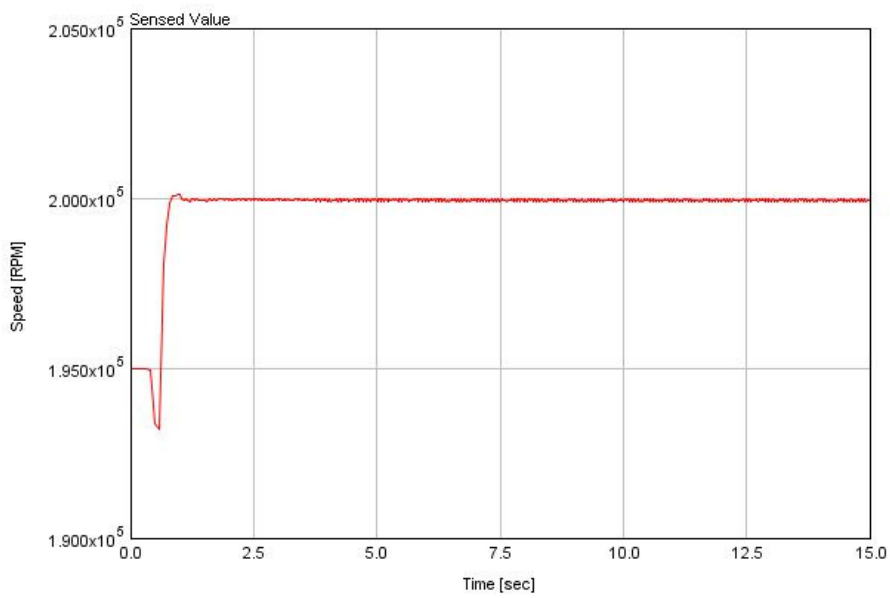
Fig. 5.17 Turbocharger shaft speed.

The maximum value of turbine inlet flow of 0.3kg/s and pressure of 3 bar is selected as an input to the rig design from the Fig. 5.15, 5.16 and 5.17.

The above analysis lead to the finalisation of centrifugal axial entry and radial exit type supercharger of the model name 'Rotrex C38-91 supercharger' (specification given in Table. 5.3). The pulley diameter obtained and the drive ratio is an input for the drive mechanism design and the motor design.

Description	Value	Unit
Max flow rate	0.63	kg/s
Max pressure ratio	2.94	--
Drive ratio	1:7.5	--
Pulley diameter	70	mm
Weight	6	kg
Rotational direction	Clock wise from the pulley side	--
Peak input shaft speed	12000	rpm
Peak impeller speed	90000	rpm

Table.5.3 Specification of Rotrex C38-91 supercharger

5.5.1.2 Selection of motor

The function of the motor is to drive the supercharger using an appropriate drive mechanism. The compressor map is used as an input to determine the motor specification. The motor is required to have enough power to drive the supercharger at sufficient speed and load to perform experiment at dynamic inlet manifold conditions.

The corrected mass flow rate which is a function of the pressure and the temperature at the outlet of the compressor is determined using the following equation:

$$m_{act} = m \sqrt{\frac{\left(\dfrac{T_{in}}{T_{ref}}\right)}{\left(\dfrac{P}{P_{ref}}\right)}} \qquad - \qquad 5.1$$

Where m_{act} - corrected mass flow rate, kg/s

T_{in} - Temperature at compressor inlet, K

T_{ref} - Reference temperature, K

P - Pressure at compressor inlet, bar

P_{ref} - Reference pressure, bar

The next step is to find the temperature after isentropic compression, at compressor outlet

$$T_2^{'} = \left[\left(\frac{p_2}{p_1} \right)^{\left(\frac{\gamma-1}{\gamma} \right)} \right] T_i \qquad - \qquad 5.2$$

where

$T_2^{'}$ - Temperature after isentropic compression, K

P_2 - Pressure at compressor outlet, bar

γ - Ratio of specific heats

Temperature at compressor outlet after non isentropic compression

$$T_2 = \left(\frac{T_2^{'} - T_i}{\eta} \right) + T_i \qquad - \qquad 5.3$$

Where

T_2 - Temperature at compressor outlet after non isentropic compression, K

η - Compressor efficiency

Power to drive the compressor is given by the equation

$$P_w = m_{act} C_p (T_2 - T_1) \qquad - \qquad 5.4$$

Where

   P$_w$ - power to drive the compressor, kW

   C$_p$ - Specific heat at constant pressure

Calculating the power to drive the compressor using the above equations

From the energy conservation and cost effectiveness point of view, the aim is to keep the motor power to a minimum required value. From the operating points of the compressor map in the previous simulation, a flow rate and pressure ratio of 0.1 kg/s and 3 :1, respectively are selected. Using these values the motor specification with a 20% margin is selected.

$$m_{act} = m \sqrt{\frac{\left(\dfrac{T_i}{T_{ref}}\right)}{\left(\dfrac{P}{P_{ref}}\right)}} = 0.1 \sqrt{\frac{\left(\dfrac{300}{288}\right)}{\dfrac{1}{1}}} = 0.102 \, kg/s$$

$$T_2^{'} = \left[\left(\frac{p_2}{p_1}\right)^{\left(\frac{\gamma-1}{\gamma}\right)}\right] T_i = \left[\left(\frac{3}{1}\right)^{\left(\frac{1.4-1}{1.4}\right)}\right] 300 = 410.62 \, K$$

$$T_2 = \left(\frac{T_2^{'} - T_i}{\eta}\right) + T_i = \left(\frac{410.62 - 300}{0.55}\right) + 300 = 501.13 \, K$$

$$P = m_{act} C_p (T_2 - T_1) = 0.102 \times 1.005 \times (501.13 - 300) = 20.63 \, kW$$

With a 20% over rating, the motor power required is arrived as 24. 76 kW. This overrating is included to consider the frictional losses in the drive mechanism. The closest available motor with 30kW is selected. The important specification of the motor considered for the rig design is given in the following table.

Description	Value	Unit
Motor manufacturer	ABB	--
Product code	Cast iron, 2 pole, 3 phase M3BP180MLB	--
Rated output	30	kW
Rated frequency	50	Hz
Nominal torque	97	Nm
Total weight of motor	208	kg
Rated speed	2950	rpm

Table. 5.4 Specification of motor

5.5.1.3 Supercharger drive mechanism

The normal drive mechanisms used are gear, belt, hydraulic or electrical drive in similar experimental rig arrangements. The belt drive is very compact and economical for this experimental rig arrangement.

The rated speed of the selected motor is ~3000 rpm and the peak required speed of the supercharger input shaft is 12000 rpm (the internal reduction within the supercharger) leads to a peak input speed of impeller to a value 90000 rpm [40]. Hence a belt drive from the motor to the supercharger is designed with the following ratio

Pulley ratio = Speed of supercharger pulley/speed of motor = 12000/3000 = 4:1

The pulley diameter at the motor end is determined from the supercharger pulley available diameter described in the previous section of supercharger selection.

Pulley outer diameter at motor end = Pulley diameter at supercharger end x pulley ratio=
70 mm x 4 = 280 mm

An automatic spring loaded rolling type tensioner system is used for the belt to maintain sufficient contact and wrap angle on the pulleys. This is also to provide tension in the belt system even when belt expands over a period of time and to accommodate any deviation of the belt system during its operation.

5.5.1.4 Lubrication and cooling system for supercharger

The only mechanical component requiring lubrication is the supercharger shaft and bearing in the experimental rig. This is because the supercharger shaft works at a very high speed of a maximum value of 90000 rpm and with loads. The Rotrex supercharger consists of an oil pump which is driven by the supercharger pulley during the operation. The pump acts as a dry scavenging pump and also an oil supply pump. The lubrication system is of self-contained type and does not require an auxiliary pump and drive mechanism.

The lubricant oil acts as a coolant for the supercharger system in the test rig. As it is circulated through the supercharger, considerable amount of heat is carried by the oil. For the safe operation of the supercharger, the temperature of the oil must not cross +80 deg C. Hence a plate type heat exchanger was used to cool the oil to a safe limit. Under extreme operating conditions the plate type heat exchanger that can be connected to a refrigerated recirculating chiller is planned. The schematic layout of the lubricating system is shown in the Fig. 5.18.
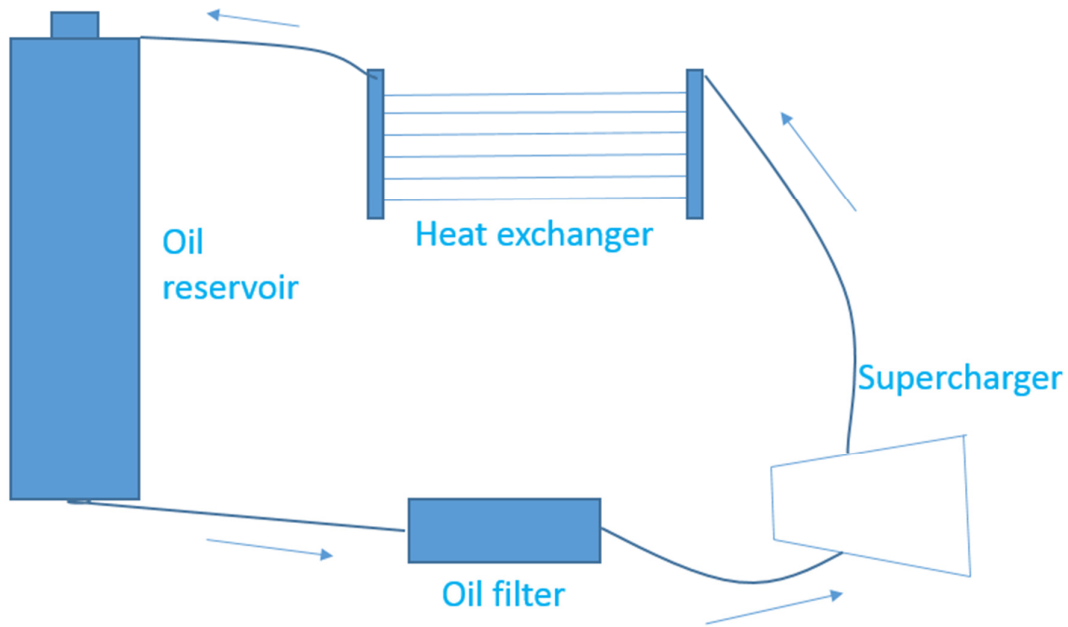
Fig. 5.18 Lubrication system schematic diagram

5.5.1.5 Inverter drive selection

As the motor selected for driving the supercharger is of a high power rating, 30kW, an inverter drive is required to control the speed of motor. Without the inverter drive and with high motor speeds, the induced voltage in the motor can damage the motor or blow off the fuses. Also the motor speed is directly proportional to the supercharger speed as they are linked using belt drives. To control the supercharger speed and hence the flow and pressure characteristics of outlet air, the motor speed need to be maintained according to a profile against time or constant speed. Hence, an inverter drive is selected having the specification WEG CFW11 37 kW. This equipment has an human machine interface and also computer software to change the motor speed.

5.5.1.6 Air intake system

An automotive engine's air intake system is used in the experimental rig. The major parts include the air filter and the intake system ducts. (Fig. 5.19 and 5.20). The major dimensions are tabulated as follows
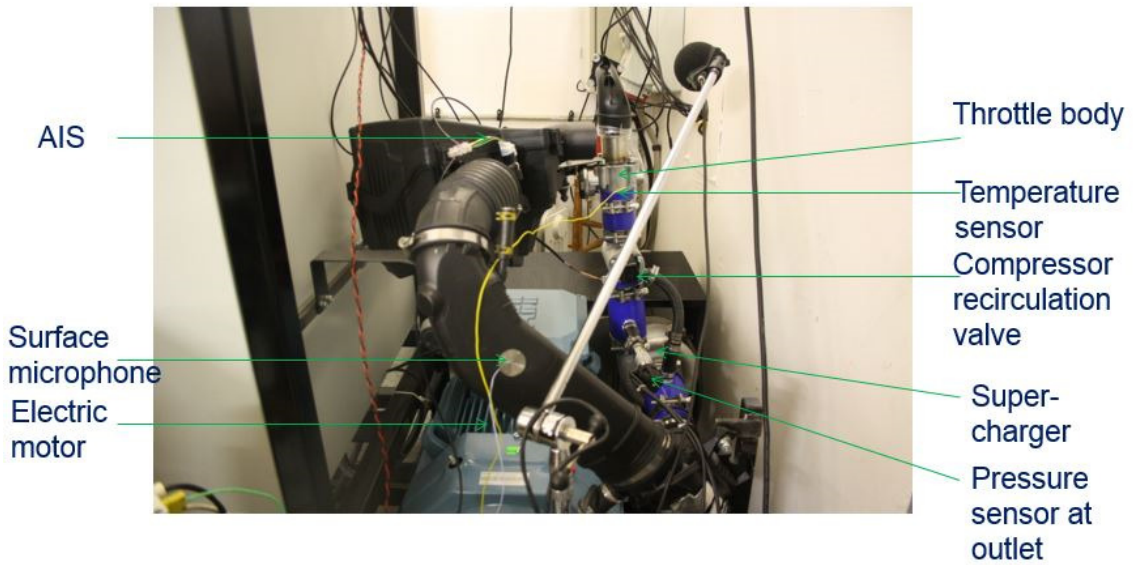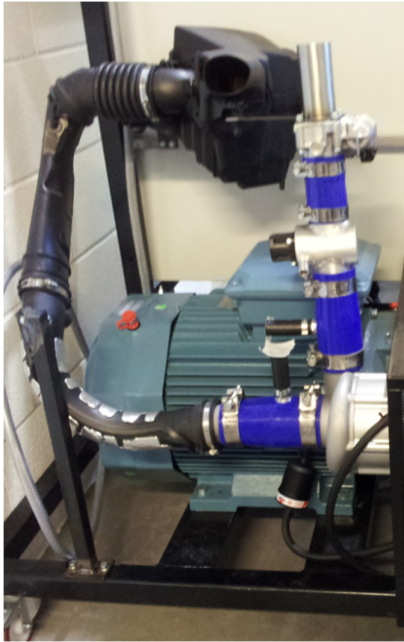
Fig. 5.19 Intake system layout on the supercharger rig (AIS – Air intake system).
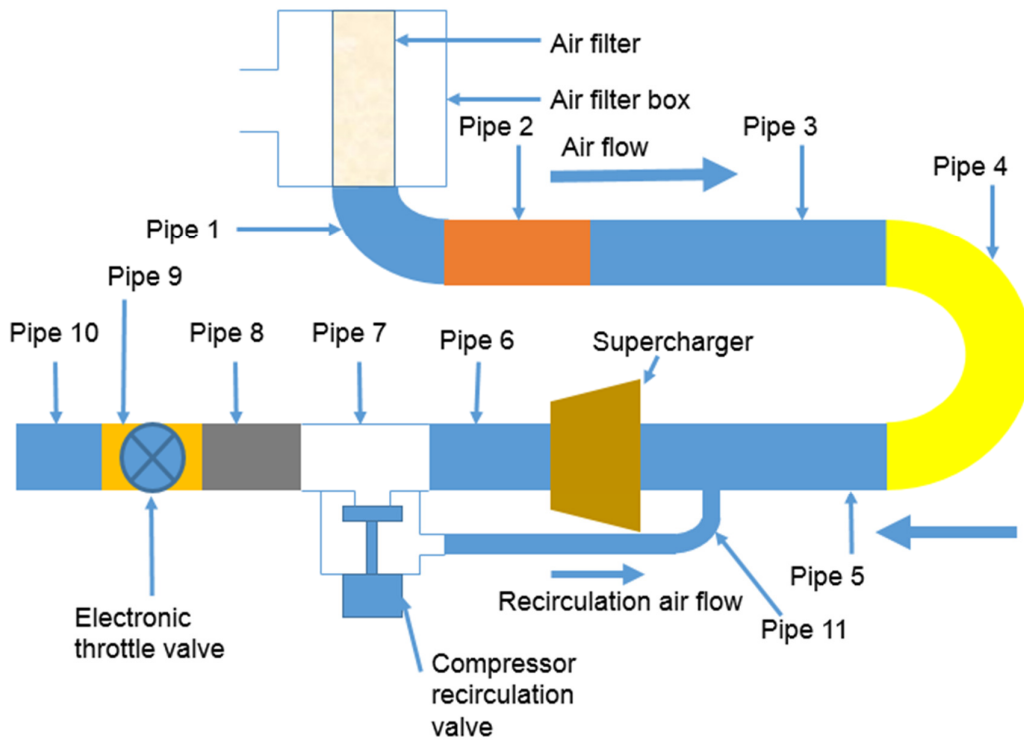
Fig. 5.20 Schematic representation of the air intake system arrangement

Description	Inlet diameter, mm	Outlet diameter, mm	Length, mm
Pipe 1	66.9	70.9	130
Pipe 2	79	66.6	160
Pipe 3	76.4	72.2	370
Pipe 4	63.5	76.2	535
Pipe 5	76.2	50	165.5
Pipe 6	63	57	164.8
Pipe 7	53.5	53.5	163.9
Pipe 8	58	58	101
Pipe 9	53.5	50	80.5
Pipe 10	48	48	109
Pipe 11	15	15	200

Table.5.5   Air intake system major dimensions

5.5.1.7 Test rig layout and integration of mechanical components

This section outlines the installation details of various individual components selected in the previous section into a supercharger rig. The main mechanical construction involves installing the motor, supercharger and the air intake system into the rig. A basic frame is designed with tubular structure as given in the appendix. The square shape of the frame allows compact design. The motor is mounted on the base of the frame and the supercharger is mounted on a plate attached to the rotor side of the motor. A belt drive is connected on the pulley attached to the rotor shaft of the motor to the supercharger pulley. The belt is operated in tension using an automatic belt tensioner.

The major drawings used for the base frame and the supercharger support manufacture are given in the appendix. A schematic diagram explaining the mechanical and electric connections are shown in the Fig. 5.21. The connection details of various instruments used are given below.
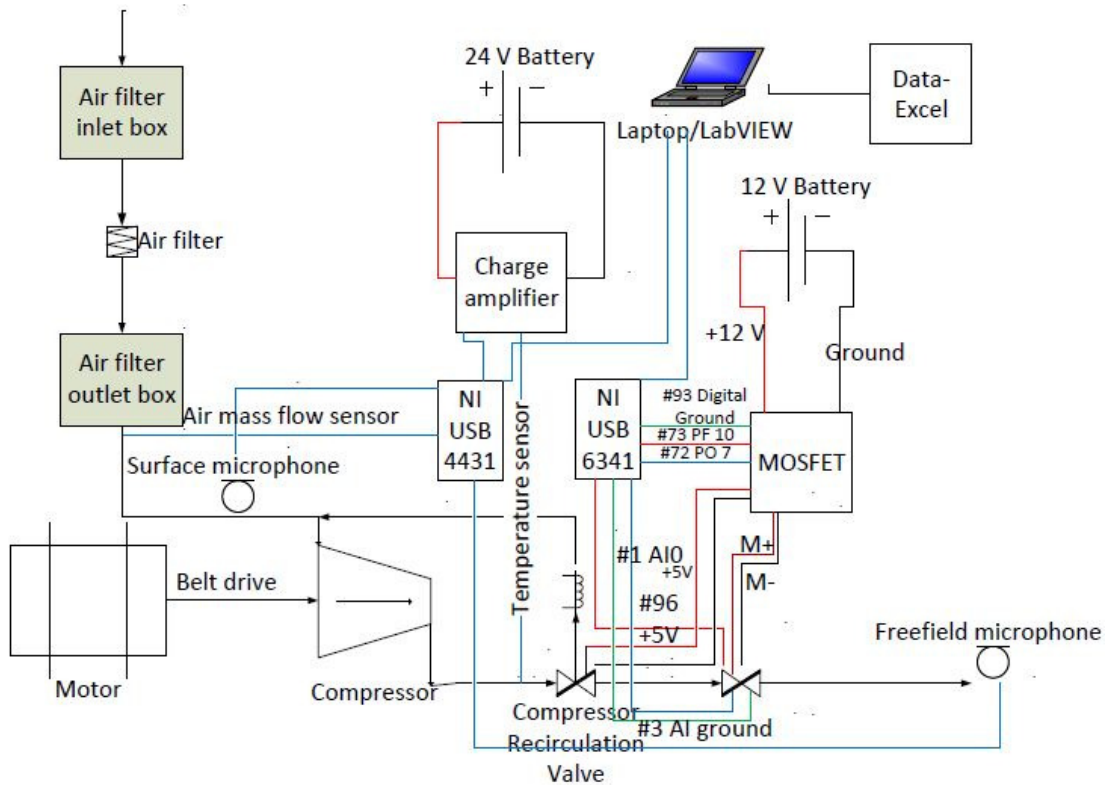
Fig. 5.21 Electrical and mechanical connections of the experimental supercharger rig

5.5.2 Electrical components – sensors and actuators, data acquisition and control modules

5.5.2.1 Data acquisition system

Data acquisition systems were decided to be used along with a computer to acquire the data at a sampling frequency of 12000 Hz. The signals to be measured are the voltage from the surface microphone, freefield microphone and accelerometer mounted on the housing of the compressor, frequency signals from the mass flow sensor, voltage signals from the temperature sensors, pressure sensors and throttle position sensor of the throttle body. The two data acquisition system chosen are NI USB 4431 and NI USB 6341 and operated by the LabVIEW program using a computer. The block diagram interface used in the LabVIEW software is shown in Appendix (Fig. 9.4). The signals acquired during the experiments are calculated within the program for conversion to proper units. Synchronisation of the signals are performed using the time stamps recorded at each data acquisition device. The connection details of the data acquisition system are given in the Fig. 5.21.

5.5.2.2 Control system

Hardware such as the NI devices, sensors and actuators and the LabVIEW software are integrated to perform as a control system. This includes providing base voltages to the devices such as throttle body, mass flow sensor, temperature sensors and pressure sensor. The main operating square signals with appropriate characteristic is performed using PID control and will be described in the electronic throttle valve section.

5.5.2.3 Free field microphone

Freefield microphone of the make GRAS 40 AE and a pre amplifier is selected to be at the compressor outlet. The specification of the microphone is given in the Table.5.5. The calibration of the microphone is done using a G.R.A.S sound calibrator using an input frequency of 1000Hz and 114 dB. The sensitivity value in the analyser is modified as suggested by the calibration experiment.

Sl No.	Description
	Microphone
1	1/2" pre polarised free field microphone type G.R.A.S 40AE
2	Serial number 56592
3	Normal open circuit sensitivity 50mV/Pa
	Microphone pre amplifier
4	1/2" CCP pre amplifier type G.R.A.S 26CA
5	Serial number 58364
	Calibrator
6	Sound calibrator G.R.A.S 42 AB
7	Output 1000 Hz 114 dB

Table.5.5 Free field microphone specification

The free field microphone is positioned at a distance of 15 cm from the outlet pipe of the compressor as given in the Fig. 5.22.
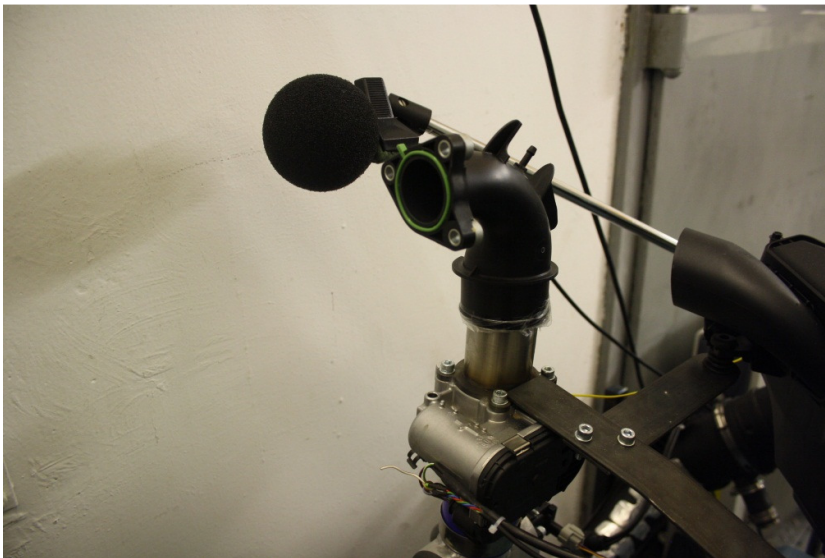
Fig. 5.22 Outlet duct and free field microphone orientation

5.5.2.4 Surface microphone

Surface microphone of the make B&K 4949 is mounted at the intake system as shown in Fig.5.23. A hole is drilled such that the microphone diaphragm is exposed to the interior of the duct. The diaphragm in turn is flush mounted with the microphone housing [44]. The flange of the microphone is mounted on the wall of the duct using screws.

Fig. 5.23 Surface microphone [44]

SI No.	Description
	Surface microphone
1	Type 4949 B&K 2574636
2	Sensitivity 10.7mV/Pa

Table 5.6 Surface microphone specification

The calibration of the surface microphone is performed using the freefield microphone as a reference. The freefield microphone is calibrated as per the procedure given in the previous section. The freefield microphone and surface microphone were used to measure a sinusoidal waveform by a loudspeaker. The result shows that the measured results of both the microphones are closely matching as in the Fig 5.24. The corresponding sensitivity is used as a calibrated value for the surface microphone in the analyser settings.
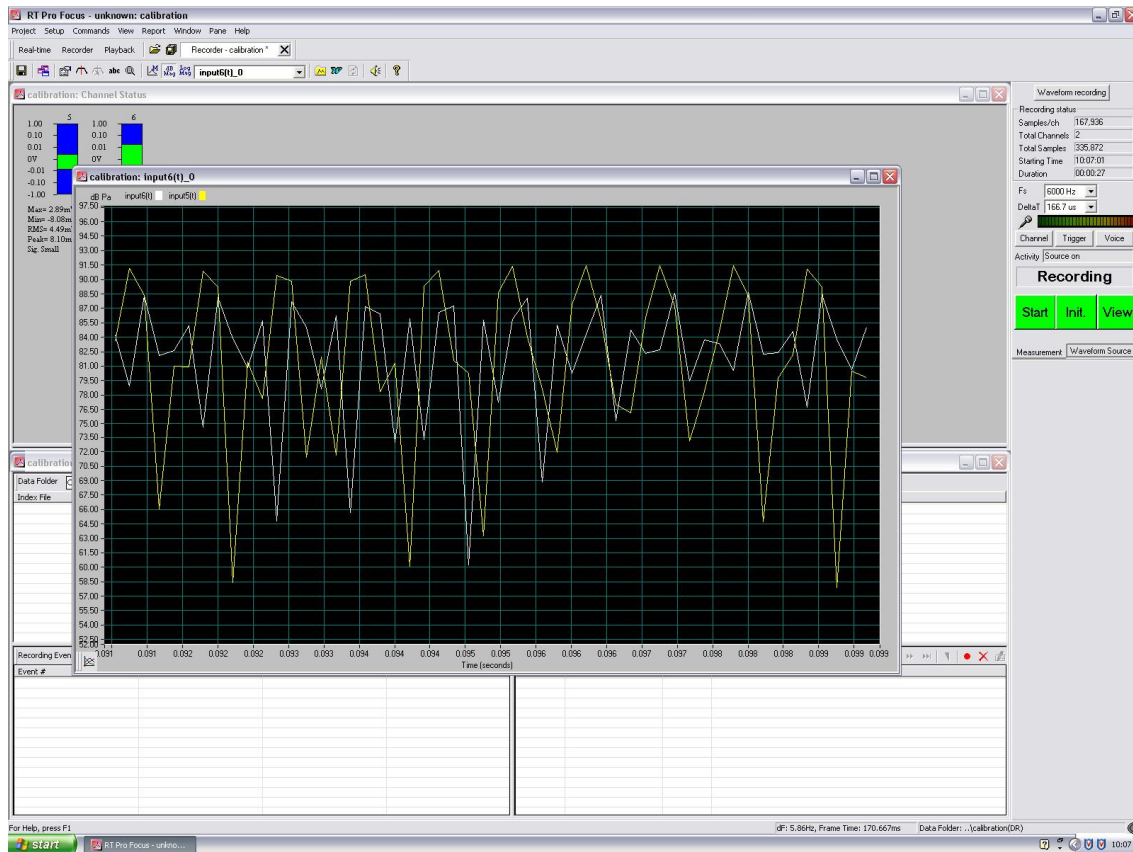
Fig. 5.24 Surface microphone (white) and microphone (yellow) reading with a loudspeaker excitation.

5.5.2.5 Pressure sensor

Static pressure at the intake system wall is a useful indication of surge occurrence and pressure fluctuations which leads to noise. Also, the operating point on the compressor map can be plotted by noting this measurement and further calculations. PMP/PTX 1400 sensor was used as pressure sensor with a capability of measuring 0 to 6 bar and the operating temperature zone of -40 to 80 deg C. As the air temperature at the outlet of compressor can exceed 100 deg C at high load operating conditions, an adaptor is required to fix the pressure sensor at a remote location at a safe temperature. The pressure sensor is connected to the outlet duct using a pipe of small internal diameter. This pipe is used to communicate the pressure at the compressor outlet to the sensor at the pressure sensor.

The specification of the pressure sensor is given in the following table (Table.5.7). The pressure sensor is calibrated using a standard calibrator. A known pressure is applied by the pump in

the calibrator into the sensor and the corresponding voltage output of the pressure sensor is measured and tabulated. The tabulated values are plotted in the form of a graph as given in the Fig. 5.25. The output voltage from the sensor increases as the pressure applied to the sensor is increased. As suggested by the graph (Fig. 5.25), the pressure against voltage shows a linear trend and is represented by the equation,

$y=0.841x-0.0189$ – 5.5

This equation can be used to calculate the instantaneous pressure from the instantaneous voltage signals measured from the sensor using a data acquisition device.

Pressure, bar	Voltage output, V
0.5	0.413
1	0.827
1.5	1.242
2	1.661
2.5	2.068
3	2.488
3.5	2.909
4	3.38

Table 5.7 Calibration results for the pressure sensor
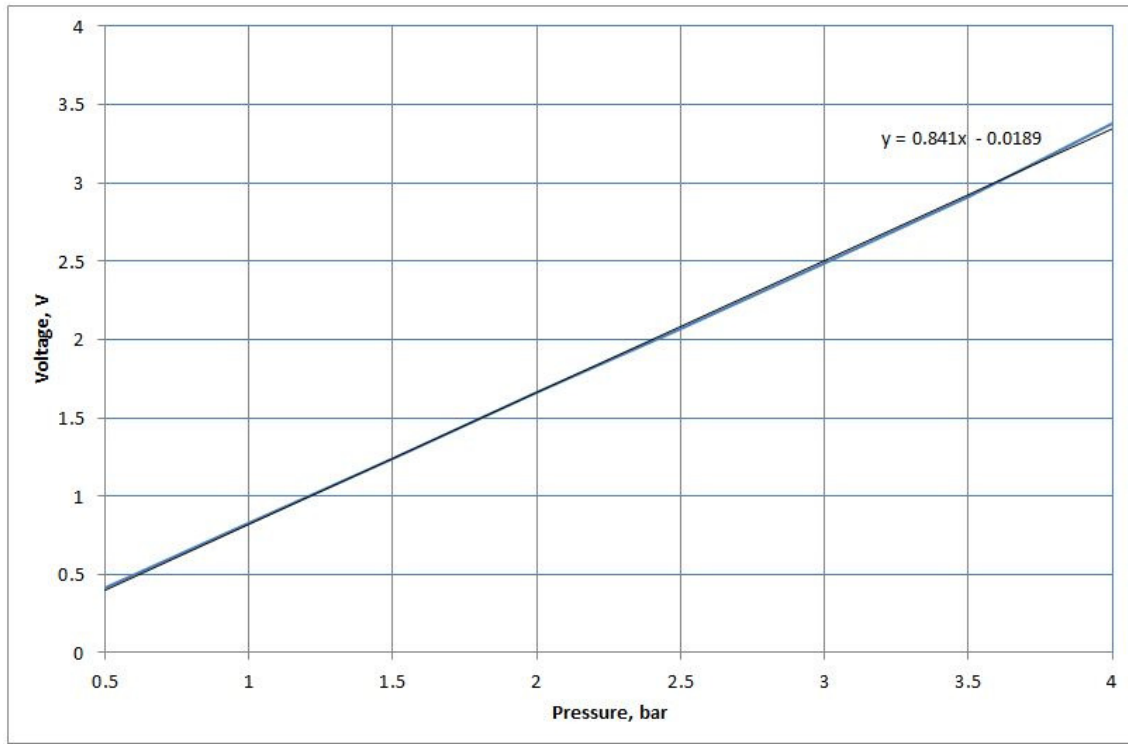
Fig. 5.25 Experimental result to calibrate the pressure sensor

5.5.2.6 Mass flow sensor

A mass flow sensor (make: Hitachi) is used on the intake duct of the supercharger rig at the outlet side of the air filter. A pre calibrated value by the supplier is used for converting the frequency of the signal into voltage as given in the following equation.

$$m=A_0+A_1*F+A_2*F^2+A_3*F^3+A_4*F^4 \quad - \qquad 5.6$$

Where,

m=mass flow rate in kg/h

A_0=

A_1=

A_2=

$A_3=$

$A_4=$
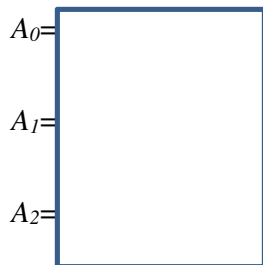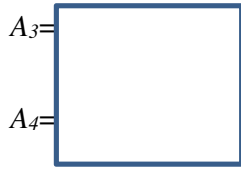
F=Frequency of the output signal in Hz

Frequency of the signal is measured using counter channel of the NI USB 6341 and LabVIEW software program. The block diagram developed in the LabVIEW software is shown in the Appendix (Fig.9.5). From the measured frequency, the instantaneous mass flow rate can be calculated using the equation given.

5.5.2.7 Temperature sensor

KX type thermocouples are used to measure the temperature at the compressor inlet and outlet. This will form a basis for compressor mass flow correction to help to determine the corrected compressor map operating points. Also, increase in temperature is a direct indication of the change in pressure within the intake system. Hence, temperature can indirectly suggest the occurrence of surge. An amplifier (Seneca K109TC) is used to scale the voltage signal. The following linear relation is used to convert the output voltage into temperature. 0 to 5 V output corresponds to 0 to 200 deg C temperature. Hence, the temperature reading is 40 times the voltage output by the sensor. (individual circuit)

5.5.2.8 Electronic throttle valve operation and throttle position sensor

The measured transient throttle profile data on a car with turbocharged engine is used as an input for the electronic throttle valve control. During this measurement noise was observed from the turbocharger in the car. The function of the electronic throttle valve operation control unit is to operate the throttle valve at the same throttle angle against time as measured in the car during tip-in and tip-out manoeuvre. Hence the throttle control system acts as a driver acting transient force on the accelerator pedal to create the surge noise.

The electronic throttle valve is fitted at the outlet side of the compressor. This unit comprises of butterfly valve (to restrict the flow at the outlet side of the compressor), electric motor (to operate the butterfly valve against a spring force), and potentiometer (to feedback the throttle position in the form of voltage of the range 0 to 5 V). The actual throttle opening percentage is measured from the feedback voltage from the throttle valve using the linear equation:

Throttle opening percentage=25.64*V-21.54   - 5.7

Where V is the feedback voltage from the electronic throttle valve

This equation was derived by opening the throttle valve to known angles and noting the voltages.

The throttle opening position (percentage) against time is loaded into the LabVIEW software in the form of a .xls table. Pulse width modulation technique is used to vary the power input to the motor and hence the opening angle of the throttle valve. Hence, square waves are generated using the hardware by the LabVIEW software program. Pulse width modulation is achieved by varying the duty cycle of the pulses generated. Duty cycle is a measure of the proportion of time when the pulse is at its highest amplitude to the period and is given by:

Duty cycle=Width of the pulse/Period of the pulse   -5.8

The higher the duty cycle, the more is the power input to the motor in the throttle valve and larger is the operating angle.

With the signals produced by an inbuilt potentiometer in the throttle body, throttle position was measured. The voltage output of the signals is linearly proportional to the throttle valve opening position. The throttle position signals are loaded into the PID (proportional-integral-derivative) control programme in the controller using the hardware. The input throttle profile is also loaded into the PID control programme. The set point for the PID control is the throttle opening percentage against time as given in the input. The PID programme controls the parameters of duty cycle by the software. By varying the duty cycle of the pulses, the PID control achieves the desired throttle opening percentage.

A schematic diagram of the throttle valve operation control and the position sensing is shown in the Fig. 5.26. The block diagram used for the PID control of throttle valve and the CRV opening is given in Appendix (Fig. 9.6).
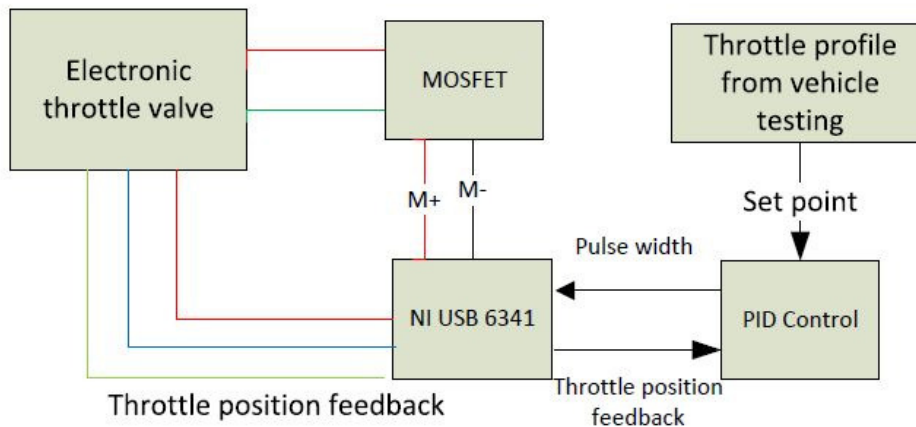
Fig. 5.26 Electronic throttle valve layout

5.6 Summary

The aim of this chapter is to document the design of supercharger rig from concept level. Two selected concepts were presented. Simulation was performed by building the design concepts on a one dimensional software to evaluate the feasibility of using a supercharger as a surge generating source. The signals measured on the experimental method followed in a literature is simulated and compared. The best concept which is a supercharger rig, based on rating of various factors was chosen. From this exercise, the measurements to be noted during the transient experiments were understood, i.e. pressure, temperature, mass flow, sound pressure, throttle position, supercharger speed and crv position. The values and the boundary conditions needed to measure these factors were obtained and the sensor/actuator design and selection was performed. The next step was to integrate the mechanical components and also electrical components. The major sensors and actuators used are given in the following table (Table.5.8). To co-ordinate the functioning of all the components, to acquire the data from the sensors and to perform the actuators, LabVIEW software was used. The use of this software enabled to consider the actuators and sensors as individual components by means of controlling those separately using codes. At the same time, their operation were co-ordinated to perform a defined steady state or transient action without minimum human intervention. Flexibility for the boundary condition definition of this transient and steady state manoeuvres was ensured.

The system as a whole was capable of performing steady state and transient manoeuvre to generate surge condition. Also, modularity of the experimental rig was ensured to enable to remove the individual components in the intake system and replace them with other parts (i.e. from other automotive intake system). It was very important to package the instrumentation into the test rig. The accessibility of the rig for instrumentation was also considered during the design phase. The following chapters explain the application of this experimental rig to predict surge noise, find the source of noise, determine the mechanism and find an economical passive solution.

Sl No	Component and Description	Supplier	Specification
1	Supercharger	Rotrex	C38-91, Mass flow - 0.63 kg/s, Pressure ratio - 2.9
2	Motor	Beta power	2 Pole, 30 kW motor, 3000 rpm rated speed
3	Inverter drive speed controller	Inverter drive	37 kW
4	Compressor inlet and outlet temperature sensor	TC Direct	KX type
5	Temperature amplifier	Seneca	K109TC
6	Compressor inlet and outlet static pressure	GE Sensing	PMP/PTX 1400
7	Surface microphone	B&K 4949	5 to 20000 Hz, 30-140 dB
8	Compressor outlet flow sensor	From an automotive intake system	Make Hitachi
9	Cooling system for lubrication	Bowman/ThermoFisher	Plate type HEX/Refrigerated recirculating chiller, 4540 W
10	Pulley system for supercharger drive	Hopkinson and Hopwood	4:1 gear ratio

Table. 5.8 List of components and sensors

CHAPTER 6
RESULTS AND ANALYSIS OF EXPERIMENTS ON SUPERCHARGER RIG

6.1 Introduction

Experiments were conducted on the supercharger rig to input the same boundary conditions as that of a car operation during surge noise occurance. Steady state and transient experiments were performed on supercharger rig. The main aim was to create the surge occurance and subsequently vary the parameters involved to reduce the surge noise. The data output from the experiments are useful to correlate with the simulation results. The experimental rig was then used to solve the problem of noise ocurrance.

The measurements taken were using the surface microphone at the inlet duct, pressure sensor at the compressor outlet, temperature sensor at the compressor inlet and outlet and mass flow sensor at the air intake system. From the literature review, the surge noise is identified to be of the order of 1500 to 7000 Hz and hence the sampling frequency for the surface microphone is maintained as 24000 Hz. Short time Fourier transform (STFT) is used to find the frequency of the local sections in the case of transient experiments and Fast Fourier transform is used in the case of steady state experiments along with STFT.

6.2 Background noise

The objective of the study is to identify the background noise and to differentiate those from the surge noise. Supercharger was not connected while doing any of these experiments. Hence, the frequency of operation of the other components involved in the rig can be separated from the actual surge frequency. The important sources of background noise are the external and mechanical and electric components.

6.2.1 Ambient noise

All the equipment related to the compressor rig are switched off in this experiment. The measurement is taken at the surface microphone which is installed at the intake duct near to the inlet side of the compressor. The objective of this study is to understand the background noise in the lab which can be considered during the main transient surge experiments. Fig. 6.1 shows

the raw data and the processed STFT results. The sound pressure is of very low amplitude with a maximum value of 0.1 Pa. The STFT result shows that the background noise is of around 60 dB. The frequency is around 50Hz and is of constant tone nature. This frequency is corresponding to the AC mains supply to the noise and vibration lab and will be always present during the experiments.
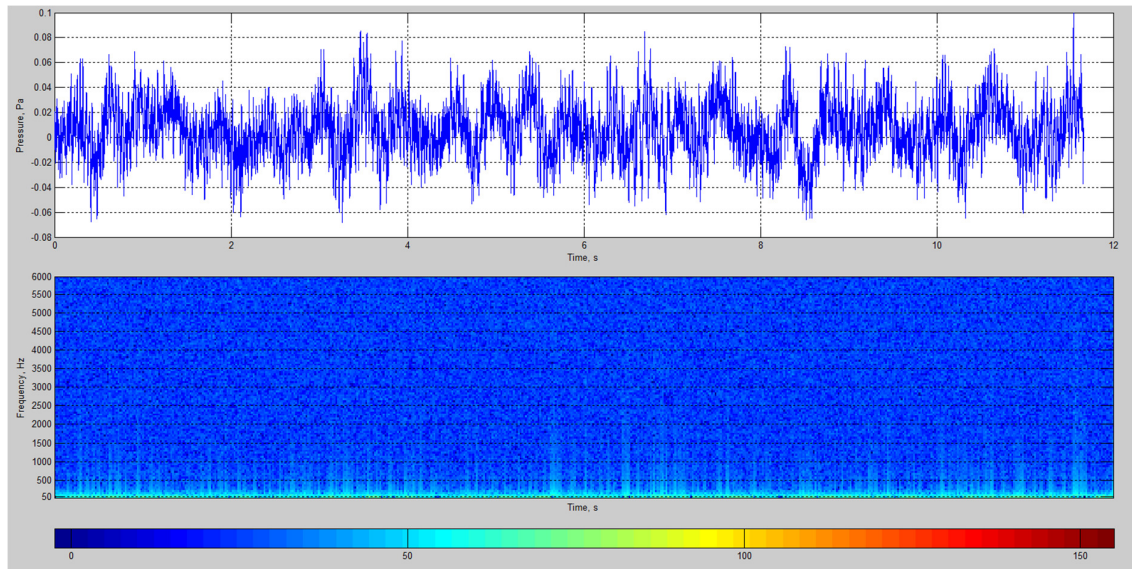
Fig. 6.1 Ambient noise (Exp# 160) (colour code shows the sound pressure level in dB)

6.2.2 Inverter noise

In this experiment, the inverter is switched on and other devices are switched off. The inverter consists of electrical components and mainly noise generating cooling fans. The noise measurements are made at the compressor inlet duct using a surface microphone. The sound pressure data shows that the noise measured is higher than the previous experiment. The maximum sound pressure recorded is 0.25 Pa. The measurement shows a maximum noise level of 73 dB occurring at a frequency of 50Hz as in the Fig. 6.2. This is possibly due to the electrical frequency of 50 Hz. The inverter fans were switched on when the thermostat senses higher temperature in the system. As this experiment was done at a no load condition, the fans were not operated.
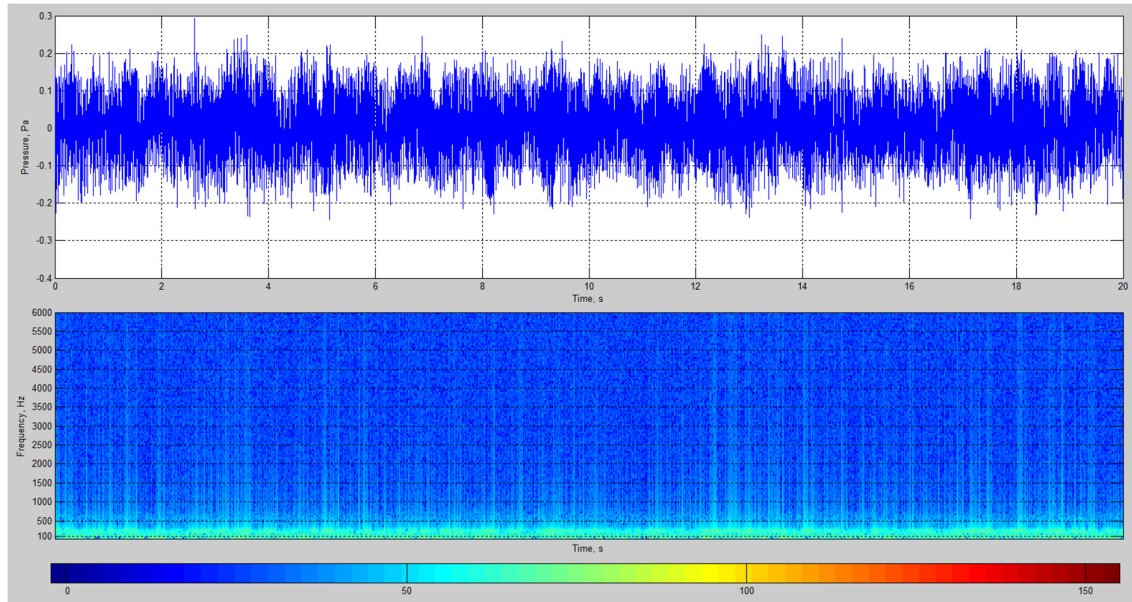
Fig. 6.2 Measurement using surface microphone at the compressor inlet pipe location (Expt ref no.161) (colour code shows the sound pressure level in dB)

6.2.3 Inverter and fan noise

The inverter and the cooling fans in the inverter are in operation during the functioning of the electric motor. These are incorporated to maintain the optimum operating temperature of the electrical circuits and to avoid any breakdown due to overheat. Hence it is important to understand the behaviour of these components in the frequency and amplitude domain. The reading of the surface microphone is analysed as given in the Fig. 6.3. . An additional frequency band appears in the figure when compared to the previous experiment. This is clearly due to the operation of the electrical fans. The sound pressure shows a slightly higher level than in the previous experiment. The maximum level of sound pressure is 75 dB for the inverter fans and corresponds to frequencies 590 and 600 Hz. The frequency may be due to the number of blades and the speed of the fan in question.
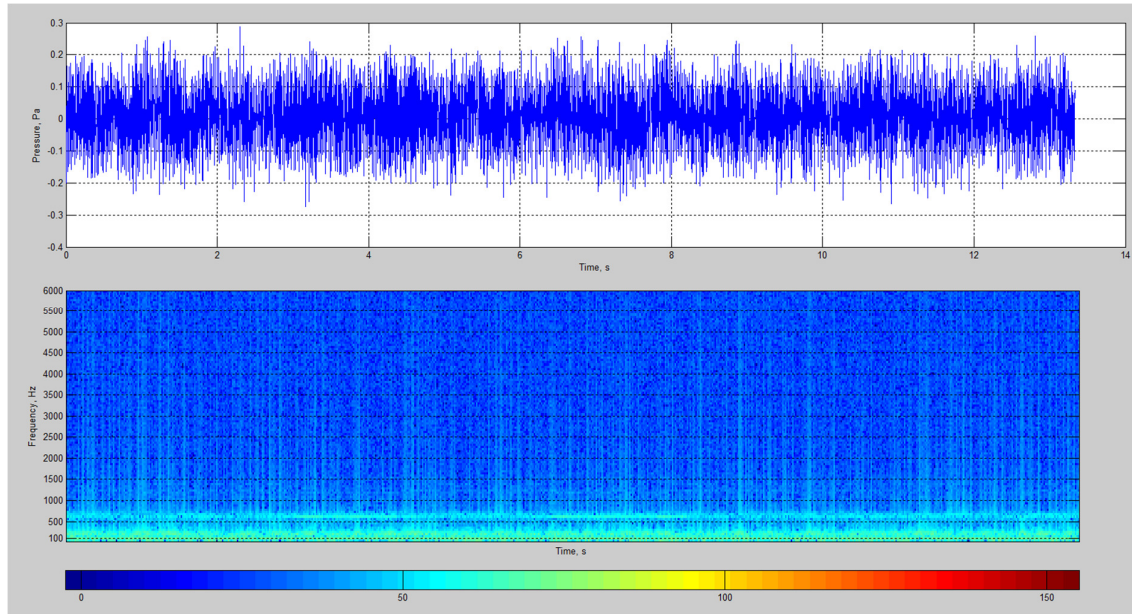
Fig. 6.3 Measurement using surface microphone at the compressor inlet pipe location – inverter and fan switched on (Expt ref no.162) (colour code shows the sound pressure level in dB)

6.2.4 Inverter, fan and motor noise

This experiment is developed from the previous experiment to identify the effect of electric motor. The results of surface microphone readings and the STFT shows additional frequency bands apart from than that of the inverter and fan noise. The motor speed is maintained at a constant value of 1000 rpm in this experiment. This corresponds to a frequency of (1000/60) 16.7 Hz. This frequency band coexists with the inverter frequency band and not distinctly visible in the following Fig.6.4. However, operation of the motor created harmonic and other frequency band as evident in the analysis. The additional frequency bands are possibly due to the harmonics of the motor speed and also excitation of the experimental rig frame structure. The maximum sound pressure level also shown an increase to 0.6 Pa as in the Fig.6.4. This experiment helped to understand the effect of forces exerted by the motor on the experimental rig.
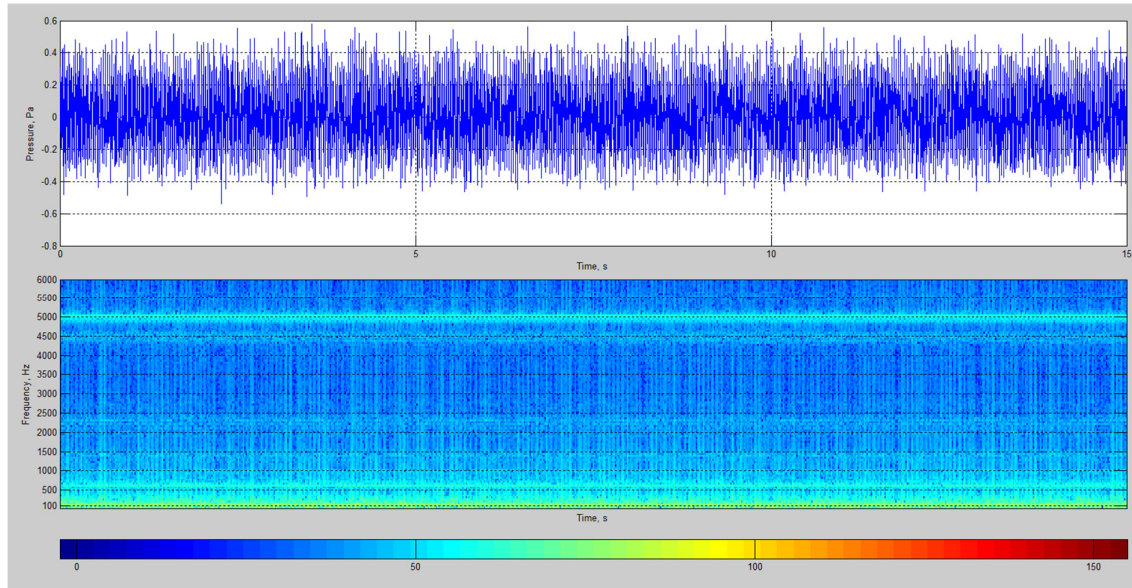
Fig. 6.4 Measurement using surface microphone at the compressor inlet pipe location –

inverter, fan and motor switched on. Compressor drive disconnected (Expt ref no.163)

(colour code shows the sound pressure level in dB)

6.2.5 Inverter, fan, and throttle valve noise

This experiment is an upgrade from the previous experiments. The inverter, inverter fan, electric motor, supercharger and throttle is operated. As mentioned in the previous sections, throttle is operated using a pulse width modulated motor and gear arrangements. The frequency of the square pulses used for the operation is 200 Hz. The frequency obtained from the analysis of the surface microphone readings are 100-300, 500, 1100, 1500, 4000 and 4500 Hz and the maximum sound pressure level observed is 75 dB. The frequency of the square pulses, electrical noise, inverter and fan operation are observed in the lower frequency range. The higher frequency in the Fig.6.5 are possibly due to the gearing operation of the throttle valve and also due to the structural vibration. There are also predominant frequencies in the region of 2000 Hz observed during the operation of solenoid valve. The solenoid valve is energised and lifted from its closed position only during this region. In other operating conditions the solenoid valve is in its initial state and not energised electrically.

159
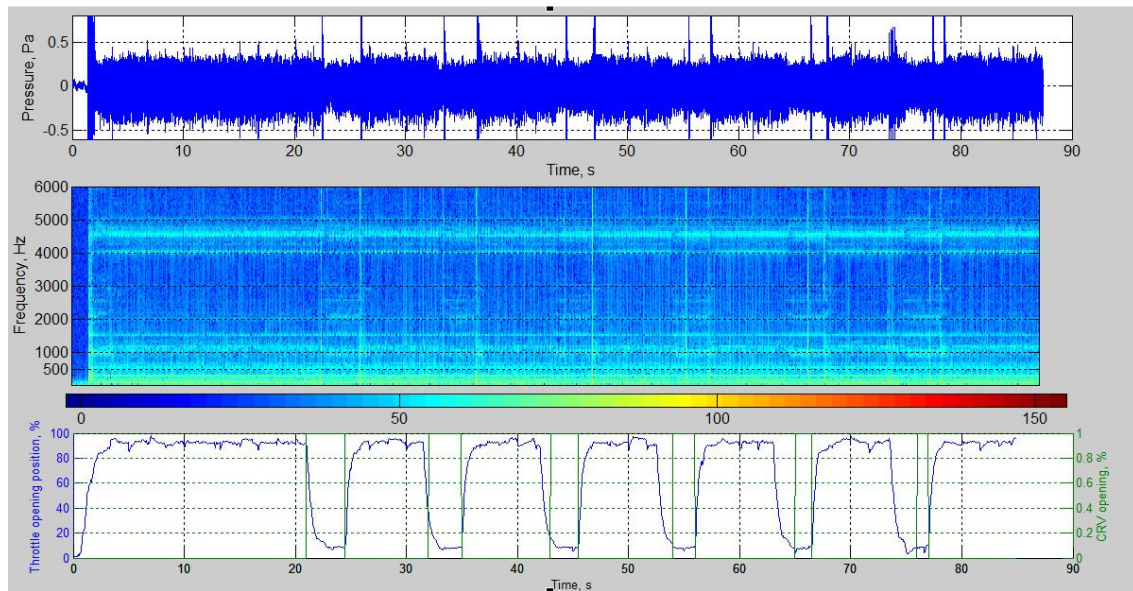
Fig. 6.5 Measurement using surface microphone at the compressor inlet pipe location –

inverter, fan, and throttle switched on. Compressor drive disconnected (Expt ref no.165)

(colour code shows the sound pressure level in dB)

6.2.6 Summary of experiments to determine background noise

The summary of the background noise experiments is given in the Table.6.1. The predominant experiments are noted and the source is identified as given in the previous sections. As all the background noise contributions are considered, the surge noise can be highlighted while doing transient and steady state experiments.

Sl No	Frequency (Hz)	Source
1	16.7	Electric motor
2	50	AC mains
3	66.7	Supercharger pulley
4	200	Throttle body
5	590, 600	Inverter fan
6	4000, 4500, 5000	Throttle body gearing, structural vibration

Table.6.1 Results of experiments on background noise

6.3 Steady state experiments

In the steady state experiments, the speed of the motor and hence the supercharger shaft speed, throttle angle position, compressor recirculation valve position are kept constant throughout. The compressor shaft speed of 30000 and 35000 rpm has been chosen as a steady state speed. The speed is chosen to clearly identify the surge occurance against the background noise. The motor speed was run at a speed of 1000 rpm and 1167 rpm to maintain a compressor speed of 30000 rpm and 35000 rpm (transmission ratio =30:1). This adjustment is done using the inverter drive which controls the motor speed. The throttle valve opening is also maintained same throughout the experiment by producing and inputting square waves of constant pulse width using the NI 6341 and the LabVIEW software. The compressor recirculation valve was kept at fully closed condition and hence there is no recirculation of air back in to the inlet. The sampling frequency for the measurements except mass flow rate has been to set to a value of 12000 Hz. The aim of the steady state experiments is to compare the noise levels and other compressor operating parameters at wide open throttle (WOT) and part throttle conditions. This will help to correlate the surge occurance and the noise occurance in the intake system. These experiments will form the base for the future transient operations. The following experiments are designed.

Compressor speed, rpm	Throttle open position (0% - fully closed, 100% - fully open)		
30000	100%	30%	0%
35000	100%	30%	0%

Table.6.2 Experiments for steady state operation

6.3.1 Wide open throttle opening

In this experiment, the throttle angle is maintained at a constant value of 100% open and the position is monitored by measuring and logging the feedback voltage from the potentiometer within the throttle body. The steady state of throttle is achieved from 13 s to 24 s as in the Fig. 6.8 and 6.9. The measurement by a surface microphone at the inlet of the compressor are processed using Short Time Fourier Transform.

The operating point of the compressor determined using the measured values of the mass flow rate of the air and the pressure ratio is overlapped on the compressor map (Fig. 6.6 and 6.7). The compressor maps presented in this chapter (steady state conditions) are not corrected for inlet temperature and pressure variations compared to that at the published compressor map data. A detailed correction procedure is explained in chapter 7. Fig. 6.6 and 6.7 shows clearly that the compressor operates at a safer surge margin, i.e. very much away from the surge line. It is also noted that the operating point closely follows the supercharger shaft speed line of 30000 rpm and 35000 rpm in Fig.6.7 and Fig.6.6.
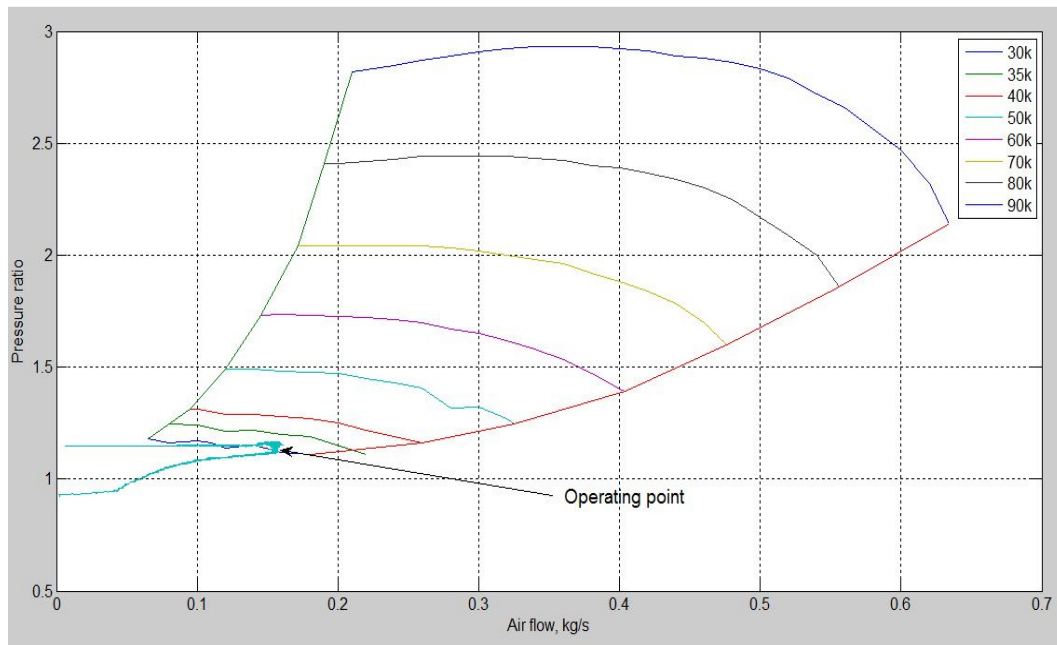
Fig.6.6 operating point of the compressor overlapped on the compressor map at WOT, 30000 rpm (expt #193)
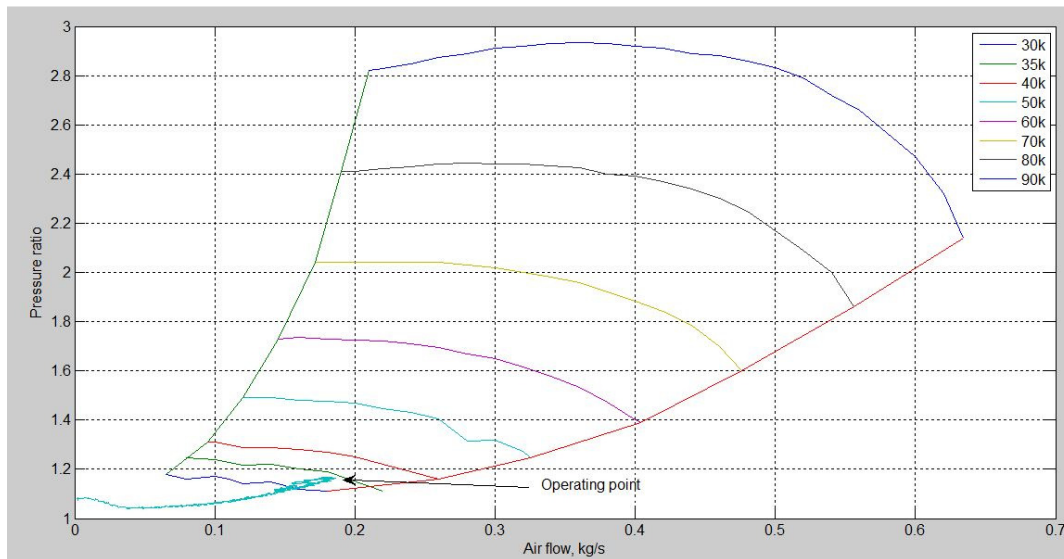
Fig.6.7 operating point of the compressor overlapped on the compressor map at WOT , 35000 rpm (expt #199)

The Short Time Fourier Transform of the surface microphone readings has been computed using MATLAB code and overlapped with other compressor parameters. Fig.6.8 shows that the mass flow rate and the pressure at the outlet fluctuates within a small range during the WOT operation. The surface microphone readings show a broad band characteristic and a constant frequency behaviour at the region of 3200 Hz, 4000 to 5000 Hz, and below 2000 Hz for both 30000 rpm and 35000 rpm experiments. The sound pressure level measured for the higher speed (35000 rpm) is much higher than the lower speed (30000 rpm). This is due to increased mechanical and flow induced noises at higher speeds.

Fig.6.8 STFT of the surface microphone measurement at compressor inlet at WOT-dB, 30000 rpm (expt #193) (colour code shows the sound pressure level in dB)

Fig.6.9 STFT of the surface microphone measurement at compressor inlet at WOT-dB, 35000 rpm (expt #199) (colour code shows the sound pressure level in dB)

6.3.2 Part throttle operation – 30% throttle opening

Throttle was closed to 30% level in this experiment. Compressor operating point move very close to the surge line compared to fully open throttle condition. Mass flow has been also reduced very much. Also there was a significant increase in the compressor output pressure ratio. The sound pressure level measured are also of a higher value than other throttle conditions. Constant frequency characteristics are observed in this operating condition for the readings of surface microphone.

The experiment with higher compressor shaft speed demonstrated a higher noise level at all conditions as given in the Fig.6.10, 6.11, 6.12 and 6.13. It is noted that the compressor operating point did not go into the surge zone. Also the STFT results did not show a characteristic higher noise level at low throttle conditions.
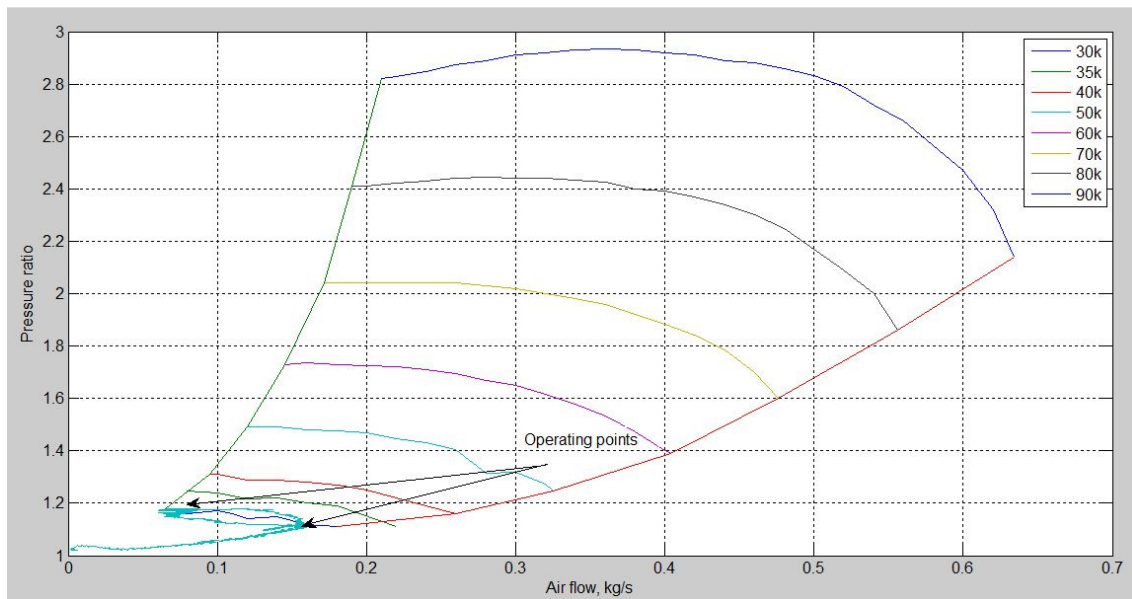
Fig.6.10 Operating point of the compressor overlapped on the compressor map at 30%, 30000 rpm - expt 190
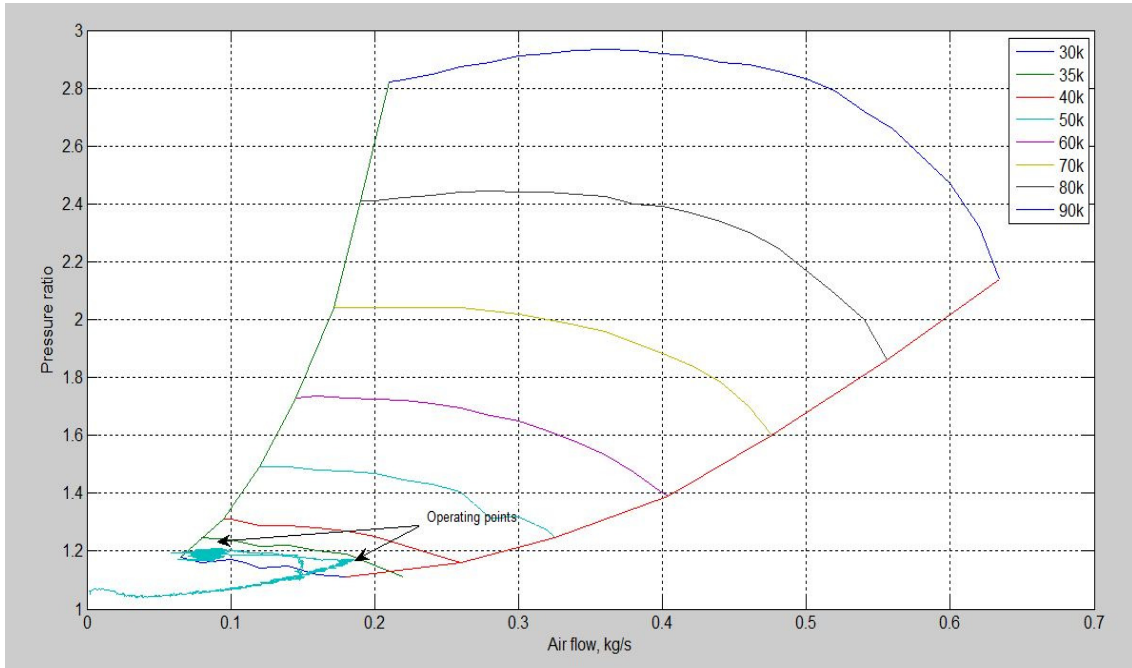
Fig.6.11 Operating point of the compressor overlapped on the compressor map at 30%, 35000 rpm - expt 196
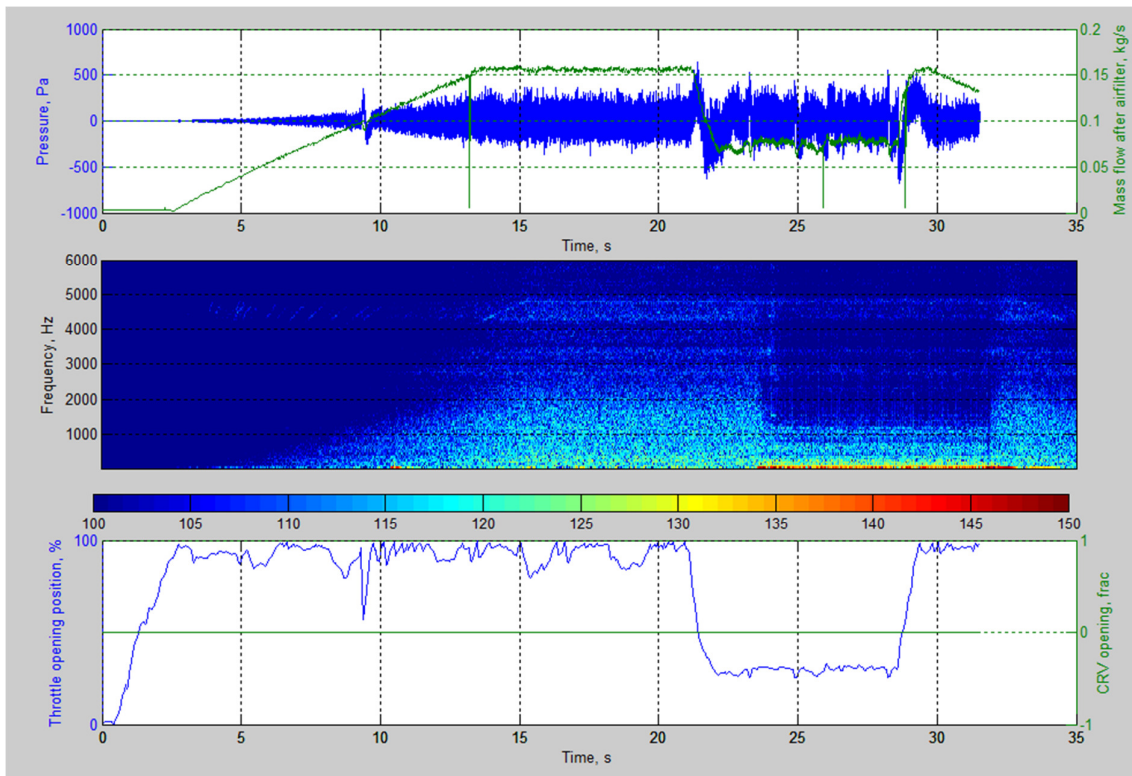
Fig.6.12 STFT of the surface microphone measurement at compressor inlet at 30% throttle opening – 30000 rpm (expt 190) (colour code shows the sound pressure level in dB)
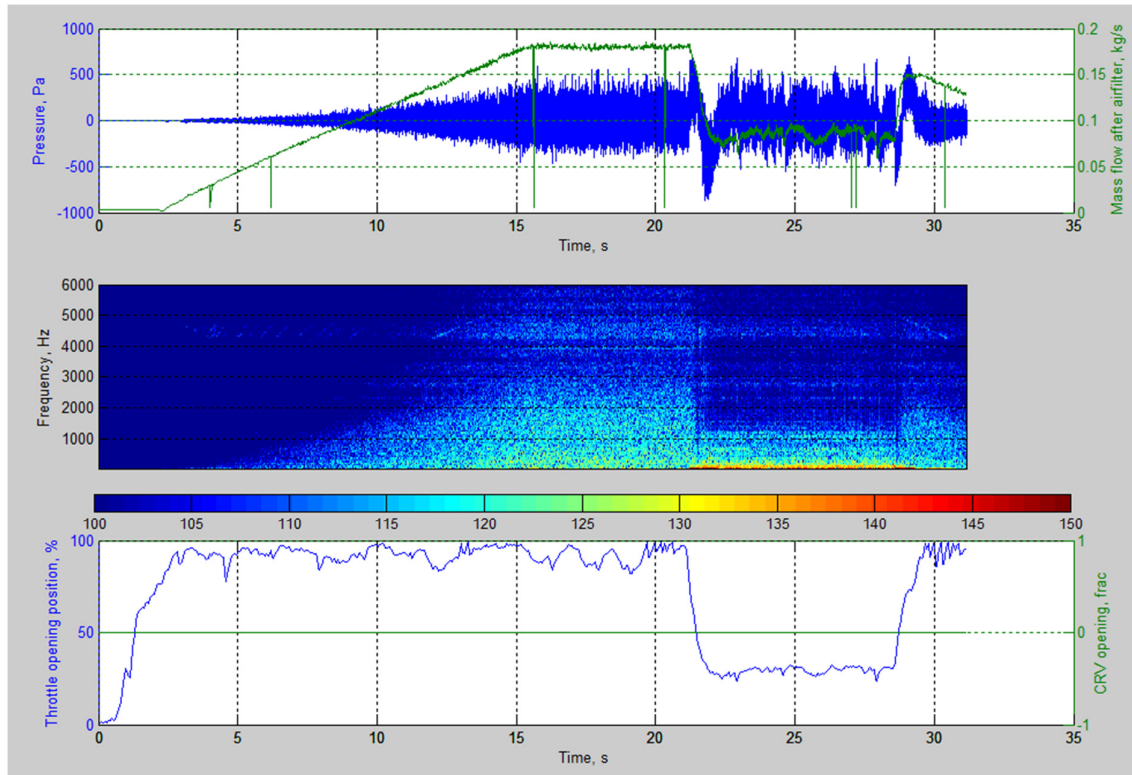
Fig.6.13 STFT of the surface microphone measurement at compressor inlet at 30% throttle opening – 35000 rpm (expt 196)

6.3.3 Part throttle operation – 0% throttle opening

Throttle was fully closed in these experiments. The mass flow of air through the intake system is reduced to lowest possible level. There is a system designed leakage of air through the throttle valve at fully closed condition. The operating point on the compressor map indicates that the compressor is working in the surge zone when the throttle is closed (Fig. 6.14 and 6.15). The STFT results (Fig. 6.16 and 6.17) shows a high amplitude noise due to surge at the region of 3250 Hz. Noise generation at this frequency is due to the flow at fully open throttle condition as evident in the previous experiment. However, when the throttle is closed, the high amplitude is created due to the flow dynamics at the surge operation.

167
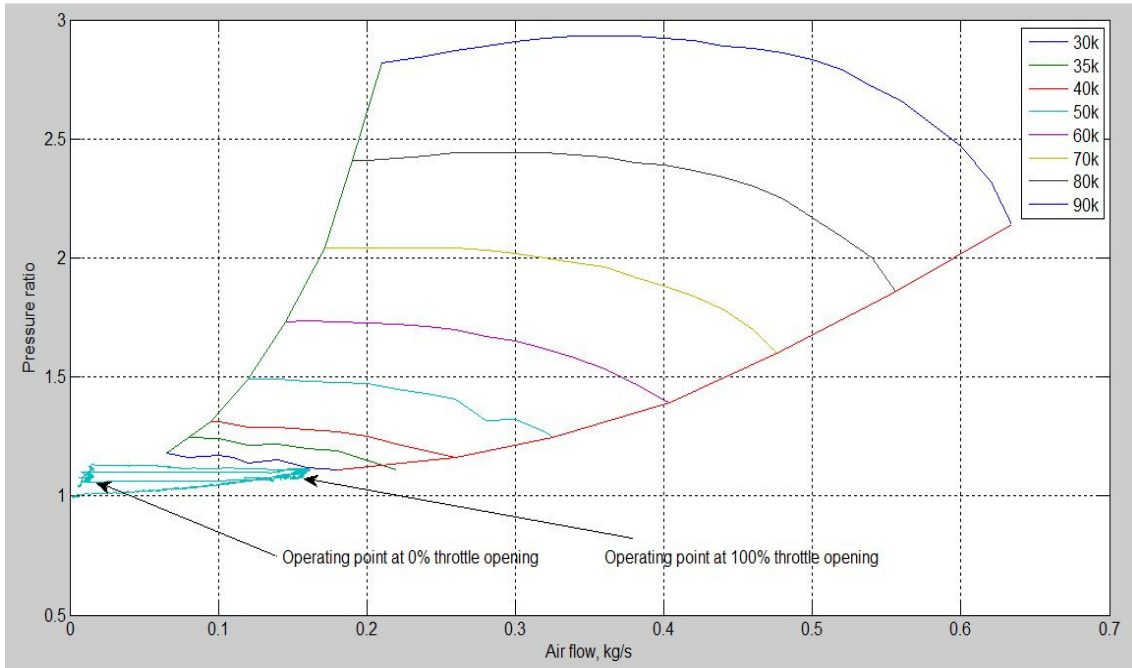
Fig.6.14 Operating point of the compressor overlapped on the compressor map at 0% throttle, 30000 rpm - expt 188
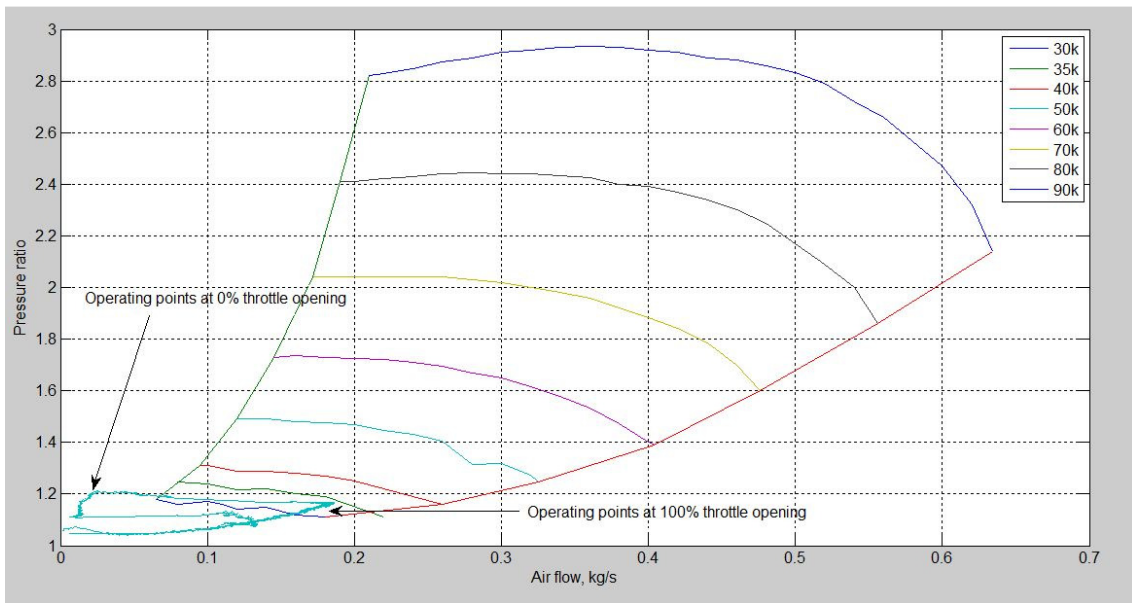
Fig.6.15 Operating point of the compressor overlapped on the compressor map at 0%, 35000 rpm - expt 194
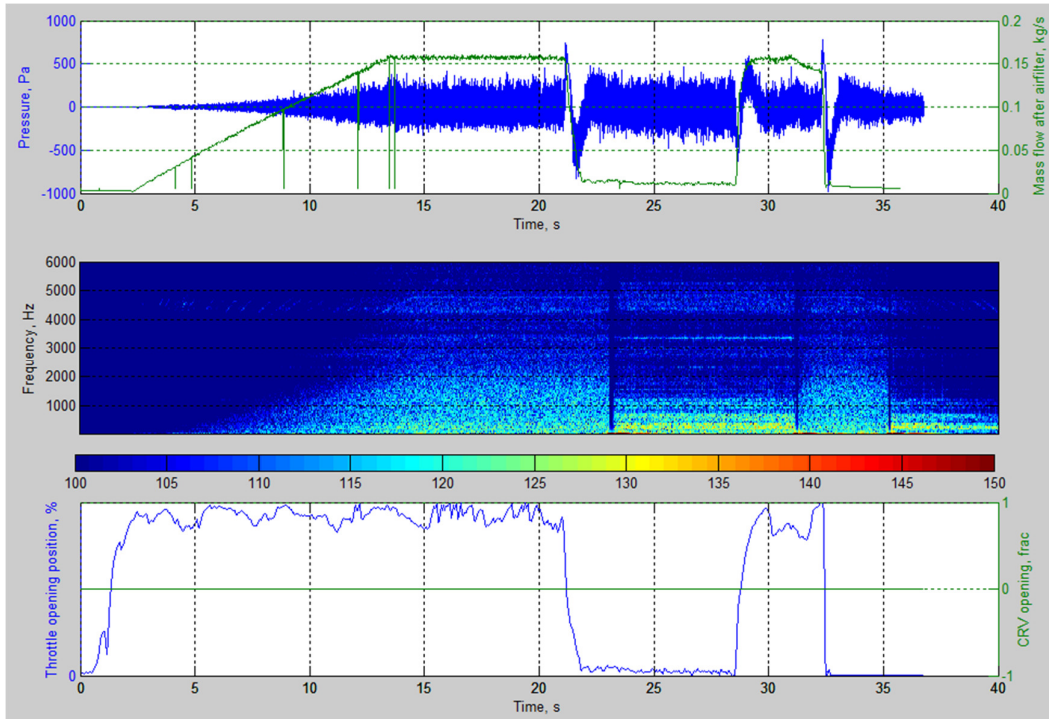
Fig.6.16 STFT of the surface microphone measurement at compressor inlet at 0% throttle

opening – 30000 rpm-Expt #188(colour code shows the sound pressure level in dB)
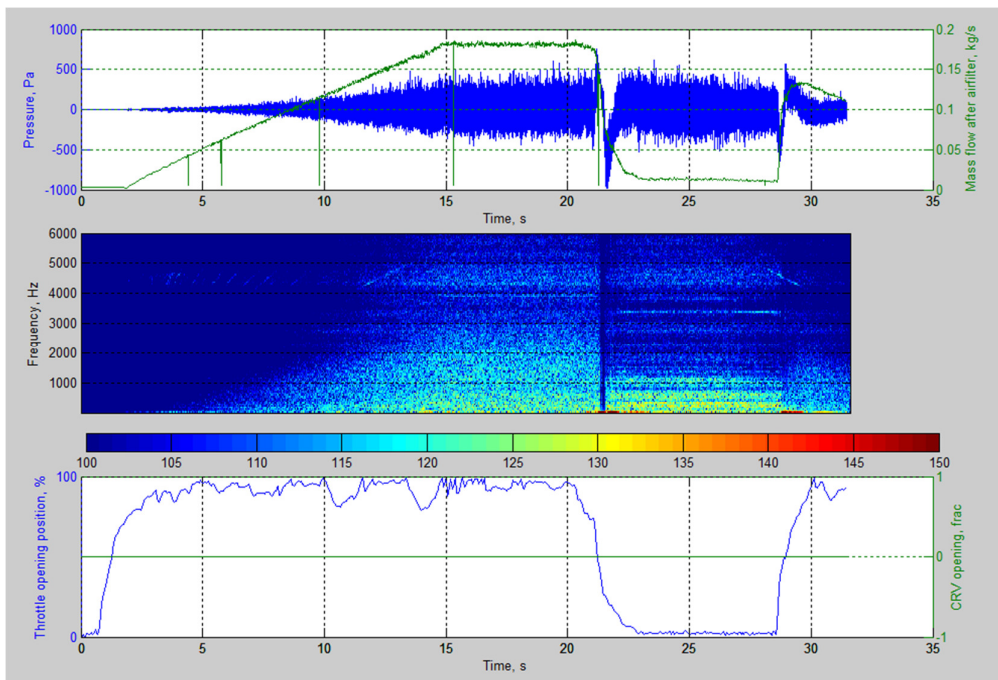
Fig.6.17 STFT of the surface microphone measurement at compressor inlet at 0% throttle

opening – 35000 rpm – Expt #194(colour code shows the sound pressure level in dB)

169

6.3.4 Summary of steady state experiments

The additional frequency content obtained during the steady state experiments using the compressor rig is added to the background noise to obtain a clear understanding of the frequency regions of interest. Surge noise is identified at 3250Hz in the steady state experiments

Sl No	Frequency (Hz)	Source
1	16.7	Electric motor
2	50	AC mains
3	66.7	Supercharger pulley
4	200	Throttle body
5	590, 600	Inverter fan
6	3250	Surge noise
7	4000, 4500, 5000	Throttle body gearing, structural vibration

Table.6.3 Results of steady state experiments

6.4 Transient experiments

Design of Experiments (DoE) [45] [46] was used to study the transient operating conditions. In DoE technique, factors are systematically varied during an experiment in order to determine their effect on the response variable. The factors chosen in the experiment can have only few values which are known as factor levels in the design. Factors can assume continuous values or specific values in the boundary condition definition. In the case of continuous factors, specific levels are chosen to perform the experiment.

The first step is to identify the factors and also the levels to be considered. The previous experiments are used to select the factors. The objective of this study is to understand the causes of surge noise generation and then lead to the analysis to find out the mechanism.

A half factorial experiment comprising of 3 factors and two levels were designed using Minitab software. The factors considered were the compressor shaft speed, throttle open position and the CRV open position. The response noted is the maximum sound pressure level measured during the lesser throttle open condition. The design of experiment is given in the table below.

Sl No	Compressor speed, RPM	Throttle open position, %	CRV open position, open or closed	Expt reference number
1	40000	0	Closed	150
2	30000	50	Closed	191
3	40000	50	Open	151
4	30000	0	Open	175

Table.6.4 Design of experiments

6.4.1 Experiment 1

Compressor recirculation valve is closed in this experiment and hence recirculation flow is blocked from the compressor outlet to inlet (Fig. 6.18). The throttle valve is closed near to 0% to reduce the air flow. The airflow is represented as green coloured curve at the top plot varies linearly with the throttle angle change. The blue coloured region in the STFT plot at the beginning and the end is due to the starting up and closing down of the experimental rig operation. The green coloured at the bottom plot represents the opening conditions of CRV. CRV remains closed for a period of 2 to 3 seconds after the throttle is closed fully. During this period the sound pressure level at the surge frequency is noted. The high energy signal in the Fig. 6.18 is reduced when the CRV is opened.
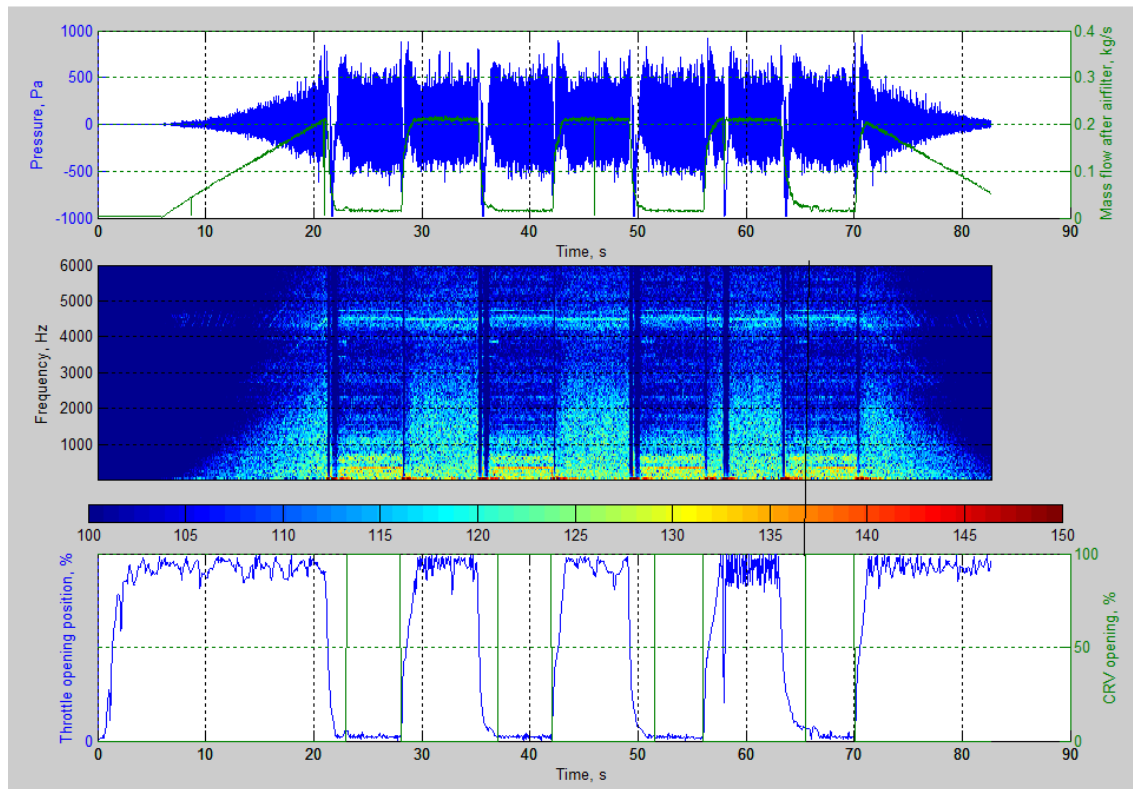
Fig.6.18 STFT of the surface microphone measurement at compressor inlet at 0% throttle opening – 40000 rpm expt 150 (colour code shows the sound pressure level in dB)

6.4.2 Experiment 2

The compressor speed is maintained at 30000 rpm and minimum throttle opening position is set to 50% and the recirculation flow is blocked (Fig. 6.19). This facilitates more air flow through the throttle valve than through the CRV. High energy noise as shown in the previous figure is not seen in this experimental result in the surge frequency region.
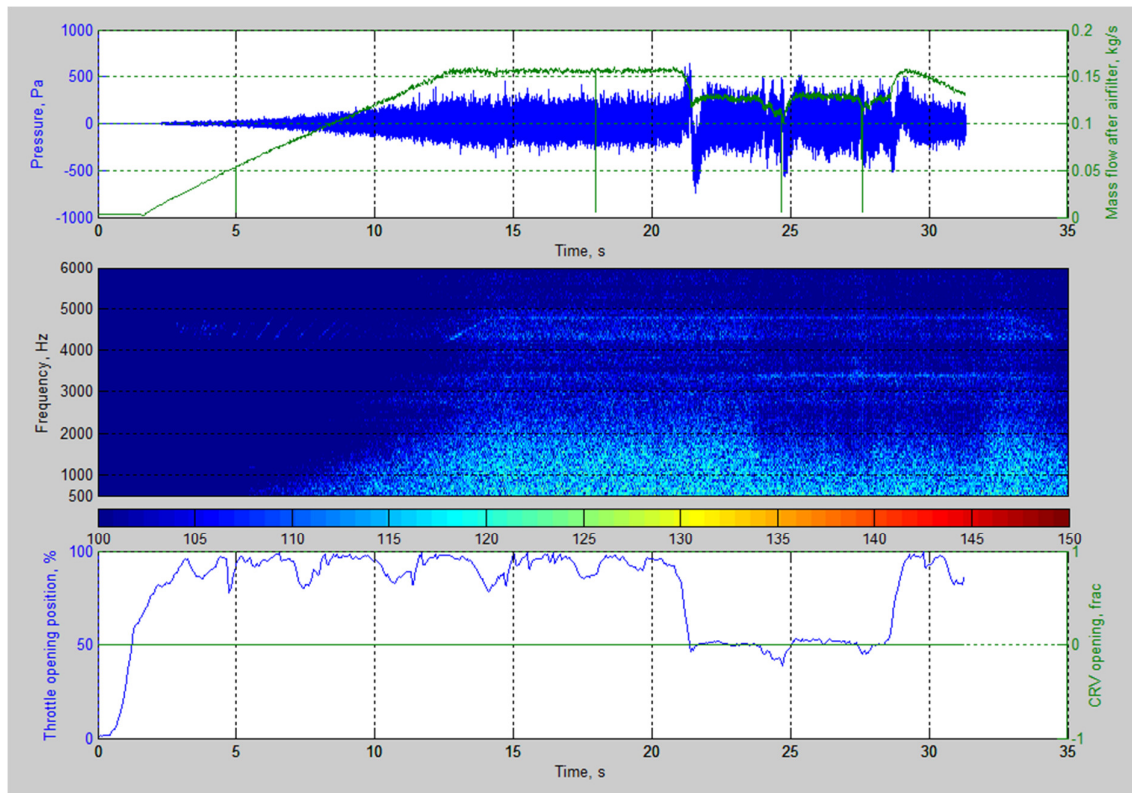
Fig.6.19 STFT of the surface microphone measurement at compressor inlet at 50% throttle

opening – 30000 rpm expt 191(colour code shows the sound pressure level in dB)

6.4.3 Experiment 3

The minimum throttle opening position is maintained at 50% and the supercharger speed is set
to 40000 rpm. The CRV is opened at lower throttle opening conditions. This experiment is
performed to see the effect of CRV opening and throttle position on the surge noise. As the Fig.
6.20 indicates, there was no high energy noise region in the surge frequency zone.
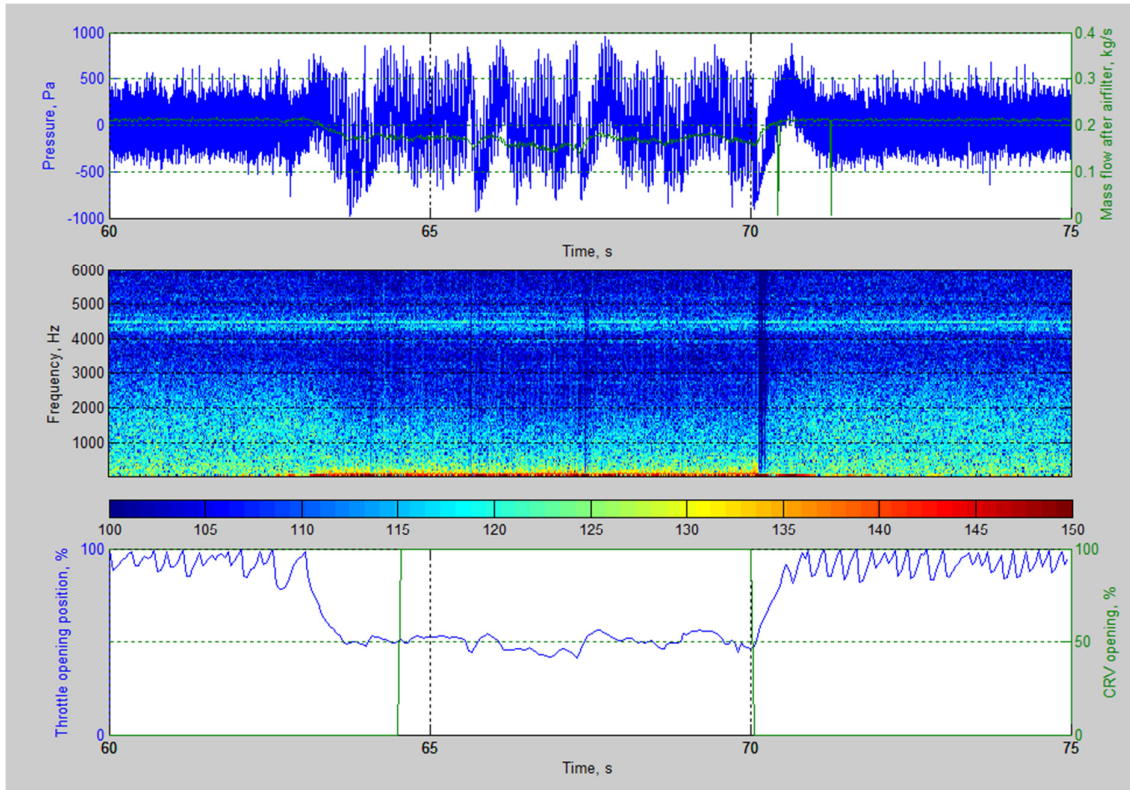
Fig.6.20 STFT of the surface microphone measurement at compressor inlet at 50% throttle opening – 40000 rpm expt 151(colour code shows the sound pressure level in dB)

6.4.4 Experiment 4

The motor speed is controlled to maintain supercharger speed of 30000 rpm in this experiment. The minimum throttle position is set to 0%, during the transient operation and the CRV is opened after a delay. As the experiment definition is to maintain the CRV in the open condition, the surge noise, if any, is measured at the region when the CRV is opened. Delayed opening of the CRV presents a clear high energy surge noise in the Fig. 6.21.
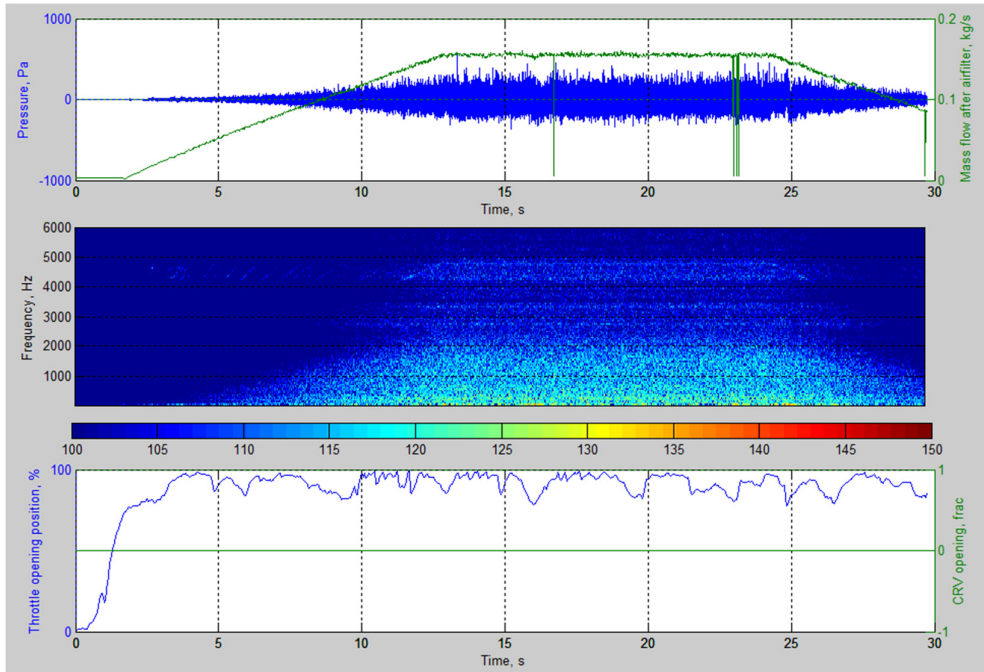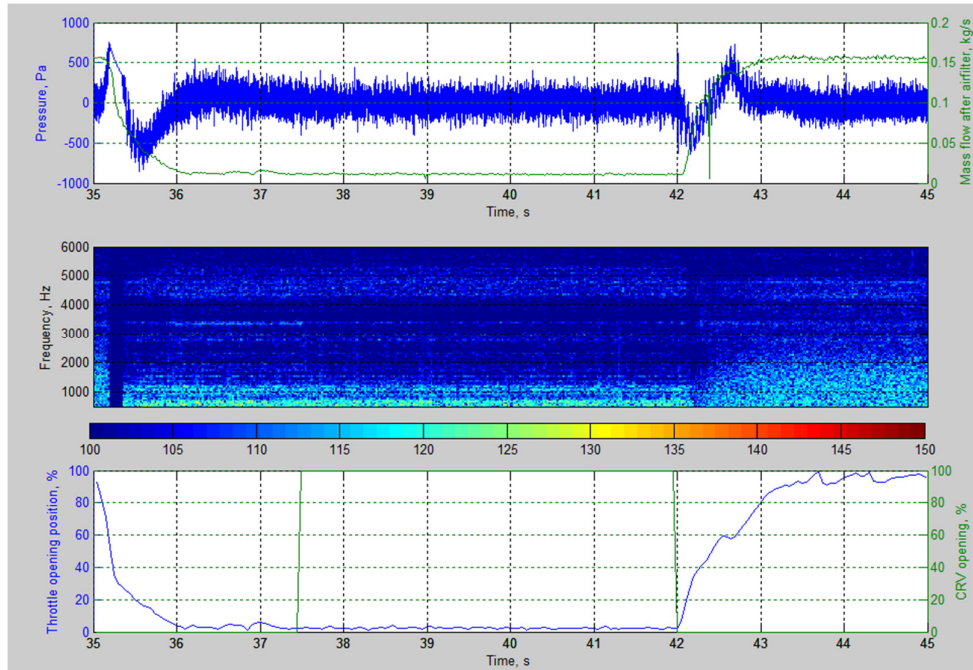
Fig.6.21 STFT of the surface microphone measurement at compressor inlet at 0% throttle

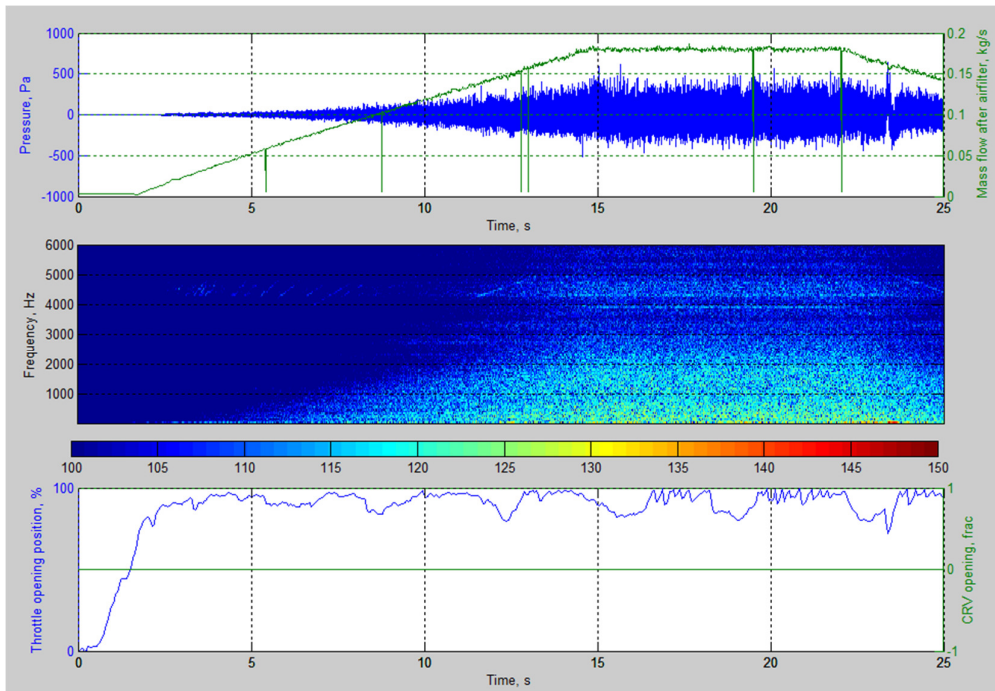opening – 30000 rpm expt 175(colour code shows the sound pressure level in dB)

6.4.5 Summary and analysis of response for the DoE

The results of transient experiments are tabulated below. The response, i.e. the maximum sound pressure level is noted for the surge region of operation and the corresponding frequency is recorded.

Sl No	Compressor speed, RPM	Throttle open position, %	CRV open position, open or closed	Sound pressure level (max), dB	Frequency, Hz	Expt reference number
1	40000	0	Closed	120.7	3450	149
2	30000	50	Closed	116.2	3400	191
3	40000	50	Open	118.6	3140	151
4	30000	0	Open	111.5	3400	175

Table.6.5 Results

The interaction of factors to generate maximum sound pressure level is difficult by just observing the results in a tabular form. Hence, a plot is generated using the ANOVA section of the Minitab software [45]. Interaction plot is used to a matrix of plots for the present set of experiments. These plots are useful for judging any interaction as they represent plot of means for each level of factor with the level of a second factor held constant. Data means are used for

presenting responses in this study. Interaction between levels of two or more factors can influence the response levels in experiments. Interaction is absent when the lines in the interaction plot are parallel. More departure from the parallel state indicates higher interaction between levels.
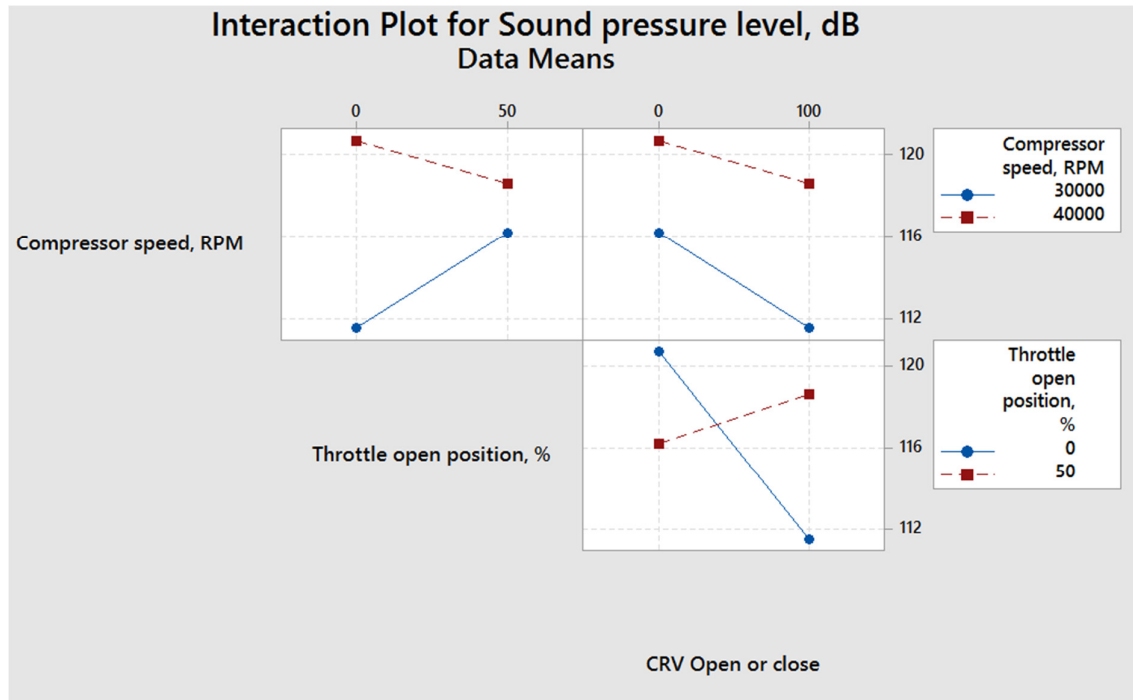
Fig.6.22 Interaction plot

6.4.5.1 Interaction between levels of compressor speed and CRV open position

The interaction plot for these factors are given in the top right hand of Fig.6.22. Observing the lines, it can be concluded that the surge noise levels are not dependent on the compressor speed variation for the same CRV open position. Hence the surge noise is likely to occur during different compressor speeds. It is noted that the surge noise amplitude is higher in the closed CRV condition irrespective of the compressor speeds.

6.4.5.2 Interaction between level of compressor speed and throttle open position

The top left hand of Fig. 6.22 represents this interaction. The lines at different levels of compressor speeds are not parallel and highly deviating from the parallel condition. This indicates a strong interaction between the throttle open position and the response. The lines shows that at 0% throttle condition, 40,000 rpm shaft speeds demonstrates a higher noise level

than the 30,000 rpm. The higher noise level at 40000 rpm is due to higher flow rate and associated dynamics. However, the noise level at 30000 rpm is lower at 0% throttle than at 50% throttle open condition. This is due to the fact that the CRV is opened at 0% throttle and this reduces the sound pressure level as per the result and the plot. At 50% throttle condition, the noise level at 40000 rpm is reduced as the CRV is opened in this case also there is no surge occurance noted.

It is derived that the throttle opening position has a strong contribution to the surge noise occurance. The lower throttle open position generates a higher surge noise. However, in actual automotive engine operations, the throttle positions can't be restricted from being closed fully.

6.4.5.3 Interaction between level of throttle open position and CRV open position

The interaction plot for this section is provided in the bottom right of the interaction plot matrix. The blue coloured line which is for the throttle fully closed condition, shows that CRV opening condition has a strong influence on the response. CRV fully closed position creates a higher sound pressure level at fully closed throttle condition. The sound pressure level is reduced considerably when the CRV is opened at the same throttle condition.

CHAPTER 7
Design of a passive solution to reduce the surge noise

7.1 Introduction

In the previous chapter, the procedure used to prepare the experimental rig was explained. The background noise was measured and the design of experiments were completed to find the effect of components on the acoustic response of the supercharger under surge conditions. The design of experiments suggested that the compressor recirculation valve (CRV) opening and throttle opening have more effect on the creation of noise.

In automotive product development process, the engine is developed from concept stage to final mass production stage using design gates. Usually, the initial phases of the product do not involve extensive testing of engine components such as turbochargers for design verification. Also, most of the time initial tests are done using prototype parts and not final design parts. During the initial and intermediate design and development phase, the intake system and turbocharger components could change due to calibration, packaging, manufacturing, aesthetic and service requirements. As a result, the operating characteristics of turbocharger could change. This can create surprises such as turbocharger surge noise during the later phase of the development. During this stage, modification of the individual components is very difficult and costly as it involves expensive tooling changes, iteration of other processes and delay in the launch of the vehicle. Hence normally, quick solutions are arrived by the component engineers to solve the problem. Most of the time, the solution is costly in terms of the component cost. This cost involved multiplies as the mass production ramps up. Hence, identification of the problem during the initial stages of the design is very important. Also, solution to the problem is equally important. This chapter focusses on the detailed investigation to the identification of the problem and also to find a solution which is less costly without affecting the performance of the engine.

The methodology followed in this chapter is given in the Fig. 7.1. The first major step is to identify the problem and is completed in the previous chapter. The next step is to characterise

the changes in the throttle angle, delay in CRV opening and the speed of the supercharger against the noise generated. This is an important step to find out the mechanism of noise generation. A parallel step is planned to verify the results using simulation software. From further analysis of results, development of a cheaper solution is planned and then validation on the experimental rig. A further step is to include the solution on engine simulation software to understand the effect of engine performance before and after implementation of the solution. The aim is that the solution do not affect the engine performance.
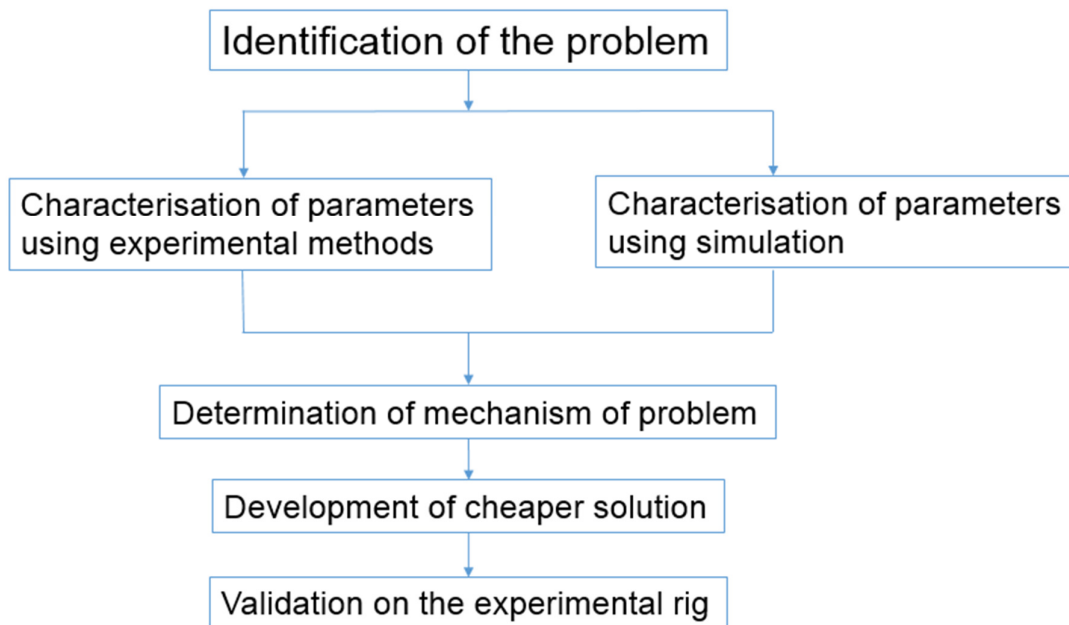
Fig. 7.1 Flow chart for the solution methodology

7.2 Characterisation of the problem using experimental method

The problem defined here is the level of sound pressure observed during the transient manoeuvre. The aim of this study is to identify the effect of finer levels of noise generating factors identified during the DoE explained in the previous chapter. The first step of this process is to identify the factors to be considered. The identified factors can then be varied in the experimental rig to arrive at the effects on the response, which is the sound pressure level. As the experimental rig is modular, the factors can be individually varied using LabVIEW software. Specific variations to the functioning of the individual components can be made by changing the input parameters to the components.

7.2.1 Identification of factors

Some literatures [6] [14] identify that the operation of the compressor in the surge and the near surge zone is the cause of the surge noise. One solution to the problem is to select a compressor with a wider compressor map to constrain the operation within the stable zone. However, during dynamic engine operations [6], there could be instances of operating point crossing the surge line, momentarily. Hence, instead of focussing on the enhancement of the map width, factors and mechanisms causing the problem were explored.

The interaction plot in the previous chapter concluded that the CRV opening and the throttle position have major influence on the noise generation. Hence these factors were chosen for characterisation study. The throttle valve position and CRV are near the source of the noise generation and hence studying the effect of the variabilities of these factors will be very useful for understanding the problem in detail. The objective is to identify the noise occurance by varying these factors in steps. The amplitude of the noise and the frequency of occurance will be noted.

Characterisation of noise occurance against factors helps to identify the solution to reduce the influence of noise occurred by these factors. In other words, the factors can be controlled to reduce the noise occurance. Independent effect of these factors on the problem can be understood using this method.

7.2.2 Characterisation of noise against CRV position – delay in opening the CRV

The temperature inlet to the cylinder of the internal combustion engines, is an important consideration in the petrol engines. The maximum temperature level is aimed to be maintained below a threshold level. If the temperature crosses a defined level at the given engine operating conditions, it could lead to knocking and will be detrimental to the engines. Hence, a compressor recirculation valve (CRV) as defined in the Fig.7.2 is used in the automotive petrol engine [10].

CRV can be operated by various means and mechanical as well as electrical means are the commonly used ones. In the case of a mechanically operated CRV, pressure difference between two chambers, i.e. primary and secondary chamber is used to control a diaphragm which is

loaded with a spring. The primary and secondary chamber pressures are maintained by the boost pressure (compressor outlet pressure) and the atmospheric pressure. The diaphragm operates the opening and closing position of a valve. The operation of this valve recirculates the high pressure air from the compressor outlet to the atmosphere or back to the compressor inlet. The leakage of high pressure air back into the atmosphere limits the charge air temperature into the cylinder.
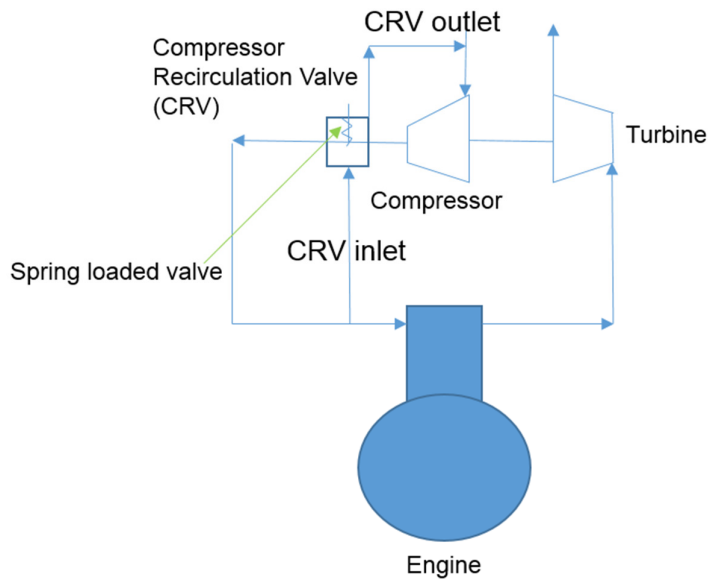
Fig. 7.2 Schematic representation of a mechanical CRV in the intake system of an IC engine

As explained in the previous chapter of literature review, surge noise is caused at high load and low speed operating conditions. It can also occur when the throttle is moved from the fully open condition to closed condition in transient engine operation in the case of petrol engines. CRV is functional in the case of this sudden transient tip-in to tip-out manoeuvre by the throttle valve. When the pressure downstream of the CRV is increased by means of sudden closure of the throttle valve, the CRV is forced to open and the excess air is recirculated back to the compressor inlet.

The response time of the mechanical CRV to the change in the intake manifold conditions, is highly dependent on the individual components such as chamber volume, diaphragm property, spring rating and also the pre load. There could be considerable delay in the operation of the CRV during the tip-in and tip-out manoeuvre of the throttle. Ideally, the CRV must start to leak the air as soon as the throttle is moved from fully opened to fully closed condition to avoid the compressor going into the surge zone of operation and thereby reduce or avoid the surge noise.

Electronic CRV is costlier alternative part to the mechanical CRV. It is operated by using a solenoid valve to recirculate the airflow. The electronic control unit of the engine controls the activation of the CRV during the defined operation time. In the present experimental rig, an electronic CRV is used to simulate a mechanical valve. By this approach, the mechanical complexities involved can be avoided and purely functional part of the valve operation, i.e. the delay in lifting and closing of the valve, can be focussed up on. The definition of delay is given in the following Fig. 7.3. The opening delay is defined as the time delay for the CRV to fully open from the start of closure of the throttle valve and the closing delay is defined as the time between the CRV start to close to throttle start to open. The delay in the opening and closing of the CRV is due to insufficient pressure and insufficient mechanical properties to force open the valve. In the case of the electronic CRV used in the test rig, delay can be introduced to study the effect on the noise generation.
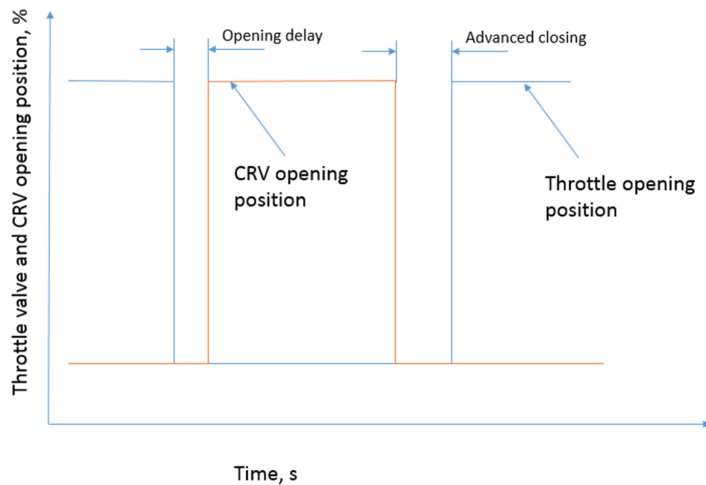
Fig. 7.3 Delta T, i.e. delay in opening or advancement in closing of CRV compared to throttle position

7.2.2.1 Experiments to determine the effect of CRV opening delay and the effect on the surge noise

So far in this chapter, the importance of characterisation of each factors on the effect i.e. amplitude of surge noise is described. The characterisation of each factor will result in identifying the major contributors to the noise. Further, the influence of design/operational aspects of each factor or component on the noise can be quantified. This will help to modify or optimise the design of the component or to change the operational parameters to reduce the noise.

In this section of the chapter, the effect of CRV is analysed by varying the time to open the valve after the start of closure of the throttle. The setup of the experimental rig was maintained same as described in the previous chapter (chapter 6). The profile of the throttle valve was defined using a excel spreadsheet. The data in the spreadsheet was processed using the LabVIEW software and the algorithm in the programme is used to delay the opening of the CRV as per the design of experiments. The entire process is automated and the results are acquired during the experiment using the NI modules and the LabVIEW software as described in the previous chapters (chapter 5 and 6). The following table (Table. 7.1) shows the details of the experiment conducted. The speed mentioned is the speed of the supercharger shaft during each experiment.

Speed (RPM)	40000	30000			
delta T (s)	0	0.5	1	1.5	2	2.5

Table.7.1 Range of speeds and delta T considered for the experiments

7.2.2.2 Experiments at 30000 RPM – 0s delay after throttle closure

The supercharger speed of 30000 rpm is selected for describing the effect of delay in the CRV opening on the level of noise. The supercharger shaft speed is regulated to 30000 rpm by maintaining the motor speed to 1000 rpm (transmission ratio 30:1). Fig. 7.4 explains the transient manoeuvre of the throttle valve and the CRV. The throttle opening position and the CRV opening condition is represented in the percentage units. The throttle is opened to 100%

and CRV is closed to 0% in the initial stage. In the first cycle, approximately at 20th s, the throttle valve is closed to 0%. The throttle valve is opened at 28th sec. In this experiment, the CRV is opened instantly as soon as the throttle valve is closed to 0%. There was no delay introduced from the moment throttle valve is closed to the moment CRV is opened. It can be noted in the Fig.7.4 that the throttle valve moves from 100% to 0% almost instantaneously. This defines the transient tip-in manoeuvre. This ramp of the throttle profile is controlled by the profile input into the LabVIEW software by controlling the pulse shape transmitted to the motor of the electronic throttle valve. As the CRV is operated by solenoid, the motion of the CRV from the closed to the open position is almost instantaneous and there is almost no ramp present in the manoeuvre. Hence, the effect of delay in the time between CRV start to open and CRV close is almost zero and has no effect on the experimental outcome. When the CRV is opened, the high pressure flow recirculates from the high pressure side of the compressor to the low pressure side of the compressor, i.e. the inlet side of the compressor. The above mentioned cycle is repeated at close intervals.

Fig.7.4 also shows the mass flow (green curve) through the air intake system (measured at the air filter). As expected, the mass flow is reduced to a very low value when the throttle valve is closed from the fully open condition. The mass flow is reduced to a very low but not zero as there is air flow through the system even at the closed condition of the throttle valve.

The green curve in the Fig.7.4 represents the sound pressure level measured at the intake system during the throttle tip-in and tip-out manoeuvre. It is noted that when the throttle is in open condition and during higher mass flow rate, the sound pressure level amplitudes are of lower values. The maximum sound pressure measured in this region are of the order of 250 Pa. The amplitude considerably increased when the throttle is closed and the maximum value observed is in the region of 500 Pa.

Fig. 7.4 also shows the Short Time Fourier Transform (STFT) of the sound pressure measured as described above. From the back ground noise observed in the previous chapter, it was understood that the surge noise occurs in the region between 3000 to 4000 Hz. The maximum noise observed in the throttle fully closed region is 112.6 dB and at 3190 Hz. There was very less surge noise energy observed from the Fig.7.4.
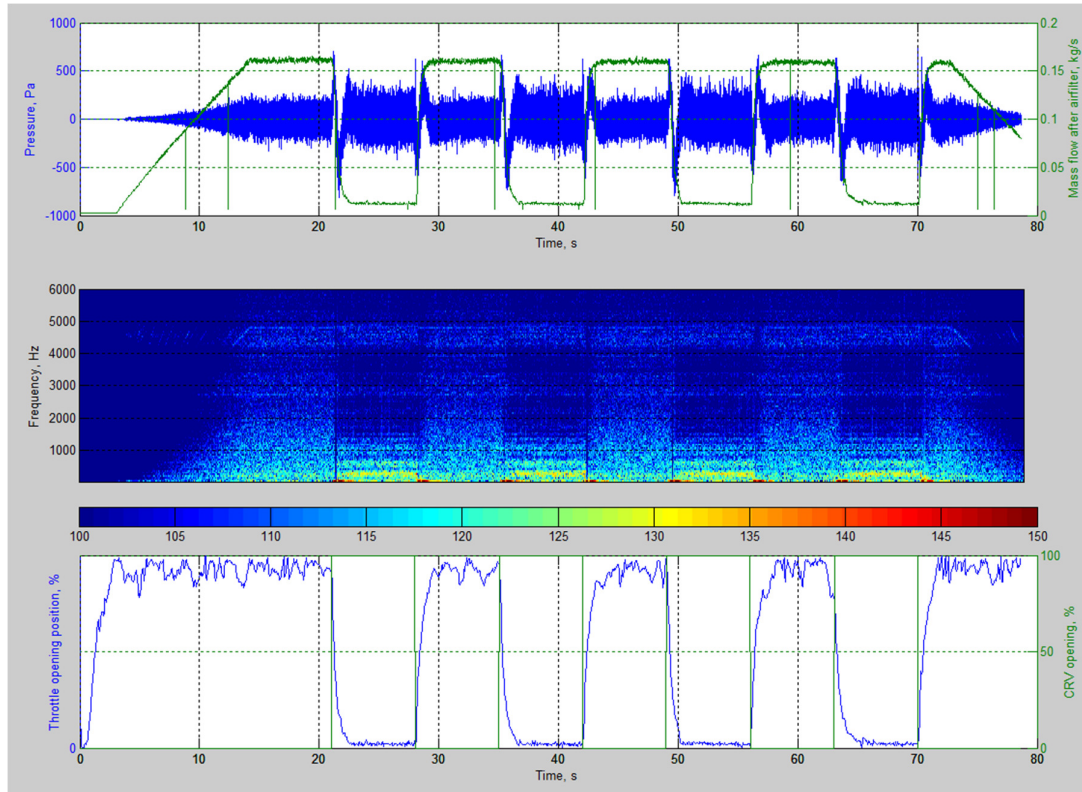
Fig. 7.4 STFT of the surface microphone data measured – during 0s CRV delay – Expt #124 (colour code shows sound pressure level in dB)

As explained in the previous sections, the mass flow is measured at the air filter and the mass flow through the compressor increases as explained in the following figure (Fig. 7.5) when the CRV is opened. The air flow direction is represented in the form of arrows in the diagram. Assuming no leakage in the experimental rig, the air entering the rig through the air filter must leave through the pipe fitted on the outlet of the rig. The mass flow rate at the entry of the air intake system is given as mf_{air} in kg/s. As a portion of air is recirculated between the compressor outlet pipe to the compressor inlet pipe(Fig. 7.5), the air flow entering the compressor is a sum of air flow through the recirculation pipe (mf_{crv}) and the mass flow entered through the air filter (mf_{air}). At the outlet of the compressor, the portion of air flow i.e. mf_{crv} is recirculated back to the inlet of the compressor. The original air flow entered into rig, mf_{air}, exits through the system outlet. The mass flow through the compressor recirculation pipe (mf_{crv}) is assumed to be 80% more than the mf_{air}, as obtained from the simulation.
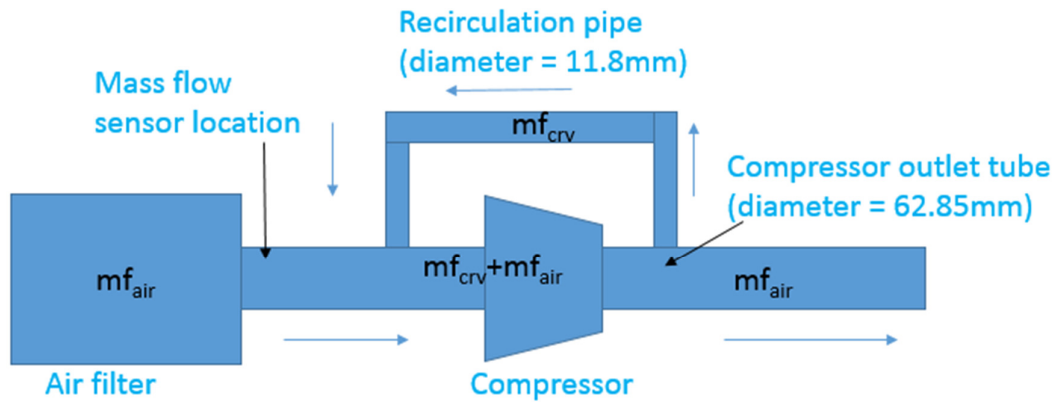
Fig.7.5 Schematic diagram of the experimental rig explaining the mass flow rate through the pipes.

The compressor map is shown in the Fig. 5.9. The original compressor map published by the manufacturer of compressor is measured on a gas stand at a reference compressor inlet temperature of 15 deg C and Pressure 101.3 kPa. Normally, during the generation of the map on a gas stand test rig, this reference pressure and temperature is maintained at a constant value. However, in an actual automotive engine, the actual temperature and pressure at the compressor inlet will be of different values. The same concept applies to the present experimental test rig used for the noise measurement. Also, at transient operating conditions of the test rig, in this map, the airflow is corrected to the inlet temperature and inlet pressure. The detailed procedure adopted is as follows [2] [10].

In the experimental test rig, pressure and temperature at the outlet of the compressor and the temperature at the inlet of the compressor is measured. The pressure ratio of the compressor is calculated as

$$PR = P_2 / P_1 \qquad - \qquad 7.1$$

PR – pressure ratio,

P_2 – total pressure at the inelt of the compressor

P_1 – total pressure at the outlet of the compressor

Pressure-volume diagrams are conventionally used to represent the Otto and Diesel cycles whereas, temperature-entropy (T-s) plot is used in the case of compressor and turbine [2] [10]. The ideal compressor and turbine operation is isentropic and also reversible. The isentropic process is represented as a vertical line in the T-s plot. In the case of original compressor as in the present experimental rig, the process is irreversible and also results in the increase of entropy at the end of the compression. The ideal processes are identified as bold lines in the Fig.7.6 and the real processes are shown as dashed lines.

Fig.7.6 T-s diagram of the compressor [10]

Efficiency of a compressor is defined by Watson et al. [2] as the ratio of the work required for ideal (isentropic) compression divided by the actual work. A common reference of same pressure ratio is considered for the numerator and the denominator. Using second law of thermodynamics, this definition is used to define the compressor isentropic efficiency

η_c =work (isentropic)/work (actual)

The compressor isentropic work and the actual work is derived from the first law of thermodynamics. The steady flow energy equation derived from this law is given as:

$$\qquad\qquad\qquad\qquad\qquad\qquad\qquad\qquad - \qquad 7.2\ [2]$$

Subscript 1 defines the inlet condition and 2 defines the outlet condition

Where

$\dot{Q}$ - heat transfer rate to the system

$\dot{W}$ - work transfer rate from the system

$\dot{m}$ - mass flow rate

h - specific enthalpy

KE - specific kinetic energy

PE - specific potential energy

The potential energy change is assumed to be negligible. Hence the equation is modified to

$$\qquad\qquad\qquad\qquad\qquad\qquad - \qquad 7.3\ [2]$$

The stagnation enthalpy is defined as

$$\qquad\qquad\qquad\qquad - \qquad 7.4\ [2]$$

The steady flow energy equation is modified to

$$\qquad\qquad\qquad\qquad - \qquad 7.5\ [2]$$

Since the heat transfer from the compressor is negligible and usually difficult to measure, it is usually neglected. Thus,

$$\qquad\qquad\qquad\qquad - \qquad 7.6\ [2]$$

As the air is used as a working medium in the compressor and is considered to be perfect or semi perfect gas, the equation of state is obeyed.

$$\qquad\qquad\qquad - \qquad 7.7\ [2]$$

Specific heat capacities are defined as

$$\boxed{}$$ -   7.8 [2]

$$\boxed{}$$ 7.9 [2]

where

$$\boxed{}$$

For a semi perfect gas, the specific heat capacity are functions of temperature only

$$\boxed{}$$ -   7.10 [2]

and

$$\boxed{}$$ -   7.11 [2]

$$\boxed{}$$ -   7.12 [2]

The reduced SFEE equation now becomes,

$$\boxed{}$$ -   7.13 [2]

The definition of isentropic efficiency can be given as

$$\boxed{}$$ -   7.14 [2]

For isentropic compression, the inlet and outlet pressure and temperature are related by the expression

$$\boxed{}$$ -   7.15 [2]

Where

$\gamma = c_p / c_v$ is the ratio of the specific heats

Substituting this in the equation for compressor efficiency

$\eta \boxed{}$ -   7.16 [2]

Rearranging the above equation,

$$\boxed{}$$

7.17 [2]

-    7.18   [2]

-    7.19 [2]

-    7.20 [2]

The pressure inlet at the compressor is calculated from the above equation from the measured values of pressure outlet, temperature inlet and temperature outlet. The compressor efficiency is looked up from the compressor map for that operating point.

Once the pressure inlet value is known at any time instant, the pressure ratio for that time instant is calculated from

$PR = P_2 / P_1$

The next required parameter to be corrected is the mass flow. As the mass flow originally measured from the gas stand by the supplier and that measured during this experiment is from different source and different setup, it is important to represent mass flow as a function of temperature and pressure. In this case, the temperature and the pressure are the variables needed to define the mass flow in the form of a mass flow parameter [7]. Independent variables are used by Watson et al. [2] to express the parameters of compressors such as mass flow rate

The parameters thus reduced are [2]

The values of R and γ are specified for different gases (air and exhaust) passing through the turbocharger, the group of parameters become [2]
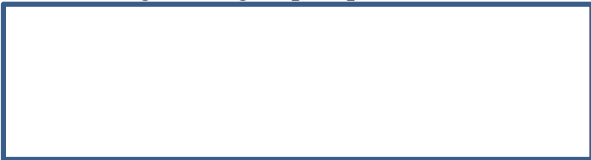
The Reynolds number is expected to have a little effect on the performance of the machine, the groups now become [2],

For this compressor, the diameter (D) is a constant and may be ignored. And also, the working fluid using this experimental rig is air. This reduces the above parameters to [2]

Using the above parameters the compressor map can be re-plotted to represent the current inlet conditions in the experimental rig. Also the mass flow can be represented in the form of mass parameter with the unit kg/s T^{-1}/MPa. The original compressor map supplied is modified in terms of mass flow by multiplying the parameters in the x axis with the constant parameter of

$$\frac{\sqrt{(15+273)}}{0.1013}$$

The advantage of this process is that the compressor map supplied by the manufacturer can be adopted to the present laboratory ambient conditions.

The next step is to convert the measured values of the mass flow into mass flow parameter. The mass flow is measured at the air filter side at a different sampling rate than that of the pressure and temperature measurement at the inlet of the compressor. This is due to the limitation of the hardware and data acquisition system used for the measurement of massflow. Hence interpolation technique has been used by the application of MATLAB using the command interp1 and a spline function. The original mass flow data and the interpolated data is shown in Fig.7.7 and Fig.7.8
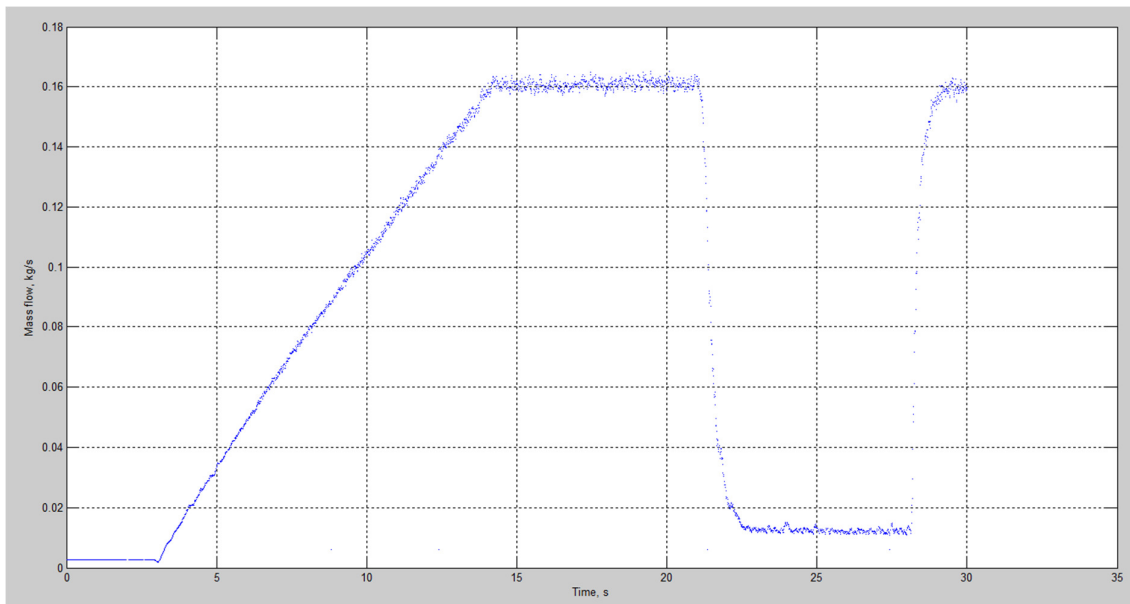
Fig. 7.7 Original mass flow sensor data
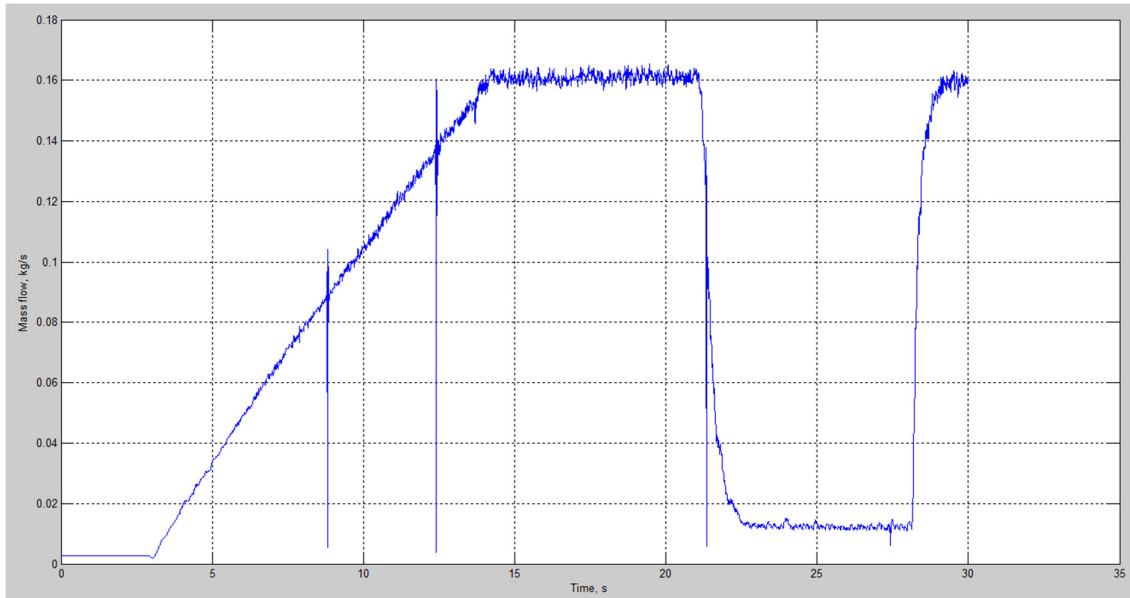
Fig. 7.8 Interpolated mass flow sensor data

The mass flow parameters for the experiments are determined using instantaneous temperature inlet, pressure inlet and the interpolated mass flow data. During the experiment, if the CRV is closed, the mass flow through the compressor is equal to the measured values by the mass flow sensor. However in the event of CRV open condition, the mass flow is assumed to be 1.8 times as measured by the mass flow sensor. This is due to the additional mass flow through the compressor due to the opening of the CRV. The new mass flow parameter thus calculated, represents the actual mass flow through the compressor. The operating points is plotted on the corrected maps as in the Fig.7.9.
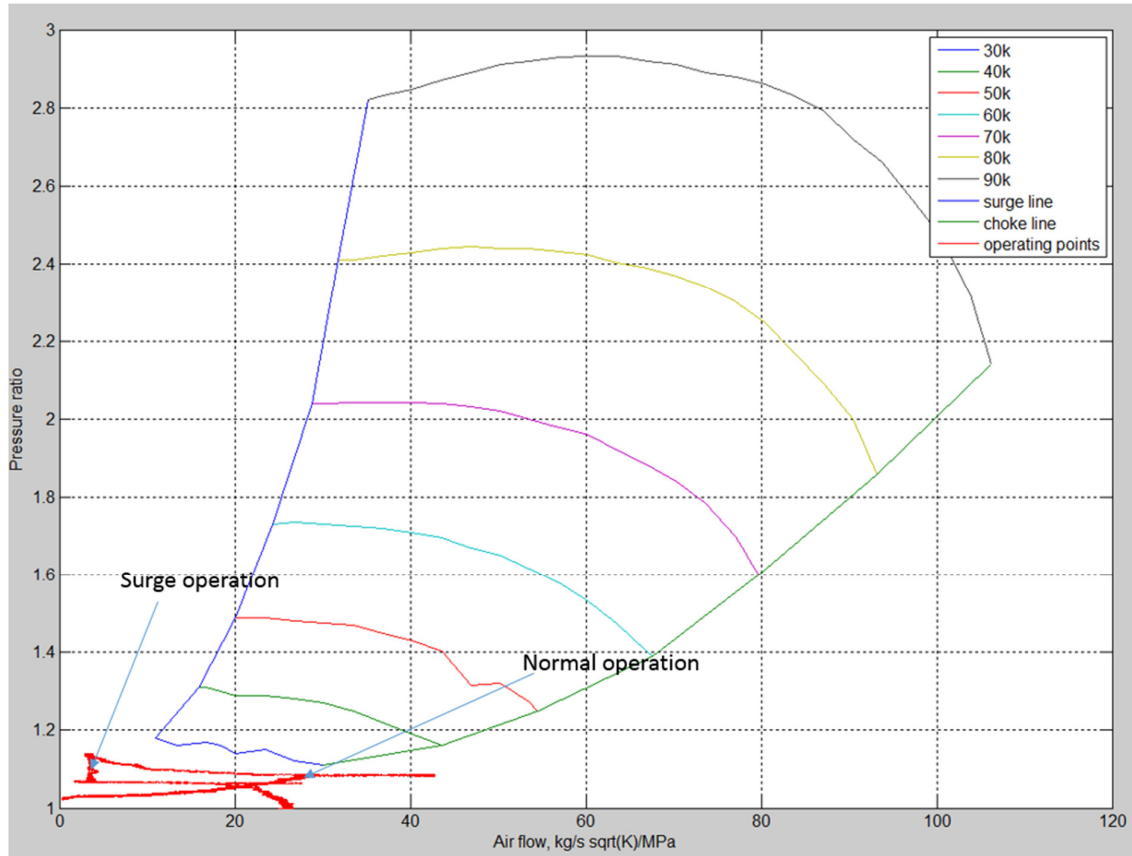
Fig.7.9 Operating points on the compressor map at 30000 rpm – 0s delta T-expt #124

The normal operating points represent during the 100% throttle valve open condition. However, as the throttle is closed, the operating points move to the surge zone. The compressor recirculation valve open condition helps to maintain the flow not to go to the much deeper surge position.

7.2.2.3 Experiment at 30000 RPM – 1.5s delay after throttle closure

This experiment is performed to understand the effect of delay in the start to opening of the CRV in the occurance of surge noise. By using an input excel (.xls) profile, a delay of 1.5 second is introduced for the CRV opening as in the Fig.7.10.
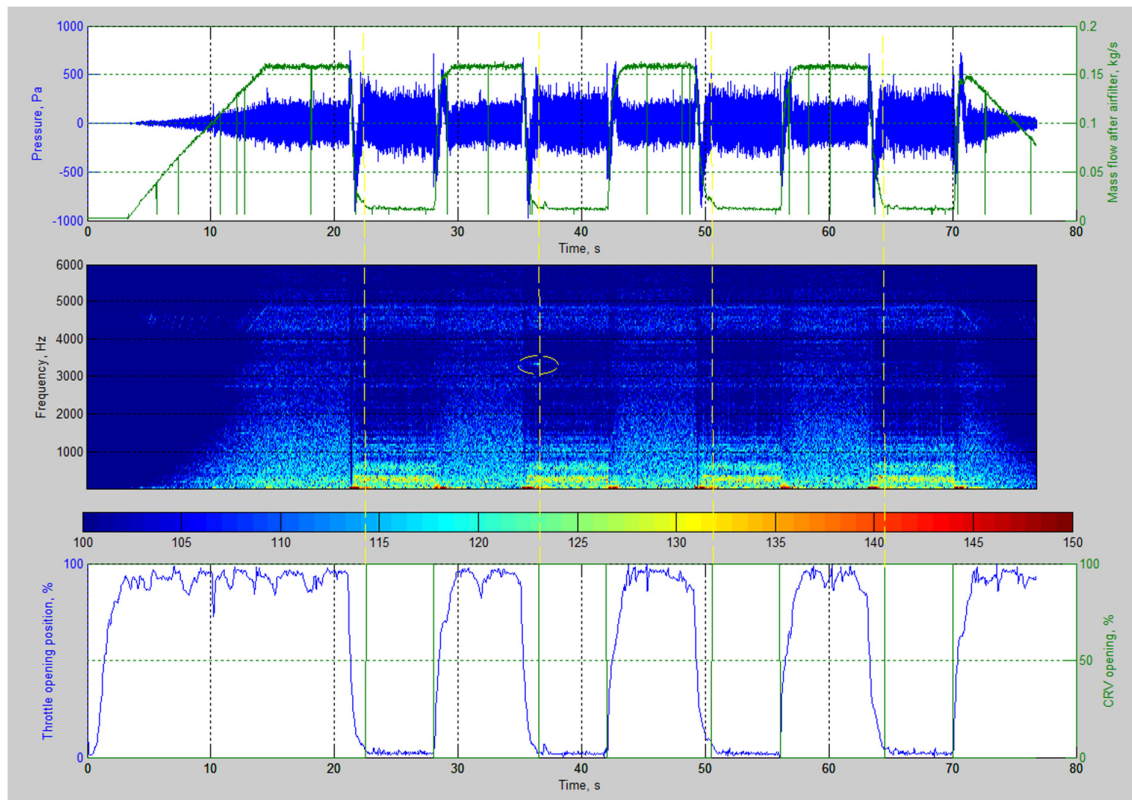
Fig. 7.10 STFT of the surface microphone data measured – during 1.5s CRV delay – Expt #127- (colour code shows the sound pressure level in dB)

As in the previous experiment, as the supercharger shaft speed increases from rest, the mass flow and sound pressure level increase to a maximum value (at 13 s) during the 100% throttle open condition. Broadband noise is noticed in this manoeuvre. As the throttle is closed to zero, the relatively quiet zone is observed from around 20 s to 28 s. The CRV is delayed by 1.5 s as explained. From the time the throttle closure to CRV open, a high intensity noise is observed in the frequency zone of 3000 to 4000 Hz. As soon as the CRV is opened, this noise disappears.

Fig. 7.10 shows four transient cycles of the throttle operation and the CRV operation. The surge noise is more evident in the first two and the fourth cycle. In the third cycle, the surge noise is very weak as the throttle valve closed to the minimum level later than the other three cycles. In other words, CRV has opened earlier than the throttle valve closure to the minimum position. This facilitated increased mass flow through the compressor and hence moving the operating point more closer to the surge line. The sound pressure level recorded during the surge operation and CRV closed condition is 116.8dB at 3350 Hz.

The corrected mass flow (mass flow parameter) is plotted against the pressure ratio at instantaneous points in the Fig.7.11. Referring to this figure, the time portion between 35s to 45s is selected for the analysis. As evident from the Fig.7.11 at around 36.5s, the CRV is opened and at 42s, the CRV is closed. It is clearly understood from the graph that the mass flow through the compressor increases as soon as the CRV is opened. This moves the operating point more closer to the surge line and reduces the surge noise. The surge line at this point of operation is not available from the supplier and hence it is assumed that the operating point is moved more closer to the extrapolated surge line.
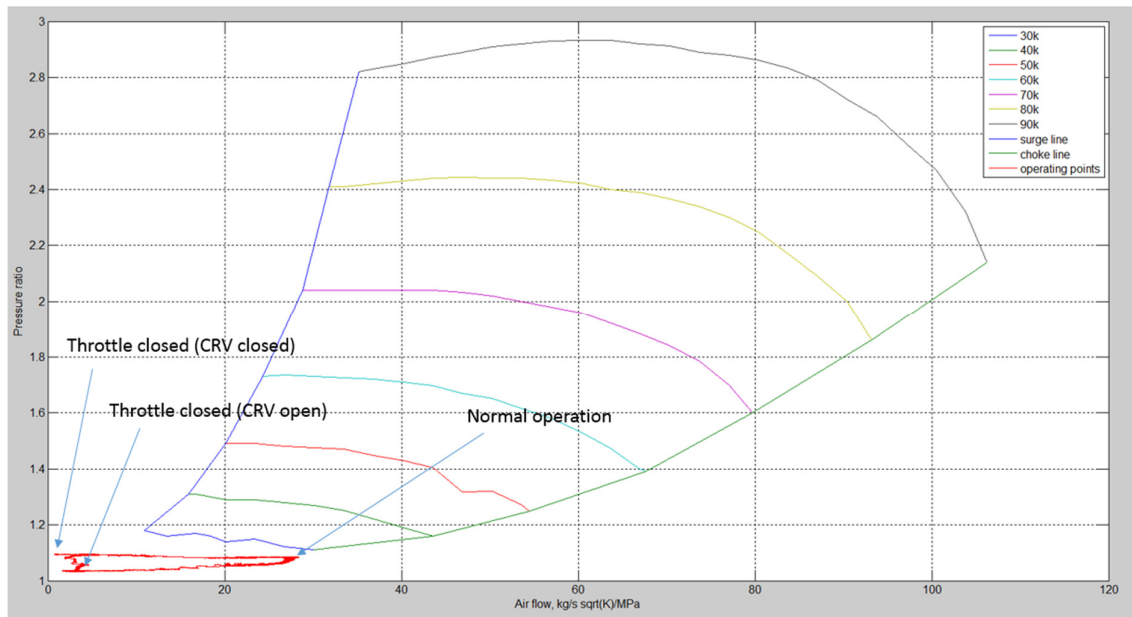
Fig. 7.11 Operating point overlapped on the compressor map-Expt #127

7.2.2.4 Experiment at 30000 RPM – 2.5s delay after throttle closure

The opening delay of CRV is further increased in this experiment to 2.5 s. This experiment is performed to quantify and observe if the CRV delay causes a continued surge noise in the event of full throttle closure. As explained in the literature review chapter, some of the surge occurance is cyclic in the case of diesel engines. This follows a surge operating zone and the system then readjusts to the normal operating zone under certain conditions. However, so far in the case of present experimental rig which simulates petrol engine air intake system, there was no stable operating zone observed when the throttle is moved to the fully closed condition. One of the objectives of this experiment is to observe if the surge is sustained during a time delay of 2.5s.

196

Fig.7.12 STFT of the surface microphone data measured – during 2.5s CRV delay – Expt #129

- (colour code shows the sound pressure level in dB)

As in the previous experiment description, four cycles are repeated for understanding the effect of CRV delay in the surge noise occurance and presented in the Fig.7.12. The throttle manoeuvre has been maintained same as in the previous experiment, i.e. moved from 100% open condition to 0% open condition, very quickly. The CRV delay (delta T) is maintained 2.5 s in all the cycles. The overall mass flow through the air intake system did not change compared to the previous experiments. This is because the throttle profile is unchanged across the experiments. Further analysis can be done for the modified mass flow across compressor. The sound pressure graph shows no much difference in the case of throttle fully open condition and during the opening duration of the CRV. However, as highlighted in the Fig.7.12, there is a considerable increase in the sound pressure level during the region of CRV closure and when the throttle is in the zero operating condition. This translates to an increase of 35% from the 'normal' operating condition, i.e. 328 Pa to 442 Pa. As soon as the CRV is closed, this sound pressure level reduces to its normal level. The graph of STFT (Fig. 7.12) shows the increased sound pressure level during the closure of the CRV. The measured value is 120.6 dB at a

197

frequency of around 3350 Hz. This high sound pressure level noted in the STFT plot disappears as soon as the CRV is opened. It is also noted that, as expected, this noise occurrence starts as soon as the throttle valve is closed fully.
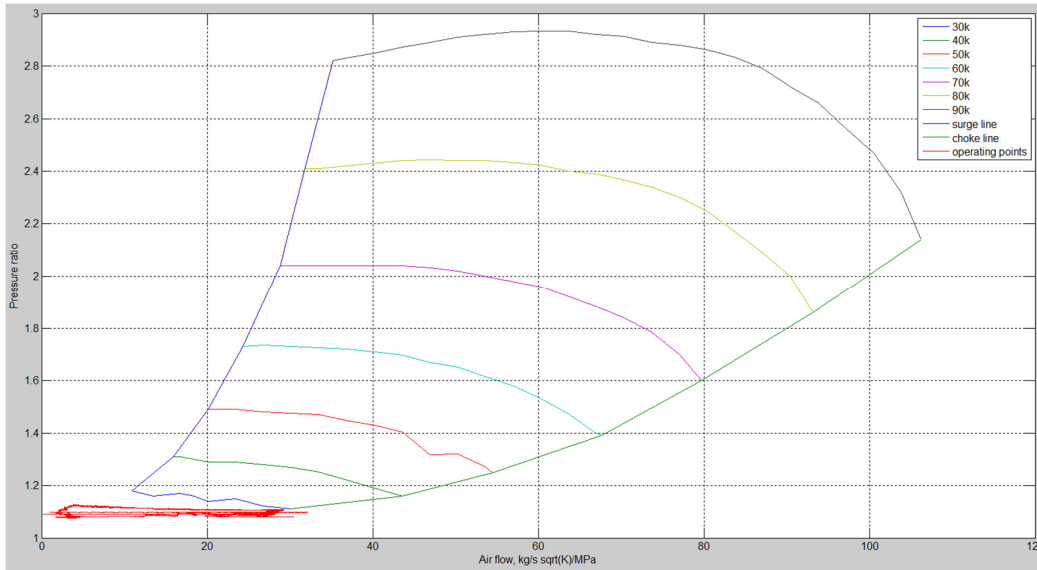
Fig.7.13 Operating point overlapped on the compressor map-Expt #129

The operating point on the compressor map is presented in the figure. As in the previous experiment, the air flow parameter reduces as the CRV is opened. However, this fact is unclear from the figure as all the data has collapsed to a narrow band. The effect of CRV opening on the mass flow and the pressure ratio is not clear from the Fig. 7.13. Hence, the mass flow and pressure ratio are analysed separately using Fig.7.14 and Fig.7.15. Fig.7.15 shows the mass flow parameter against time, CRV and throttle opening position. As calculated, the mass flow parameter increases by 50%. Fig.118 shows the pressure ratio variation against time, CRV and throttle opening position. It is noted from the Fig.7.15 that the pressure ratio decreases after a certain delay. As the CRV is opened, it is observed that the pressure ratio reduces at a faster rate and hence the average amplitude is reduced. As a result, sound pressure level is reduced considerably.
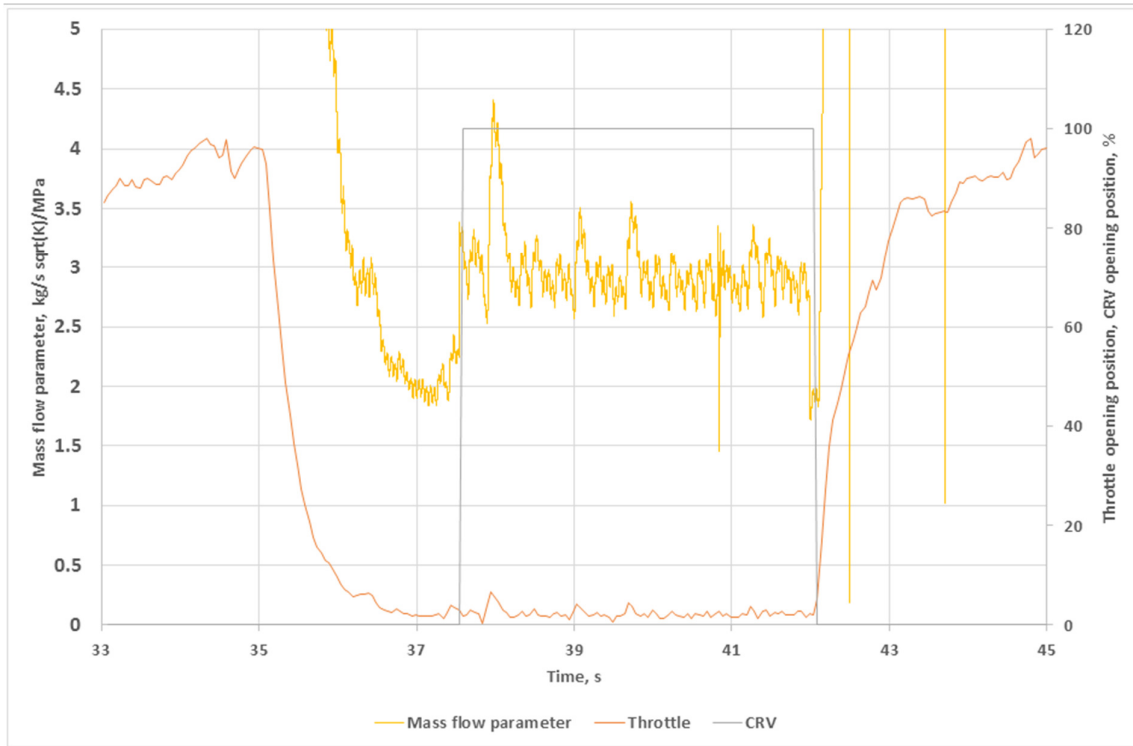
Fig. 7.14 Mass flow parameter variation against time during surge operation
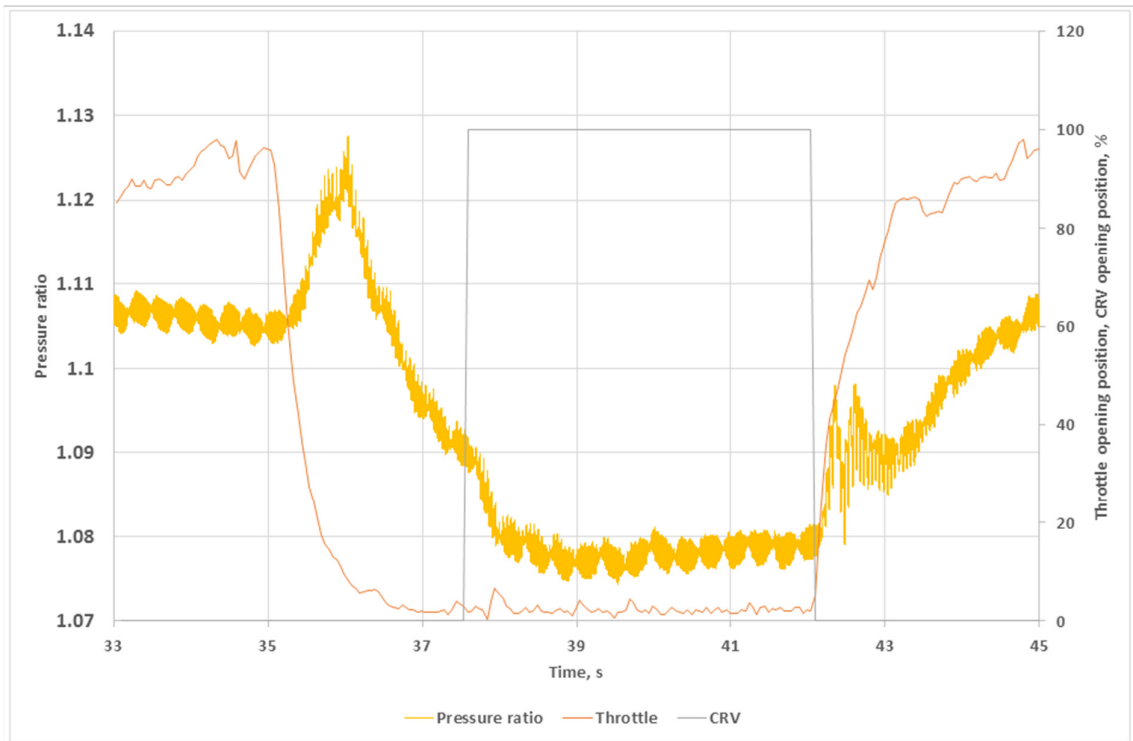
Fig. 7.15 Pressure ratio variation against time during surge operation

7.2.2.5 Experiment at 30000 RPM – 2.5s advance before throttle opening

So far in this chapter, the effect of CRV opening delay was discussed. It was concluded that the delay caused an increase in intensity of the surge noise. In the current and next two sub sections, the effect of CRV delay before the throttle opening from the full closed position is explained. This translates to the mechanical condition of delay in CRV due to friction, response to pressure , damping of the system and spring rating.
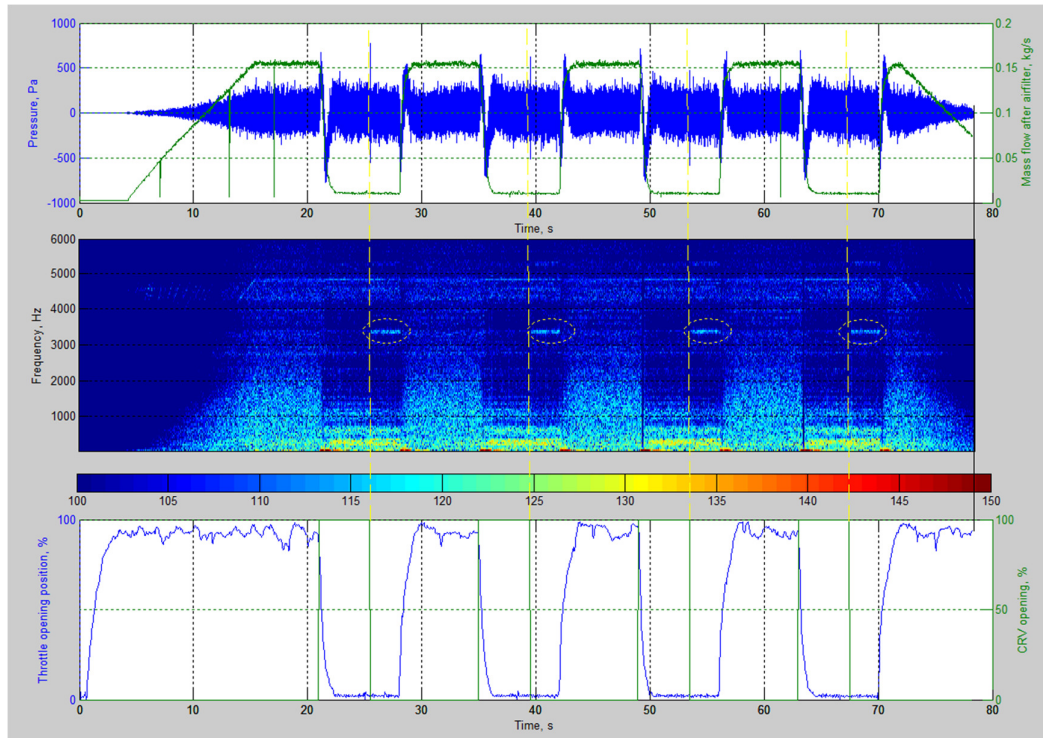
 Fig.7.16 STFT of the surface microphone data measured – during 2.5s CRV delay – Expt #135

(colour code shows the sound pressure level in dB)

Fig.7.16 shows the analysed surface microphone recorded values at the compressor inlet. The throttle profile is maintained same as in the previous experiment. The CRV is opened as soon as the throttle starts to close. The variation introduced in this experiment is that the CRV is closed much before the opening of throttle valve. The opening advance is set as 2.5 s. The sound pressure measured by the surface microphone increases by 10% once the CRV is closed early. In the STFT graph, high intensity surge noise is observed for the duration of CRV closure at throttle closed condition. Hence, it can be concluded that advance in CRV closure is equally a noise generating factor as the delay in the CRV opening.

7.2.2.6 Experiment at 40000 RPM – 0s delay after throttle opening

The speed of the supercharger is increased to 40000 RPM and the CRV delay is set to 0 s. No surge noise is noted in the STFT result in the Fig.7.17. The compressor map presents the operating point. As the mass flow through the compressor has increased due to opening of the CRV, the operating point moves closer to the surge line. This reduces the surge noise intensity. The maximum sound pressure level noted in the STFT graph (Fig. 7.17) is 118.5 dB at 3875 Hz.
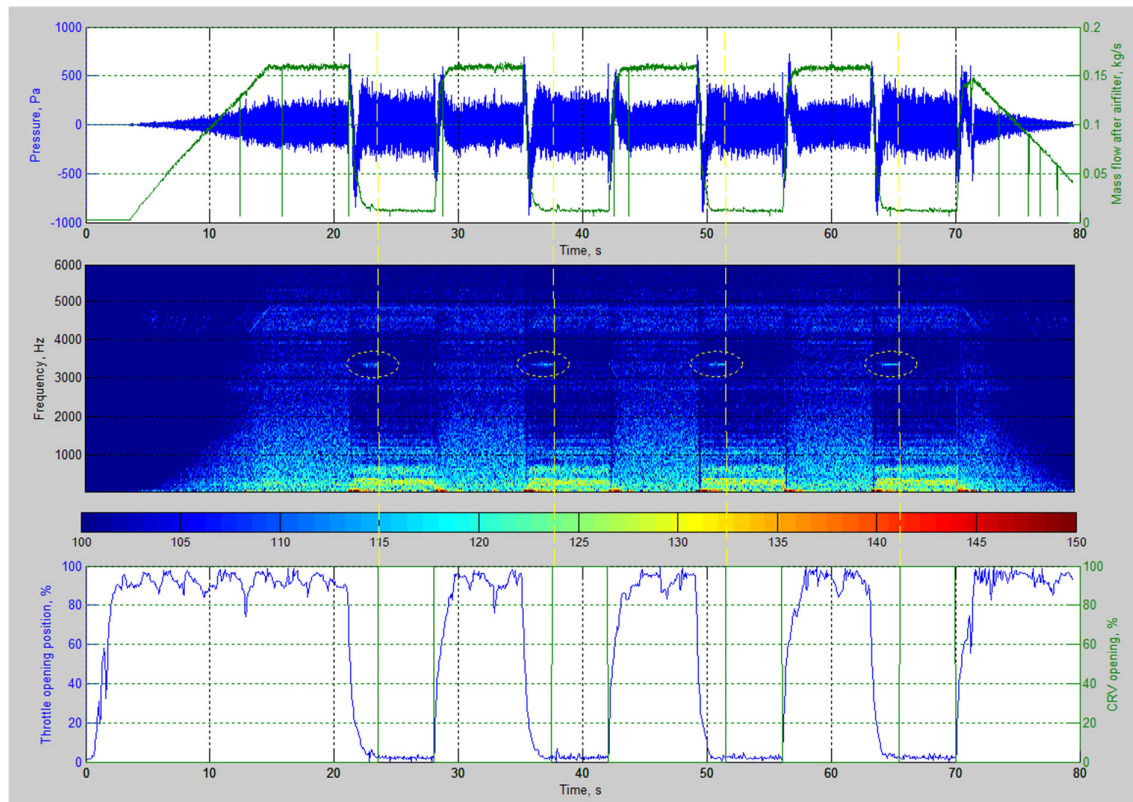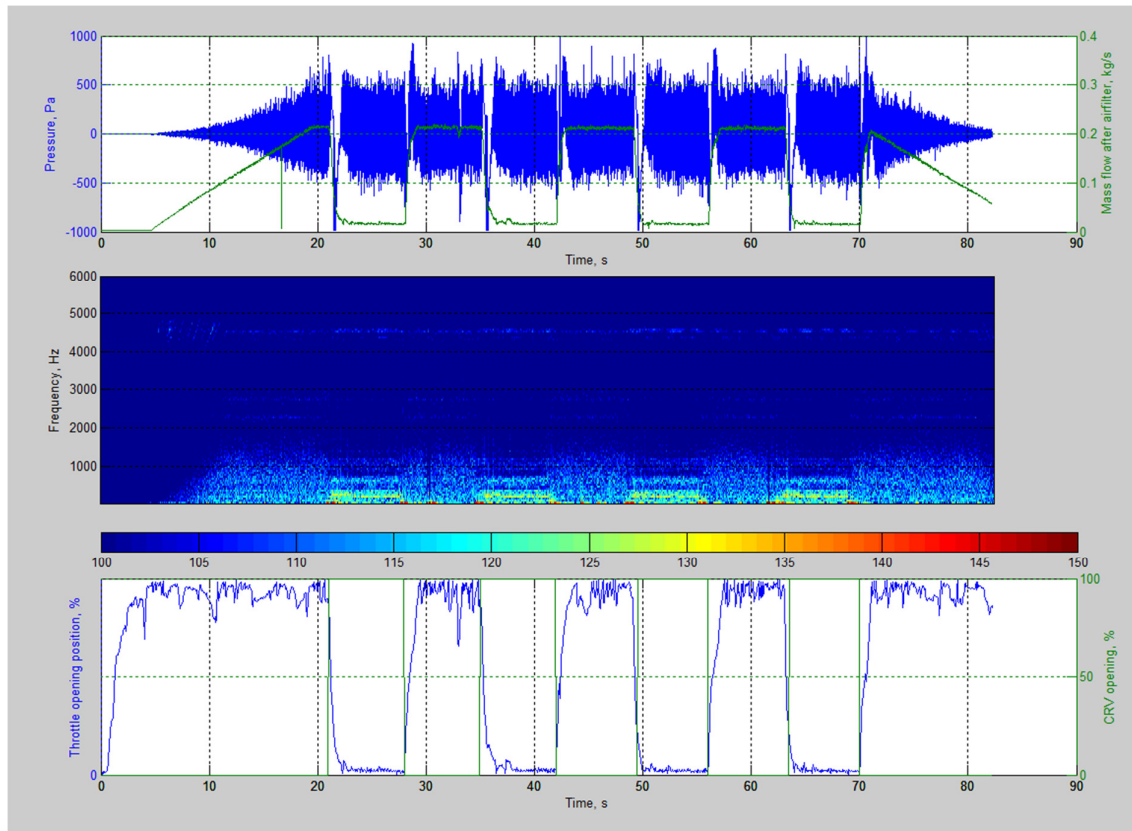

Fig.7.17 STFT of the surface microphone data measured – during 0s CRV delay – Expt #148 (colour code shows the sound pressure level in dB)

7.2.2.7 Experiment at 40000 RPM – 1.5s delay after throttle closure

From Fig. 7.18 the maximum noise measured in this experiment is 120.5 dB at a frequency of 3450 Hz. This increase in noise level when compared with the 30000 rpm case is possibly due to the increase in the flow at 40000 rpm and hence the increase in the surge intensity. The compressor map represented shows that at WOT, as expected the operating point remains on

the 40000 rpm line and in the part throttle, compressor operates in the surge region As in similar experiments, the operating point moves more closer to the surge line reducing the intensity of the surge noise.
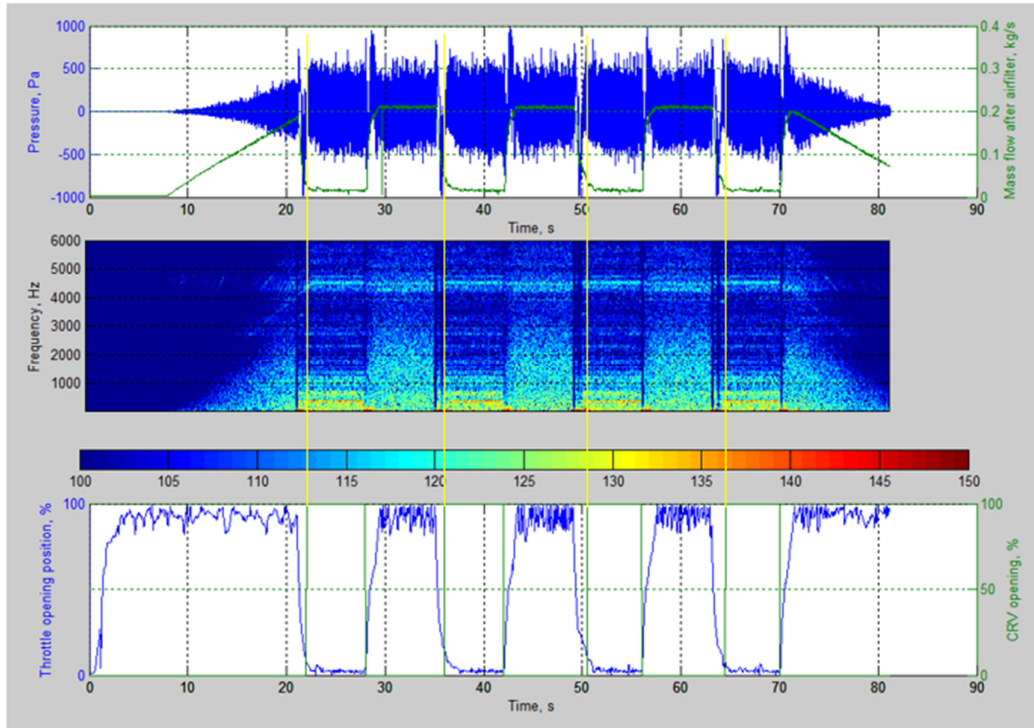
Fig. 7.18 STFT of the surface microphone data measured – during 1.5s CRV delay – Expt #149 (colour code shows the sound pressure level in dB)
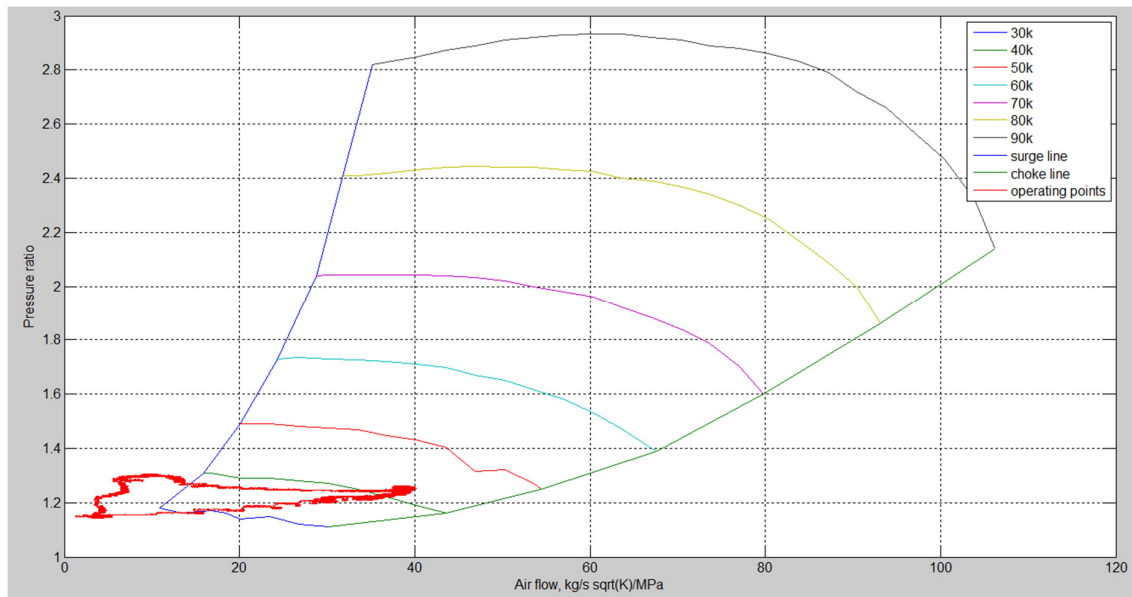
Fig.7.19 Operating point overlapped on the compressor map-Expt #149

7.2.2.8 Experiment at 40000 RPM – 2.5s delay after throttle closure

The experimental results with delayed opening of the CRV is shown in Fig. 7.20 and the operating point is overlapped on the compressor map in the Fig. 7.21. The maximum sound pressure level recorded is 121.5 dB at 3875 Hz during the surge operation.
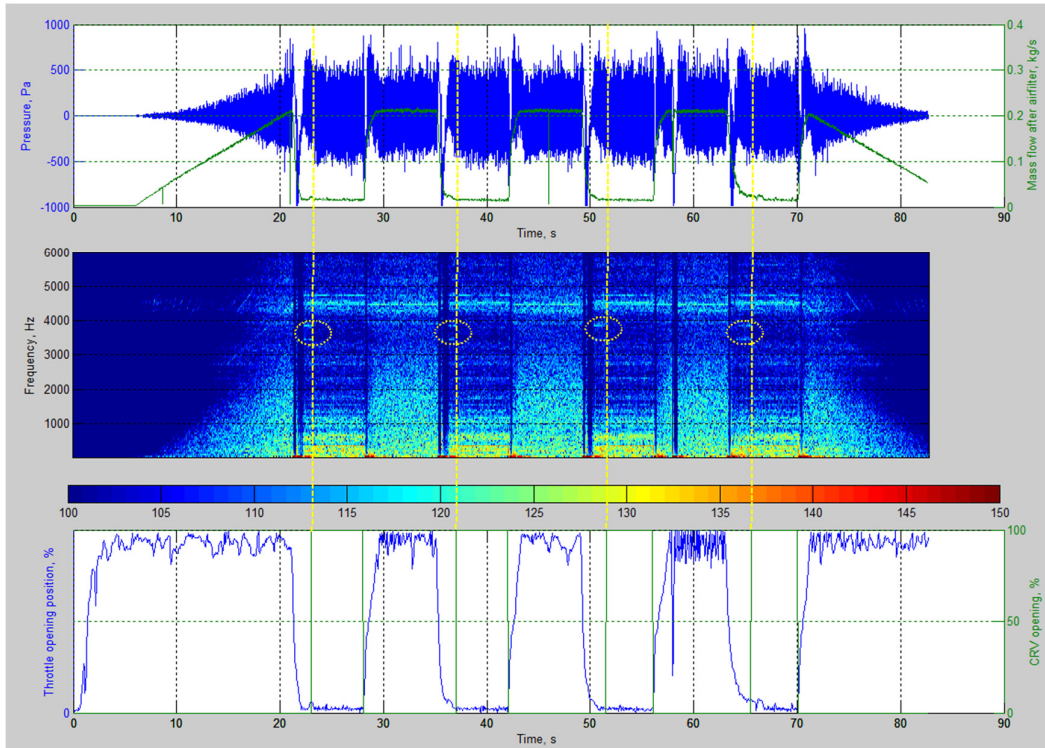
Fig.7.20 STFT of the surface microphone data measured – during 2.5s CRV delay – Expt #150

(colour code shows the sound pressure level in dB)
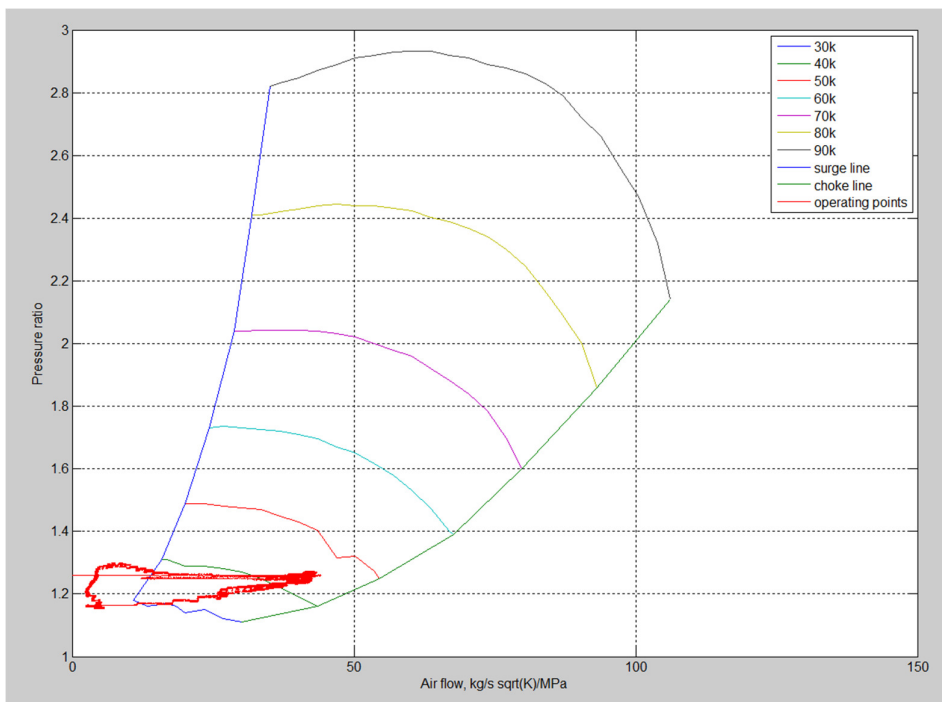
Fig. 7.21 Operating point overlapped on the compressor map-Expt #150

7.2.3 Effect of CRV delay against the level of surge noise

In the previous sections, at two different speeds of supercharger i.e. 30000 and 40000 rpm, the effect of delay in the CRV opening was studied. The characteristics of sound pressure level, pressure ratio, mass flow during the transient manoeuvre was understood for the given compressor and intake system combination. The effect of the CRV delay in opening on the mass flow through the compressor, on the pressure ratio and hence on the noise pressure level is understood. The delay used in the previous experiments were 0, 1.5 and 2.5 s.

Transient throttle manoeuvres were performed at each experiments to get the maximum sound pressure levels and the frequency. The measurements for this section are performed at the region between the throttle start to close and when the CRV is in the closed condition. The aim of this study is to characterise the delay in CRV in terms of sound pressure level and frequency. Even though the STFT figures give a visual representation of the surge noise occurrence as explained in the previous sections, the aim of this exercise is to quantify the noise level.

In a mechanical CRV, the delay is quiet prominent and is influenced by various factors such as damping of the chambers, spring rate, and pressure difference experienced by the diaphragm. Also the system inertia may not allow faster opening of the mechanical CRV. This effect is important in the case of quick transient manoeuvre of the throttle. This can happen when the driver moves the accelerator pedal from fully open or partially open to closed condition and releases back in a short time period. The time period used in the test rig is around 8 seconds and may not be happening in the actual driving cycle. In the case of the shorter cycle period, the pressure in the intake manifold may not be sufficient to open the CRV. Also, the inertia, spring rate and the damping of the system may prevent the faster opening of the valve. Hence, the main issue encountered in the petrol engine is the delay in the opening of the CRV during transient manoeuvres. Hence, the cycle period is maintained longer and the delay of the CRV is varied to see the effect.

7.2.3.1 Effect of CRV delay at 30000 rpm

The measurements during the CRV and the throttle closure at constant supercharger speed of 30000 rpm has been plotted against the delta T, that is the time for the CRV to open after throttle is closed in the Fig.7.22. The noise at fully open throttle and CRV conditions are ignored for this study. This is because of presence of increased flow noise, during these

operations. Whereas, during the closed condition of the throttle and the CRV, the engine/test rig flow noise will be quieter and the surge noise will be standing out.

The noise observed at zero 'delta T' is around 112.5 dB. As the 'delta T' is progressed to 0.5s, the maximum noise level increased to 115 dB. There is a dip in the noise level as in the Fig.7.22. However, this could be due to the selection of the experiment at which this noise drop occurs. This may be able due to the effect of momentary increase in the throttle valve open condition from the fully closed condition or the difference in the profiles. After observing the third cycle at experiment #127 (reference Fig.7.10), it was noted that the CRV is opened earlier than the other cycles in the same experiment. Hence this point may be ignored for understanding the effect of 'delta T'. However, this effect helped to understand the correlation between the throttle closed condition and the CRV delay.

The effect of CRV delay was continued to be more prominent on the surge noise at 1.5 s (117 dB), 2 s (120.75 dB) and at 2.5 s (121 dB) 'delta T'. The sound pressure level is shown to be of considerable increase from the 'delta T' value of 0s to 2.5 s. The minimum and the maximum sound pressure level values ranged from 112.5 dB to 121 dB. However, the difference in the increase in the sound pressure level is 8.5 dB. This value is challenge in the real automotive engine scenario to reduce back to the normal level. This also involves costly modifications or additions to the intake system or the engine components to reduce this unwanted noise. Also, there could be fatigue damage to the compressor blades, casing vibrations, bearing damage and excitations of the intake pipes [17].

Corresponding frequencies are also noted using the STFT plot and shown in the Fig.7.22. This shows an interesting trend that the frequency of noise remains within narrow range (3150Hz to 3350 Hz) with the delay in the CRV operation. Hence, it is concluded that the frequency do not increase or decrease with the change in the delta T for the given supercharger speed of 30000 rpm. This reduces the complexity in the solution to the problem. This is because mainly the noise solutions generally offered are dependent on the frequency of the excitation. The reduction in the sound pressure levels are normally the outcome of the solution.
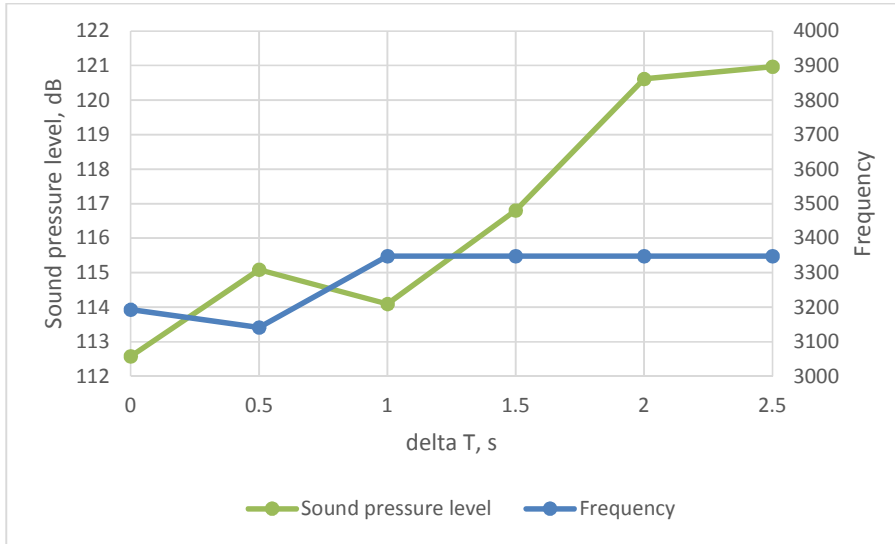
Fig 7.22. Maximum sound pressure level and corresponding frequency measured at CRV and throttle valve closed condition, Expt #124-#129

7.2.3.2 Effect of CRV delay at 40000 rpm

In this experiment, the supercharger speed is maintained at 40000 rpm. Hence, clearly the flow is increased throughout the intake system compared to the 30000 rpm. Other factors such as throttle angle profile, CRV opening profile and the instrumentation are maintained the same as in the previous discussion. Hence the major variable changed in the present experiment is the mass flow through the intake system and the blade passing frequency. The blade passing frequency is increased as the speed of the supercharger shaft is increased.

As a similar trend to the previous study at 30000 rpm, the sound pressure level at this experiment has shown an increasing trend as the 'delta T' was increased. At 'delta T' of 0 s, a high sound pressure level of 118.5 dB is observed. As the 'delta T' is increased to 0.5 s, the sound pressure did not increase as expected. This is due to increased opening of throttle due to the controlled profile shift, which allowed reduced surge zone operation. The same effect is seen at the 'delta T' of 1.5 s. A 2 dB increase is observed at 1s compared to 0 s. At 2.5 s, the overall sound pressure level increase from the 0s 'delta T' is 3 dB.

The frequency range for the 'delta T' of 0 s to 2.5 s is 3450 to 3875 s. One of the reason for the frequency increase could be the blade passing frequency variation compared with the experiment with 30000 rpm shaft speed. The blade passing frequency is a function of the speed

of the supercharger shaft. The ratio of the supercharger shaft speed and that of the frequency of noise generation should match, if the noise is created due to the blade passing. The extreme frequencies recorded are

Ratio of supercharger speed = 40000/30000=1.33:1

Ratio of the frequencies = 3875/3150 = 1.23:1

Hence, it is concluded that the blade passing difference is not the cause of difference in measured frequencies.
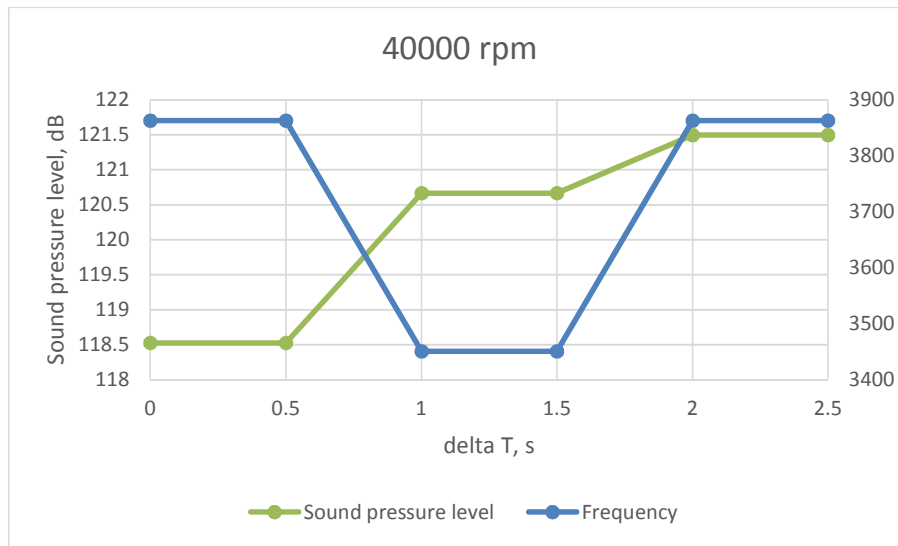
Fig 7.23. Maximum sound pressure level and corresponding frequency measured at CRV and throttle valve closed condition, Expt #148-#150

7.3 Characterisation of the parameters using simulation method

The simulation rig as described in chapter 5 is modelled using a one dimensional code (GT-Power). The aim of the exercise is to determine the massflow through the CRV and to implement the ratio between between the mass flow through the CRV and the mass flow through the air filter inlet into the measured values and further analysis. The objective is to input the design data of the compressor rig into the model and to run the simulation using the same boundary conditions such as throttle opening profile, CRV opening profile and the supercharger speed of 30,000 RPM. The next step adopted was to compare the simulated and measured pressure outlet and mass flow during the minimum throttle condition. Finally, the ratio of the mass flow through the CRV against mass flow through the air inlet is noted and used as an input for the calculation using measured values.

Fig. 7.24 Layout of experimental rig in GT Power

7.3.1 Results

The boundary conditions in the simulated rig, i.e. throttle and CRV opening positions are given as input to the simulation model. This means that the throttle and CRV in the model operates at the same profile as in the experimental rig. The speed of the supercharger is maintained at 30,000 rpm. Results from the simulated model are compared with the measured values. Pressure outlet and massflow rate are presented in Fig.7.25 and 7.26. As the massflow and the pressure outlet are matching closely, the mass flow through the CRV is noted. The ratio of mass flow through the CRV and the intake system is noted as 1.8. This means that the mass flow through the CRV is 80% more than that of the massflow through the inlet.

Fig. 7.25 Throttle and CRV opening position against time – simulated and measured
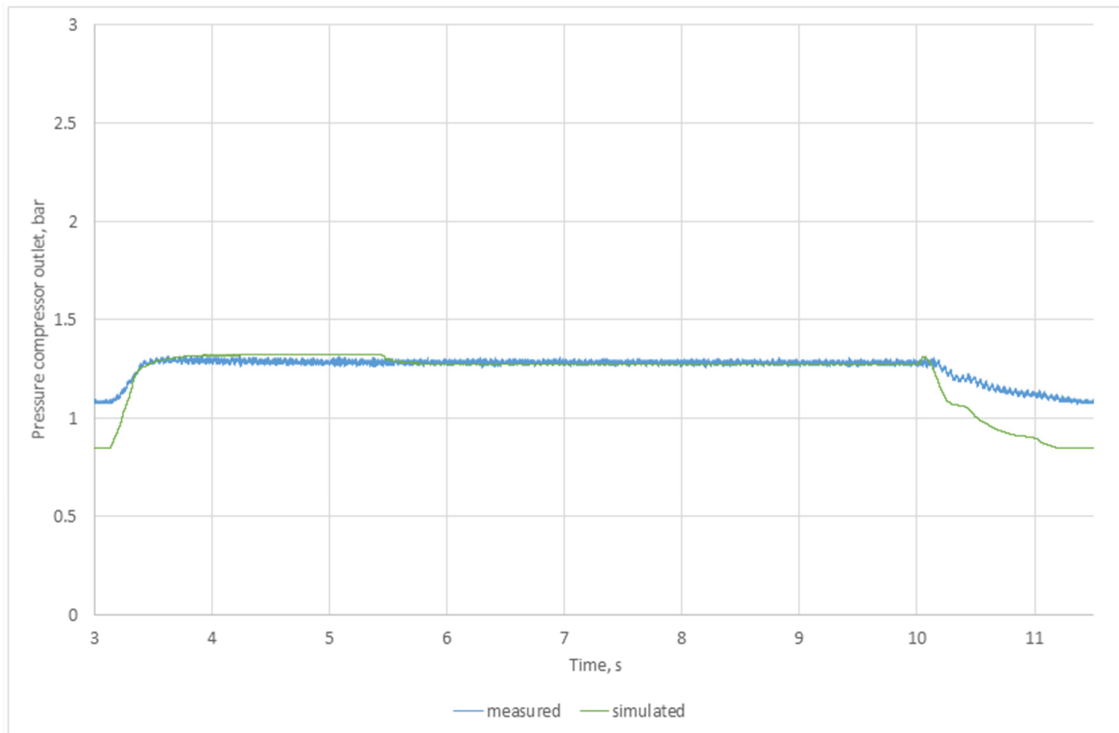
Fig. 7.26 Pressure at compressor outlet – simulated and measured
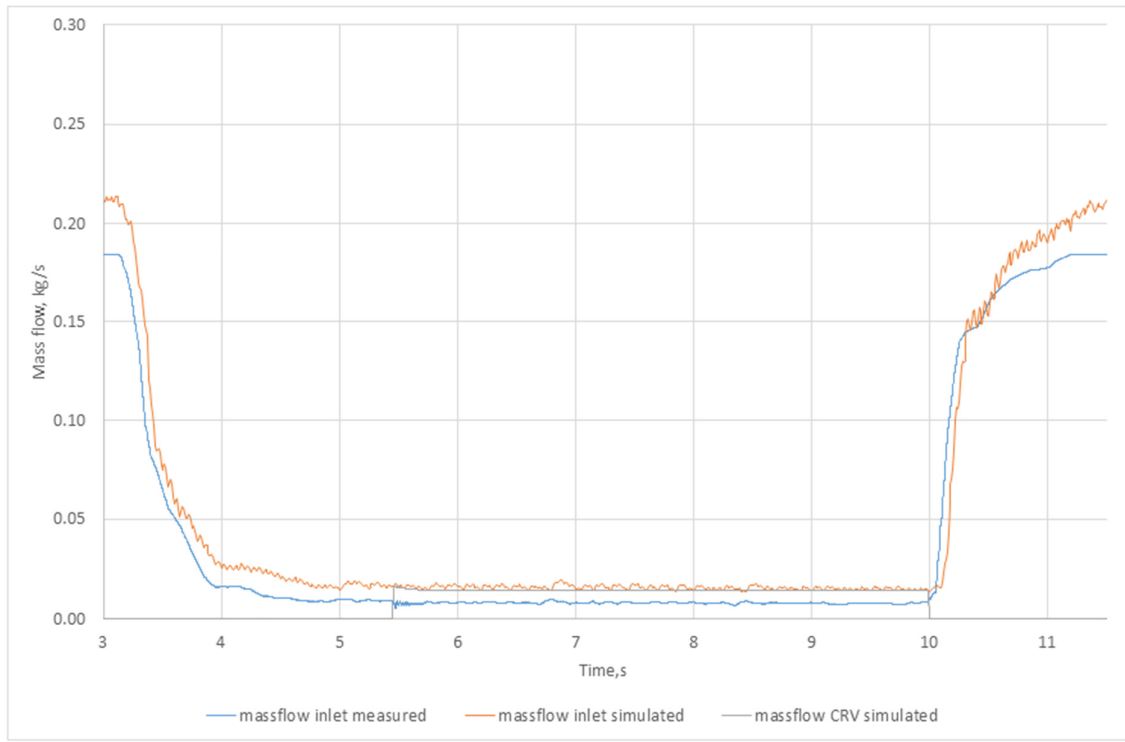
Fig. 7.27 Mass flow inlet – simulated and measured and mass flow through CRV simulated

7.4 Mechanism of the problem

The effect of CRV, throttle opening on the noise intensity during the surge region is understood from the experimental and analytical work performed so far in this chapter. As proved by the previous experiments, the surge noise occurs during the throttle and CRV closed condition, if the pressure and flow dynamics in the intake system are favourable to create the noise. The surge noise creating frequency is found to be generally independent of the speed of the supercharger. It was evident from the experiment at different speeds of 30000 rpm and 40000 rpm that the frequency remains within narrow bands. Also the variation in the frequency was not found to be proportional to the change in the speed of the supercharger. However, it was found that the intensity of the noise was much higher in the 40000 rpm shaft speed than with the 30000 rpm shaft speed . This phenomena is possibly due to the increase in the flow velocity at higher supercharger shaft speeds [17] and hence higher pressure dynamics. Hence, it may be concluded that the surge occurrence is a flow induced phenomena.

It is observed from the experiments that the surge noise increased with the increase in flow, i.e. with the increase in the compressor impeller speed. Jungbauer et al. [17] suggested that the

flow induced problems are due to coincidence of vortex shedding with an acoustic frequency in the turbomachinery system. It is stated that each geometrical discontinuity for the flow is the site of vortex shedding [39]. At the geometrical discontinuities the acoustic waves in the fluid can induce vortex shedding. The dynamic pressure fluctuations which occur due to the transient tip in – tip out throttle manoeuvre are then amplified. The amount of amplification of the fluctuations is controlled by the acoustic damping of the intake system, either downstream or upstream of the compressor. Damping is caused by different factors, such as internal friction, interface friction and radiation of energy into contagious fluids or structures [47]. The structures in the case of automotive application are the compressor housings and the plastic intake system ducts which can vibrate and radiate the noise to the passenger compartment.

The frequency distribution of vortex shedding as a function of fluid flow velocity and geometrical dimension is given as [17]

$$f_s = N_s \frac{c_f}{d} \qquad - \qquad 7.21$$

Where N_s - Strouhal number (dimensionless)

c_f – Flow velocity, m/s

d – Basic hydraulic (geometric) diameter of obstruction or constriction (pipe or passage diameter), m

It is stated that the obstructions or constrictions shed vortices efficiently at or near a Strouhal number of approximately 0.2. The vortex shedding frequency does not refer to a specific frequency, but to a band of frequencies around the Strouhal number of 0.2.

Another type of resonances explained in the literatures are the radial acoustic resonances or the cross mode resonances [47]. The intake duct represented in the design of the turbocharger acts as a waveguide for the acoustic waves in the intake air media. Pierce [48] and Fahy et al. [47] showed that the modes proper to a rigid – walled, uniform, cylindrical waveguide of infinite length take the form

$$p_{np}(r,\phi,z) = \tilde{p}_{np} \frac{\cos}{\sin}(n\phi) J_n(k_r r)\exp(-jk_z z) \quad - \qquad 7.22$$

Where

J_n - Bessel function

k_r - radial wavenumber is determined from the equation $[J_n^{'}(k_r r)]_{r=a} = 0$

n – number of diametral pressure nodes

p – number of concentric circular pressure nodes

A particular mode cannot propagate freely and carry energy in an infinitely long duct below a certain cut-off frequency given by [47]

$$k_z^2 = k^2 - \left(k_r^{np}\right)^2 = 0 \qquad - \qquad 7.23$$

Or

$$ka = k_r^{np} a \qquad - \qquad 7.24$$

The ring frequency of the shell is expressed as $\Omega_{np} = (k_r^{np} a)(c/c_i^{''})$

Jungbauer et al. [17] suggested that the cavity resonance frequency for the cylindrical wave equation is defined as,

$$f_{np} = J_{np}(c/d) \qquad - \qquad 7.25$$

Where

c – speed of sound in the contained fluid, m/s

d - basic hydraulic (geometric) diameter of obstruction or construction, m

The values of J_{np} for different values of n, i.e. the number of diametral pressure nodes and p, i.e. the number of concentric circular pressure nodes are given in the table (Table 7.2). The representation of nodal pattern as examples are given in the Fig.7.28.
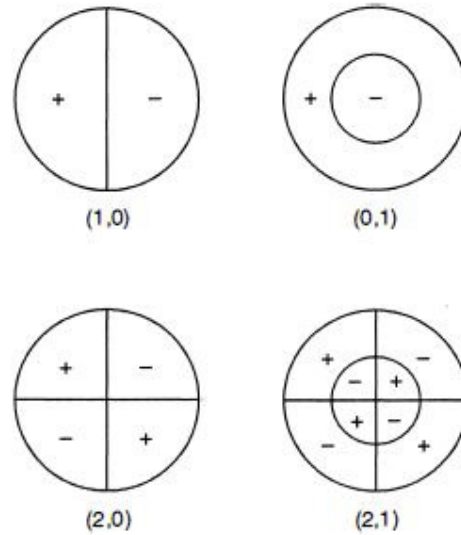
Fig.7.28 Nodal pattern for Acoustic Radial Modes [17]

n	p				
	0	1	2	3	4
0	0	1.2197	2.2331	3.2383	4.2411
1	0.5861	1.697	2.714	3.7261	4.7312
2	0.9722	2.1346	3.1734	4.1923	5.2036
3	1.3373	2.5513	3.6115	4.6428	5.6624
4	1.6926	2.9547	4.0368	5.0815	6.1103
5	2.0421	3.3486	4.4523	5.5108	6.5494
6	2.3877	3.7353	4.86	5.9325	6.9811
7	2.7304	4.1165	5.2615	6.3477	7.4065
8	3.0709	4.4931	5.6576	6.7574	7.8264

Table.7.2 values of J_{np} [17]

The type of resonance described here is of three-dimensional acoustic resonance which can be represented as standing acoustic wave pattern as given in the Fig.7.27. They are oriented perpendicular to the pipe and flow passage axes. The nodal patterns represented in the Fig. 7.27 rotates and propagates up and down the piping as a helical wave. The velocity is given as per the following equation [17]

$$v_x = \frac{c}{\sqrt{1 - \dfrac{f_{np}}{f}}} \qquad - \qquad 7.26$$

Where

v_x – velocity of propagation, m/s

f – excitation frequency, Hz

if the excitation frequency, *f* is less than the ring frequency of the shell, the pulsation decays exponentially. If the frequencies are equal, the resonance is said to be excited and if the excitation frequency is greater than the ring frequency, acoustic cross mode propagate up and down the system.

7.4.1 Calculation of resonant frequencies for the experiment on the compressor rig

This section of the chapter explains the application of theory presented in the previous section, i.e. the radial acoustic resonance and the vortex shedding on a typical experimental result. The aim of this exercise is to identify the mechanism of noise generation during the surge operation. The frequency range of surge noise generation has been identified by performing transient operation of the compressor rig. The objective of the exercise is to find out the resonant frequency at different temperature for each mechanism. In the case of radial acoustic resonance, the determination of resonant frequency at different nodal pattern and different temperature are performed. Also, vortex shedding frequency is determined. By overlapping all the frequencies at the STFT graph, the mechanism can be identified.

Anlaysed results of experiment #129 are used for calculation of the resonant frequencies. As a summary of the experiment the supercharger shaft speed is maintained at a constant value of 30000 rpm and the throttle and crv transient profile is defined as in the Fig. 7.12. The analysed results are also presented in the Fig.7.12. The range of frequencies obtained from the background noise check and also using the experiment #129 are given in the following table (Table. 7.3).

Sl No	Frequency (Hz)	Source
1	16.7	Electric motor
2	50	AC mains
3	66.7	Supercharger pulley
4	200	Throttle body
5	590, 600	Inverter fan
6	3193.1, 3141.6, 3347.6, 3450.6, 3863	Surge noise
7	4000, 45000, 5000	Throttle body gearing, structural vibration

Table 7.3 Summary of frequencies

Four pipes of the supercharger rig are identified for the study. The pipes are chosen from the consideration of proximity of compressor and also in which flow difference occurs during the throttle closed condition in the transient maneuver. Compressor inlet pipe (blue), supercharger inlet (aluminium), supercharger outlet (aluminium), throttle inlet and CRV hose are the parts selected for the resonant frequency calculation. The region of interest is divided into three :- 1. at the inlet side of the compressor and the pipes include compressor inlet pipe (blue), supercharger inlet (aluminium and is integral to the supercharger), 2. At the outlet side of the compressor and the pipes include compressor outlet (aluminium and integral to the supercharger), throttle inlet and 3. CRV hose which connects the outlet side of the compressor to the inlet side.

7.4.2 Vortex shedding

Using the equation, a sample calculation is presented.

Ns=0.2

d= 50 mm; at supercharger inlet tube at the intake side

velocity at any pipe section is defined from the equation

$$\dot{m} = \rho_o vA$$

Where

$\dot{m}$ - mass flow rate, kg/s = 0.0105 kg/s

ρ_o - density of air, kg/m^3 = 1.114 kg/m^3 at 45 deg C

c_f – velocity, m/s

A – cross section area, m^2 = $\dfrac{\pi}{4}d^2 = \dfrac{\pi}{4}0.05^2 = 0.002$ m^2

$v = \dfrac{\dot{m}}{\rho_o A} = 0.0105/(1.114*0.002) = 4.71$ m/s

$f_s = N_s \dfrac{v}{d} = 0.2 \times (4.71/0.05) = 18.84$ Hz

The calculation is repeated for the inlet and outlet sections of the compressor, where more flow dynamics may occur during the transient manoeuvre (Table.7.4). Throttle and CRV sections are also selected as these have major actions during the experiment.

Location	Supercharger inlet pipe (blue)		Supercharger inlet (aluminium)	Supercharger outlet (aluminium)	Supercharger outlet pipe (blue)	Throttle inlet	CRV hose
Diameters (mm)	50	76	70	53	63	57.5	52	12
Frequency	19	5	7	16	10	13	17	1395

Table 7.4 Results of vortex shedding calculation

The results show that as the flow diameter reduces, the frequency increases as the flow diameter is decreased. Hence the maximum frequency calculated is at the CRV hose location and is 1395 Hz. The surge frequency measured using the experimental rig is of the range 3193 to 3863 Hz. Hence it may be concluded that the vortex shedding is not the cause of surge noise in the experimental rig.

7.4.3 Acoustic radial resonances

An example calculation is given below for finding the acoustic radial resonance frequencies. Referring to the Fig.7.27, containing nodal pattern, the combinations of n, i.e. number of diametral pressures nodes and p, i.e. number of concentric pressure nodes, (n=1, p=0); (n=0, p=1); (n=2, p=0) and (n=0, p=2) are selected for the analysis. The value of α_{mn} is selected for the corresponding values of n and p from the table. The speed of sound is given by

$c = \sqrt{\gamma R T}$

γ - ratio of specific heat for air (1.4)

R – universal gas constant 287 J/kg/K

T – temperature of the air, K

As the temperature varies across the outlet and inlet of the compressor, the previous equation is used to calculate the speed of sound. Fig.7.28 and Fig.7.29 shows the variation of temperature during the transient manoeuvre and the value range from 15 to 60 deg C for the compressor speed of 30000 and 40000 rpm.
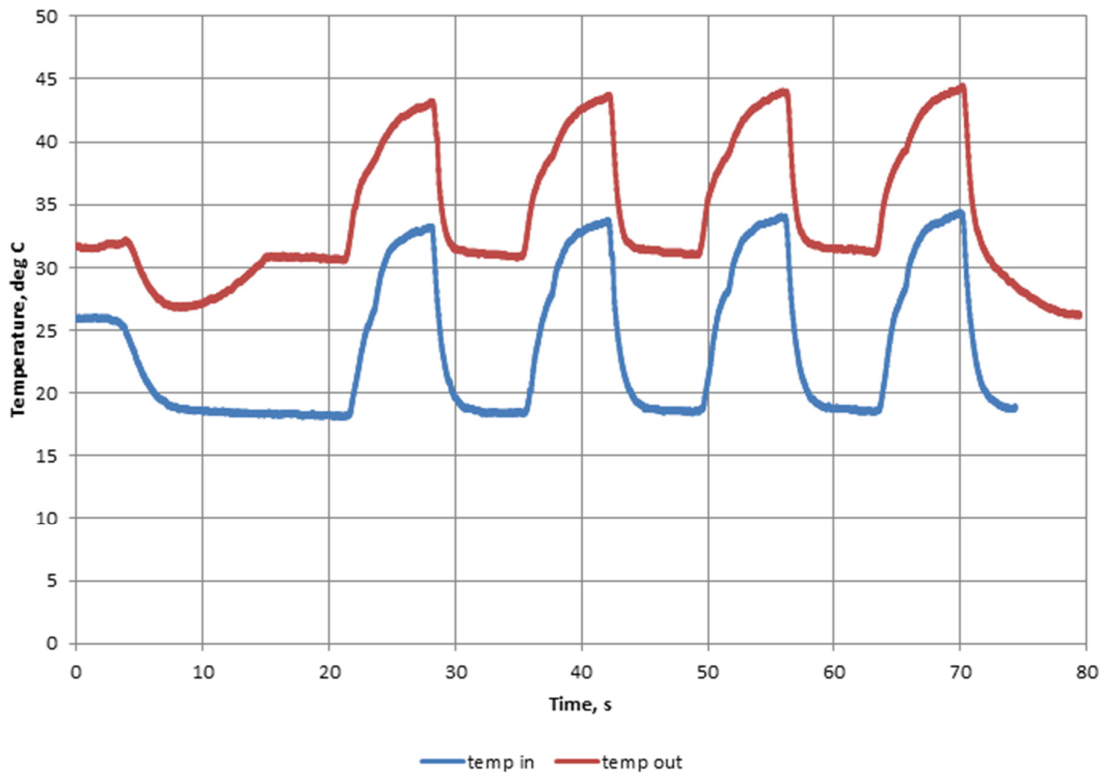
Fig.7.29 Temperature inlet and outlet values – 30000 rpm shaft speed, expt #129
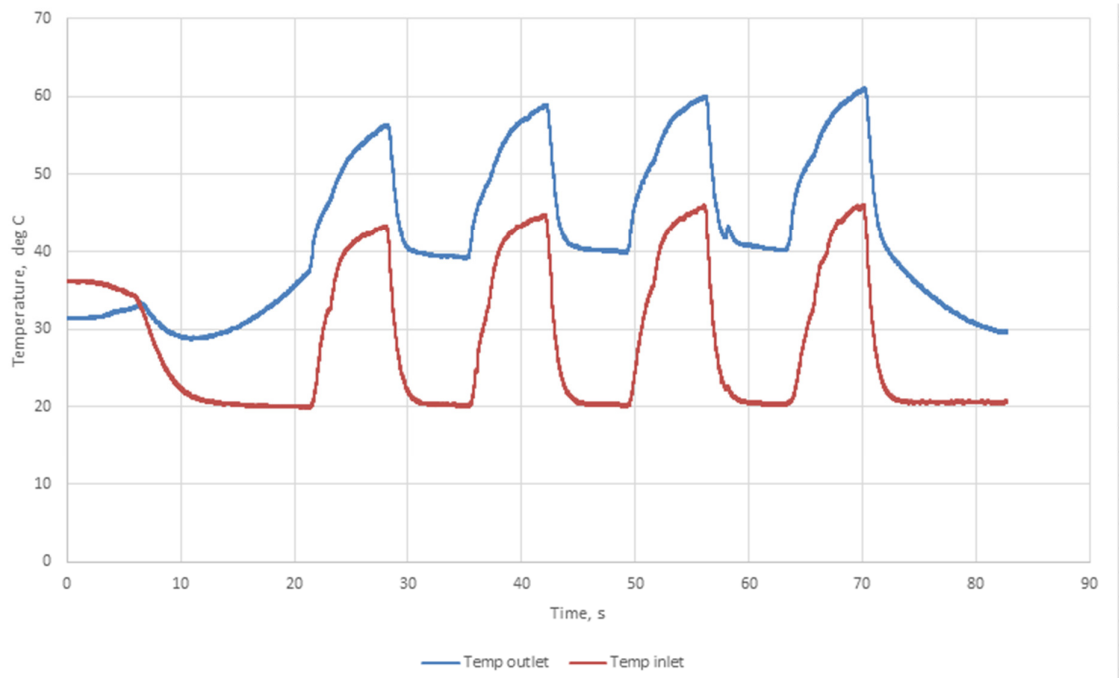
Fig.7.30 Temperature inlet and outlet values – 40000 rpm shaft speed, expt #150

As an example calculation, the following values are selected

T=15 deg C

n=1

p=0

$J_{np} = 0.5861$

$$c=\sqrt{\gamma RT} = \sqrt{1.4x287x(15+273)} = 340.2 \text{ m/s}$$

d=63.5mm, is the inlet diameter of the flow section at supercharger inlet tube

Therefore, radial acoustic resonant frequency is given as,

$$f_{np} = J_{np}\left(\frac{a}{d}\right) = 0.5861\left(\frac{340.2}{0.0635}\right) = 3140 \text{ Hz}$$

The above calculated value of 3140 Hz shows the radial acoustic frequency for the conditions as given above.

The resonant frequency calculated corresponding to the temperatures of 15, 45 and 60 deg C are given in the tables (Table 7.5. Table 7.6 and Table 7.7) .

Location	Supercharger inlet pipe (blue)		Supercharger inlet (aluminium)	Supercharger outlet (aluminium)	Supercharger outlet pipe (blue)		Throttle inlet	CRV hose
Diameters (mm)	50	76	70	53	63	57.5	52	12
Resonant frequency (1,0)	3987	2623	2848	3762	3165	3467	3834	16614
Resonant frequency (0,1)	8298	5459	5927	7828	6586	7216	7979	34575
Resonant frequency (2,0)	6614	4351	4724	6240	5249	5752	6360	27559
Resonant frequency (0,2)	15193	9995	10852	14333	12058	13211	14608	63303

Table 7.5 Resonant frequencies corresponding to 15 deg C

Location	Supercharger inlet pipe (blue)		Supercharger inlet (aluminium)	Supercharger outlet (aluminium)	Supercharger outlet pipe (blue)		Throttle inlet	CRV hose
Diameters (mm)	50	76	70	53	63	57.5	52	12
Resonant frequency (1,0)	4190	2757	2993	3953	3325	3644	4029	17458
Resonant frequency (0,1)	8720	5737	6228	8226	6920	7582	8384	36332
Resonant frequency (2,0)	6950	4573	4964	6557	5516	6044	6683	28959
Resonant frequency (0,2)	15964	10503	11403	15061	12670	13882	15350	66518

Table 7.6 Resonant frequencies corresponding to 45 deg C

Location	Supercharger inlet pipe (blue)		Supercharger inlet (aluminium)	Supercharger outlet (aluminium)	Supercharger outlet pipe (blue)		Throttle inlet	CRV hose
Diameters (mm)	50	76	70	53	63	57.5	52	12
Resonant frequency (1,0)	4288	2821	3063	4045	3403	3729	4123	17866
Resonant frequency (0,1)	8923	5870	6374	8418	7082	7759	8580	37180
Resonant frequency (2,0)	7112	4679	5080	6710	5645	6185	6839	29635
Resonant frequency (0,2)	16337	10748	11669	15412	12966	14206	15709	68070

Table 7.7 Resonant frequencies corresponding to 60 deg C

The flow diameters at each components of the supercharger rig are given in the table. The corresponding resonant frequencies at different temperatures exposed at the inlet and outlet side of the compressor are tabulated. The resonant frequencies increase with the reduction in the flow diameter. Also, at higher modes the resonant frequency values increases. If the trends on different temperatures are compared, the resonant frequency values increase as the temperature is increased. This is due to the fact that the speed of sound increases with the increase in temperature of the gases. As given in the table, the surge frequency ranges from 3140 Hz to 3870 Hz in the current experiment at compressor rig at shaft speeds 30000 rpm and 40000 rpm. This resonant frequency zone is marked in the tables as yellow coloured box. It may be concluded that the radial acoustic resonant frequencies are closer to the surge

frequency. Hence, it may be concluded that the mechanism of surge noise in the intake system is due to radial acoustic resonance at supercharger inlet or outlet locations.

7.5 Solution to the problem

This section discusses the methodology adopted to solve the problem of surge noise. The aim is to reduce the intensity of noise. More focus of the solution is given to the passive method. However, the active solution is also discussed for the completeness. One of the major difficulty in the implementation of the active solution is that the additional electronics and hardware could cause a cost increase in the turbocharger part. However, compressor map based corrections are possible with the active solution. In the case of passive solution, the design should lead to a more cost effective solution. In the case of both solutions, verification of the engine performance should be conducted to understand the effect.

7.5.1 Design of parts- passive solution

Passive solution is generally employed using stationary parts such as a silencer, sound-absorbing tiles, insulation. The following two sections explain the method used to design parts for passive solution.

Referring to the calculation performed for radial acoustic resonance, it has been found that the compressor inlet and compressor outlet are the regions for which the frequency occurrence matches with the measured surge noise frequency. Hence modifications or addition of parts for passive solution was planned for the compressor inlet and outlet locations. Modification of parts has been given a low priority as the shape of the parts affects the packaging of the intake system on the powertrain system.

Referring to the table, n=1, i.e. number of diametral pressures nodes and p=0, i.e. number of concentric pressure nodes correspond to the case where the calculated radial acoustic frequency matches with the measured surge noise frequency. Fig. 7.27, with the nodal pattern is referred for the combinations and a part has been designed as given in the Fig.7.31. The parts are designed to enable them to be bolted into the inside of the compressor inlet and outlet pipes. The ribs and the wall of the parts are designed with adequate thickness to withstand the pressure due to high mass flow rate and temperature. Minimum thickness is very important to maintain the pressure drop of the part to the minimum. Additional pressure drop due to the part can cause increased pumping loss for the engine and hence increased fuel consumption. The wall thicknesses of the final part can be reduced by integrating the part with the compressor inlet

and outlet pipes. The prototype parts were manufactured using rapid prototyping machine. Computer aided design models were provided as an input to the machine. The picture of installed parts are given in the Fig. 7.32.
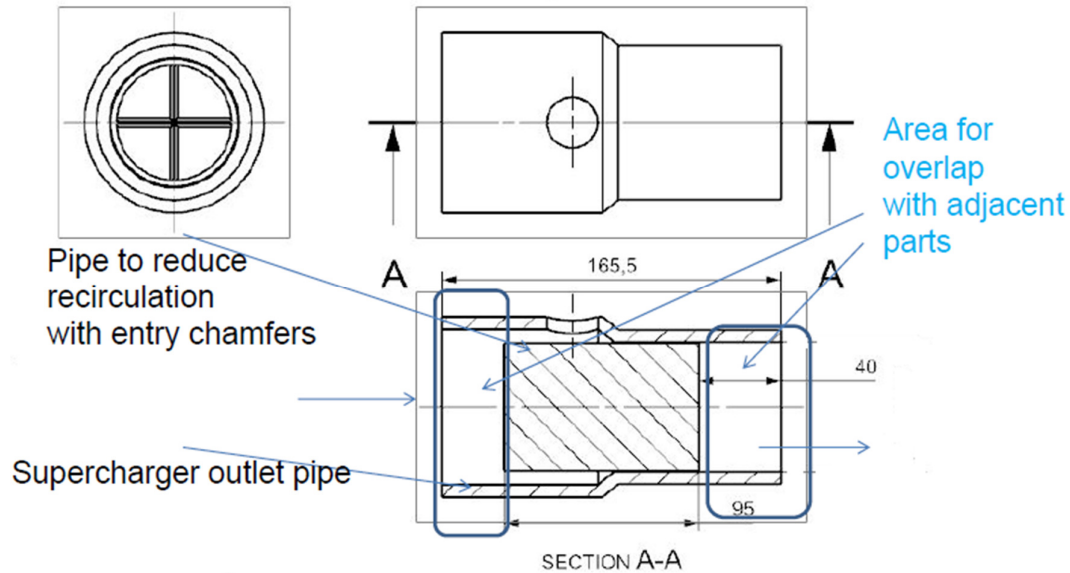
Fig. 7.31 Sectional view of the supercharger pipe
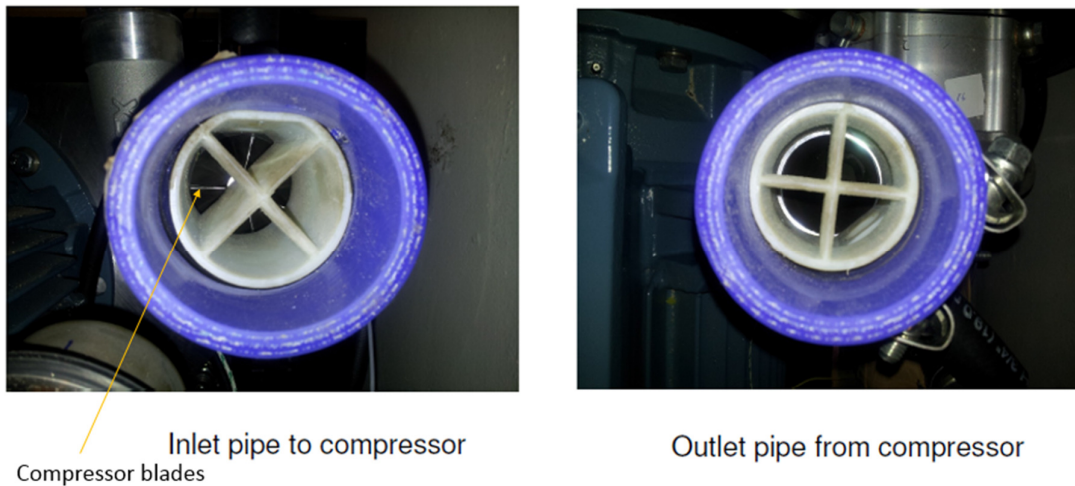
Fig. 7.32 Parts for passive solution fitted inside the compressor inlet and outlet pipes.

7.6 Validation of solution on the experimental rig

Four experiments were planned to quantify and understand the effect of introduction of the passive solution parts inside the compressor inlet and outlet pipes. The installation details are

shown in Fig.7.30 and Fig. 7.31. The experiments conducted are 1. Without using passive solution pipes, 2. With passive solution pipes at the outlet of the compressor, 3. With passive solutions pipes both at the inlet and outlet of the compressor and 4. With passive solution only at the inlet of the compressor. The supercharger shaft speed is maintained at 30000 rpm for all the experiments.

7.6.1 Without using pipes for passive solution

This experiment is a repetition of previous experiments without any passive solution used. The aim is to quantify the surge noise amplitude and to compare with the other experiments in this section.
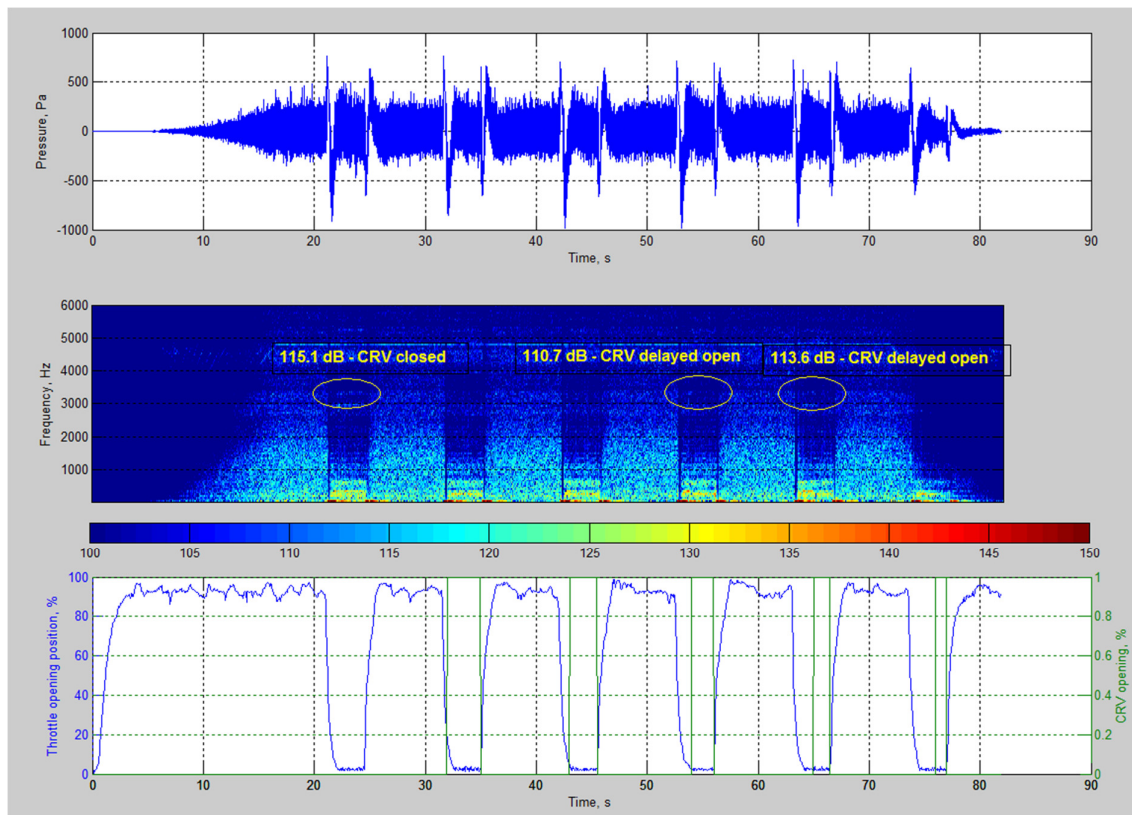
Fig.7.33 Experimental results with no pipes for passive solution fitted – Expt #215

In the first cycle, CRV is completed closed and this resulted in higher noise levels. In the last two cycles, CRV is opened with a delay, which resulted in slight drop in the noise level. The results presented in the Fig.7.32 shows that the maximum value of surge noise measured in this experiment is 115 dB

7.6.2 Pipes for passive solution installed at the outlet of the compressor

In this experiment, the pipe is attached at the outlet duct of the compressor. The inlet duct is retained same as the original specification.
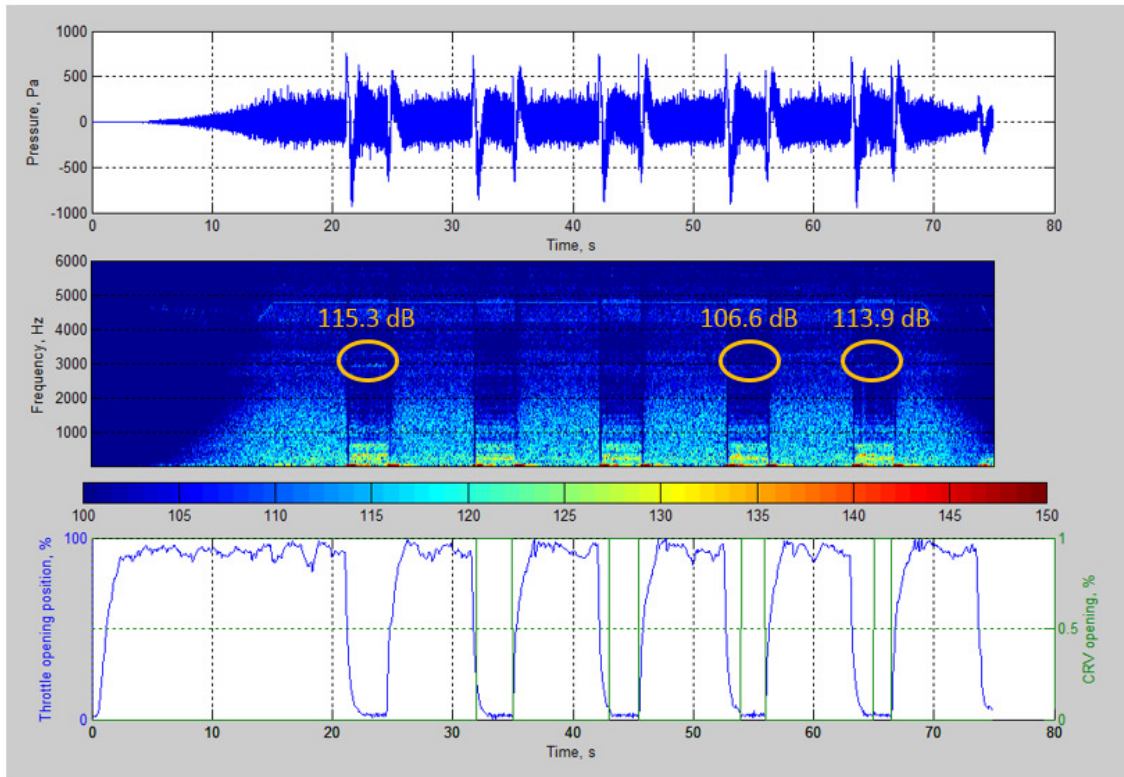
Fig.7.34 Experimental results with pipes for passive solution fitted at the compressor outlet–

Expt #214 (colour code shows the sound pressure level in dB)

As in the previous experiment, the CRV is kept closed in the first cycle and opened with a delay in the other cycles. The noise levels are similar to the previous experiment and did not decrease. The introduction of the pipe at the compressor outlet did not help to arrive at the solution.

7.6.3 Pipes for passive solution fitted at the inlet and outlet pipes of the compressor

The throttle and CRV profiles are maintained same as in the previous experiments. The pipes are installed inside the intake pipe and outlet pipe near the compressor. It is found that the noise amplitude at other regions are remaining fairly same and that at the surge zone has reduced by 10 dB. Hence, pipes installed at the inlet and outlet pipe of the compressor are possibly a good passive solution

Fig.7.35   Experimental results with passive solution installed at the inlet and outlet pipes of the compressor - Expt #212 (colour code shows the sound pressure level in dB)

7.6.4 Pipe for passive solution installed at the inlet pipe of the compressor

The results displayed in the Fig.7.35 clearly shows that the noise is significantly reduced (10 dB) from the original condition. This reduction is comparable to the use of the CRV on the turbocharger. The passive solution installed displayed a noise reduction of 10 dB inspite the fact that the CRV is not opened. Hence, it may be concluded that passive solution is as effective solution as the operation of CRV (active costlier solution), in terms of noise reduction.
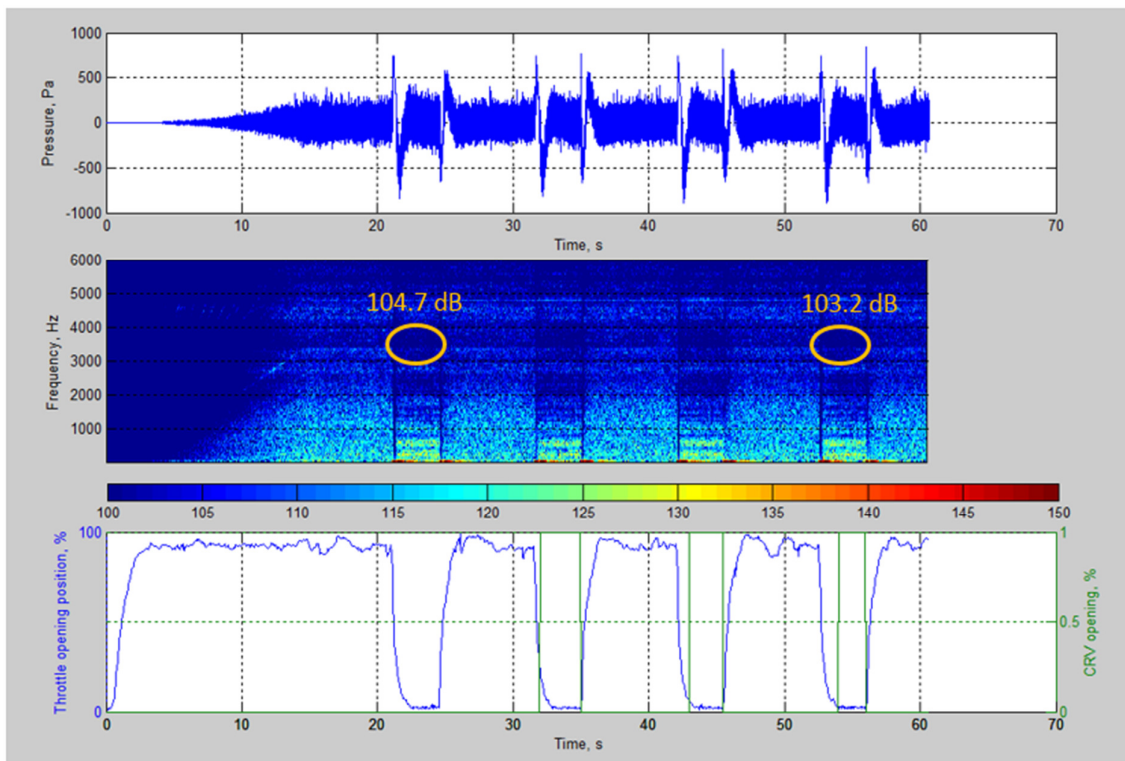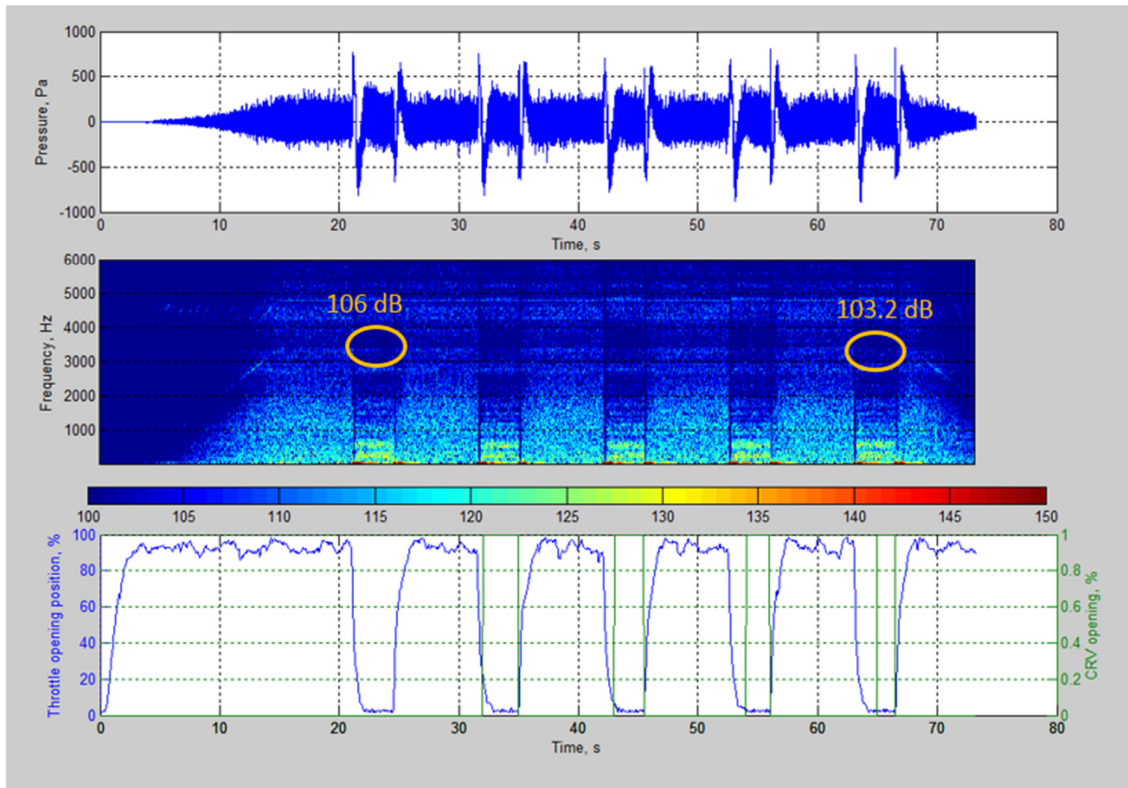
Fig.7.36   Experimental results with passive solution installed at the inlet pipe of the compressor-Expt#213 (colour code shows the sound pressure level in dB)

CHAPTER 8
Conclusion and future work

This thesis focuses on the transient manoeuvres of the throttle system in a petrol engine, analysis of experimental results to identify the turbocharger (compressor) noise, determination of mechanism of noise generation, arriving at a cost effective, passive, specific solution for an intake system and finally verifying the noise reduction obtained, using the specific solution on an experimental rig.

Chapter 2 covered the literature review performed to understand the types of turbocharger noise, possible identification techniques, theory for surge noise generation and finally solutions adapted by various authors. The identification of the source of noise is made usually from the frequency, turbocharger speed and the engine operating conditions. Among the types of noise reviewed, the surge noise may be categorised in to the blow noise or whoosh noise and the frequency range of interest is 1500-3000Hz. This type of noise is generally caused during the operating conditions of less air flow and low turbocharger speed. Many noise generating mechanism in the turbocharger surge period is caused by flow as explained by D.E. Jungbauer et. al [17] and Watson and Janota [2]. The principle mechanism is the disruption of flow due to the effect of non-uniform flow leaving the impeller which can then cause rotating stall of the diffuser. Coincidence of vortex shedding with the acoustical resonance results in the amplification of dynamic pressure fluctuations and hence noise problems. Zero dimensional, one dimensional and CFD modelling are the numerical techniques used to predict the occurrence of surge. Zero dimensional modelling have simplifying assumptions such as ignoring the wave propagation effects and spatial effects in the compressor system.

Main conclusions from this chapter are

- Review of the techniques in the literatures helped to choose the one dimensional numerical technique for this project due to the limitations of zero dimensional modelling.
- Suggested solutions to overcome the noise problem include pre whirl devices and broad band resonators. With the help of pre whirl devices, the operating point on the compressor is moved to the stable region. However, the effect on the pressure drop in

the intake system which can affect the engine performance is not documented. Broad band resonators provided a transmission loss of 23.5dB. This type of solution can be difficult to introduce due to packaging constraints.

Preliminary experiments were conducted on a non turbocharged, Ford Fiesta car engine to measure the noise and vibration characteristic under idle and tip in and tip out manoeuvres, as explained in chapter 3. Fast Fourier Transform (FFT) was used in the idle operation condition to identify the dominant frequencies, whereas Short Time Fourier Transform(STFT) was used in the transient operation to identify the dominant frequencies and corresponding sound pressure levels. As seen in section 3.4.2, characteristic whoosh noise behaviour was not observed in the Fig. 3.9.

The important conclusion of this chapter is:

- Much of the energy as observed in the figure 3.9 is in the lower frequency range of 150 Hz to 620 Hz and do not give a characteristic surge, whoosh or chirpy noise. Hence, it was concluded to try to identify the whoosh noise in an experimental rig and also on one dimensional turbocharged engine model.

The work was extended to predict the pressure pulsations and noise in intake system using one dimensional simulation on a spark ignition engine model, as presented in the chapter 4. Surface microphone model was developed and integrated to the model to measure the pressure fluctuations and to perform the FFT (section 4.5.2). The patterns of the simulated dominant frequencies show a good match with that obtained from the idle operation in the preliminary experiment. Further, a DoE with various contributing factors to the noise in a turbocharged engine, is explained for transient simulation in section 4.5.4. The factors considered were engine speed, throttle profile, CRV profile and compressor surge line position. The compressor surge line is usually determined using a test stand at turbocharger's manufacturing facility using standard piping layout. However, when the turbocharger is installed into the engine, this profile can shift. One dimensional simulation helped to understand the effect of this shift on the intake system noise. The results explained in the section 4.11 show that the CRV closure position along with the shift of the surge line to the stable zone is having an influence on the sound pressure level of the intake system. Characteristic chirpy noise was not observed in the engine simulation model results. This is possibly due to the limitation of one dimensional modelling tool to predict frequencies above 1000 Hz.

In chapter 5, an experimental rig design is explained in detail including the simulation work performed to get input data, component design, layout and manufacturing details. A modular test rig was designed, built and instrumented in the Noise and Vibration laboratory, Loughborough University. The main advantage of the experimental rig over an engine is that the individual components such as throttle body, CRV and shaft speed can be varied independently using the LabVIEW software. The profiles of operation of these components which were measured from the automotive vehicle, during surge operation. These profiles were replicated in the experimental rig. The throttle profile was varied using PID control using LabVIEW software. Modular construction is another advantage of the experimental rig. This helps to adapt intake system of different engines into the rig. Also, this helps to exclude any component or make any changes to the component or its operation to understand the effect on the surge noise. The rig constructed may be a good tool for an automotive NVH engineer to measure the noise characteristic of intake system.

After commissioning the compressor rig in the noise and vibration lab, the next step followed was to simulate the surge operation in the rig (Chapter 6). Initially the background noise was measured to characterise the frequency and amplitude of various components of the experimental rig as explained in section 6.2. The aim was to identify the surge noise frequency from that of the background noise. This kind of identification is achieved with difficulty in the case of an engine dynamometer, as there are many mechanical components involved. Hence, one of the novelty in this project is the use of a modular test rig which can characterise the surge noise clearly from the background noise. As defined in section 6.3, steady state experiments were conducted with throttle in different positions. Experiments with fully closed throttle profile demonstrated characteristic surge noise at a frequency of 3250 Hz. Summary of experiments was presented in Fig. 6.22 in the form of an interaction plot using Minitab software. This figure outlines the interaction of compressor speed, throttle open position and the CRV open or close position on surge noise. As a conclusion of this chapter, it was found that CRV open or close position and throttle position have a major contribution to the cause of surge noise.

It was concluded from this chapter that

- The CRV open or close position and the throttle position are the major contributing factors to the surge noise

Design of a passive solution to reduce the surge noise is explained in chapter 7. From the conclusion of the previous exercise it was found that the CRV delay has a major influence on the surge noise. It was also identified that the surge noise is a flow induced phenomena. Hence, characterisation of the problem at different compressor shaft speeds and CRV delay values were conducted using simulation and experimentation methods. It was found that CRV delay has a strong influence in the surge noise generation. The surge noise occurrence frequencies identified at 30000 rpm of shaft speed fell in a narrow range of 3150 Hz to 3350 Hz and for the 40000 rpm – 3450 to 3875 Hz. Section 7.4 explains the steps followed to determine the mechanism of the problem. From the subsequent analysis, radial acoustic resonance may be a mechanism of surge noise generation as given in the section 7.4.3.

Another novelty of this thesis is that a passive solution has been derived following a solution methodology which may be used by NVH engineers in the automotive industry to reduce the noise at transient conditions, with less effect on the engine calibration or performance. Solution by improving the mechanical CRV by modification of the spring rate and other damping characteristics may be adopted to reduce the delta T, i.e. the time delay in opening or closing of the CRV. A passive solution was derived using the radial acoustic resonance calculation and the nodal patterns and is presented in section 7.5. The passive solution results in a less cost increase than using complex electronic means such as electronic CRV to reduce the surge noise. Experiments using newly designed part for passive solution show (section 7.6) that the sound pressure levels are reduced to almost the same levels (10 dB reduction) even without opening the CRV. From the STFT results, more suitable location for the part introduction for solution is found to be at the compressor inlet than at the outlet, thus confirming the fact that the turbocharger surge noise occurs at the inlet section.

The main conclusions of the thesis are:

- The surge noise frequencies at 30000 rpm falls in a narrow range of 3150Hz and 3350Hz and for the 40000 rpm-3450 to 3875 Hz.
- The mechanism of whoosh noise generation may be the radial acoustic resonance in the intake duct of the compressor.
- A passive solution was derived using the radial resonance calculation and the nodal patterns

Due to limited time available for this research, some extension of the current work was described as future work. Adaptation of supercharger rig to drive the turbocharger can be used as a possible extension in future. This would help to make the rig completely modular, i.e. use the intercooler, turbocharger as in an actual engine. Also, with the introduction of pulse supercharging and by considering mechanisms to include the number of cylinders, the effects of these can be understood. However, this extension requires extensive control facilities such as flow control valve and a dedicated lubrication circuit to the turbocharger.

Improved flow visualisation could be another possible future work. Laser anemometry or multi axial flow probes could be used in the intake system to understand the modal pattern of radial acoustic waves. Laser anemometers can help in less obtrusive method to visualise the flow.

References

[1]   R. Kunze, "The environmental challenge for the automotive industry," MSc in Automotive
         Systems Engineering course note, Loughborough University, 2004-05.

[2]   N. Watson and M. S. Janota, Turbocharging the Internal Combustion Engine, The Macmillan
         Press Ltd, 1993.

[3]   J. B. Heywood, Internal Combustion Engine Fundamentals, McGraw-Hill Series in Mechanical
         Engineering, 1988.

[4]   R. V. Basshuysen and F. Schafer, Internal Combustion Engine Handbook, SAE International,
         2002.

[5]   M. Schroeer and H. Stoffels, "NVH aspects of a downsized turbocharged gasoline powertrain
         with direct injection," in *Noise and Vibration Conference and Exhibition, SAE Technical Paper
         Series, 2003-01-1664*, Traverse City, Michigan, 2003.

[6]   D. Evans and A. Ward, "Minimising Turbocharger Whoosh Noise for Diesel Powertrains," in
         Noise & Vibration Conference and Exhibition, SAE Technical Paper Series, 2003-01-1664,
         Traverse City, Michigan, May 16-19 2005.

[7]   J. March, G. Strong, S. Gregory and B. Rediers, "Achieving Diesel Vehicle Appeal Part 1: Vehicle
         NVH Perspective," in *SAE Technical Paper, 2005-01-2484*.

[8]   Y.W.Lee, D.J.Lee, KAIST, Y.So, D.Chung, GMDAT, "Control of Airflow Noise From Diesel Engine
         Turbocharger," in *SAE 2011-01-0933*.

[9]   H. Rammal, M.Abom, KTH CICERO, "Acoustics of Turbocharger," in *SAE 2007-01-2205*.

[10] R. Stone, Introduction to Internal Combustion Engines, MacMillan Press Ltd, 1999.

[11] M. V. Casey and M. Schiegel, "Estimation of the performance of turbocharger compressors at extremely low pressure ratios," *Proc. IMechE Part A: J. Power and Energy,* vol. 224.

[12] S. Pischinger, RWTH Aachen, H. Stoffels, Ford Werke GmbH, C. Steffens, FEV Motorentechnik GmbH, R. Aymanns, RWTH Aachen, R. Stohr, FEV Motorentechnik GmbH, M. Atzler, RWTH Aachen, "Acoustics development for exhaust gas turbochargers," *MTZ Worldwide 03, Vol 69,* March 2008.

[13] E. P. Trochon, "A new type of silencers for turbocharger noise control," in *Proceedings of the 2001 Noise and Vibration Conference, SAE technical paper series, 2001-01-1436*.

[14] C. Teng and S. Homco, "Investigation of whoosh noise in automotive turbocharger," in *SAE 2009-01-2053*.

[15] G. Capon, T. Morris, Ford Motor Company Limited, "The effect of air inlet system features on automotive turbocharger compressor performance," in *Turbochargers and turbocharging, 9th international conference*, London, 19-20 May 2010.

[16] R. Chen, ""Introduction to Centrifugal Compressors," MSc 2004 Course Notes, Aeronautical and Automotive Engineering, Loughborough University.

[17] D. Jungbauer and L. Eckhardt, "Flow-induced turbocompressor and piping noise and vibration problems-identification, diagnosis and solution," in *Proceedings of the 26th turbomachinery symposium, Texas A&M University, College Station, Texas*.

[18] S. Ziada, A. Oengoren and A. Vogel, "Acoustic resonance in the inlet scroll of a turbocompressor," *Journal of fluids and structures,* vol. 16(3), pp. 361-373, 2002.

[19] F. Archibald, "Self-excitation of an acoustic resonance by vortex shedding," *Journal of Sound and Vibration,* vol. 38(1), pp. 81-103, 1975.

[20] F. Williams and X. Y. Huang, "Active stabilisation of compressor surge," *J. Fluid Mech.,* vol. 201, pp. 245-262, 1989.

[21] E. Greitzer, "The stability of pumping systems," *Journal of Fluids Engineering,* 1981.

[22] H. Chen, I. Hakeem, R. F. Martinez – Botas, Mechanical Engineering Department, Imperial college of Science, Technology and Medicine, London, "Modelling of turbocharger turbine under pulsating inlet conditions," *Proceedings of Institution of Mechanical Engineers,* vol. 210, 1996.

[23] H Rammal, KTH CICERO, J Galindo, CMT-Motores Termicos, "The passive acoustic effect of turbo-compressors," in *9th International Conference on Turbochargers and Turbocharging*, London, May 2010.

[24] P. Keller, M. Becker, Borg Warner Inc., R. Dehner, A. Selamet, The Ohio State University, "Simulation of Mild Compressor Surge using GT-POWER," in *GT-2010 Conference*.

[25] R. Dehner, A. Selamet, Ohio State University, P. Keller. M. Becker, BorgWarner Inc, "Prediction of Surge in a Turbocharger Compression System vs. Measurements," in *SAE 2011-01-1527*, 17/05/2011.

[26] N. C. Baines, Concepts NREC USA, "Turbocharger turbine pulse flow performance and modelling – 25 years on," in *9th International Conference on Turbochargers and Turbocharging*, London, May 2010.

[27] K.S. Peat, Loughborough University, A.J. Torregrosa, A. Broatch, T. Fernandez, CMT-Motores Termicos, Universidad Politecnica de Valencia Camino de Vera, "An investigation into the passive acoustic effect of the turbine in an automotive turbocharger," *Journal of Sound and Vibration,* vol. 295, pp. 60-75, 2006.

[28] N. Aretakis, K. Mathioudakis, M. Kefalakis, K. Papiliou, Laborary of Thermal Turbomachines, National Technical University of Athens, "Turbocharger unstable operation diagnosis using vibroacoustic measurements," *Transactions of the ASME,* vol. 846/Vol 126, October 2004.

[29] J. Galindo, J.R. Serrano, C.Guardiola, C. Cervello, "Surge limit definition in a specific test bench for the characterisation of automotive turbochargers," *Experimental Thermal and Fluid Science,* no. 30, pp. 449-462, 2006.

[30] I. L. Ver and L. L. Beranek, Noise and Vibration Control Engineering-Principles and Applications, Second ed., John Wiley & Sons, Inc., 2006.

[31] J Galindo, J R Serrano, X Margot, A Tiseria, N Schorn, H Kindl, "Potential of flow pre-whirl at the compressor inlet of automotive engine turbochargers to enlarge surge margin and overcome packaging limitations," *International Journal of Heat and Fluid Flow,* no. 28, pp. 374-387, 2007.

[32] 30 Nov 2011. [Online]. Available: http://www.forcedinductions.com/help.htm.

[33] S. Usuda, M. Otsuka, M. Nagata, Toyota Motor Corporation, "Noise and vibration reduction of newly developed 3.01 direct injection diesel engine," in *JSAE Review 23, 285-289*, 2002.

[34] S. Walsh, "Vehicle systems-Vehicle NVH - MSc 2004 Course Note".

[35] S. K. Mitra, Digital Signal Processing – A Computer Based Approach, Mc Graw Hill Series in Electrical and Computer Engineering, 2001.

[36] "MATLAB help guide, MathWorks, 2011".

[37] "GT Suite Flow theory manual," 2014.

[38] R. L. Street, G. Z. Watters and J. K. Vennard, Elementary Fluid Mechanics, John Wiley & Sons, 1996.

[39] D E Winterbone and R J Pearson, Design Tehniques for Engine Manifolds – Wave Action Methods for IC Engines, Professional Engineering Publishing Limited, 1999.

[40] L. Landau, Fluid Mechanics, Pergamon Press, 1999.

[41] "SAEJ1826, "Turbocharger gas stand test code", SAE standards (Reaffirmed 1995-03)".

[42] J. Galindo, J.R. Serrano, H. Climent, A. Tiseira, "Experiments and modelling of surge in small centrifugal compressor for automotive engines," *Experimental Thermal and Fluid Science,* vol. 32, pp. 818-826, 2008.

[43] Rotrex Technical Datasheet C38 Range (8), accessed from, "http://www.rotrex.com/Home/Technology/Product_Technical_Data," 01 February 2013. [Online].

[44] "http://www.bksv.co.uk/doc/bp2055.pdf, http://www.bksv.com/Products/transducers/acoustic/microphones/microphone microphone preamplifier-combinations/4949.aspx," Feb 2013. [Online].

[45] Help manual, Minitab17.

[46] R. Fisher, Design of Experiments, 8th ed., Oliver and Boyd, 1966.

[47] F. Fahy and P. Gardonio, Sound and structural vibration, Academic Press, 2007.

[48] A. Pierce, Acoustics: An introduction to its physical principles and applications, Acoustical
Society of America, 1989.

[49] M. Harrison, Vehicle Refinement Controlling Noise and Vibration in Road Vehicles, Elsevier
Butterworth-Heinemann, 2004.

[50] "Flow Theory Manual – GT Suite, Gamma Technologies," 2010.

[51] "GT Power User's manual Version 6.2, September 2006".

[52] Y. Mochkaai, "GT-Power as a tool for acoustic and dynamic optimisation of exhaust sytems," in
GT-SUITE user conference 2009, Frankfurt, Nov 2009.

[53] B. Schweizer, "Total instablility of turbocharger rotors-physical explanation of the dynamic
failure of rotors with full-floating ring bearings," *Journal of Sound and Vibration,* vol. 328, pp.
156-190, 2009.

[54] S. Bennet, A history of control engineering 1930-1955, IEE control engineering series 47.

[55] F. Payri, J. Benajes and M. Reyes, CMT-Motores Termicos, Universidad Politecnica de Valencia
Camino de Vera, "Modelling of supercharger turbines in internal combustion engines,"
International Journal of Mechanical Science, no. 38, pp. 853-869, 1996.

[56] F. Willems, M. Heemels, B de Jager, A. Stoorvogel, "Positive Feedback Stabilization of Compressor Surge," in *Proceedings of the 38th conference on Decision & Control*, Phoenix, Arizona USA, December 1999.

[57] J. T. Gravdhal, F. Willems, B. de Jager, O. Egeland, "Modelling for surge control of centrifugal compressors: comparison with experiment," in *Proceedings of the 39th IEEE Conferenc eon Decision and Control*, Sydney, Australia, December 2000.

[58] P. W. Sachaberg, T. Priede, R. K. Dutkiewicz, "Effects of a rapid pressure rise on engine vibration and noise," in *900013, SAE Technical Paper Series, International Congress and Exposition*, Detroit, Michigan, 1990.
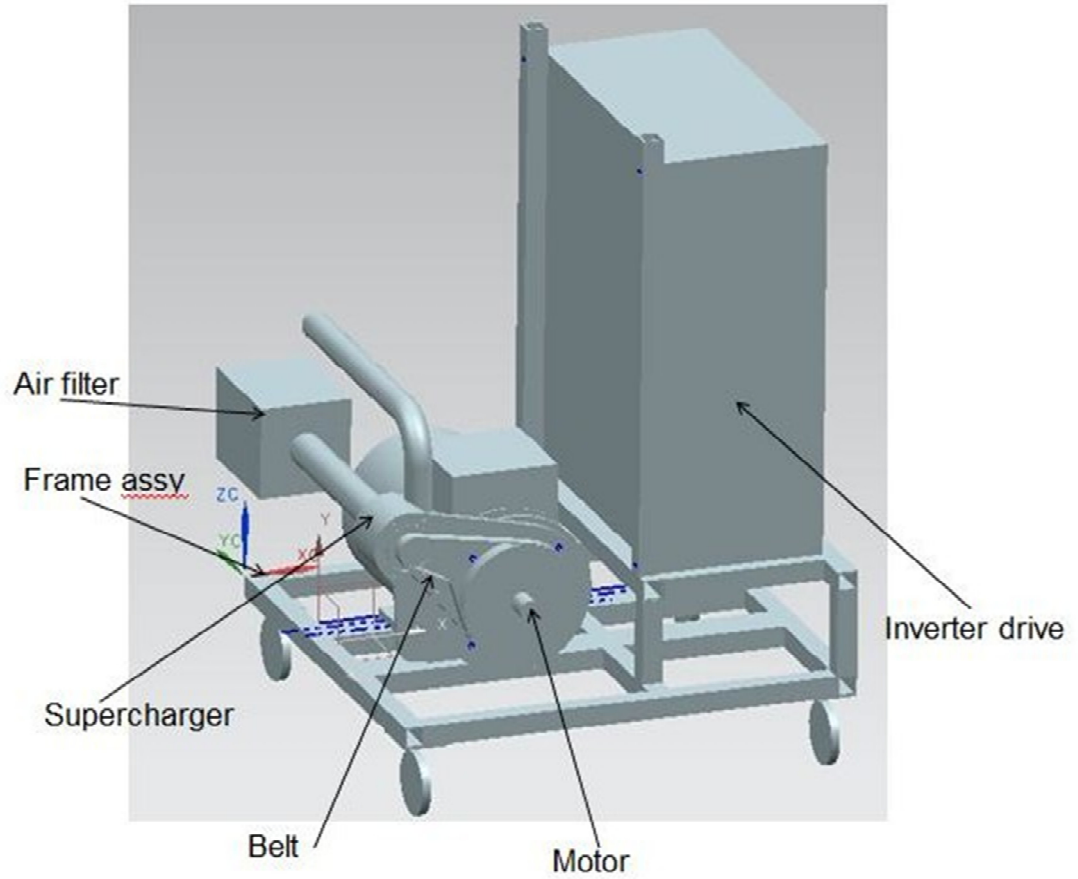
Appendix 1 – Experimental rig drawings
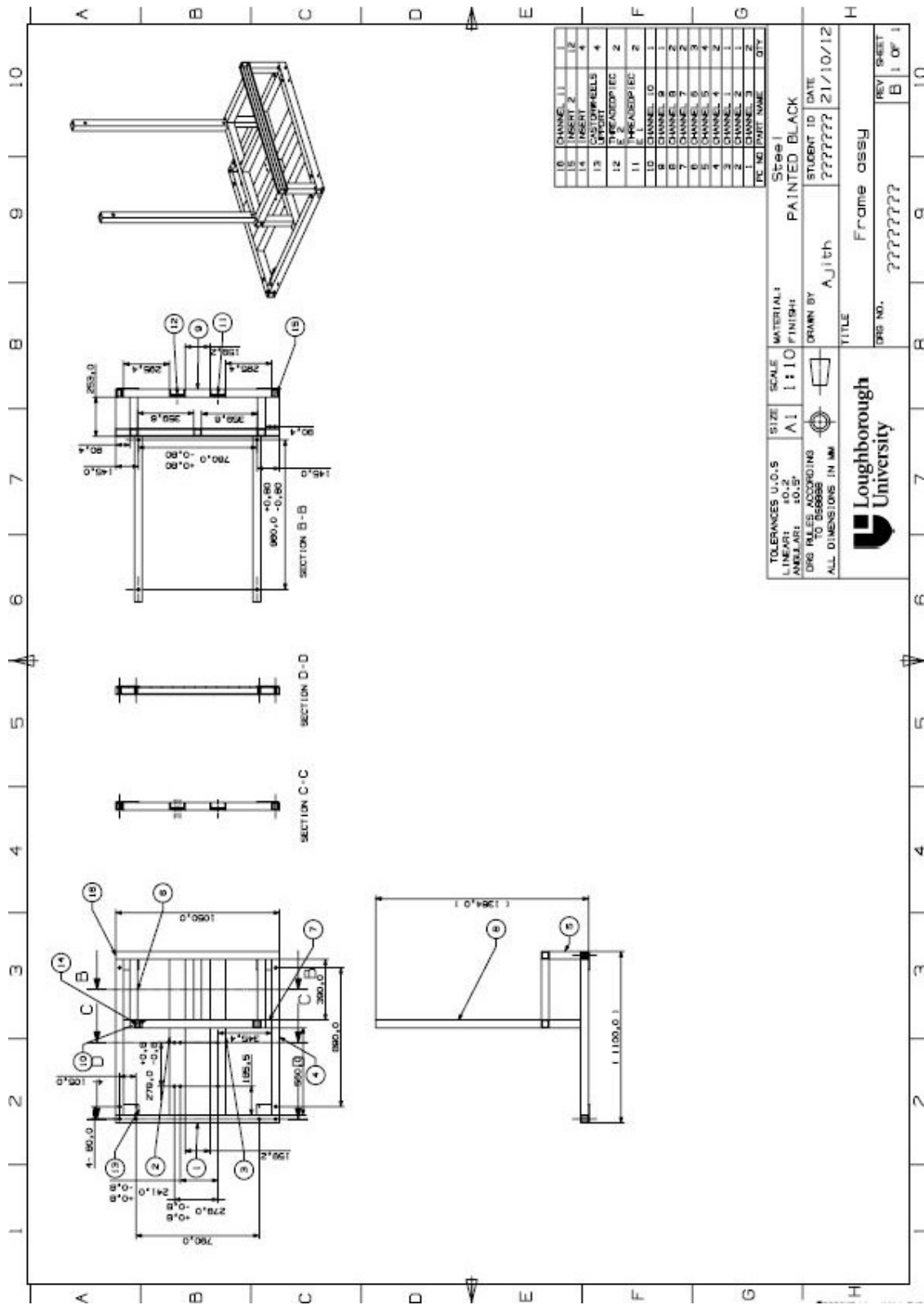

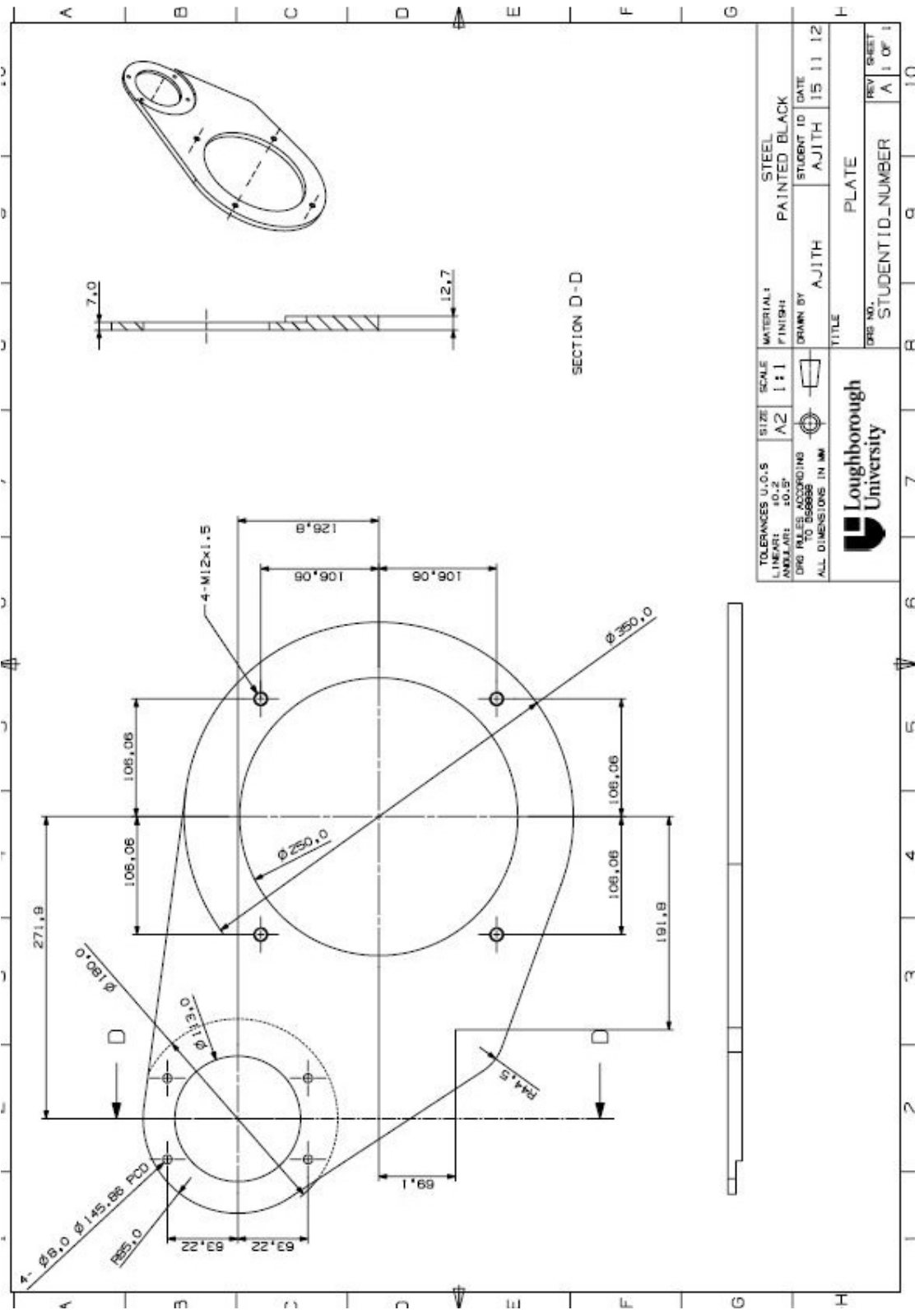Fig.9.1 Supercharger rig model

Fig. 9.2 Frame assy

Fig. 9.3 Plate drawing
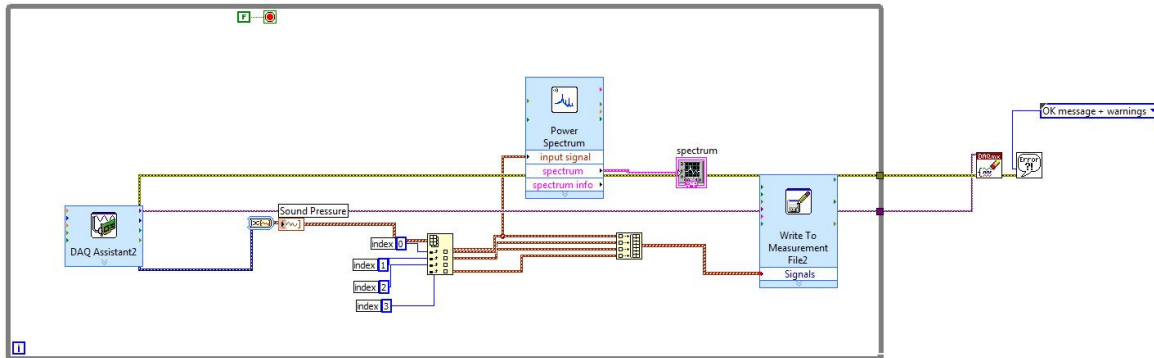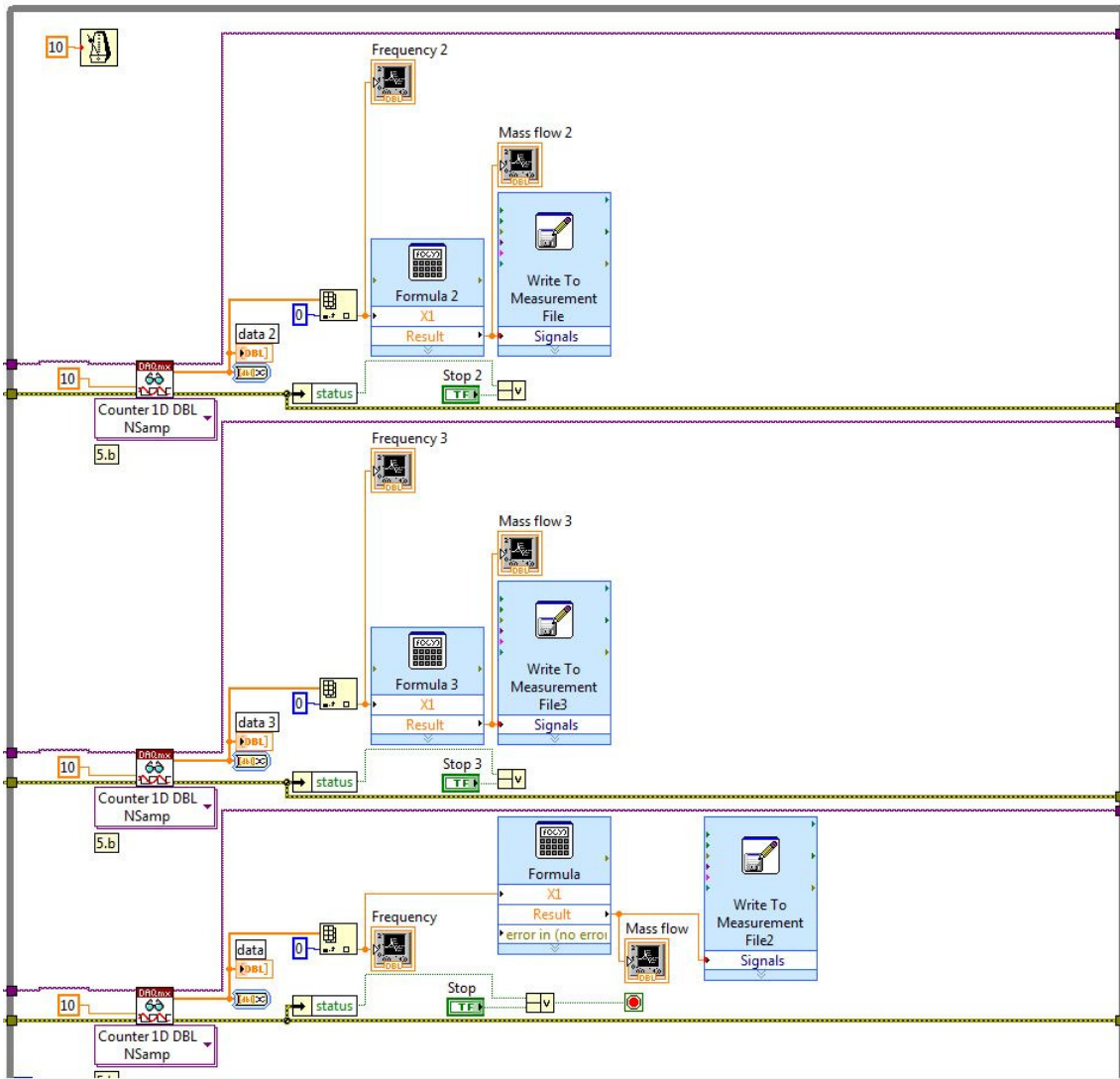
Appendix 2- LabVIEW block diagrams

Fig. 9.4 Data acquisition layout

Fig. 9.5 Massflow measurement layout

Fig. 9.6 Throttle and CRV control layout